Transcriptional regulation of intestinal epithelial homeostasis and regeneration

Angelis, Nikos

Awarding institution:
King's College London

Thesis title:

“Transcriptional regulation of intestinal epithelial homeostasis and regeneration”

Nikolaos Angelis

King’s College London

and

The Francis Crick Institute

PhD supervisor: Vivian Li

A thesis submitted for the degree of

Doctor of Philosophy

June 2022

Abstract

Intestinal stem cells (ISCs) reside at the bottom of intestinal crypts. They divide and give rise to early progenitor cells (+4/+5 cells) when entering the transit-amplifying zone (TA), and eventually differentiate into various mature epithelial cell types. Wnt, Notch and Tgf-β/Bmp signalling pathways form gradient of expression along the crypt-villus axis and play a central role in regulating ISC homeostasis and lineage commitment. Despite the good understanding of the signalling pathways in regulating ISC self-renewal and fate decision, the underlying mechanism of the dynamic lineage selection and plasticity of the +4/+5 early progenitors remains largely unknown.

Here, we identify Arid3a as a novel regulator of intestinal epithelial cell differentiation and maturation. Arid3a is expressed at the early progenitors at +4/+5 cell positions and most differentiated cells with an expression gradient that accumulates at the tip of the villus. We show that Wnt signalling has an inhibitory role on the expression of Arid3a, while Tgf-β signalling promotes its expression. Intestinal epithelial-specific deletion of Arid3a leads to decreased numbers of proliferating TA cells at the upper crypt and a reduction of Wnt signalling which is associated with a moderate decrease of Paneth cell numbers. Interestingly, ISC numbers are not affected. Most importantly, loss of Arid3a perturbs the zonation programme of the entire intestinal epithelium. Expression analysis of the Arid3a cKO intestine showed a reduced gene signatures of committed cells at the upper crypt and a strong enrichment of mid-villus to villus-tip gene signatures of enterocytes, goblet, enteroendocrine and tuft cells. Our findings suggest that TA cells enter their differentiated states earlier at the expense of their proliferative capacity. Finally, using an irradiation mouse model, we show that loss of Arid3a impairs the regenerative process by altering the dynamics of proliferation and apoptosis.

We conclude that Arid3a drives maintenance of epithelial homeostasis across the crypt-villus axis and supports the regenerative capacity of the intestinal epithelium. Our work provides an important advancement in understanding the regulation of TA cells state and the transdifferentiation process in the intestinal epithelium.

Acknowledgment

Pursuing a PhD can be a challenging, stressful but, at the same time, rewarding experience. Finding the ideal place where you really fit and feel comfortable is key to a successful PhD. First of all, I would like to thank my supervisor Dr. Vivian Li for her support throughout these years. While in the process of looking for a PhD position, I wanted to work with a young, aspiring scientist who creates a positive lab atmosphere and who would allow me to own my project, encourage me to test my scientific ideas, and be always there for me when I need help. Vivian offered me all of that and even more and I will be eternally grateful to her. Next, I would like to thank all past and current lab members who made my PhD experience truly unforgettable. We definitely had a lot of fun over coffee or lunch and we never stopped supporting each other in the lab. Especially, massive thanks to Anna Baulies for being my lab sister for the past 5 years and a friend for life.

Thanks to Dr. Karen Liu, Dr. Francois Guillemot and Dr. Axel Behrens who formed my thesis committee and greatly supported my project by providing excellent scientific discussions, ideas and feedback.

Thanks to the Academic team of the Crick for providing guidance throughout the PhD programme, to the Crick Science Technology Platforms for their continuous scientific support, to everyone at 3NW quadrant for making it such a nice place to work and to the members of the Development and Stem Cell interest group.

Big thanks to all of my friends that supported me all these years. Throughout my High School studies in my hometown, my BSc studies at the University of Patras, my MSc studies at the University of Groningen, my post-bac experience at the National Institutes of Health and my PhD studies at the Crick, I was lucky enough to meet amazing and inspiring people who are all an indispensable part of my life and have never stopped to support me.

A special thank you to my former supervisor Dr. Swee Lay Thein. She is the reason I decided to pursue a PhD and she taught me what it takes to be a good scientist.

Lastly, but most importantly, a massive thank you to my parents, my brother, my grandparents and my partner. I would have never been able to do anything without their unconditional love and support. I owe everything that I have done to them.

Table of contents

Table of figures

List of tables

List of abbreviations

5-HT	Serotonin
AB-PAS	Alcian Blue-Periodic Acid Schiff
ADAM	A-disintegrin-and-metalloprotease
Agr2	Anterior gradient protein 2 homolog
Alpi	Alkaline phosphatase
Apc	Adenomatous polyposis coli
Apoa4	Apolipoprotein A4
Arid	A+T rich interaction domain
Ascl2	Achaete-Scute homologue 2
ATAC-seq	Assay of Transposase Accessible Chromatin sequencing
Atoh1	Atonal BHLH Transcription Factor 1
Axin2	Axis inhibition 2
BCR	B-cell antigen receptor
Bmp	Bone morphogenetic protein
Bmpr	Bone morphogenetic protein receptor
Btk	Bruton's tyrosine kinase
CBC	Crypt base columnar
Ccnd1	Cyclin D1
CD24	Cluster of differentiation 24
Cdc	Cell division cycle
ChgA	Chromogranin A
ChIP	Chromatin immunoprecipitation

Ck1	Casein kinase 1
cKO	conditional knockout
Clu	Clusterin
CM	Conditioned medium
CRD	Cysteine-rich domain
DAPI	4’,6’-diamidino-2-phenylindole
Dclk1	Doublecortin-like kinase 1
Ddx5	DEAD box containing 5
Dll	Delta-like
DNA	Deoxyribonucleic acid
DNase-seq	DNase I hypersensitive sites sequencing
DSG	Di(N-succinimidyl) glutarate
DSL	Delta/Serrate/Lag-2
DSS	Dextran sulfate sodium
DTT	Dithiothreitol
Dvl	Dishevelled
EC	Enterocytes
EDTA	Ethylenediaminetetraacetic acid
EdU	5-ethynyl-2’-deoxyuridine
EE	Enteroendocrine
Egf	Epidermal growth factor
Egfr	Epidermal growth factor receptor
Eph	Erythropoietin-producing human hepatocellular

Ephrin	Eph-receptor interacting protein
ESC	Embryonic stem cells
Fabp1	Fatty acid binding protein 1
FACS	Fluorescence-activated Cell Sorting
FAIRE-seq	Formaldehyde-Assisted Isolation of Regulatory Elements sequencing
FBS	Fetal bovine serum
FDR	False discovery rate
Fgf2	Fibroblast growth factor 1
Fzd	Frizzled
GC	Goblet cells
Gfi1	Growth factor independent 1
Gfp	Green fluorescent protein
Ghrl	Ghrelin
Gip	Gastric inhibitory peptide
Gli	Glioblastoma family of transcription factor
Glp1	Glucagon-like peptide 1
GSEA	Gene set enrichment analysis
Gsk3	Glycogen synthase kinase 3
Gy	Gray
H&E	Haematoxylin and Eosin
Hdac	Histone deacetylase 1
Hes	Hairy and enhancer of split
Hgf	Hepatocyte growth factor

Hh	Hedgehog
Hnf	Hepatocyte nuclear factor
Hopx	Homeodomain-only protein
IBD	Inflammatory bowel disease
IF	Immunofluorescence
Ifn-γ	Interferon-γ
Igf1	Insulin-like growth factor 1
IgH	Immunoglobulin heavy chain
IHC	Immunohistochemistry
Ihh	Indian hedgehog
Il	Interleukin
Il11ra1	Interleukin 11 receptor a1
ILC	Innate lymphoid cell
IP	Immunoprecipitation
ISC	Intestinal stem cell
Jagged	Serrate-like
JAK	Janus kinase
JNK	c-Jun N-terminal kinases
Klf4	Krüppel-like factor 4
Krt19	Keratin19
Lats1/2	Large tumour suppressor 1/2
Lef	Lymphoid enhancer-binding factor
Lgr5	Leucine-rich-repeat-containing G-protein-coupled receptor 5

LRC	Label-retaining cell
Lrig1	Leucine-rich repeats and immunoglobulin-like domains 1
Lrp5/6	Low-density lipoprotein-related protein 5/6
Lyz	Lysozyme
MAPK	Mitogen-activated protein kinase
MEF	Mouse embryonic fibroblasts
Met	Mesenchymal-epithelial transition
Mex3a	Mex-3 RNA Binding Family Member A
Mst1/2	Mammalian Ste20- like kinases 1/2
mTert	Mouse telomerase reverse transcriptase
Mtg	Myeloid translocation gene
Muc2	Mucin2
Neurog3	Neurogenin 3
NICD	Notch Intracellular Domain
NSC	Normalized strand coefficient
Nts	Neurotensin
Olfm4	Olfactomedin 4
PC	Paneth cells
PCA	Principal Component Analysis
PEI	polyethylenimine
PFA	Paraformaldehyde
PI3K	Phosphatidyl- inositol 3-kinase
Pou2f3	Pou class 2 homeobox 3

Pp2a	Protein phosphatase 2a
Ptch1/2	Patched 1/2
QC	Quality control
qRT-PCR	Quantitative real-time polymerase chain reaction
Rbpj	Recombination Signal Binding Protein for Immunoglobulin Kappa J Region
Reg4	Regenerating islet-derived family member 4
RIN	RNA integrity number
RNA	Ribonucleic acid
RNA-seq	RNA sequencing
Rnf43	Ring Finger Protein 43
RSC	Relative strand correlation
Rspo	Rspondin
S1K	Schedule 1 killing
Sca-1	Stem cell antigen 1
Scf	Stem cell factor
scRNA-seq	single cell RNA sequencing
Sec	Secretin
Shh	Sonic hedgehog
Slc	Solute carrier family
Smad	Mothers against decapentaplegic
Smoc2	SPARC-related modular calcium-binding 2
Smo	Smoothened
Sox	SRY-Box containing transcription factor

Spdef	SAM pointed domain containing ETS transcription factor
Sst	Somatostatin
STAT	Signal transducer and activator of transcription
TA	Transit-amplifying
Taz	Transcriptional co- activator with PDZ-binding motif
TC	Tuft cells
Tcf4	Transcription factor 4
Tff3	Trefoil factor 3
TFII-I	Transcription factor II-I
Tgf	Transforming growth factor
Tgfbr	Transforming growth factor β receptor
TOBIAS	Transcription factor Occupancy prediction By Investigation of ATAC-seq Signal
Tph1	Tryptophan hydroxylase 1
TSS	Transcription start site
WB	Western blot
Wnt	Wingless-related integration site
WT	Wild type
Yap	Yes-associated protein
Zg16	Zymogen granule protein 16
Znrf3	Zinc And Ring Finger 3

Chapter 1: Introduction

1.1 Biology of the intestinal epithelium

1.1.1 Organisation of the intestinal epithelium

The gastrointestinal tract is a digestive system that includes the oesophagus, stomach, small and large intestines, caecum and rectum, which facilitates food uptake, digestion, nutrient absorption, waste disposal and provides barrier function (Collier et al., 2022). The small intestine serves as the main point of food digestion and nutrient absorption, but it also secretes mucus and hormones, interacts with microbiota and protects the body from pathogenic microbes and toxins (Noah and Shroyer, 2013). In order to achieve these functions, the small intestine has a complex, multilayer structure. The outermost layer is serosa that mainly includes mesothelial cells and connective tissue. Next, there are two muscle layers that are important for the bowel movement (peristalsis). The next layer is submucosa which consists of neural, lymphatic and vascular components, fibroblasts and immune cells. The submucosa is bound from one of the two outer muscle layers as well as muscularis mucosa, another very thin muscle layer. After muscularis mucosa, there is the last layer of the intestinal tube termed mucosa. Mucosa consists of the mesenchymal lamina propria that includes fibroblasts, nerves and immune cells and the monolayer of columnar intestinal epithelium which faces the lumen (Meran et al., 2017, Noah and Shroyer, 2013).

The intestinal epithelium is one of the fastest renewing and regenerating tissues. It has a highly organized structure that consists of finger-like projections towards the lumen called villi, and small glandular invaginations towards the submucosa called crypts, which are the proliferative compartment (Santos et al., 2018) (figure 1.1). Each villus structure is attached to at least six proliferative crypts (Barker, 2014). Due to their continuous exposure to pathogenic organisms and substances that are present in the intestinal lumen, up to 10^{11} epithelial cells are lost daily in humans, while the whole epithelium is renewed every 5-7 days (Leblond and Walker, 1956). This extremely high turnover in cell composition is facilitated by stem cells residing at the intestinal crypts. Over the past decades, two models of stem cell identity have been

proposed based on different functional analyses: the “stem cell zone model” suggests the existence of columnar stem cells residing at the bottom of the crypt (Bjerknes and Cheng, 1999), while the “+4 model” (based on their cell position counting from the crypt base) suggests that stem cells reside immediately above a population of differentiated cells called Paneth cells (Potten, 1977). Recent transcriptomic and proteomic analyses of the two populations, as well as lineage tracing experiments, have led to the proposal of a stochastic model (Munoz et al., 2012, Van der Flier et al., 2007). It is now proposed that intestinal stem cells (ISCs) reside at the bottom of the crypt, where they will divide to generate a daughter cell that will either self-renew to regenerate another stem cell or will enter the transit-amplifying (TA) zone for subsequent lineage specification (Barker, 2014, Barker et al., 2007, Tetteh et al., 2015).

Intestinal lineage decision takes place at cell positions +4/+5, where progenitor cells are located (Clevers, 2013). These cells are highly plastic and are able to re-acquire stemness for tissue regeneration upon injury (see section 1.3 in detail) (Tetteh et al., 2016, van Es et al., 2012, Baulies et al., 2020b). The progenitor cells in the intestinal epithelium can be broadly divided into two main subtypes: absorptive and secretory progenitors. Absorptive progenitors differentiate into enterocytes (EC), the most abundant cell type of the intestinal epithelium, while secretory progenitors give rise to enteroendocrine cells (EE), Paneth cells (PC), goblet cells (GC) and tuft cells (TC) (figure 1.1). As the ISCs differentiate, daughter cells migrate up the crypt-villus axis and eventually die and shed into the intestinal lumen when they reach the tip of the villus after 4-5 days (Artavanis-Tsakonas et al., 1999, Demitrack and Samuelson, 2016, Noah et al., 2011, Noah and Shroyer, 2013). On the other hand, Paneth cells are the only differentiated cell type that move to the bottom of the crypt and reside in between stem cells, serving as crypt niche (figure 1.1) (Sato et al., 2011b).

The stem cell-to-daughter cell transition in the intestinal epithelium is a highly dynamic and plastic process. Maintenance and regulation of the stem cell pool is controlled both by the cellular niche as well as by the stromal microenvironment including fibroblasts, immune cells, neural cells and the extracellular matrix (Meran et al., 2017). A variety of signalling cascades, including Wnt, Notch and Tgf-β/Bmp, has been well-described in regulating ISC maintenance and lineage commitment, and their contributions in intestinal homeostasis will be further discussed in section 1.2.

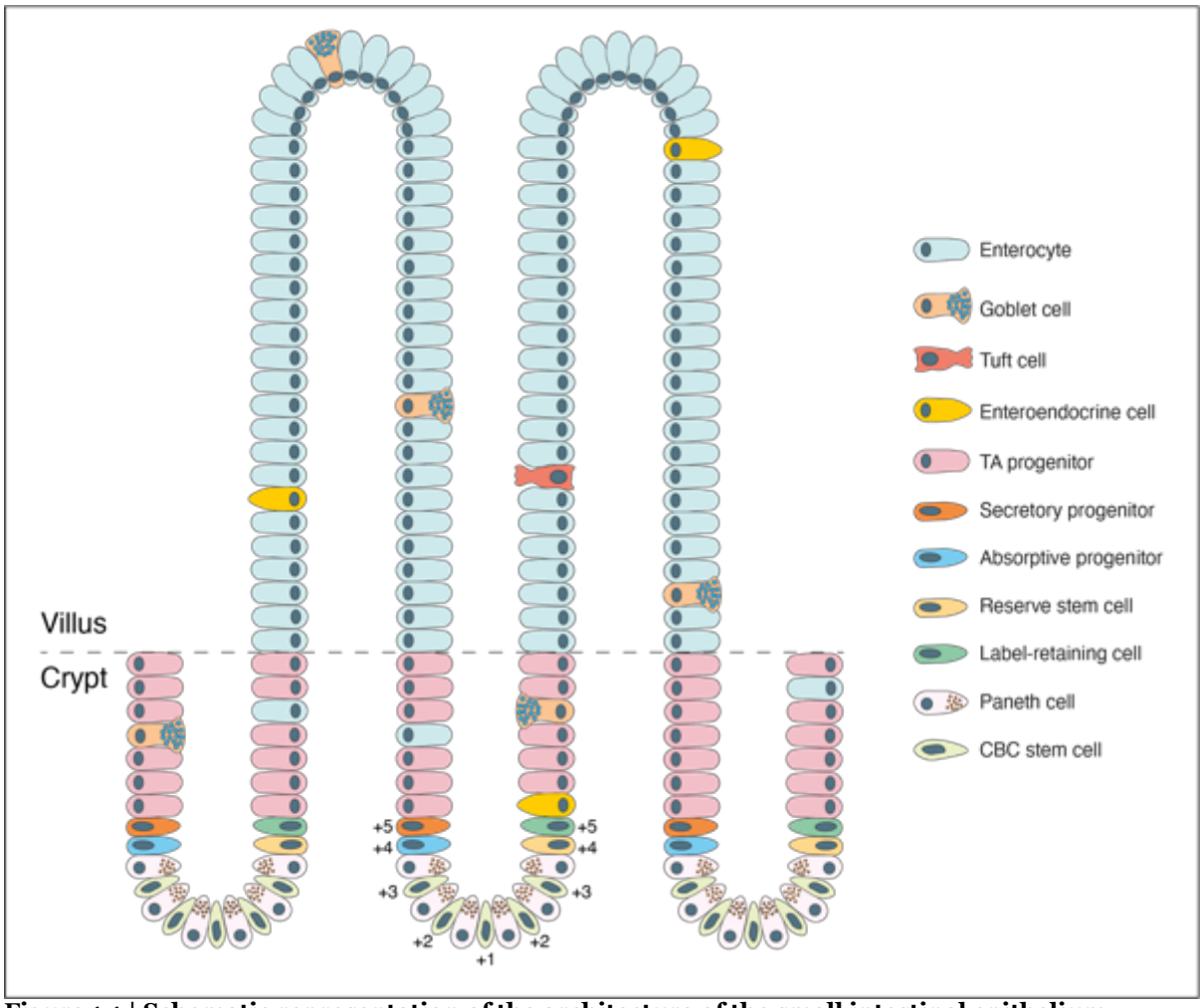

Figure 1.1 | Schematic representation of the architecture of the small intestinal epithelium. Lgr5-positive CBC stem cells reside at the bottom of the crypt and actively proliferating to give rise to all differentiated populations all serving different functions to maintain homeostasis. The +4/+5 positions represent a highly diverse and dynamic population of reserve stem cells and secretory/absorptive progenitors.

1.1.2 Intestinal stem cells

As mentioned in section 1.1.1, a decades-long scavenger hunt-like search of the bona fide ISC led to the identification of two distinct stem cell populations, both carrying characteristics of stem cell identity but residing at different physical positions within the intestinal crypt: 1) the actively proliferating crypt base columnar (CBC) cells and 2) the slow cycling +4 cells (figure 1.1). CBC cells are slender cells that are interspersed between Paneth cells that occupy positions 1-3 from the base of the crypt, while +4 cells reside right above CBCs at position 4 (Cheng and Leblond, 1974, Potten, 1977, Potten et al., 1978, Potten et al., 1974).

The landmark study from Barker et al. in 2007, led to the identification of leucine-rich-repeat-containing G-protein-coupled receptor 5 (*Lgr5*) as the bona fide

marker of ISCs (Barker et al., 2007). Lgr5 is exclusively expressed at CBCs and lineage tracing experiments showed that these Lgr5-positive cells are actively cycling to maintain homeostasis by fine-tuning of proliferation and differentiation and are able to generate all distinct differentiated cell types in the villus (Barker et al., 2007, Snippert et al., 2010). Subsequently, many more transcriptomic and proteomic analyses reported additional markers that are either exclusively expressed at Lgr5-positive CBCs, such as Olfactomedin 4 (*Olfm4*) and SPARC-related modular calcium-binding 2 (*Smoc2*), or show an enrichment at the CBCs compared to their progeny, such as Achaete-Scute homologue 2 (*Ascl2*), SRY-Box containing transcription factor 9 (*Sox9*) and Axis inhibition 2 (*Axin2*) (Munoz et al., 2012, Van der Flier et al., 2007). Interestingly, it has been showed that Lgr5-positive cells exhibit higher telomerase activity compared to their immediate progeny (Schepers et al., 2011). This higher activity is a mechanism to prevent telomere shortening and DNA damage caused by the fast and continuous cycling property of ISCs. Previous studies showed that every intestinal crypt has ~15 stem cells at any time and this number remains constant due to neutral competition of stem cells for niche space, while Paneth cells appear to be the key determinant of the available space (Cheng et al., 1969, Snippert et al., 2010). Of note, single Lgr5-positive cells have the ability to generate long-term *ex vivo* stromal-free 3D intestinal organoid cultures under supplementation of several growth factors that recapitulate the stem cell niche (Sato et al., 2011a, Sato et al., 2009).

On the other side, +4 cells were initially identified from label-retaining studies that showed long-term incorporation and retention of tritiated thymidine (^{3}HTdR), indicating that ISCs are slow-cycling or quiescent (Potten, 1977, Potten et al., 1978, Potten et al., 1974). More recent studies focusing on identification of molecular markers of the +4 position have identified cells that rarely divide to sustain genome integrity, yet they are capable of generating all intestinal lineages. These markers include polycomb complex protein BMI_1 (*Bmi1*) (Sangiorgi and Capecchi, 2008), homeodomain-only protein (*Hopx*) (Takeda et al., 2011), mouse telomerase reverse transcriptase (*mTert*) (Montgomery et al., 2011) and leucine-rich repeats and immunoglobulin-like domains 1 (*Lrig1*) (Powell et al., 2012, Wong et al., 2012). However, extensive expression analyses at single-cell level demonstrated that these markers are not exclusively expressed at the +4 cells but are also detected at Lgr5-positive CBCs (Itzkovitz et al., 2011, Munoz et al., 2012). In another landmark study, Buczaki et al shed more light into the true identity of the +4 label-retaining cells

(LRCs). These cells are Lgr5-positive that do not contribute to tissue renewal during homeostasis. Instead, they resemble precursors of Paneth and enteroendocrine secretory cells (Buczacki et al., 2013). These findings were later confirmed by an independent study, showing that a small fraction of Lgr5-low cells located mainly at the +4 position is not cycling (Basak et al., 2014).

These recent advances in ISC biology have helped the formation of a broadly accepted and plastic model of stem cell identity in the intestinal crypt. Lgr5-positive active cycling stem cells reside at the bottom of the crypt and are capable of differentiating into all differentiated cell lineages under normal homeostasis. On the other hand, the +4 position cells contain a more heterogeneous population that includes quiescent or reserve stem cells, LRC precursors of Paneth and enteroendocrine cells, as well as absorptive and secretory progenitors that are rapidly proliferating before terminal differentiation. Most of these +4 cells can acquire Lgr5-positive identity upon injury. However, what differentiates the true ISCs to their progeny is not only restricted to their multipotency and self-renewal ability, but also extends to their cell cycle properties, physical position within the crypt and distinct metabolic (high mitochondrial respiration) and epigenetic (increased chromatin accessibility of stem cell genes) signatures (Baulies et al., 2020b).

Although Lgr5-positive cells are widely accepted as the bona fide ISCs of the adult intestinal epithelium, it was only until recently that the true origin of these cells was identified. Lgr5-positive cells first emerge at embryonic stages E13.5 with a stronger expression at the posterior end of the premature intestine (Nigmatullina et al., 2017). However, embryonic and adult Lgr5-positive cells have a remarkably different transcriptional and epigenetic signature (Kazakevych et al., 2017). By combining lineage tracing and biophysical approaches, Guiu et al showed that all cells of the fetal mouse epithelium at E16.5 can contribute to the adult Lgr5-positive stem cell pool, independently of their position and Lgr5 status. This unexpected event is caused by a continuous remodelling and fission events that can physically bring non-diving Lgr5-negative cells back to the proliferative fetal intervillus regions leading them to re-acquire an Lgr5-positive identity (Guiu et al., 2019). This result is of great importance in stem cell biology and indicates that stemness is induced by external cues rather than hard-wired, which can justify the remarkable capability of the small intestinal epithelium to self-renew and respond to damage.

1.1.3 Paneth cells

Paneth cells are highly specialised antimicrobial peptide-secreting cells of the intestinal epithelium. Unlike other differentiated cells, Paneth cells are big granular cells which move downwards to the crypt base residing among ISCs. Interestingly, Paneth cells do not renew as frequent as other epithelial cell type. Instead of the usual turnover at around 5 days, PCs remain at the crypt base for approximately 14 days (Bjerknes and Cheng, 2005, Ireland et al., 2005). They serve as a critical epithelial niche for CBCs by secreting Wnt3A, Notch ligands, transforming growth factor -α (Tgf-α) and epidermal growth factor (EGF) to support ISC proliferation (Sato et al., 2011b). This is evident by a study showing that co-culture of Lgr5-positive stem cells with Paneth cells greatly improves the organoid formation capabilities (Sato et al., 2011b). However, several independent studies have demonstrated that epithelial-specific ablation of Paneth cells did not impair Lgr5-positive stem cell population, suggesting that the role of Paneth cells as ISC niche *in vivo* is dispensable (Durand et al., 2012, Garabedian et al., 1997, Kim et al., 2012). Importantly, Paneth cells are absent from colonic crypts where cKit-positive/CD24-positive goblet cells seem to reside next to Lgr5-positive stem cells and support their function (Rothenberg et al., 2012). Moreover, regenerating islet-derived family member 4 (*Reg4*) -positive deep crypt secretory cells that are intermingled with Lgr5-positive colonic stem cells have also been reported to be function as Paneth cell-equivalent functioning as epithelial niche (Sasaki et al., 2016).

Differentiation of Paneth cells requires a downregulation of Notch signalling and is promoted by secretory-lineage Atonal BHLH Transcription Factor 1 (Atoh1), while epithelial-specific deletion of Atoh1 leads to complete abrogation of Paneth cells (figure 1.2) (Kim et al., 2012). Most importantly though, Wnt signalling is absolutely necessary for the formation and maturation of Paneth cells in both embryonic and adult intestine through the Wnt - Rspondin1 (Rspo1) - Lgr4/5 axis (Farin et al., 2012, van Es et al., 2005) (discussed in detail in section 1.2).

Apart from their role as stem cell niche during homeostasis, Paneth cells are important defence gatekeepers protecting the epithelium by secreting granules in response to microbial ligands and acetylcholine agonists (Clevers and Bevins, 2013). These granules contain antimicrobial peptides that mainly include α-defensins and immune modulators that not only protect from enteric pathogens, but also help

establishing the microbiota composition (Clevers and Bevins, 2013). Importantly, germ-free housed mice show a high expression of α-defensins, indicating that their presence in Paneth cells is not triggered by bacterial exposure, but rather as part of their intrinsic transcriptional programme (Breault et al., 2008, Roberts et al., 1995). On the other hand, other antimicrobial peptides are secreted by Paneth cells as a response mechanism to pathogens (Kim et al., 2012, Sangiorgi and Capecchi, 2008).

The diverse role of Paneth cells functioning as the stem cell niche and protecting from pathogens highlights their functional significance in both homeostatic and non-homeostatic conditions. Conversely, expression of several susceptibility genes related to inflammatory bowel disease (IBD) and mis-regulation of secretion of antimicrobial peptides by Paneth cells has placed them as key modulators of intestinal disease (Elphick and Mahida, 2005, Wehkamp and Stange, 2020, Yang and Shen, 2021).

1.1.4 Enterocytes

Enterocytes are the most abundant cell type of the intestinal epithelium that account for more than 80% all small intestinal epithelial cells (Cheng and Leblond, 1974). Like every villus epithelial cell, enterocytes exhibit microvilli structures that increase apical membrane surface area and facilitate more efficient absorption. These structures consist of a membrane protrusion that is supported by actin filaments and cross-linking proteins Villin, Espin and Fimbrin, and form a continuous brush border (Maury et al., 1995, McConnell et al., 2009, Mooseker, 1985).

Differentiation towards the absorptive enterocytes requires active Notch signalling at the early progenitor cells and it's driven by Mtg8 and Mtg16 to supress Atoh1 expression (figure 1.2) (Baulies et al., 2020a). Most importantly, downregulation of Wnt is a key step in enterocyte differentiation (Yin et al., 2014) (more details in section 1.2). Recent studies have demonstrated a key role of hepatocyte nuclear factor 4A and 4G (Hnf4a and Hnf4g) in enterocyte differentiation, since simultaneous loss of these transcription factors greatly impairs enterocyte numbers at the intestinal villus (Chen et al., 2019, Lindeboom et al., 2018).

The small intestinal epithelium facilitates the absorption and transport of macromolecules through two distinct mechanisms: transcellular transport via enterocytes and paracellular transport via adjacent epithelial cells. Enterocytes

facilitate absorption mainly via endocytosis (Karasov, 2017, Snoeck et al., 2005). To facilitate absorption, enterocytes express a high variety of transporters which include apolipoproteins to transport lipids, solute carrier family 7 (Slc7) to transport amino acids, Slc2 to transport carbohydrates and Slc15 to transport peptides (Karasov, 2017, Moor et al., 2018).

Enterocytes are highly specialised cells that execute not only the bulk of nutrient absorption, but also express antimicrobial and immunomodulatory programmes. To achieve that, after the lineage decision enterocytes continue to trans-differentiate as they move along the villus to facilitate different functions based on nutrient availability and other environmental cues (Moor et al., 2018). In other words, enterocytes upregulate the baseline expression of specific genes at different zones of the crypt/villus axis to execute diverse functions (Moor et al., 2018). This unravels an unexpected cellular plasticity, where committed enterocytes can modulate their gene expression programme to maintain homeostasis. A recent study suggested that zonation of enterocytes is largely co-ordinated by Lgr5-positive telocytes at the villus tip (Bahar Halpern et al., 2020). More recently, another study showed that Bmp signalling promotes the transdifferentiation of enterocytes (Beumer et al., 2022) (to be discussed in detail in section 1.2.5). Whether exogenous stimuli is the only determinants of enterocyte transdifferentiation, or an internal clock also exists to tightly regulate this process is yet to be examined.

1.1.5 Goblet cells

Goblet cells are the most abundant secretory cells of the small intestinal epithelium that consist about 8% of the total epithelial cells (Pelaseyed et al., 2014). They secrete mucus as an essential preventive mechanism against pathogen invasion and intestinal inflammation and contribute to the barrier function alongside with enterocytes (Yang and Yu, 2021). Mucin 2 (Muc2) is the major component of the small intestinal mucus and form large polymers along with other mucus components such as Zymogen granule protein 16 (Zg16), Anterior gradient protein 2 homolog (Agr2) and Trefoil factor 3 (Tff3) (Birchenough et al., 2015, Nowarski et al., 2015). Moreover, goblet cells have an immunomodulatory role by obtaining antigens from the lumen and present them to underlying dendritic cells (McDole et al., 2012).

Goblet cell differentiation requires inactive Notch signalling and is controlled by Atoh1, which, in turn, upregulates the SAM pointed domain containing ETS transcription factor (Spdef) that drives differentiation of goblet cells (figure 1.2) (Lo et al., 2017). Notably, Atoh1 expression remains high in mature villus goblet cells and intestinal-specific loss of Atoh1 leads to complete loss of goblet cells (Gracz et al., 2018). Moreover, inactivation of Wnt in common goblet and Paneth cell progenitor cells favours formation of goblet cells (Yin et al., 2014). Mitogen-activated protein kinase (MAPK) signalling is a third molecular pathway involved in goblet cell formation and its genetic inactivation in the gut leads to reduced goblet cell numbers (Heuberger et al., 2014). Krüppel-like factor 4 (Klf4) is another essential transcription factor for goblet cell differentiation and its genetic deletion leads to an almost complete elimination of goblet cells (up to 90%) (Katz et al., 2002).

Similar to enterocytes, a recent study showed that goblet cells also have a spatial zonation across the crypt villus axis with distinct expression of their ligands, receptors and transcription factors as well as the secreted mucus (Manco et al., 2021). Of note, the immunomodulatory programme of goblet cells shows an enrichment at the villus tip, possibly to facilitate their communication with luminal antigens. Whether goblet cells transdifferentiate as they move up the villi or whether they simply acquire their final identity at specific locations is yet to be determined.

1.1.6 Enteroendocrine cells

The small and large intestines are the biggest endocrine organs of the human body. Enteroendocrine cells are a rare population of the intestinal epithelium that consist less than 1% of the total epithelial cells and secrete more than 20 different hormones (Gehart and Clevers, 2019). Despite their limited presence, enteroendocrine cells are key mediators of metabolism and appetite control. A recent study showed that enteroendocrine cells can be divided into 8 distinct sub-lineages based on their hormone production: N cells (Neurotensin, *Nts*), D cells (Somatostatin, *Sst*), K cells (Gastric inhibitory peptide, *Gip*), S cells (Secretin, Sec), X cells (Ghrelin, *Ghrl*), I cells (Cholecystokinin, *Cck*), L cells (Glucagon-like peptide 1, *Glp1*) and enterochromaffin cells (Serotonin, *5-HT*) (Gehart et al., 2019). Interestingly, it has been reported that several enteroendocrine lineages can transdifferentiate into other lineages. Several of these hormones appear to have a gradient of expression with

enrichment either at the crypt (*Glp1*, *Tac1*) or at the villus tip (*Nts*, *Sec*) in a Bmp-dependent way. Of note, hormones like serotonin and somatostatin are uniformly produced at the intestinal epithelium (Beumer et al., 2018).

Reduced Wnt and Notch signalling is essential for early progenitors to acquire enteroendocrine identity which are derived from LRCs at the +4 position (figure 1.2) (Buczacki et al., 2013, Wang et al., 2007). Expression of Neurogenin 3 (Neurog3) at LRCs is driving their differentiation towards the enteroendocrine lineage over Paneth cell. Neurog3 is the master regulator of enteroendocrine cells and its genetic ablation in the gut leads to total loss of enteroendocrine cells (Jenny et al., 2002, Lopez-Diaz et al., 2007). Growth factor independent 1 (Gfi1) promotes goblet and Paneth cell formation by directly suppressing Neurog3-mediated differentiation of enteroendocrine cells, adding an extra layer of secretory lineage specification (Bjerknes and Cheng, 2010, Shroyer et al., 2005). Recent studies have greatly advanced our understanding in the dynamic regulation of this diverse cell type by demonstrating a spatiotemporal dynamic expression of these cells at single cell resolution (Gehart et al., 2019, Haber et al., 2017, Manco et al., 2021, Yan et al., 2017a). Using a slow-decaying Neurog3 reporter, Gehart et al showed that all sub-lineages exhibit a clear temporal hierarchy where expression of each lineage is tightly controlled by a specific and distinct transcriptional signal (Gehart et al., 2019). Moreover, Enterochromaffin and L cells revealed a time-dependent hormonal plasticity. A subsequent study further dived into the spatial resolution of enteroendocrine cell migration over time and confirmed that although some hormones have a time-regulated expression mediated by Neurog3 expression, cells secreting these hormones can be physically residing at various positions of the crypt-villus axis (Manco et al., 2021). For example, somatostatin-expressing D-cells have a late time stamp and, yet their expression is restricted at the crypt and intervillus junction.

1.1.7 Tuft cells

Tuft cells are another very rare population of chemosensory cells (~0.4% of the total epithelium) which are present throughout the digestive and respiratory systems. Since their initial discovery and until recently, little was known about their exact function. However, recent studies have started unravelling their role in the gut

epithelium (Sato, 2007). Tufts cells have a very unique structure where they appear to have a brush border on their apical side and a swelling of the nucleus (Gerbe et al., 2012). They act as sentinels for infectious organisms such as Helminths, noroviruses and bacterial microbiota, as well as taste-chemosensory cells (Gerbe et al., 2012, Sato, 2007, Sbarbati and Osculati, 2005, Wilen et al., 2018). They are involved in immune function in a process known as "weep and sweep" where they form part of the host defence against infection by regulating the intestinal type 2 innate lymphoid cell (ILC2)-epithelial response, leading to secretion of the cytokine Interleukin 25 (Il25) (Gerbe et al., 2016, Nadjsombati et al., 2018, von Moltke et al., 2016). Tuft cells express the marker doublecortin-like kinase 1 (*Dclk1*) that was previously associated with expression at quiescent stem cells at the +4 position (Long et al., 2021).

Differentiation of Tuft lineage is not fully dependent on Notch and Atoh1. Tuft cells arise from Atoh1-positive progenitors and an initial study showed that loss of Arid3a leads to reduced Tuft cells (Gerbe et al., 2011). Importantly, loss of other secretory lineage-specific transcription factors (such as Neurog3, Spdef and Gfi1) does not affect Tuft cells (Gerbe et al., 2011, Herring et al., 2018). Instead, it has been previously shown that tuft cell differentiation is mainly dependent of the transcription factor Pou class 2 homeobox 3 (Pou2f3) during homeostasis whilst loss of Pou2f3 eliminates Tuft cells. Pouf2f3 expression is regulated by two distinct pathways: one downstream of interleukin 13 (Il-13) (figure 1.2) and one downstream of the DEAD box containing RNA binding protein (Ddx5) that drives Rho GTPase Cell Division Cycle 42 (CDC42) expression to stimulate Tuft cell hyperplasia (Gerbe et al., 2016, Long et al., 2021). Another study demonstrated that SRY-box transcription factor 4 (Sox4) regulates tuft and enteroendocrine cells in an Atoh1-independent manner (Gracz et al., 2018). Recent advances in single cell transcriptomics have helped better understanding of Tuft cell specification and differentiation. There are now two confirmed Tuft sub-populations, termed "Tuft1" and "Tuft2" with distinct functions (Haber et al., 2017). Tuft1 cells have a neuronal-like transcription programme, while Tuft2 have enrichment of immunomodulatory programme. Similar to enterocytes and goblet cells, expression of tuft cell-related markers shows a broad zonation from the crypt to the villus tip (Manco et al., 2021). Interestingly, Tuft1 markers are enriched at the villus bottom, while Tuft2 cells are enriched towards the mid-villus and villus tip.

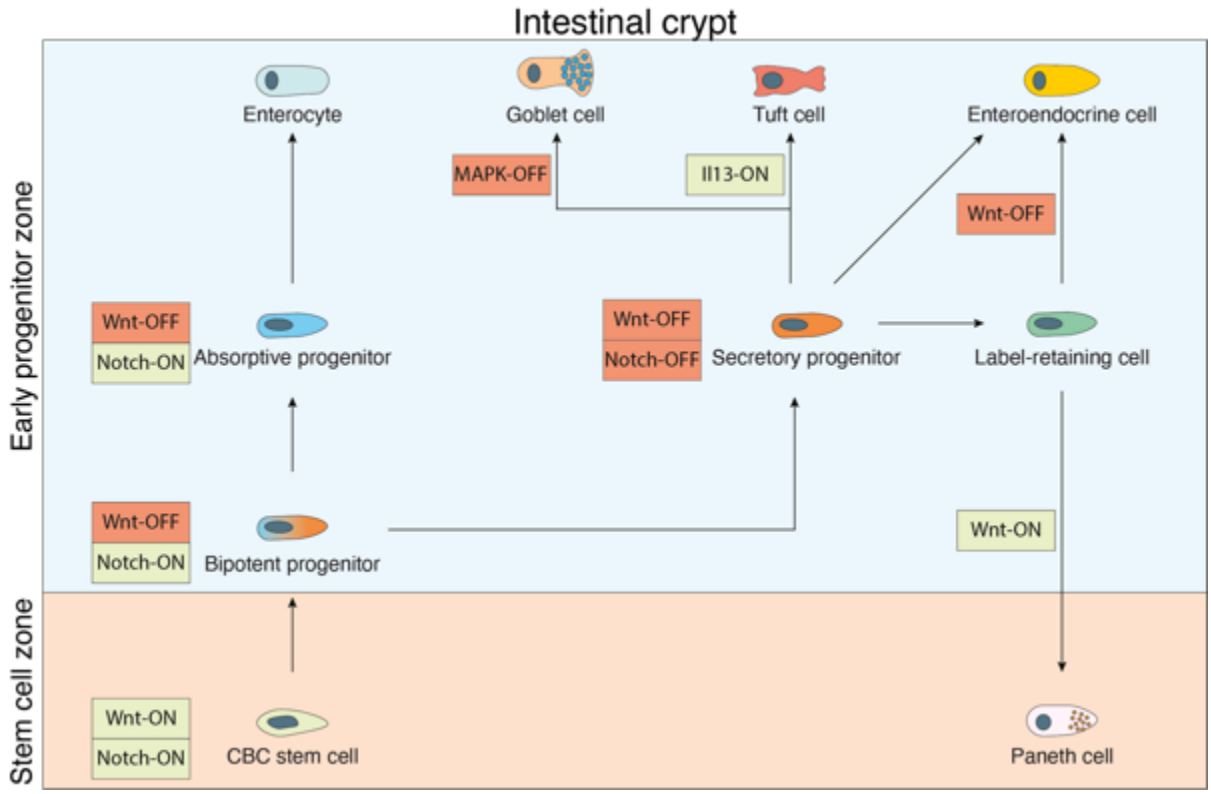

Figure 1.2 | Wnt and Notch signalling regulate the lineage decision at the early progenitor zone. Active Wnt and Notch are both required for maintenance of Lgr5-positive CBC stem cells at the bottom of the crypt. Upon Wnt downregulation Notch acts as a switch at the +4/+5 positions to determine lineage decision. "Notch-ON" drives absorptive differentiation, while transient "Notch-OFF" leads bipotent progenitors to acquire a secretory fate. Upon initial absorptive vs secretory decision, Wnt and Notch continue to regulate the final differentiation and maturation of secretory cells in combination with other pathways (e.g., MAPK for goblet cell specification). Tuft cells are the only secretory cells that their terminal differentiation is Notch-independent.

1.2 Signalling in gut homeostasis

The proliferation and differentiation of ISCs is tightly regulated by a combination of signalling cascades which act collectively to ensure small intestinal homeostasis (figure 1.3). Dysregulation of these pathways is associated with cancer and other gastrointestinal diseases. Signalling cues from the developmentally conserved Wnt, Notch, Egf, Bmp, Eph/Ephrin, Hedgehog and Hippo pathways are all involved in this process, highlighting the complexity of homeostatic mechanisms required to support a diverse set of functions from many short-lived differentiated cell types. Of note, the same signalling cascades play a central role not only in adult tissue homeostasis, but also during early development and damage-induced epithelial regeneration. Moreover, the combined epithelial and mesenchymal origin of these signals highlights the importance of the underlying molecular inputs from all different cell types in epithelial cell turnover.

In sections 1.2.1 – 1.2.7, the molecular basis of each one of these pathways as well as their contribution in stem cell self-renewal or differentiation will be discussed in detail.

1.2.1 Wnt signalling

Wnt (Wingless-related integration site) signalling is a highly conserved pathway that is linked to proliferation from early development throughout adulthood. It can be further divided to canonical (β-catenin dependent) and non-canonical (β-catenin independent) Wnt pathways, the former plays a key role in ISC maintenance (Clevers and Nusse, 2012). In the gut, Wnt drives proliferation in early developmental stages and villus morphogenesis at E15.5 in mice (Chin et al., 2016). Canonical Wnt pathway provides the most influential signals to regulate proliferation and differentiation of Lgr5-positive ISCs, while its aberrant activation is the most frequent event in the initiation of colorectal and other gastrointestinal cancers (Nusse and Clevers, 2017).

In mammals, there are 19 different Wnt ligands that have unique and overlapping functions. Wnt proteins are relatively small in size (40 kDa), and they are rich in cysteines. Before their secretion, Wnt ligands undergo post-translational modifications at the endoplasmic reticulum, a process mediated by Porcupine (Rios-Esteves and Resh, 2013). The modification includes attachment of glycoproteins and lipids to the Wnt ligands (Takada et al., 2006, Willert et al., 2003). After Wnt becomes lipid bound, Wntless/Evi (Wls) regulates its exit from the Golgi apparatus and its translocation to the plasma membrane (Nusse and Clevers, 2017).

Wnt ligands bind to Frizzled (Fzd) receptors of the signal-receiving cells. Fzd proteins are seven-pass transmembrane receptors that carry an extracellular N-terminal cysteine-rich domain (CRD) where Wnt ligands bind (Bhanot et al., 1996). In the absence of Wnt signals, β-catenin, the key downstream effector of the canonical Wnt signalling, is phosphorylated by its destruction complex. The destruction complex consists of Axin, Adenomatous polyposis coli (Apc), glycogen synthase kinase 3 (Gsk3), casein kinase 1 (Ck1), protein phosphatase 2a (Pp2a) and E3-ubiquitin ligase β-TrCP (Koch, 2017). B-catenin is not only phosphorylated by the destruction complex but it is also ubiquitinated by β-TrCP and targeted for proteasomal degradation (Aberle et al., 1997, Liu et al., 2002). In the nucleus, the transcriptional repressor

Groucho binds to the transcription factor (Tcf)/ lymphoid enhancer-binding factor (Lef) complex and blocks transcription of Wnt targets (Cavallo et al., 1998). Upon Wnt binding, Fzd receptors dimerise with the single transmembrane receptors low-density lipoprotein-related protein 5/6 (Lrp5/6). Dishevelled (Dvl) facilitates the interaction of Lrp with Axin and, as a consequence, β-catenin ubiquitination and degradation is inhibited, leading to saturation of the destruction complex (Li et al., 2012b). This results in accumulation of newly synthesised β-catenin in the cytosol and subsequent translocation to the nucleus where it displaces Groucho, binds to the Tcf / Lef complex, and drives Wnt targets transcription (Molenaar et al., 1996).

Under normal homeostatic conditions in the adult intestine, Wnt forms an expression gradient radiating from the crypt bottom to the crypt/villus junction (Clevers, 2013, Farin et al., 2016). Wnt ligands can be secreted by both stromal (Wnt 2b/4/5a/5b) and epithelial cells (Wnt 3/6/9b). Stromal Wnts are produced by Foxl1+ telocytes as well as Gli1+ and CD34+/GP38+/αSMA- sub-epithelial mesenchymal cells (Aoki et al., 2016, Degirmenci et al., 2018, Stzepourginski et al., 2017). As mentioned before, Paneth cells secrete short-range epithelial Wnt3 at the bottom of the crypt that is crucial for the formation of the Wnt gradient to drive ISC proliferation (Farin et al., 2016, Gregorieff et al., 2005, Kabiri et al., 2014). Of note, a mouse intestinal organoid-based study showed that expression of Wnt3a from Paneth cells is coupled to the circadian clock and cell cycle that utilises Cyclin D1 (Ccnd1) to drive proliferation (Matsu-Ura et al., 2016). Stromal-derived Wnts are essential for stem cell homeostasis since their depletion leads to loss of intestinal crypts (Valenta et al., 2016). On the other hand, loss of epithelial Wnt3 does not affect the proliferative status of intestinal crypts, although its presence is essential for maintenance of organoid cultures lacking stromal-derived Wnt signals (Farin et al., 2012).

Wnt signalling can also be enhanced by the Rspondin (Rspo) agonists. Rspo family has four different members which bind to another category of seven-pass transmembrane receptors, the Leucine-rich repeat-containing G-protein coupled receptors 4/5/6 (Lgr4/5/6) which, in turn, bind to the single transmembrane molecules Ring Finger Protein 43 (Rnf43) and Zinc and Ring Finger 3 (Znrf3). In the absence of Rspo, Rnf43/Znrf3 bind to Fzd receptors limiting their availability. Rspo enhances Wnt signalling by occupying Rnf43/Znrf3 and increasing the availability of Fzd receptors to be bound by the Wnt molecules (de Lau et al., 2011, Hao et al., 2012). Of note, Lgr receptors as well as Rnf43 and Znrf3 are not only essential components

of the Wnt signalling but are also Wnt transcriptional target genes signifying one of the many negative feedback loop mechanisms of the Wnt pathway (Nusse and Clevers, 2017). Rspo2 and Rspo3 are the two most important members of the family in the gut to modulate Wnt signal and maintain Lgr5-positive ISCs (de Lau et al., 2014, Storm et al., 2016). Rspo3 ligands are secreted by the Platelet-derived growth factor receptor alpha (Pdgfrα)-positive pericryptal stromal cells (Greicius et al., 2018). Of note, it has been recently shown that Rspo is the key driver of ISC self-renewal, whereas Wnt is important for establishment of the Lgr/Rspo/Rnf43 axis by regulating transcriptional expression of Lgr and Rnf43, (Yan et al., 2017b).

1.2.2 Notch signalling

Notch signalling requires direct contact between the membranes of two neighbouring cells to promote signal transduction. The signal-sending cell expresses type I transmembrane ligands of the Delta/Serrate/Lag-2 family (DSL), while the signal-receiving cell expresses Notch receptors that are also a type I transmembrane protein. In mammals, there are 5 different ligands (Delta-like 1/2/3 and Serrate-like 1/2) (Dll1/2/3 and Jagged1/2) and 4 Notch receptors (Notch 1/2/3/4) (Artavanis-Tsakonas et al., 1999, Carulli et al., 2015). Upon ligand-receptor binding two main events occur. First, a proteolytic cleavage of an extracellular juxtamembrane site by a member of the a-disintegrin-and-metalloprotease (ADAM) family. Secondly, a cleavage step of the transmembrane facilitated by γ-secretase leads to the release of the Notch Intracellular Domain (NICD) to the cytoplasm and subsequent re-localisation to the nucleus. In the nucleus, NICD binds to the transcription factor Recombination Signal Binding Protein for Immunoglobulin Kappa J Region (Rbpj) that recruits other transcriptional co-activators and results in transcription of Notch target genes such at the members of the Hairy and enhancer of split (Hes) family.

Paneth cells at the crypt bottom express Dll1 and Dll4 ligands to amplify Notch signalling at the crypt bottom and generate a signalling gradient similar to that of Wnt (Shroyer et al., 2007, Stamataki et al., 2011, van Es et al., 2005). Notch activation promotes proliferation and maintenance of Lgr5-positive ISCs in the crypts. Olfm4 is a transcriptional target downstream of Notch and has been validated as an ISC-specific marker with similar expression pattern as Lgr5 (van der Flier et al., 2009). A series of elegant experiments have proved the indispensable role of Notch in stem cell

maintenance. Deletion of Notch1 and Notch2 leads to stem cell loss, while Notch1 activation increases stem cell proliferative capacity (Carulli et al., 2015, Fre et al., 2011). Similarly, loss of Dll or Hes genes leads to loss of crypt proliferation (Pellegrinet et al., 2011, Ueo et al., 2012).

Apart from ISC maintenance, Notch plays another crucial role in binary cell fate decision at the +4/+5 cell positions to maintain ratios between absorptive and secretory lineages via a mechanism termed "lateral inhibition" (Sancho et al., 2015). According to it, transient Notch inactivation at the progenitor cells leads to downregulation of the transcriptional suppressor Hes1 and subsequent de-repression of its target gene Atoh1. Atoh1 is the master regulator of secretory lineage, and its activation promotes expression of Dll1/4 at Atoh1-expressing cells. Presentation of Dll1/4 at these cells, activates Notch at the immediate adjacent cells, supresses Atoh1 and drives differentiation towards the enterocyte lineage (Kim et al., 2014, Lo et al., 2017). This mechanism translates the binary fate decision into an "Notch-ON" and "Notch-OFF" state (Gehart and Clevers, 2019). Genetic or pharmacological inhibition of Notch or overexpression of Atoh1 pushes differentiation towards the secretory lineage. In contrast, loss of Atoh1 leads to loss of all secretory cells. Importantly, Atoh1 also has a role in ISC proliferation. Loss of Atoh1 restores Hes1 expression in mice with intestinal-specific deletion of Rbpj (Kim and Shivdasani, 2011), while its upregulation upon γ-secretase inhibition leads to suppression of stem cell proliferation (van Es et al., 2010).

It is important to note that while Notch drives the initial fate decision at the +4/+5 positions, it is equally important for terminal differentiation of secretory fate within the TA zone. For example, stochastic Notch expression determines specification of bipotential goblet/enteroendocrine progenitors (Kay et al., 2017, Li et al., 2012a). It also acts synergistically with Wnt to determine the Paneth versus enteroendocrine cells of Lgr5-low LRCs at the +4 position (Beumer and Clevers, 2021, Buczacki et al., 2013).

1.2.3 Egf signalling

Epidermal growth factor (Egf) is a ligand that activates the signal-receiving cell via its binding to the epidermal growth factor receptor (Egfr) to promote proliferation and differentiation (Gehart and Clevers, 2019). Egfr has an intrinsic protein-tyrosine

kinase activity, and ligand-receptor binding causes its transition to an active homodimer state (Cohen et al., 1980). Tyrosine residues at the C-terminus of Egfr are auto-phosphorylated leading to activation of downstream effectors. These effectors include pro-survival and proliferation pathways such as MAPK, Janus kinase (JAK)-signal transducer and activator of transcription (STAT), phosphatidyl- inositol 3-kinase (PI3K)/Akt and c-Jun N-terminal kinases (JNK) (Spit et al., 2018).

Contrary to Wnt and Notch pathways, Egf does not form a signalling gradient in the small intestinal crypts and Egfr is expressed at both CBCs and TA cells (Yang et al., 2017). It is required to drive proliferation and maintain stem cells. Egf ligands as well as Tgf-α, which can also activate Egfr, are secreted by Paneth cells, although other unidentified mesenchymally-derived sources of Egf signals have been suggested (Farin et al., 2012, Sato et al., 2011b). This hypothesis is based on the fact that exogenous Egf supply is necessary for establishment of human and mouse intestinal organoid cultures (Sato et al., 2011a, Sato et al., 2009). However, its role in these cultures has been challenged by two recent independent studies. Joosten et al. showed that hepatocyte growth factor (Hgf) can substitute Egf function by promoting proliferation through its Mesenchymal-epithelial transition (Met) receptor and CD44 (Joosten et al., 2017). Subsequently, it was shown that replacement of Egf and p38 inhibitor by insulin-like growth factor 1 (Igf-1) and fibroblast growth factor 1 (Fgf-2) does not affect the proliferative capacity of human organoids, but, instead, drives differentiation more efficiently (Fujii et al., 2018). On the other hand, direct blockage of Egf signalling in organoids has been shown to induce Wnt-independent quiescence of Lgr5-positive ISCs and promotes differentiation towards enteroendocrine fate (Basak et al., 2017).

Tight regulation of Egf is necessary for controllable proliferation within the intestinal crypt. Mutations of the Kirsten rat sarcoma virus (KRAS) are central in the progression of colorectal cancer (Tan and Barker, 2015). In homeostasis, tight regulation of Egf signalling is controlled by Lrig1. Lrig1 induces expression of ErbB receptors that are negative regulators of the canonical Egfr receptors, whereas intestinal-specific deletion of Lrig leads to increased stem cell numbers and crypt size (Powell et al., 2012, Wong et al., 2012).

1.2.4 Eph/Ephrin signalling

Erythropoietin-producing human hepatocellular (Eph) receptors are another member of the tyrosine kinase in response to the binding of Eph-receptor interacting proteins (Ephrins). Interestingly, Eph and Ephrins can both induce downstream signalling on a bidirectional basis (Kania and Klein, 2016). For signal transduction, Eph and Ephrins form arrays with variable size which correlates to the signal strength (Kania and Klein, 2016). Eph/Ephrin signals exist in most adult stem cell niches that are linked to the regulation of cell positioning, adhesion and migration by modulating the organisation of actin cytoskeleton and affecting functionality of integrins (Genander and Frisen, 2010). Ligand-receptor binding leads to Eph auto-phosphorylation and activation of MAPK and Ras signalling cascades (Kalo and Pasquale, 1999).

In adult intestine, Eph/Ephrin signalling controls interaction between cells and regulates positioning along the crypt-villus axis. Eph and Ephrin form opposite gradients of expression, where EphB accumulates at the crypt bottom and EphrinB at the villus tip. This is controlled by Wnt signalling that induces expression of EphB2 and EphB3 at the bottom of the crypt and supresses expression of EphrinB1, which is activated at differentiating cells by Notch. ISCs express high levels of EphB2, while Paneth cells express EphB3. In fact, the high expression of EphB3 is required to drive Paneth cells to move against the cell flow of the intestinal epithelium and migrate to the crypt bottom (Batlle et al., 2005, Batlle et al., 2002, Koo et al., 2009, Solanas et al., 2011). In the absence of EphB3, Paneth cells are randomly positioned across the villus, underlying the importance of Eph/Ephrin signals in crypt compartmentalisation and niche formation (Batlle et al., 2002).

1.2.5 Tgf-β/Bmp signalling

Bone morphogenetic protein (Bmp) pathway is one of the branches of the Transforming growth factor -β (Tgf-β) superfamily of signalling cascades that have been linked to cell proliferation and differentiation, cell cycle arrest as well as organ development (Massague, 2012). Bmps are extracellular signalling cytokines that bind to Bmp type 1 and type 2 receptors (Bmpr1/2) that are transmembrane proteins and carry tyrosine kinase activity in their intracellular domain. As a result of Bmp binding

to these receptors, Bmpr2 trans-phosphorylates Bmpr1 which, in turn, phosphorylates R-Smads1/5/8 that are bound on the receptor. Smad1/5/8 are transcription factors and members of the Smad (mothers against decapentaplegic) family (Zhang and Que, 2020). In fact, different R-Smad proteins are associated with different branches of the Tgf-β signalling superfamily (Shroyer and Wong, 2007). Phosphorylated Smad1/5/8 first bind to the common core Smad4 (c-Smad) and subsequently translocate to the nucleus to drive expression of Bmp target genes (Zhang and Que, 2020).

In the adult small intestinal epithelium, Bmp forms a gradient of expression that is opposite to that of Wnt. Bmp expression is the highest at the villus tip and regulates differentiation at the post-mitotic villi. Bmps are secreted by mesenchymal cells across the villus and the formation of such a gradient is driven by the presence of Bmp antagonists Noggin and Gremlin1/2 at the pericryptal region (He et al., 2004, Kosinski et al., 2007). These antagonists directly suppress the Bmp-driven differentiation, and their importance has been demonstrated both *in vivo* and *in vitro*. On one hand, overexpression of Noggin or Gremlin1 at villi cells induces ectopic crypt formation (Davis et al., 2015, Haramis et al., 2004). On the other hand, Noggin is an indispensable component for the maintenance of intestinal organoid cultures and its withdrawal from the culture medium leads to exhaustion of the stem cell compartment (Sato et al., 2009). These findings indicate that Bmp inactivation is sufficient to define stemness and promote crypt compartmentalisation. Mechanistically, it has been recently shown that Bmp signalling directly supresses transcription of stem cell genes including Lgr5 by Smad4 via histone deacetylase 1 (Hdac1) recruitment (Qi et al., 2017).

As discussed in Chapter 1.1, enterocytes and goblet cells show a broad zonation of gene expression from the upper crypt to the villus tip. In a recent study, Beumer et al. showed that this switch of gene expression programme is facilitated by the Bmp gradient of the villus both *in vivo* and *ex vivo* (Beumer et al., 2022). Moreover, Bmp4 induces the hormone switch of enteroendocrine cells as they move upwards the villi. (Beumer et al., 2018). The data highlight the crucial role of Bmp in driving not only differentiation but also the spatial gene expression programme of various cell lineages.

Apart from adult tissue homeostasis, Bmp is also key to the establishment of the architecture of the fetal small intestinal epithelium. At E15.5, Bmps derived from the fetal mesenchyme directly supress Wnt signalling and restrict the presence of Lgr5-positive cells at the proliferative intervillus region (Shyer et al., 2015, Shyer et

al., 2013). The findings reveal a well-conserved role of Bmp on Wnt signalling from the establishment of the epithelial architecture in developing gut to the maintenance of adult homeostasis.

Compared to Bmp signalling that has been extensively studied on intestinal epithelial differentiation, the role of Tgf-β in intestinal homeostasis is less characterised (Meran et al., 2017). Tgf-β ligands are secreted by both epithelial and non-epithelial cells and bind to the type 1 and type 2 Tgf-β receptors (Tgfbr1/2) (Ihara et al., 2017). Tgf-β signalling acts in a similar manner to Bmp. Although both pathways act via nuclear translocation of a Smad4/R-Smad complex, Tgfbr1/2 receptors activate different R-Smads than Bmpr1/2, namely Smad2/3 (Massague, 2012). Tgf-β has been extensively characterised for its dysregulation in several gastrointestinal diseases, including colorectal cancer, inflammatory bowel disease and fibrosis (Stolfi et al., 2020). During homeostasis, Tgf-β has been shown to regulate barrier function by controlling expression of tight junction proteins, such as Claudin-1 (Howe et al., 2005). Most importantly, Tgf-β has also been established as a modulator of intestinal epithelial differentiation where treatment of intestinal epithelial cells with recombinant Tgf-β induces their differentiation (Liao et al., 2013). Of note, presence of a Tgf-β receptor inhibitor is necessary for the establishment and maintenance of human intestinal organoids (Sato et al., 2011a).

1.2.6 Hedgehog signalling

Hedgehog (Hh) signalling can be activated by binding of one of the hedgehog ligands to the twelve-pass transmembrane receptors Patched 1/2 (Ptch1/2). Although three different group of Hh ligands have been discovered, intestinal epithelial cells express only two of them: high levels of Indian hedgehog (Ihh) and lower levels of Sonic hedgehog (Shh) (Spit et al., 2018). Upon ligand binding, Ptch receptors release the seven-pass transmembrane protein Smoothened (Smo) that can activate the Glioblastoma family of transcription factors 1/2/3 (Gli1/2/3), which drive expression of target genes. In the absence of upstream Hh ligands, Smo activity is blocked by Ptch receptors resulting to a proteolytical cleavage of the C-terminus of Gli transcription factors. This truncated version of Gli proteins acts as a repressor to supress expression of Hh target genes (Madison et al., 2005, Stone et al., 1996, Taipale et al., 2002, Zacharias et al., 2011).

Under homeostatic conditions of the adult intestine, Hh ligands are secreted in a paracrine manner by TA cells and trigger activation of the pathway in surrounding stroma cells to increase of their proliferation. This results in production and subsequent secretion of Bmp ligands and suppression of stemness at the villus (Kosinski et al., 2010). Downregulation of Ihh leads to disruption of the mesenchymal architecture including deterioration of the extracellular matrix and reduces crypt myofibroblasts (Kosinski et al., 2010, Zacharias et al., 2011). On the other side, overactivation of Hh signalling results in an accumulation of mesenchymal cells (Zacharias et al., 2011), but that does not affect Wnt signalling or epithelial cell proliferation as it was initially proposed (van Dop et al., 2009)

Sub-epithelial Gli-positive myofibroblasts have been previously shown to act as a supportive source of Wnt ligands and are considered an essential niche component. Upon loss of Paneth cells-derived Wnt3, Hh signalling drives an increase in Gli-positive stromal cells helping the maintenance of homeostasis (Degirmenci et al., 2018, Valenta et al., 2016). In fetal intestine, Shh ligands secreted from epithelial cells drive the production of Bmps from the surrounding mesenchyme to supress Wnt (discussed in Chapter 1.2.5). This highlights the complex crosstalk of signalling pathways in regulating intestinal development and adult tissue homeostasis.

1.2.7 Hippo signalling

The Hippo pathway mainly relies on extracellular mechanical cues to activate its gene expression programme and its function is related to organ development, adult stem cell self-renewal and regeneration (Li and Clevers, 2013). However, increasing evidence has shown that inputs of Hippo pathway are not limited to mechanical forces but also include hormone signals, intracellular energy levels, actin cytoskeleton and cell-cell contact (Meng et al., 2016). When Hippo signalling is inactive, the transcriptional co-activators Yes-associated protein (Yap) and transcriptional co-activator with PDZ-binding motif (Taz) translocate to the nucleus and bind to TEA domain transcription factors 1-4 (Tead1-4) to activate gene transcription. Of note, Yap/Taz proteins do not have DNA-binding domains and their interaction with Tead proteins is crucial for downstream signalling (Meng et al., 2016). When Hippo is activated, Mammalian Ste20- like kinases 1/2 (Mst1/2) phosphorylate and activate Large tumour suppressor 1/2 (Lats1/2). These proteins also possess kinase activity to

phosphorylate Yap and Taz, leading to their retention in the cytoplasm and their gradual degradation (Li and Clevers, 2013, Meng et al., 2016).

In adult small intestinal epithelium, Hippo has a major role during intestinal regeneration and tumorigenesis (discussed in Chapter 1.3) but is dispensable in adult tissue homeostasis. However, recent findings have demonstrated that it is also involved in small intestinal homeostasis. Imajo et al used an artificial intestine-specific gene transfer to show that Yap and Taz influence the status of progenitor cells depending on their transcriptional partners: they utilise Tead proteins to stimulate their proliferation or they bind to Klf4 to drive their differentiation towards goblet cells (Imajo et al., 2015). Intestinal-specific loss of Yap/Taz does not alter crypt architecture and stem cell proliferation *in vivo*, but their continuous nuclear translocation upon Lats1/2 deletion leads to crypt hyperplasia and an increase of proliferative capacity of TA cells (Guillermin et al., 2021).

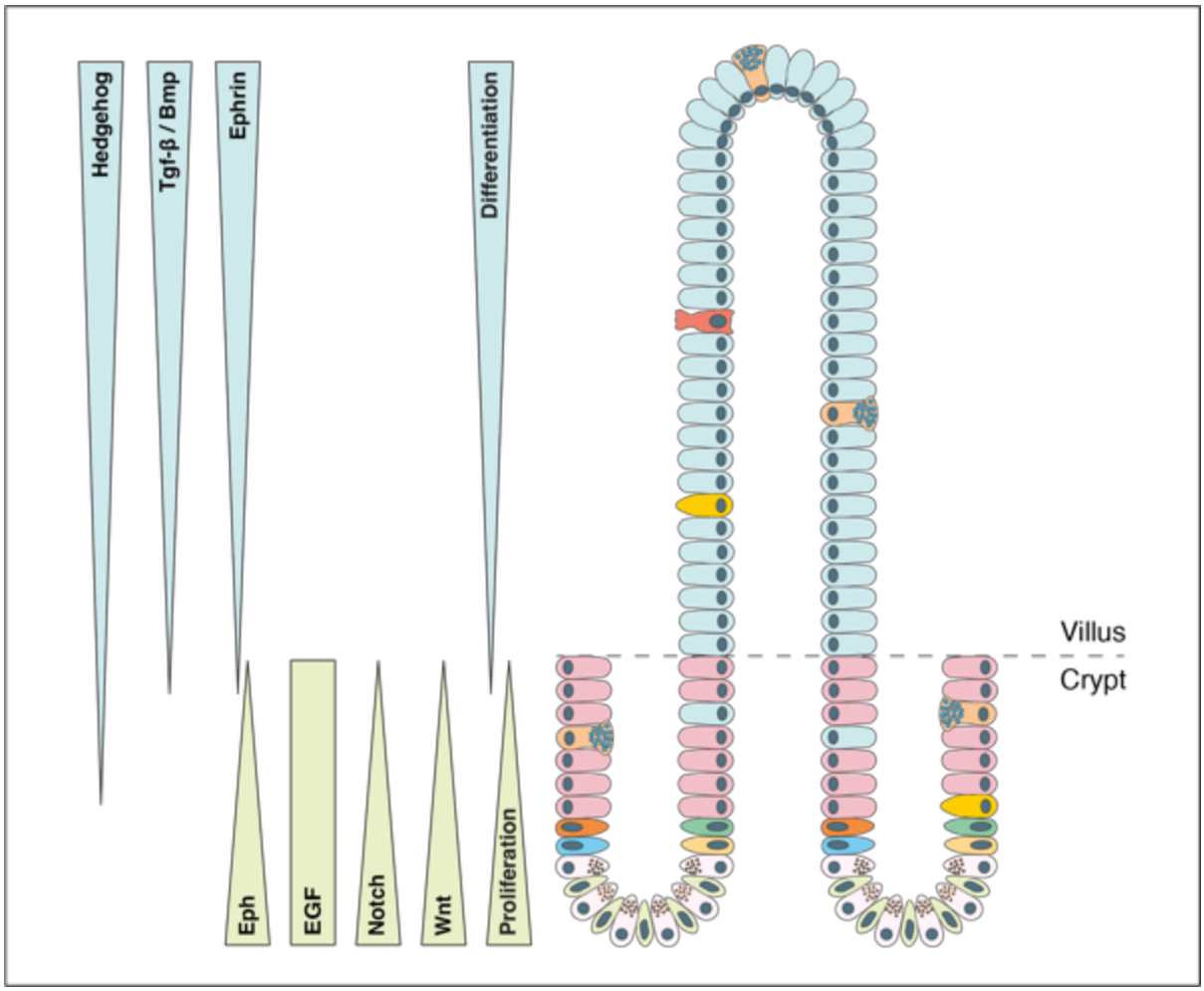

Figure 1.3 | Signalling pathways orchestrate intestinal epithelial homeostasis.
Various signalling cascades have been established to control the high cell turnover of the intestinal epithelium. Wnt, Notch and Egf are the main regulators of proliferation. Notch drives the initial lineage decision, while Tgf-β/Bmp and Hedgehog signal drive terminal differentiation at the villus.

1.3 Regeneration and plasticity

1.3.1 Injury and repair of the small intestinal epithelium

Homeostasis of the small intestinal epithelium is a highly dynamic process that relies on an equilibrium between cell death and replenishment of dead cells. This continuous cell turnover follows a linear way of cell migration from the crypt bottom (stem cell division and daughter cell generation) to the villus tip (cell shedding), with Paneth cells being the exception to this rule (discussed in detail in Chapters 1.1 and 1.2). Upon injury and disruption of the homeostatic mechanisms, epithelial cells that are located right above the ISC zone at the crypt bottom exhibit high cellular plasticity. They can de-differentiate and reacquire stem cell-like properties, migrate downwards to the ISC zone and replenish the damaged Lgr5-positive ISCs. Tissue damage can be caused by various events, including exposure to pathogenic organisms, inflammatory disease and or irradiation/chemotherapy-induced genotoxic stress (Meyer et al., 2022). Several *in vivo* mouse models as well as *ex vivo* organoid models have been developed over the past decades to re-capitulate tissue damage and study repair mechanisms. These include infection models using helminths or other parasites, delivery of a sub-lethal γ-irradiation dose, chemically induced colitis, administration of chemotherapy drugs that induce cell death as well as genetic ablation of Lgr5-positive ISCs (Baulies et al., 2020b, Beumer and Clevers, 2016).

Extensive research over the past few years has unravelled several key mechanisms of intestinal repair upon injury. These include dedifferentiation of several Lgr5-negative cell populations driven by several signalling cascades (see section 1.3.2 below). Of note, the key pathways involved in tissue homeostasis and diseases are often activated upon injury to drive regeneration by transiently altering their target gene expression. In particular, Wnt and Hippo-Yap/Taz signalling play the most pivotal role in regulating response to injury.

Wnt regulates regeneration through the transcription factor Ascl2. In homeostasis, *Ascl2* is a Wnt target gene exclusively expressed at CBCs and acts together with the β-catenin/Tcf complex to activate expression of stem cell genes (Schuijers et al., 2015). Upon injury, Ascl2 is crucial in cellular dedifferentiation of non-ISC crypt cells. Expression dynamics revealed that Ascl2 is expressed prior to Lgr5 in the progenitor cells to initiate dedifferentiation by upregulating Wnt.

Transcriptional analysis of dedifferentiating cells has showed that Ascl2 utilises Interleukin 11 receptor a1 (Il11ra1) to drive this process (Murata et al., 2020). Importantly, it has been previously shown that epithelial Wnts secreted from Paneth cells are dispensable for intestinal regeneration, since stroma secreted Wnts can fully support the regeneration process (Kabiri et al., 2014).

Yap signalling is another key player in the regenerative process by translocating to the nucleus and driving cell proliferation (Cai et al., 2010). Yap localisation is highly dynamic and several Yap activation models upon injury have been proposed. Upon DSS treatment, extracellular matrix remodelling orchestrates colonic crypts to supress adult stem cell markers and activate fetal markers instead to drive regeneration (more details in Chapter 1.3.2) (Yui et al., 2018). Moreover, stromal cells have been reported to activate Yap upon regeneration. Recent studies have implicated group 3 innate lymphoid cells (ILC3s) as main regulators of the dynamic control of Yap via interleukin 6 (Il-6)-dependent way to activate gp130 (a co-receptor of Il-6) and subsequent increase of Yap signalling (Romera-Hernandez et al., 2020, Taniguchi et al., 2015). It is interesting to note that Hippo/Yap signalling drives the regeneration process by cross-talking with other pathways including Wnt, Egf and Notch (Beumer and Clevers, 2021). For instance, Yap-driven suppression of Wnt signals is believed to be crucial during the regeneration process since by restricting Paneth cell differentiation and thereby promoting ISC expansion (Barry et al., 2013, Gregorieff et al., 2015). On the other hand, it has been recently shown that, upon regeneration, transcription of Yap and its downstream effector Tead1/2/4 are driven by Wnt whereas Yap nuclear localisation is regulated by Src family kinase (Guillermin et al., 2021).

1.3.2 Epithelial cell dedifferentiation during regeneration

As mentioned before, several early or terminally differentiated populations can contribute to intestinal regeneration. However, many studies focused on identifying specific cell markers at the progenitor cell population contributing to dedifferentiation, while the underlying mechanism of the regenerative response remains unclear. Below, we discuss the current knowledge of intestinal epithelial regeneration regarding cellular plasticity of different cell types.

+4 reserve stem cells. The +4 position comprises of various cell populations, including the quiescent or reserve stem cells. Initial studies linked these cells with marked expression of *Bmi1*, *Hopx* and *mTert*. Interestingly, all these studies confirmed that cells marked by these genetic markers has the ability to convert to actively cycling stem cells in response to either irradiation or genetic ablation of Lgr5-positive cells upon administration of diphtheria toxin (Lgr5-DTR-EGFP mouse model) (Montgomery et al., 2011, Takeda et al., 2011, Tian et al., 2011). Similarly, LRCs residing at position +4 can not only give rise to enteroendocrine and Paneth cells during homeostasis, but also possess regenerative capacity after irradiation or drug-induced injury (doxorubicin and hydroxyurea) (Buczacki et al., 2013). A very distinct sub-population of Keratin 19 (*Krt19*)-positive cells at the +4 position has also been shown to be radioresistant and can generate Lgr5-positive ISCs in response to injury. These cells exist in both small intestinal and colonic crypts and are considered cancer-initiating stem cells (Asfaha et al., 2015). Of note, Bmi1-positive, Hopx-positive, mTert-positive and Krt19-positive cells are all great examples of a bidirectional cell differentiation. Under homeostasis, these populations are direct progeny of Lgr5-positive ISCs and upon injury can re-acquire stem cell identity. Lastly, a more recent single cell RNA sequencing (scRNA-seq) study of the regenerating epithelium identified a very rare sub-population of quiescent revival stem cells marked by Clusterin (*Clu*). These Clu-positive cells are dispensable under homeostasis but essential for regeneration upon irradiation, Lgr5-positive stem cell ablation and dextran sulfate sodium (DSS)-induced colitis (Ayyaz et al., 2019). After injury, these revival stem cells express Stem cell antigen-1 (Sca-1) that signifies a fetal-like transcriptional programme to drive regeneration of Lgr5-positive ISCs in a Yap-dependent manner (Ayyaz et al., 2019). These findings come in accordance with two other independent studies that indicated acquisition of a fetal-like identity as a mechanism to drive regeneration. Firstly, Nusse et al. showed that helminth infection and irradiation activate an Interferon-γ (Ifn-γ) transcriptional programme that is marked by Sca-1 and drives Lgr5-positive cell regeneration (Nusse et al., 2018). In parallel, Yui et al. showed that colonic epithelium is remodelled to supress adult stem and differentiation markers and to acquire a more primitive fetal-like state, which is facilitated by remodelling of the extracellular matrix and activation of Yap/Taz via increased Fak/Src signalling (Yui et al., 2018).

Early progenitors. Progenitor cells of both absorptive and secretory lineages located at around +4/+5 cell positions have been linked with intestinal regeneration. As shown by lineage tracing experiments, enterocyte progenitor cells marked by Alkaline phosphatase (*Alpi*) have the ability to convert to Lgr5-positive ISCs and Paneth-like cells upon genetic deletion of Lgr5-positive cells. As these Alpi-positive cells dedifferentiate, they switch their transcriptional programme to regeneration and wound healing genes to protect the intestinal barrier (Tetteh et al., 2016).

On the other side, several secretory cell populations have been reported to have much more diverse regenerative capacities. Dll1-positive cells are the immediate progeny of ISCs and they can respond to irradiation and revert to stem cells (van Es et al., 2012). Moreover, a subset of the aforementioned Krt19-positive cells that are marked by *Atoh1* have the ability to acquire Lgr5-positive identity in the colon (Castillo-Azofeifa et al., 2019) and small intestine (Tomic et al., 2018). The ability of Atoh1-positive cells to regenerate the stem cell pool and to drive differentiation is tightly regulated at a post-translation level that requires a multisite phosphorylation (Tomic et al., 2018). Goblet cell-specific precursors that are marked by expression of surface markers Cd69 and Cd274 is another population with regenerative potential. Similar to other secretory progenitors, these cells have a unique open chromatin accessibility, which show dynamic re-organisation of their chromatin profile to one resembling Lgr5-positive cells upon irradiation or diphtheria toxin-induced ISC depletion (Jadhav et al., 2017).

Lastly, a slow-proliferating subpopulation of Lgr5-high cells has been proposed as a multilineage progenitor with regenerative capabilities and is marked by high expression of Mex-3 RNA Binding Family Member A (*Mex3a*). Under homeostasis, these cells are identified as LRCs, but they continuously re-acquire a high proliferative status. Moreover, Mex3a-positive cells exhibit high levels of resistance to irradiation and chemotherapy, and as a result they drive intestinal regeneration (Barriga et al., 2017).

Paneth cells. Although terminally differentiated, Paneth cells show a remarkable plasticity to re-acquire stemness upon injury through various mechanisms. Upon acute inflammation, Paneth cells can lose their secretory identity to re-enter the cell cycle and de-differentiate to Lgr5-positive cells. Inflammation (such as inflammatory bowel disease) is marked by increased expression of stem cell

factor (Scf) at Paneth cells. Scf binds c-Kit and leads to activation of Pi3k/Akt, inactivation of Gsk3β and subsequent activation of Wnt signalling that drives Paneth cell dedifferentiation (Schmitt et al., 2018). Interestingly, an independent study showed that irradiation induces dedifferentiation of a subset of Paneth cells and acquisition of a stem cell-like transcriptome in a Wnt-independent manner. Instead, irradiation leads to Notch activation that was sufficient to trigger Paneth cell dedifferentiation through translocation of NICD to the nucleus (Yu et al., 2018). Lastly, using an organoid model of doxorubicin treatment, Jones et al. confirmed that an Adam10-dependent Notch activation is required for dedifferentiation of Defa4-expressing Paneth cells (Jones et al., 2019).

Enteroendocrine cells. Although Bmi1 was initially identified as a marker of reserve stem cells at the +4 position, subsequent transcriptomic analyses revealed a broad expression throughout the crypt. Indeed, a recent study demonstrated that Bmi1-positive cells represent enteroendocrine cells (Jadhav et al., 2017). A subset of these cells that is marked by Prospero Homeobox 1 (*Prox1*) shows regenerative capacity and re-acquire stemness as shown by lineage tracing experiments (Yan et al., 2017a). Although this cluster was initially identified as an enteroendocrine precursor population, the study from Gehart et al identified it as mature I cells pointing to the need of adding extra layers of spatiotemporal expression to transcriptomic data to better understand differentiation dynamics (Gehart et al., 2019, Yan et al., 2017a). Moreover, terminally differentiated enterochromaffin cells marked by expression of Tryptophan hydroxylase 1 (*Tph1*) also possess stem cell-like potential upon injury both *in vivo* and *in vitro* (Sei et al., 2018).

1.4 Hypothesis

Maintenance of small intestinal homeostasis has been extensively studied over the past few decades. Complex and tight regulation is needed to maintain an intact epithelium for the vital functions of food digestion and host defence. As described in section 1.1, Lgr5-positive ISCs are actively cycling at the bottom of intestinal crypts with the capacity to generate all differentiated lineages upon niche exit. As mitotically active cells, CBCs are particularly susceptible to damage. Upon injury, progenitor cells of either lineage, quiescent reserve stem cells at the +4 position as well as differentiated cells have demonstrated plasticity to re-acquire stemness.

The complex mechanisms of stem cell self-renewal and differentiation are tightly regulated by various signalling cascades. Wnt and Egf signals govern maintenance of stemness and proliferation of both stem cells and TA cells at the upper crypt. Notch amplifies the stem cell signal at the crypt base and dictates the fate decision making process between absorptive and secretory lineages at +4/+5 cell positions. On the other hand, Bmp drives differentiation and terminal maturation at the villus compartment.

The progenitor cells residing at the +4/+5 positions are part of the TA zone that extends to the intervillus junction. +4/+5 cells are the immediate progeny of Lgr5-positive CBCs and have shown an extended level of plasticity with a high degree of epigenetic similarities with CBCs. Notch is key to determine the cell fate at these progenitor cells. Interestingly, although progenitor cells have committed to either of the lineages immediately after niche exit, they continue to undergo several more rounds of cell divisions in the TA zone before terminal differentiation and maturation closer to the intervillus junction. Previous studies have focused predominately on the signalling regulation of ISC proliferation and differentiation, whereas the precise control of lineage specification, spatial transcriptomics and plasticity at the early progenitors/TA zone remains largely uncharacterised. Here, we hypothesise the existence of a transcriptional control network at the +4/+5 early progenitor cells at the crypts of the small intestinal epithelium that drives cell lineage commitment and specification during homeostasis as well as plasticity upon injury. Genes of this network could act dependently or independently of already established regulators of epithelial homeostasis, such as Wnt, Notch and Bmp pathways, and possibly regulate niche exit, initial fate decision and subsequent terminal maturation.

1.5 Aim

The aim of this PhD thesis is to characterise the transcriptional control at the +4/+5 progenitor cells of the crypts of the small intestinal epithelium. Specifically, we aim to identify new key regulators in this region and to study their roles in ISC maintenance, lineage specification and regeneration.

Screening of transcription factors expressed at the +4/+5 cells (will be discussed in detail in Chapter 3) identified Arid3a as a putative candidate regulating intestinal epithelial homeostasis. The specific aims of this project are:

(1) to characterise of the expression pattern of Arid3a throughout the intestinal epithelium;

(2) to investigate the upstream regulation of Arid3a by various signalling pathways known to have key functions in proliferation and differentiation processes;

(3) to study the effects of Arid3a depletion in normal intestinal homeostasis; and

(4) to explore the potential role of Arid3a in irradiation-induced regeneration.

Chapter 2: Materials and Methods

2.1 Animal studies

2.1.1 Conditional knockout animals and genotyping

All animals were maintained with appropriate care according to the United Kingdom Animal Scientific Procedures Act 1986 and the ethics guidelines of the Francis Crick Institute. The full list of transgenic mice used for this study is shown below in Table 1.

Mouse strains	Genetic background	Reference
VillinCre-ERT2$^{+/-}$	C57BL/6	(el Marjou et al., 2004)
Arid3a$^{fl/fl}$	C57BL/6	(Habir et al., 2017)
Arid3b$^{fl/fl}$	C57BL/6	(Kurkewich et al., 2016)
Arid3a$^{fl/fl}$ *; Arid3b*$^{fl/fl}$	C57BL/6	In this study
VillinCre-ERT2$^{+/-}$*; Arid3a*$^{fl/fl}$	C57BL/6	In this study
VillinCre-ERT2$^{+/-}$*; Arid3b*$^{fl/fl}$	C57BL/6	In this study
VillinCre-ERT2$^{+/-}$*; Arid3a*$^{fl/fl}$*; Arid3b*$^{fl/fl}$	C57BL/6	In this study

Table 1 | List of transgenic mice.

Animal genotyping was performed by PCR amplification of genomic DNA extracted from ear punch biopsies taken from mice aged three weeks (see primer list on Table 2). Biopsies were first digested in 200µl lysis buffer (10mM Tris pH7.5, 100mM NaCl, 10mM Ethylenediaminetetraacetic acid (EDTA), 0.5% Sarkosyl) at 55°C overnight. 200ng of DNA was amplified using MyTaq™ Red Mix (Bioline, BIO-25043) and 0.4µM forward and reverse primers in a reaction with final volume of 25µl. After the initial denaturation step (95°C for 1min), the thermocycler was configured to 35 cycles of 95°C for 30s, 56-60°C for 30s (depending on the primer) and 72°C for 1min per kilobase of amplification, followed by a final 3min step of extension at 72°C. PCR products were then visualised and size-verified on a 2% w/v agarose/TAE

electrophoresis gel with 5ng/ml ethidium bromide. *Villin*Cre-ERT2 animals were genotyped by the Biological Research Facility of the Francis Crick Institute.

To induce conditional deletion, wild-type (WT) and knockout (KO) animals were injected intraperitoneally with tamoxifen at 1.5mg/10g of mouse weight (from a 20mg/ml stock solution). Mice were culled by schedule 1 procedure (S1K) at the desired timepoint.

Target	Forward primer	Reverse primer
Arid3a$^{fl/fl}$	TGCCTGTTGGAAGGATGATCTGG	CTCCTTCCTCTTGTCTCCTGTGTGG
Arid3b$^{fl/fl}$	TTGAGATGAATCCCTCAGACCT	CTCGAAAGAGCACATATTGCAG

Table 2 | List of genotyping primers.

2.1.2 EdU chasing experiments

5-ethynyl-2'-deoxyuridine (EdU) (Life Technologies, E10187) was injected intraperitoneally at 0.3mg/10g of mouse weight (from a 10mg/ml stock solution). Mice were culled by S1K at 2 hr after EdU injection.

2.1.3 Irradiation experiments

Mice were exposed to controlled 12 Gray (12Gy) total body ionising irradiation to induce damage using a Caesium (γ) irradiator. The dosage rate was 0.779Gy/min. Mice were culled by S1K at the desired timepoint.

2.2 Cell line culture

2.2.1 Culture conditions and maintenance

HEK293T and LS174T cells were maintained in DMEM GlutaMAX (Gibco, 10566-01) supplemented with 5% FBS (Gibco, 10270106) and 100 units/ml penicillin and 100 ug/ml streptomycin (Gibco, 15140122). Cells were incubated in a humidified atmosphere of 5% CO2 at 37°C. For transient overexpression, plasmids were transfected with polyethylenimine (PEI; Polysciences, 23966) according to

manufacturer's instructions. For immunoprecipitation (IP) experiments, cells were seeded 24hr before transfection in a 10 cm plate. For quantitative RT-PCR experiments, cells were seeded 24hr before transfection in 6-well plates using 1μg of pLV-ATOH1 overexpression plasmid (previously generated in the lab). For Wnt pharmacological inhibition, cells were seeded 24hr before treatment with LGK974 inhibitor (Selleck chemicals, S7143).

2.2.2 Cell line immunofluorescence

For immunofluorescence (IF) experiments, LS174T cells were grown on sterilised glass coverslips in 24-well plates. Coverslips were not coated with poly-L-lysine before seeding the cells, since LS174T cells are very adherent. Cells were fixed with 4% paraformaldehyde (PFA) for 15min and permeabilised using 0.5% Triton X-100 in PBS for 15min. Cells were blocked with 1% Bovine Serum Albumin (BSA) for 1hr at room temperature before overnight incubation with primary antibodies at 4°C (see Table 3 for full list of antibodies). Cells were washed with PBS and incubated with secondary antibodies conjugated to Alexa-Fluor 488 (Invitrogen, A32731) at room temperature for 1hr in the dark. Cells were washed and stained with 4',6'-diamidino-2-phenylindole (DAPI) and/or Phalloidin-Atto647 (Sigma, 65906) for 30min in the dark. Coverslips were washed and mounted with ProLong Gold Antifade Mountant (ThermoFischer, P36934). Images were acquired as z-stacks using a Leica SPE confocal microscope and processed using Fiji.

2.3 Mouse small intestinal organoids

2.3.1 Establishment and maintenance of organoid cultures

Organoids were established from freshly isolated adult small intestine, as previously described (Gracz et al., 2012). In brief, 2cm of jejunal small intestinal tissue was opened longitudinally and villi was scrapped using a glass cover slip. The remaining tissue was incubated in 15mM EDTA and 1.5mM (Dithiothreitol) DTT at 4°C for 10min and moved to 15mM EDTA solution at 37°C for an extra 10min. Subsequently, the tissue was shaken vigorously for 30sec to release epithelial cells from basement membrane and the remaining remnant intestinal tissue was removed.

Cells were washed once, filtered through a 70μm cell strainer, and resuspended in Cultrex BME Type 2 RGF Pathclear (Amsbio, 3533-01002). All freshly isolated organoids were maintained in either Intesticult medium (Stem Cell technologies, #06005) or in-house made basal medium containing EGF (Invitrogen PMG8043), Noggin, Rspondin and Wnt3A WENR medium), as previously described (Sato et al., 2009). The Rho kinase inhibitor Y-27632 (Sigma, Y0503) was added to the culture during first week of crypt isolation and single cell dissociation. For Wnt, Notch, Tgf-βand Bmp pathway manipulation, organoids were passaged and allowed to recover for 72 hours before treatment. For Wnt signalling inhibition, organoids were treated for 48hr with either 5μM of LGK974 inhibitor or 30μM of LF3 inhibitor (Sigma, SML1752); for Notch signalling inhibition, organoids were treated with 10μM of DAPT inhibitor (Sigma, D5942) for the indicated timepoints; for Tgf-β signalling manipulation, organoids were treated with 0.1ng/ml of recombinant Tgf-β1 (Sigma, 11412272001) for the indicated timepoints; for Bmp signalling manipulation, organoids were treated with 20ng/mL of recombinant Bmp4 (Peprotech, 120-05ET) for the indicated timepoints. For complete gene deletion, *Villin*-CreERT2;*Atoh1*$^{fl/fl}$ organoids were treated with 1μM 4-hydrotamoxifen (4-OHT) for 24hr, followed by 48h of 10μM DAPT treatment for Notch inhibition.

Noggin and Rspondin conditioned media were generated by HEK293T cells. Wnt3A conditioned medium was generated from L cells. All images were acquired using an EVOS FL Cell Imaging System (Life technologies) and image brightness was adjusted using Adobe Photoshop (exactly same parameters were applied to all samples of the same experiment).

For generation of Arid3a-overexpressing organoids, organoids derived from *Villin*-CreERT2;*Atoh1*$^{fl/fl}$ were electroporated with an empty or Arid3a-overexpression vector (PB-CMV-MCS-EF1α-GreenPuro PiggyBac; System Biosciences, PB513B-1) as previously described (Fujii et al., 2015). Selection of positively transduced organoids was performed with puromycin treatment (1μg/ml) for 48h. Performance of puromycin selection was validated by checking GFP expression of surviving organoids using an EVOS FL Cell Imaging System.

2.3.2 Organoid formation assay

Organoids were established as described in section 2.3.1. For organoid formation assay, crypts were counted using a brightfield microscope and 200 crypts were seeded in 20µl of Cultrex BME Type 2 RGF Pathclear in individual wells of a 48-well plate and cultured in WENR medium for 5 days until counted. Three technical replicates were performed per animal.

2.3.3 Rspondin withdrawal assay

For Rspondin withdrawal assay, organoids were passaged and seeded in 3 10µl droplet per well of a 24-well plate. Organoids were allowed to re-establish in normal ENR medium (5% Rspondin) for 48hr. Subsequently, organoid medium was replaced, and organoids were cultured in ENR medium containing either 5% or 1% of Rspondin.

2.3.4 Disaccharide assay

Organoids were washed twice with PBS and incubated with a 56mM solution of sucrose during 1h. Supernatants were collected and frozen until the assay was performed. To detect glucose content, Amplex® Red Glucose/Glucose Oxidase Assay Kit (Invitrogen, A22189) was used. Samples were diluted when necessary and incubated with the reaction buffer containing Amplex Red®, horseradish peroxidase and glucose oxidase. Fluorescence was measured in a Tecan microplate reader with an excitation wavelength of 540nm and fluorescence emission detection at 590nm. Glucose concentration was assessed using a glucose standard curve from 0 to 200µM.

2.3.5 Irradiation experiments

Organoids were passaged and seeded in a 24-well plate containing 500µl of Intesticult and allowed to recover for 72h. Organoids were exposed to controlled 4Gy ionising irradiation to induce damage using a Caesium (γ) irradiator. The dosage rate was 0.779Gy/min and samples were used for downstream FACS analysis of apoptotic cells (section 2.5.2).

2.4 Crypt-villus fractionation

4cm of jejunal small intestinal tissue was opened longitudinally and villi was scrapped using a glass cover slip. Villi and the remaining intestinal tissue were transferred into two separate tubes and washed once. Both parts of the small intestine were incubated in 15mM EDTA and 1.5mM DTT at 4°C for 10min and moved to 15mM EDTA solution at 37°C for an extra 10min (as described in section 2.3.1) for isolation of epithelial cells of villi and crypt fragments. Pelleted cells were re-suspended in RLT buffer (see section 2.7.1) and stored at -80°C before proceeding to RNA extraction (section 2.7.1)

2.5 Fluorescence-Activated Cell Sorting (FACS)

2.5.1 Sorting of GFP-positive cells from *Lgr5-EGFP-ires-CreERT2 mice*

Crypts were harvested from the proximal jejunum (~10cm) as described in section 2.3.1. Crypts were dissociated by incubating with Collagenase/Dispase (Roche, 11097113001) for 20min at 37oC, followed by 20min incubation with TrypLE (Gibco, 12604013) for 20min at 37oC. TrypLE was stopped by adding Advanced DMEM (Gibco, 12491015) containing 10% fetal bovine serum (FBS) (Gibco, 10270106) and dissociated cells were passed through a 20µm strainer. Cells were stained with DAPI and resuspended in PBS-0.5% BSA-2mM EDTA. Cells were separated and re-collected in Advanced DMEM plus 10% FBS based on GFP intensity. Cell sorting was performed on a BD FACSAria™ II System

2.5.2 FACS analysis of apoptotic cells

Organoids were collected at the appropriate timepoint after irradiation, mechanically dissociated and washed once. Subsequently, organoids were dissociated into single cells using ACCUMAX™ (Merck, SCR006) for 7min at RT. The reaction was stopped by the addition of Advance DMEM and washed. Cells were resuspended in Annexin-V binding buffer (10mM HEPES, 140mM NaCl and 2.5mM $CaCl_2$) and incubated with Annexin-V-FITC (Thermofischer, A13199) for 15min and DAPI for

3min and filtered before analysis. Cell analysis was performed on a BD LSRFortessa™ Cell Analyzer.

2.6 Western blot and immunoprecipitation

Cells or organoids were lysed in cold lysis buffer containing 150mM NaCl, 30mM Tris (pH 7.5), 1mM EDTA, 1% Triton X-100, 10% Glycerol, 0.5mM DTT and Halt™ Protease and Phosphatase Inhibitor Cocktail (Thermofischer, 78440). Lysates were centrifuged for 30min at 15000 rpm at 4°C and supernatants were kept for downstream protein quantification using Thermo Scientific™ Pierce™ BCA Protein Assay Kit (Thermofischer, 10741395) according to manufacturer's instructions. Upon quantification, equal amounts of protein were mixed in 4x Laemmli Sample Buffer (Biorad, 1610747), resolved in 10% sodium dodecyl sulfate-polyacrylamide gels (SDS-PAGE), and subsequently transferred to polyvinylidene difluoride (PVDF) membranes. Membranes were blocked using 5% milk in Tris-buffered saline (50mM Tris, 150mM NaCl, pH 7.6) containing 0.1% Tween-20 (TBS-T) for 1hr and primary antibodies were added to blocking solution. Primary antibody incubations were carried at 4°C overnight (see Table 3 for full list of antibodies). After washing with TBS-T, the appropriate HRP-conjugated antibody was added for 1hr at room temperature. Anti-β-actin-HRP (Sigma, A3854) was used to visualise the housekeeping gene β-actin as a loading control. Membrane was then washed, and antibodies were detected using GE Healthcare Amersham™ ECL Prime Western Blotting Detection Reagent (GE Healthcare, 12316992). Protein bands were visualised using an Amersham Imager 600.

For immunoprecipitation (IP) experiments, cells were washed and collected as described in the previous paragraph. After centrifugation, lysates were pre-cleared with IgG agarose beads (Millipore, IP10-10ML) for 2hr at 4°C. Immunoprecipitation was performed by incubating the cellular lysates with the desired antibody at 4°C overnight. Protein G PLUS/Agarose beads (Santa Cruz Biotechnology, sc-2002) were added and incubated at 4°C for 4hr. Immunocomplexes were washed with cold lysis buffer and subjected to SDS-PAGE and Western blot analysis as described above. Full list of antibodies used for Western blot and immunoprecipitation is shown in Table 3.

Antibody	Application	Dilution	Source
Arid3a	Cell line IFA WB	1:100 1:1000	Abcam
Arid3a	IHC WB IP/ChIP	1:700 1:1000 -	Proteintech
Muc2	IHC	1:200	Santa Cruz (sc-15334)
ChgA	IHC	1:200	Abcam (ab15160)
Lyz	IHC	1:2000	Dako (A0099)
Sox9	WB	1:500	Millipore (AB5535)
Cyclin D1	WB	1:1000	Cell signalling (2978)
β-Actin-HRP	WB	1:20000	Sigma (A3854)
Phalloidin-Atto647	IHC	1:500	Sigma (65906)
Fabp1	IHC	1:100	Thermo Fisher (328607)
Apoa4	IHC	1:500	R&D (AF8125)
Cleaved caspase -3	IHC	1:200	Cell signalling (9664)
Ki67	IHC	1:200	Abcam (ab15580)
Annexin-V-FITC	FACS	1:40	Thermofischer (A13199)

Table 3 | List of primary antibodies.
IFA: immunofluorescence assay; WB: Western blot; IP: Immunoprecipitation; ChIP: Chromatin immunoprecipitation; FACS: Fluorescence-Activated Cell Sorting

2.7 RNA isolation and reverse transcription

2.7.1 RNA isolation from cell lines, organoids and tissue

RNA was extracted according to the manufacturer's instructions (Qiagen RNeasy, 74106). Harvested cell lines, organoids or intestinal crypts were resuspended in RLT buffer (provided with the kit) supplemented with 40mM DTT to inhibit RNases activity. Before RNA extraction samples were undergone one freeze/thaw cycle to increase the yield of extracted RNA.

2.7.2 cDNA synthesis and qRT-PCR

500-1000ng of RNA were reverse transcribed using the cDNA Reverse Transcription Kit (Applied Biosystems, #4368813), according to manufacturer's instructions. RT-qPCR was performed in 384-well plates, in experimental triplicates, in a 12µl reaction mixture containing 6µl of 2x PowerUp™ SYBR® Green Master Mix (Applied Biosystems, A25742), 10µM of each primer and 25-50ng of cDNA. The reaction mixture without cDNA template was used as a negative control for each reaction plate. After 40 cycles of amplification, samples were normalised to housekeeping genes *Ppib* (for mouse samples) or *β-actin* (for human samples), where data was expressed as mean ± s.e.m. Primer sequences are listed in Table 3.

Gene	Forward primer	Reverse primer
	Mouse primers	
Atoh1	GCCTTGCCGGACTCGCTTCTC	TCTGTGCCATCATCGCTGTTAGGG
Hes1	ATAGCTCCCGGCATTCCAAG	GCGCGGTATTTCCCCAACA
Dll1	CCCATCCGATTCCCCTTCG	GGTTTTCTGTTGCGAGGTCATC
Mtg8	ATGGCTTTGACAGAGAGCCT	CTGGGGTGTCGATAGGAGTC
Mtg16	TCACCACCCTACAGCAGTTT	AGGGATAACAAACGGCCTCA
Arid3a	AGGCCGCCTACCTGTATCTT	AGGTGCTGTAGGAGGTGGTG
Arid3b	CCTTAGCCAGAGTTCCACCA	GATCTCTCTTCCCCTGCCTC
Gfp	ACGTAAACGGCCACAAGTTC	AAGTCGTGCTGCTTCATGTG
Lgr5	CATCAGGTCAATACCGGAGC	TAATGTGCGAGGCACCATTC
Alpi	ATCATCTTCCTGGGTGACGG	ATCATCTTCCTGGGTGACGG
Olfm4	ACCAAGCTGAAAGAATGTGAG	TAACAGCTTTCCAGGAGCA
Axin2	TCCAGAGAGAGATGCATCGC	AGCCGCTCCTCCAGACTATG
CyclinD1	GCCATCCAAACTGAGGAAAA	GATCCTGGGAGTCATCGGTA
Sox9	CTGGAGGCTGCTGAACGAGAG	CGGCGGACCCTGAGATTGC
Id1	CCTGCAGCATGTAATCGAC	TTCAGACTCCGAGTTCAGC
Lyz	ATGGAATGGCTGGCTACTATGGAG	CTCACCACCCTCTTTGCACATTG
Muc2	TCTACCTCACCCACAAGCTG	TGGTCTGCATGCCATTGAAG
ChgA	CAAGGTGATGAAGTGCGTCC	GGAGAGCCAGGTCTTGAAGT
Dclk1	CGCTTCAGATCTTTCGAGGC	CCGCAGACATAGCTTTCACC
Smad7	CCCCCGGCTGAGAGGCTCAT	CACCTGCTGCCAGTCTGCCC
Clu	ATACCTGCATGAAGTTCTATGC	GGTTTAGAAACTCCTCTAGCTG
Ctgf	Qiagen QuantiTect Primer Assay	
Cyr61	Qiagen QuantiTect Primer Assay	
Ppib	TCCATCGTGTCATCAAGGA	CATAGATGCTCTTTCCTCCTG
	Human primers	
MTG8	CGACAACGTTAACTAATGGCA	CATTGCTGAAGCCATTGGG
MTG16	GCAGGAAGAAGTGATCGAC	CAGTTCAGGAGGTTGTTGAG
DLL1	ACTCCTACCGCTTCGTGTGT	CAGGGTTGCACACTTTCTCC
DLL4	AGGCCTGTTTTGTGACCAAG	CTCCAGCTCACAGTCCACAC
ARID3A	CCCGCCCCTAAGATCAAGAA	GTTGATCTCCACCGACATGC
ARID3B	TGCTGAGAAGAAGGCATCGA	CGGGATGAGGTAGGACTTGG
AXIN2	GACAGGAATCATTCGGCCAC	CCTTCAGCATCCTCCGGTAT
ACTIN	TTCTACAATGAGCTGCGTGTG	GGGGTGTTGAAGGTCTCAAA

Table 3 | List of qRT-PCR primers.

2.8 Tissue staining

2.8.1 Immunohistochemistry

For analysis of small intestine by immunohistochemistry (IHC), tissues were fixed in 10% formalin and embedded in paraffin. Sections were deparaffinized with xylene and rehydrated in a graded series of ethanol. Antigen-retrieval was performed for 20 min at high temperature in 0.01M Citrate (pH 6) or Tris-EDTA buffer (10mM Tris base, 1mM EDTA, pH 9). Slides were then blocked using the appropriate blocking buffer (10% Normal goat serum or 10% Normal donkey serum in 1% BSA) and incubated overnight with the appropriate antibody at 4°C (See Table 3 for full list of antibodies). Finally, slides were incubated with the secondary antibody for 1h and washed three times with PBS. For colorimetric staining, with diaminobenzidine (DAB) slides were incubated with peroxidase substrate, dehydrated, counterstained with Haematoxylin solution according to Mayer (Sigma, 51275) and mounted. Slides were scanned using an Olympus VS120 slide scanner and images were processed using QuPath (Bankhead et al., 2017).

For immunofluorescence, slides were incubated with Alexa-Fluor 488 or Alexa-Fluor 568 antibody for 1h, washed three times with PBS, incubated with DAPI for 15 min to visualize nuclear DNA and mounted with ProLong Gold Antifade Mountant. Images were acquired as z-stacks using a Leica SPE or a Leica SP8 confocal microscope and processed using Fiji. For whole slide imaging, slides were scanned using an Olympus VS120 slide scanner and images were processed using QuPath (Bankhead et al., 2017).

When indicated, sections were stained for Haematoxylin & Eosin (H&E), alkaline phosphatase and Alcian Blue-Periodic Acid Schiff (AB-PAS) staining. Edu was detected according to the manufacturer's protocol (Thermo Fisher Scientific, Click-iT Plus EdU Alexa Fluor 555 imaging kit C 10638) to evaluate proliferating cell number. Edu+ cells were quantified in at least 10 crypts per mouse.

Stomach, spleen and liver tissues were also collected at the indicated timepoints, embedded in paraffin and stained for H&E for downstream analysis.

2.8.2 *In situ* hybridisation

Single-molecule in situ hybridization was performed on mouse intestine according to manufacturer's instructions (ACD; RNAscope 2.5HD Assay RED (REF 322350) or RNAscope 2.5HD (REF 322436)). The probes used were against *Arid3a* (REF 525721), *Arid3b* (REF 525731), *Atoh1* (REF 408791), *Lgr5* (REF 312171) and *Olfm4* (REF 311831). Briefly, guts were fixed in formalin overnight, paraffin-embedded and cut into 5-micron thick slices. Target retrieval was performed for 15 minutes, followed by RNAscope Protease Plus incubation for 24 minutes on the FFPE Sample Preparation and subsequent amplification steps. For brightfield analysis, slides were counterstained using 50% Haematoxylin solution according to Mayer and for immunofluorescence slides were incubated with DAPI for 10min for DNA visualisation. Images acquired with an Olympus VS120 slide scanner and images were processed using QuPath (Bankhead et al., 2017).

For combined RNAscope and immunofluorescence of *Arid3a* with Muc2, ChgA or Lyz, samples were first stained for Arid3a using the red channel of duplex RNAscope kit, followed by antibody immunostaining as described above.

2.9 Bulk RNA-seq

2.9.1 Sample preparation

Crypts or villi were isolated from 10cm of mouse jejunal small intestinal tissue as described in section 2.4 and RNA was isolated as described in section 2.7.1. RNA integrity (RIN) was examined using Bioanalyzer 2100 RNA 6000 Nano kit from Agilent and RIN cut-off was set to 7. For crypt samples, libraries were prepared using KAPA mRNA HyperPrep kit (KK8580) according to manufacturer's instructions. For most villus samples, RIN number was lower than 7 and libraries were prepared with KAPA RNA HyperPrep with RiboErase (KK8561) according to manufacturer's instructions.

2.9.2 Bulk RNA-seq data analysis

Fastq files were processed using the nf-core/RNA-seq pipeline (10.5281/zenodo.4323183) version 3.0 using the corresponding versions of STAR RSEM to quantify the reads against release 95 of Ensembl GRCm38. These raw counts were then imported into R (R Core Team (2020). R: A language and environment for statistical computing. R Foundation for Statistical Computing, Vienna, Austria. URL https://www.R-project.org/) version 4.03 /Bioconductor version 3.12 (Huber et al., 2015). We then used to DESeq2 (Love et al., 2014)version 1.30.1 to account for the different size factors between the samples, and used a generalised linear (negative binomial) model with main effects of arid3a (or arid3b) status and time (as a categorial variable) to find genes that were statistically significantly associated with arid3a (or arid3b) status (Wald test) with a false discovery rate of <0.05.

Gene set enrichment analysis (GSEA) was performed using the GSEA desktop software (version 4.1.0) using the following parameters: GSEA Preranked > no collapse of gene symbols > classic enrichment statistic > Chip platform "Mouse_Gene_Symbol_Remapping_Human_Orthologs_MSigDB.v7.5.chip". GSEA custom lists were obtained from the indicated publications. For Metacore analysis, the online software was used (https://portal.genego.com/). Gene lists of upregulated and downregulated genes were created by using FDR<0.05 and fold change>1.5 cut-offs. One click analysis included Pathway Maps and GO Processes.

2.10 ChIP-seq

2.10.1 Sample preparation

Isolated mouse crypts (see section 2.3.1) were dual cross-linked first in 2 mM Di(N-succinimidyl) glutarate (DSG; Sigma-Aldrich, 80424) for 45 min at room temperature followed by incubation in 1% formaldehyde for 10 minutes as previous described (Corces et al., 2017). The fixation was terminated by quenching with glycine (Sigma-Aldrich, 50046) for 5 minutes at room temperature. The samples were washed twice in PBS and resuspended in commercial lysis buffer containing protease inhibitors from the MAGnify Chromatin Immunoprecipitation System kit (Thermo Scientific; 492024). The chromatin was sheared using the Covaris LE220-plus

sonicator (Covaris). The sonicated chromatin was incubated for one hour at 4°C with Dynabeads protein A/G beads from the kit coupled to 8 µg of anti-Arid3a antibody (Proteintech, 14068-1-AP) per IP. 10% of the chromatin was used for the Inputs control. The beads were washed with buffers supplied with the kit and samples were de-crosslinked in buffer containing Proteinase K at 55°C for 15 minutes according to the manufactures' instructions. The DNA was purified using the DNA Purification Magnetic Beads supplied with the kit and the eluted DNA was verified using the Agilent Bioanalyzer. The DNA library for sequencing was prepared using the NEB Ultra II DNA kit (NEB, E7645). The quality of the final DNA library was confirmed on the Agilent Tapestation before the samples were submitted to sequencing.

2.10.2 ChIP-seq data analysis

The nf-core/chipseq pipeline (version 1.2.2) (Ewels et al., 2020) written in the Nextflow domain specific language (version 19.10.0) (Di Tommaso et al., 2017) was used to perform the primary analysis of the fastq samples in conjunction with Singularity (version 2.6.0) (Kurtzer et al., 2017). The command used was "nextflow run nf-core/chipseq -profile crick --input /Path_to_desing/design.csv --fasta Mus_musculus.GRCm38.dna_sm.toplevel.fa --gtf Mus_musculus.GRCm38.95.gtf --gene_bed Mus_musculus.GRCm38.95.bed --single_end --macs_gsize 2.6e9 --blacklist mm10.blacklist.bed --narrow_peak -r 1.2.2 -resume".

To summarise, the pipeline performs adapter trimming (Trim Galore! - https://www.bioinformatics.babraham.ac.uk/projects/trim_galore/), reads alignment (BWA), mark duplicates (Picard) (picard-tools - http://broadinstitute.github.io/picard) and filtering ((SAMtools) (Li et al., 2009), BEDTools (Quinlan and Hall, 2010); BamTools (Barnett et al., 2011); pysam - https://github.com/pysam-developers/pysam; picard-tools - http://broadinstitute.github.io/picard)), normalised coverage track generation (BEDTools (Quinlan and Hall, 2010); bedGraphToBigWig (Kent et al., 2010)), peak calling (MACS) (Zhang et al., 2008), annotation relative to gene features (HOMER) (Heinz et al., 2010), consensus peak set creation (BEDTools), differential binding analysis ((featureCounts) (Liao et al., 2014) R Core Team, DESeq2 (Love et al., 2014)) and extensive QC and version reporting ((MultiQC (Ewels et al., 2020), FastQC (Daley and Smith, 2013), deepTools (Ramirez et al., 2016), ataqv (Orchard et al., 2020)). All

data was processed relative to the mouse Ensembl GRCm38 release 95. A set of consensus peaks was created by selecting peaks that appear in at least one sample. Counts per peak per sample was obtained with featureCounts (Liao et al., 2014).

For Motif enrichment analysis, peaks from WT_R1 as it was the only one that gave sufficient number of peaks, was used with the "findMotifsGenome.pl" script from the HOMER suite (Heinz et al., 2010)

2.11 ATAC-seq

2.11.1 Sample preparation

Isolated mouse crypts were dissociated to single cells as described in section 2.5.1 and single cell numbers and viability were assessed using Trypan blue dye and Neubauer chamber. 25.000 cells per sample were transferred to a fresh tube, pelleted and incubated in RSB buffer (10mM Tris-Cl pH 7.4, 10mM NaCl and 3mM $MgCl_2$) supplemented with 0.1% v/v NP-40 (Sigma, 11332473001), 0.1% v/v Tween-20 (Sigma, 11332465001) and 0.01% Digitonin (Promega, G9441) to isolate intact nuclei. Isolated nuclei were subsequently treated with Tn5 transposase (Illumina, 20034197) for 30min at 37^{o}C with agitation for DNA tagmentation. DNA was immediately purified using Qiagen Mini Elute kit (Qiagen, 28004). Purified DNA was subsequently used for library preparation using NEBNext® High-Fidelity 2X PCR Master Mix (NEB, M0541S) using primers with Nextera dual indexes in a 20µl final reaction volume. PCR amplification included 5min incubation at 72^{o}C, followed by 30sec of DNA denaturation at 98 ^{o}C and 12 cycles of the following: 98 ^{o}C for 10sec, 63 ^{o}C for 30sec and 72 ^{o}C for 1min. PCR products were cleaned up using Ampure XP beads (Beckman Coulter, A63881) according to manufacturer's instructions. The quality of the final DNA library was confirmed on the Agilent Tapestation before the samples were submitted to sequencing.

2.11.2 ATAC-seq data analysis

The nf-core/atacseq pipeline (version 1.2.1) (Ewels et al., 2020) written in the Nextflow domain specific language (version 19.10.0) (Di Tommaso et al., 2017) was used to perform the primary analysis of the fastq samples in conjunction with

Singularity (version 2.6.0) (Kurtzer et al., 2017). The command used was "nextflow run nf-core/atacseq -profile crick --input /Path_to_desing/design.csv –fasta Mus_musculus.GRCm38.dna_sm.toplevel.fa --gtf Mus_musculus.GRCm38.95.gtf --gene_bed Mus_musculus.GRCm38.95.bed --macs_gsize 2.6e9 --blacklist mm10.blacklist.bed --narrow_peak -r 1.2.1 -resume".

To summarise, the pipeline performs adapter trimming (Trim Galore!- https://www.bioinformatics.babraham.ac.uk/projects/trim_galore/), reads alignment (BWA) and filtering (SAMtools) (Li et al., 2009), (BEDTools) (Quinlan and Hall, 2010); BamTools (Barnett et al., 2011); pysam - https://github.com/pysam-developers/pysam; picard-tools - http://broadinstitute.github.io/picard)), normalised coverage track generation ((BEDTools) (Quinlan and Hall, 2010); bedGraphToBigWig (Kent et al., 2010)), peak calling (MACS) (Zhang et al., 2008) and annotation relative to gene features (HOMER) (Heinz et al., 2010), consensus peak set creation (BEDTools), differential binding analysis ((featureCounts) (Liao et al., 2014) R Core Team, DESeq2 (Love et al., 2014)) and extensive QC and version reporting ((MultiQC (Ewels et al., 2020), FastQC (Daley and Smith, 2013), deepTools (Ramirez et al., 2016), ataqv (Orchard et al., 2020)). All data was processed relative to the mouse Ensembl GRCm38 release 95. A set of consensus peaks was created by selecting peaks that appear in at least one sample. Counts per peak per sample was then imported on DESeq2 within R environment for differential expression analysis. Pairwise comparisons between genotypes in each condition, and between conditions per genotype were carried out and differential accessible peaks were selected with an FDR < 0.05.

For footprinting analysis TOBIAS (v 0.12.10) (Bentsen et al., 2020) was used by running the following pipeline (https://github.com/luslab/briscoe-nf-tobias). The pipeline runs TOBIAS' ATACorrect, ScoreBigwig, BINDetect and generates PlotAggregate metaplots on merged replicate bam files. TOBIAS was run on set of consensus peaks used for the differential analysis (see above). As described before (Bentsen et al., 2020), all TFs with -log10(p-value) above the 95% quantile or differential binding scores smaller/larger than the 5% and 95% quantile are coloured. Selected TFs are also shown with labels.

Chapter 3: Identification of novel regulators of intestinal homeostasis

3.1 Introduction

Intestinal stem cell proliferation and differentiation is a highly regulated process. As extensively discussed in Chapter 1, a variety of signalling pathways is involved in this process, orchestrating the complete renewal of gut epithelial cells every 5 days. Wnt, Notch, Egf, Bmp and Hedgehog signalling pathways are the gatekeepers of proper intestinal epithelial function during homeostasis and also participate in tissue regeneration upon damage.

The remarkable ability of the small intestine to replenish its cells at such a high rate and respond to injury has traditionally turned it into an excellent model to understand adult stem cell function (Baulies et al., 2020b, Spit et al., 2018). Expanding our knowledge on how adult tissue homeostasis is regulated is the first and most important step towards identifying mutations that can drive disease. Intestinal diseases include -but are not limited to- cancer, inflammatory bowel disease (IBD), ulcers and coeliac disease. These can be a result of faulty regulation of either the rapidly diving stem cells or their progeny. Despite extensive characterisation of signalling pathways regulating ISC plasticity and fate decision, the transcriptional network underlying this process is not fully understood. We hypothesised that there is a gene regulatory network at the early progenitor cells that promotes stem cell niche exit and subsequent differentiation. Therefore, this project aims to characterise the transcriptional control at the +4/+5 early progenitor cells at the crypts of the small intestinal epithelium. Here, we report the discovery of the transcription factors Arid3a, Mtg8 and Mtg16 and we elucidate their unique contributions in intestinal epithelial homeostasis.

3.2 Results

3.2.1 Comparative transcriptomic analysis of stem cells and early progenitor cells

Soon after the identification of Lgr5 as a *bona fide* marker of the cycling stem cells residing at the bottom of the crypt, several studies attempted to identify additional markers of either CBC stem cells or quiescent +4 cells that may contribute to plasticity and regeneration. The major hurdle of studying early progenitor cells is the lack of specific cellular markers. In 2012, Munoz et al. used the combination of two different microarray platforms to screen transcriptomic and proteomic differences between the two populations and define a specific gene signature for Lgr5-positive stem cell genes. This signature included both genes that were expressed uniquely at the bottom of the crypt as well as genes that exhibited a gradient of expression similar to the one of Wnt signalling (Munoz et al., 2012). This elegant study provided an excellent database for identifying genes that may act as key modulators of intestinal homeostasis by fine tuning the stem cell-to-daughter cell transition.

For this study, the *Lgr5-EGFP-ires-CreERT2* knock-in reporter mouse line was used, where the *Lgr5* locus drives the expression of GFP. Lgr5-positive cells divide on average every 21.5h (Schepers et al., 2011). On the other side, GFP protein has a half-life of 26h (Nash and Lever, 2004), that is significantly longer that the stem cell division rate. That means that Lgr5-negative early progenitor cells positioned just above the stem cell niche at positions +4/+5 will have residual but lower levels of GFP expression. Hence, this model allows us to stratify crypt stem/progenitor cells in the absence of specific molecular markers, where Lgr5-positive cells have the highest GFP expression. Subsequently, cells were sorted in 5 fractions and these sorted populations were marked as 5+, 4+, 3+, 2+ and 1+ ranging from highest (5+) to lowest (1+) GFP expression (GSE36497).

To focus on early stem-progenitor cell transition, we decided to exclude the lowest 1+ fraction in our re-analysis, resulting in a final of 6 arrays to be analysed. We set a fold change threshold of >1.5 in at least 3 arrays and we identified a total of 2546 genes that were positively or negatively enriched at the 5+ population (figure 3.1). In contrast to the original study, our focus was shifted to the lower expressing GFP (early

progenitor) populations that may contain potential new modulators crucial for epithelial proliferation and differentiation upon stem cell niche exit. As expected, the list included genes that are already known to play a role in early fate decision, mainly downstream of Notch signalling (such as *Atoh1*, *Gfi1*, *Spdef*, *Dll1* and *Dll4*) as well as well-established markers of all differentiated cells (such as *Alpi*, *ChgA*, *Muc2*, *Dclk1* and *Gcg*). We also confirmed that the 5+ population had a significantly higher expression of the stem cell genes *Lgr5*, *Olfm4*, *Ascl2*, *Smoc2* and *Rnf43* (figure 3.1).

After exclusion of all known markers of stem cells, progenitor cells and differentiated cells and removal of duplicate genes from the microarray data, we searched for transcription factors that are enriched in early progenitor cells. We performed an extensive literature review and we shortlisted 3 candidate genes as putative modulators of ISC homeostasis: the DNA-binding transcription factor Arid3a (A+T Rich Interaction Domain3A) and two transcriptional co-repressors Mtg8 and Mtg16 (Myeloid Translocation Gene 8 / 16). Arid3a has mainly been associated with hematopoietic progenitor cell differentiation (Webb et al., 2011) and immunoglobin production (Herrscher et al., 1995). However, its role in gut homeostasis has never been explored (more details in section 3.2.3). On the other hand, Mtg8 and Mtg16 have been previously reported to be essential for ISC regulation both in development (Calabi et al., 2001) and in adult stages (Poindexter et al., 2015), but the exact mechanism of action is still missing.

This thesis will focus on the work that has been done on describing the localisation and upstream regulation of Arid3a and its paralog Arid3b (Chapter 3) as well as their role in intestinal homeostasis (Chapter 4) and irradiation-induced regeneration (Chapter 5). During my PhD, I have also supported a post-doc in the lab on her work on Mtg16 and Mtg8, mainly on characterising the upstream regulation of both genes by Notch signalling and the effects of *Mtg16* deletion in lineage commitment. These results will be presented in the next section of this chapter.

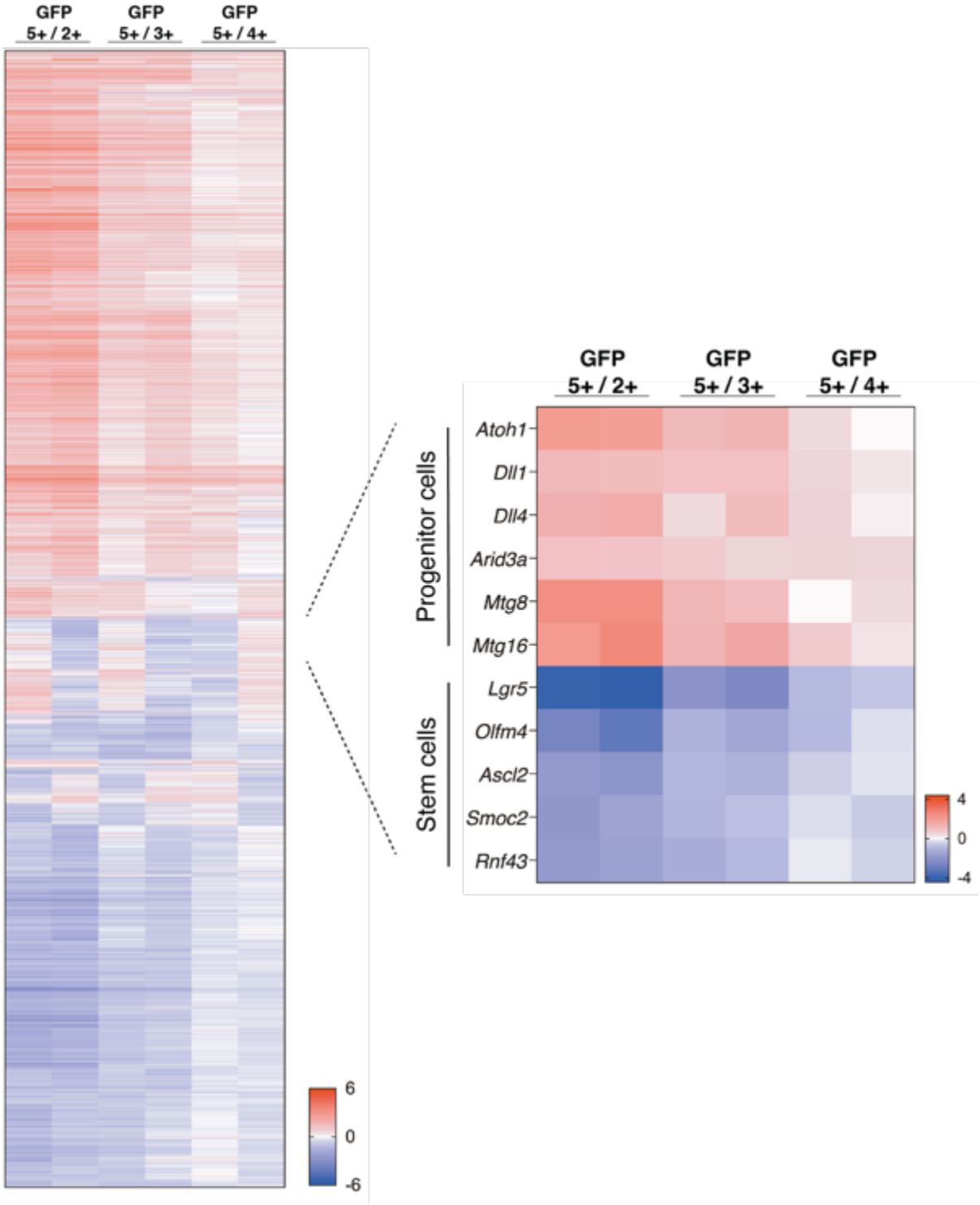

Figure 3.1 | Differential gene expression between Lgr5-positive stem cells and their immediate progeny.
Re-analysis of previously published transcriptomics data reveals two distinct gene expression signatures. Our analysis revealed an enrichment of Arid3a, Mtg8 and Mtg16 at the progenitor population. Genes shown on the left panel have >1.5-fold difference in at least 3 arrays. Representative examples are shown on the right panel.

3.2.2 Mtg8 and Mtg16 are supressed by Notch signalling and regulate niche exit and lineage specification

Mtg family of proteins facilitates transcriptional repression via binding to DNA-binding transcription factors and other co-repressors and histone-modifiers (Rossetti et al., 2004). The aforementioned microarray analysis of differential gene expression (figure 3.1) identified that two members of the Mtg family, Mtg8 and Mtg16, are enriched at the progenitor cell population. Mtg proteins have been proposed to be essential for tight regulation of spatial and temporal gene expression and were first identified in leukaemia initiating translocation fusions (Rossetti et al., 2004). The Mtg family also includes a third member, Mtgr1 (Rossetti et al., 2004). In the blood, Mtg16 regulates hematopoietic progenitor cell proliferation and lineage differentiation through interaction with Notch (Chyla et al., 2008, Engel et al., 2010). Previous studies have demonstrated the regulatory roles of Mtg genes in gut development and adult homeostasis. Mtg16 has been reported to supress ISC proliferation and regulates crypt regeneration upon injury (Poindexter et al., 2015). Moreover, Mtgr1 has been shown to regulate secretory lineage commitment and maintenance (Amann et al., 2005, Parang et al., 2015). On the other hand, the role of Mtg8 in the intestine is the least studied among the three members of the family. Most mice with homozygous loss of *Mtg8* died postnatally. Pups surviving two days after birth showed severe impairment in gut growth (Calabi et al., 2001). An intestinal epithelial-specific *Mtg8* knockout mouse model will help to further characterize its role in the intestinal epithelium. Our lab has recently generated this model and detailed analysis of the role of Mtg8 in the small intestine is currently undergoing.

The first part of the study on the role of Mtg8 and Mtg16 in ISC regulation has already been published. As mentioned before, this project was led by a post-doc in the lab and this section aims to highlight the results that were generated by me as part of the project.

The two transcriptional co-repressors Mtg8 and Mtg16 are specifically expressed at the dynamic progenitor cells. Double RNAscope staining showed significant overlapping expression of *Mtg16* and the secretory progenitor marker *Atoh1*, while *Mtg8* was only expressed in *Atoh1*-negative cells (Baulies et al., 2020a). This led us to hypothesize that Mtg8 and Mtg16 are regulated by Notch signalling at the progenitor cells to regulate niche exit and lineage specification. Indeed, treatment

of organoids with γ-secretase inhibitor DAPT (to inhibit Notch signalling) showed significant upregulation of both *Mtg8* and *Mtg16*, similar to control genes *Atoh1* and *Dll1* (figure 3.2A). To test if the Notch-regulated expression of *Mtg8* and *Mtg16* is dependent on Atoh1, organoids derived from VillinCreER;*Atoh1*$^{fl/fl}$ mice were treated with DAPT for 48h. Similar to *Dll1* and *Dll4* expression, DAPT- mediated upregulation of *Mtg8* and *Mtg16* was abolished upon hydrotamoxifen (4-OHT)-induced excision of *Atoh1* (figure 3.2B). To further confirm that the two co-repressors are regulated by Notch via Atoh1, and that the upregulation observed at the organoids was not due to changes in cell fate upon Notch inhibition, *ATOH1* was overexpressed in 293T cells. Ectopic overexpression of ATOH1 resulted in significant upregulation of both *MTG8* and *MTG16*, as well as the control target *DLL1* (figure 3.2C). We have also treated mouse organoids with DAPT inhibitor and collected samples at various early timepoints (4h, 8h, 12h, 13h, 14h, 15h, 16h) to assess gene expression changes prior to fate alteration. We confirmed that the transcriptional repressor *Hes1,* an essential component downstream of Notch, was downregulated as early as 4h after Notch inhibition. Interestingly, *Atoh1* expression was upregulated at 12h, while *Mtg16* was significantly increased at 15h and *Mtg8* only at 48h (data not shown).

Previously published data (Poindexter et al., 2015) and histological analysis of *Mtg16*-/- animals in our lab showed an increase in stem cell genes and a reduction in absorptive enterocyte markers (*Alpi, Villin, Fabp1, Apoa4*). To further investigate the role of Mtg16 in niche exit and fate decision, RNA-seq of WT versus *Mtg16*-/- intestinal crypts (N=3) was performed (figure 3.2D). Differential gene expression analysis revealed 478 genes (False Discovery Rate (FDR) <0.1) that were significantly upregulated or downregulated upon Mtg16 loss. Consistent with the immunostaining analysis, stem cell and Wnt signature genes (such as *Lgr5*, *Axin2*, *Sox9*) were upregulated whilst multiple enterocyte markers (such as *Alpi*, *Fabp1*, *Apoc2*) were decreased (figure 3.2D). In addition, markers of Paneth cells and enteroendocrine cells were increased (figure 3.2D). Gene set enrichment analysis (GSEA) confirmed enrichment of stem cell and secretory signature and loss of absorptive enterocytes in *Mtg16*-/- animals (figure 3.2E).

Taken together, these results contributed to the findings of the new regulators of intestinal stem cells: Mtg8 and Mtg16 are repressed by Notch signalling to drive stem cell niche exit and determine absorptive versus secretory fate decision and by competing with Atoh1 transcription (Baulies et al., 2020a).

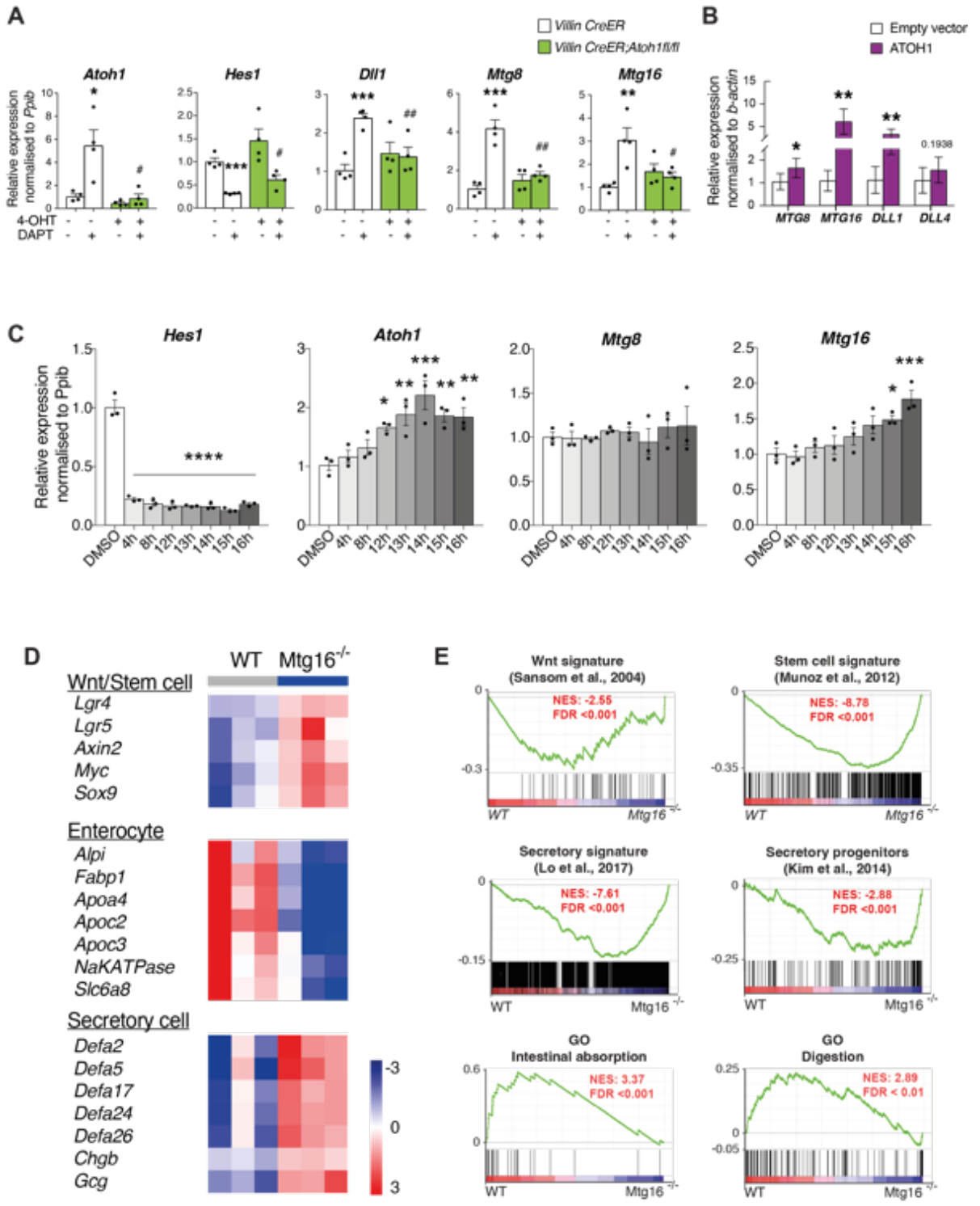

Figure 3.2 | Mtg8 and Mtg16 are master regulators of niche exit and fate decision downstream of Notch.
(A) qRT-PCR of VillinCreER and VillinCreER; Atoh1$^{fl/fl}$ mouse organoids treated with Notch inhibitor, DAPT for 48h. Four independent experiments were performed (n=4). Data represent mean ± s.e.m. *P<0.05, **P<0.01, ***P<0.001, compared with untreated control group; #P<0.05, ##P<0.01, compared with DAPT-treated control group, two-sided t-test. (B) qRT-PCR analysis of the indicated genes upon ATOH1 overexpression in HEK293T cells. Three independent experiments were performed (n=3). Data represent mean ± s.e.m. *P<0.05, **P<0.01 , two-sided t-test. (C) Time-course experiment of WT mouse organoids treated with DAPT for various timepoints. Organoids were established from three biologically independent animals (N=3). Data represent mean ± s.e.m. *P<0.05, **P<0.01 , ***P<0.001, two-sided t-test. (D) Heatmap showing selected genes differentially expressed in WT and Mtg16-/- intestine (FDR cut-off <0.1). (E) GSEA probing for various gene lists.

3.2.3 Validation of Arid3a enrichment at the progenitor population

As described in section 3.2.1, our initial re-analysis of differential gene expression of ISCs and their immediate progenitors identified Arid3a as a putative novel modulator of epithelial homeostasis. Interestingly, the role of Arid3a in ISC regulation and tissue homeostasis has never been studied in the past.

ARID3A is a transcription factor that contains a DNA binding domain which interacts with A+T rich genomic regions, and it is the founding member of the ARID family of proteins (Herrscher et al., 1995, Patsialou et al., 2005). It is a member of the ARID3 sub-family along with ARID3B and ARID3C (Korn and Schlundt, 2022). All seven sub-families of ARID-containing proteins have a highly conserved ARID domain that spans about 100 amino acid residues (Wilsker et al., 2005). All 3 members of the ARID3 sub-family share an approximately 80% similarity of their ARID domain (figure 3.3). Interestingly, the ARID3 subfamily have a unique extended ARID domain (eARID) of the N- and C-terminus of the core ARID domain that is unique to this sub-family and forms extra alpha helices in the protein structure which facilitate DNA binding (Korn and Schlundt, 2022, Kortschak et al., 2000, Wilsker et al., 2005). ARID3 family of proteins also contain a highly conserved REKLES domain (figure 3.3), which is divided in two subdomains: a N-terminal REKLES-α and a highly conserved C-terminal REKLES-β that are required for nuclear import and export, respectively. However, ARID3B lacks the ability of nuclear to cytoplasm shuttling, and is trapping ARID3A in the nucleus through its REKLES-β domain (Kim et al., 2007, Kim and Tucker, 2006, Shandala et al., 2002). ARID3A also has a N-terminus acidic transactivation domain (NCBI).

The role of ARID3A in the haematopoietic system has been extensively studied. ARID3A was initially associated with transcriptional regulation of immunoglobulin heavy chain (IgH) through a complex including Bruton's tyrosine kinase (Btk) and transcription factor II-I (TFII-I) (Lin et al., 2007). In the blood, ARID3A has been shown to drive normal development of both myeloid and B lineage specification, where deletion of the mouse Arid3a, leads to lethality at embryonic stages, due to defective haematopoiesis (Ratliff et al., 2016). Interestingly, Arid3a also regulates B-cell response to antigen. Post-translational palmitoylation of cytoplasmic Arid3a leads to its accumulation in lipid rafts which regulates B-cell antigen receptor (BCR) signalling (Schmidt et al., 2009). Moreover, Arid3a shows an enrichment in

megakaryocytes compared to haematopoietic progenitor cells and it has been proven to promote terminal megakaryocytic differentiation (Alejo-Valle et al., 2022).

Arid3a has been reported as both a positive and negative regulator of cell cycle progression. It can act as an oncogene and can induce proliferation in RAS-induced senescence (Peeper et al., 2002). It has also been reported to stimulate E2F1 transcriptional activity (Suzuki et al., 1998). On the other hand, tumour suppressor p53 activates Arid3a expression which in turn regulates p53 protein stability and control cell cycle arrest (Lestari et al., 2012, Ma et al., 2003).

Arid3a has also been implicated in chromatin remodelling, embryonic development, and epigenetic post-translational modifications (An et al., 2010, Lin et al., 2007, Popowski et al., 2014, Rhee et al., 2014). Recently, loss of Arid3a was also linked with developmental plasticity (An et al., 2010) with report showing that Arid3a represses embryonic stem cells (ESCs) and mouse embryonic fibroblasts (MEFs) reprogramming by directly binding to promoter regions of Oct4, Sox2 and Nanog (Popowski et al., 2014).

In the gut, *Arid3a* overexpression has been associated with development of colorectal cancer, although its high expression is also linked to good prognosis in patients with colorectal carcinoma due to increased chemosensitivity of cancer cells (Li et al., 2022, Song et al., 2014, Tang et al., 2021). More recently, a single-cell analysis of the developing gut identified *Arid3a* as a key regulator of epithelial cell development, whilst the mechanism remains unknown (Fawkner-Corbett et al., 2021).

ARID3A interplays with its paralogue ARID3B, in chromatin conformation and gene regulation of cancer cells (Liao et al., 2016). Moreover, the two Arid genes cooperate in gene regulation of B cells (Kurkewich et al., 2016) and have also been reported to have a large number of common target genes in ovarian cancer (Dausinas et al., 2020). Of note, their role is redundant during development (Webb et al., 2011). Although, Arid3b did not appear in our initial transcriptomics screening (Chapter 3.2.1), we hypothesized that there might be functional redundancy in their role in small intestinal epithelial cells. Hence, we decided to study the role of both genes. Arid3c has been discovered more recently and it is not expressed at the small intestine (Protein atlas), thus it was not included in our studies.

Figure 3.3 | Schematic representation of mouse Arid3a and Arid3b proteins.
Both proteins share a highly preserved ARID DNA binding domain and a C-terminal REKLES motif.

Before proceeding to further exploring the role of Arid3a and Arid3b in small intestinal homeostasis, we first validated their expression in the intestine. As extensively discussed in section 3.2.1, the initial screening was based on a published dataset of sorted crypt cells from the *Lgr5-EGFP-ires-CreERT2* mouse line based on their GFP expression. Taking advantage of the same mouse line, we FACS-sorted three different populations based on their GFP expression and we annotated them as GFP-high, GFP-low and GFP-very low (figure 3.4A-B). GFP-high are Lgr5-positive ISCs, GFP-low are the immediate +4/+5 progenitors and GFP-very low are the early TA cells. qRT-PCR analysis of the three populations confirmed that *Arid3a* was significantly enriched at the progenitor population compared to ISCs. Of note, GFP-very low cells showed an even higher but not statistically enrichment of *Arid3a* (figure 3.4C). As expected, expression of *Arid3b* did not show any variation among the three populations (figure 3.4C). *Lgr5* and *Atoh1* were used as control genes for our sorting, where *Lgr5* was more enriched at ISCs and *Atoh1* at progenitor cells (figure 3.4C).

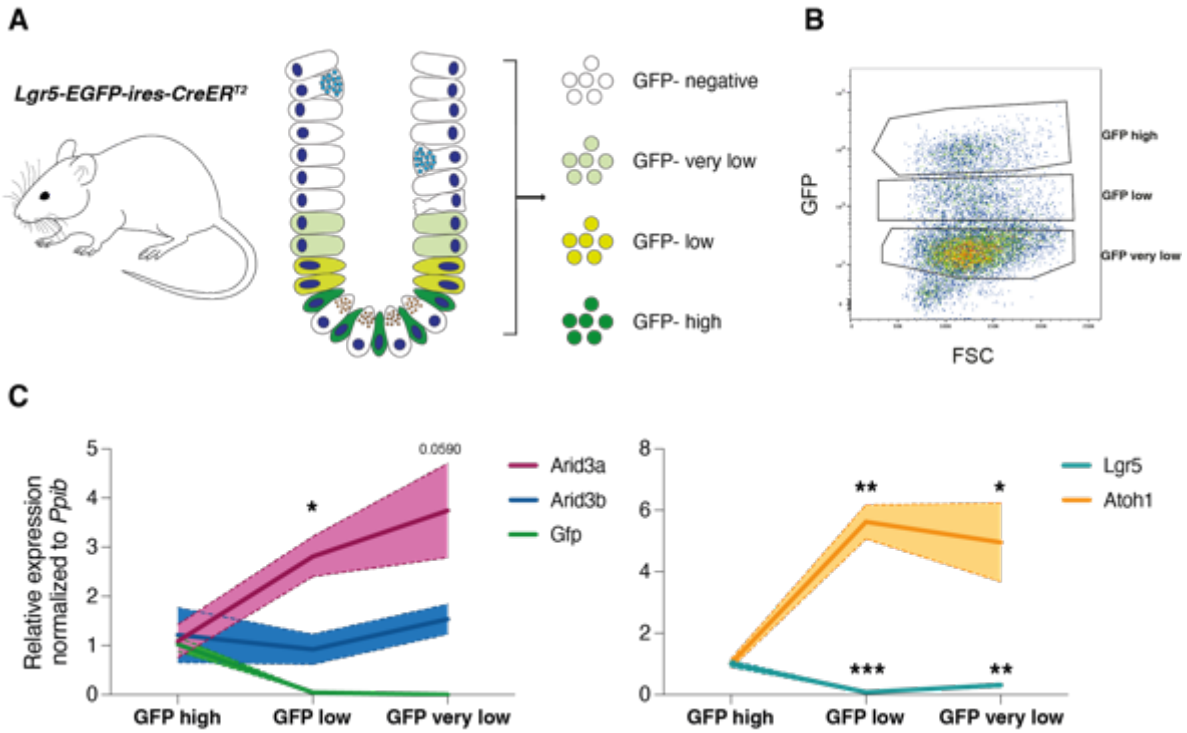

Figure 3.4 | Validation of Arid3a enrichment at progenitor cells.
(A) Schematic representation of stem cells, progenitor cells and TA cells based on their GFP expression. (B) Representative plot from our FACS sorting of GFP+ cells from the Lgr5-EGFP-ires-CreERT2 mouse line. (C) qRT-PCR analysis of the three sorted populations. Three biologically independent animals (N=3). Data represent mean ± s.e.m. (light colour area) *P<0.05, **P<0.01, ***P<0.001, two-sided t-test.

3.2.4 Arid3a expression forms a gradient and accumulates at the tip of the villus

After confirming the enrichment of *Arid3a* at the progenitor population, we sought to fully characterise the expression of Arid3a throughout the crypt-villus axis of the intestinal epithelium. RNAscope technology (figure 3.5A) and immunohistochemistry (figure 3.5B) were used to determine the expression of Arid3a mRNA and protein levels, respectively. In both cases, we uncovered a very unique pattern of expression: Arid3a forms a gradient of expression that accumulates at the tip of the villus. At the crypt level, mRNA levels of Arid3a were detected in most cells, while protein was detected only in cells at the +4/+5 position and above. Of note, at progenitor cells, expression of Arid3a was both cytoplasmic and nuclear (figure 3.5B). On the other hand, RNAscope analysis showed that Arid3b was ubiquitously expressed at both crypt and villus compartments without specific enrichment (figure 3.5E). Although we also tested antibodies against Arid3b protein, none of them produced specific staining.

To further probe the localisation of Arid3a at the crypt, we performed double RNAscope staining of *Arid3a* with *Lgr5* (ISC marker) and *Atoh1* (secretory progenitor and Paneth cell marker). At the bottom of the crypt, *Arid3a* showed both overlapping and exclusive staining with both *Lgr5* and *Atoh1,* indicating that *Arid3a* is also expressed in both stem cells and Paneth cells, although its expression at these cells was minimal (figure 3.5C). Quantification of the RNAscope data revealed that Arid3a not only was enriched at the +4/+5 cells as compared to the ISCs, but this enrichment was maintained throughout the upper crypt (figure 3.5C). This result is in agreement with our qRT-PCR data from the initial validation experiment that was discussed in section 3.2.3 (figure 3.4C). Of note, *Arid3a* was expressed in both *Atoh1*+ and *Atoh1*- cells at the +4/+5 positions (figure 3.5C). Stromal expression of *Arid3a* was also detected (figure 3.5A,B), since stromal cells of the small intestine include B cells which express high levels of Arid3a (Mowat and Agace, 2014, Ratliff et al., 2014).

To confirm the enrichment of Arid3a at the villus compartment, we performed crypt-villus fractionation of mouse proximal small intestinal tissue followed by qRT-PCR analysis of the two compartments. As expected, the stem cell-specific marker *Olfm4* was enriched at the crypt fraction, while the enterocyte marker Alkaline phosphatase (*Alpi*) was enriched at the villus. In accordance with our RNAscope data,

Arid3a showed a 20-fold upregulation in the villus compared to the crypt (figure 3.5D).

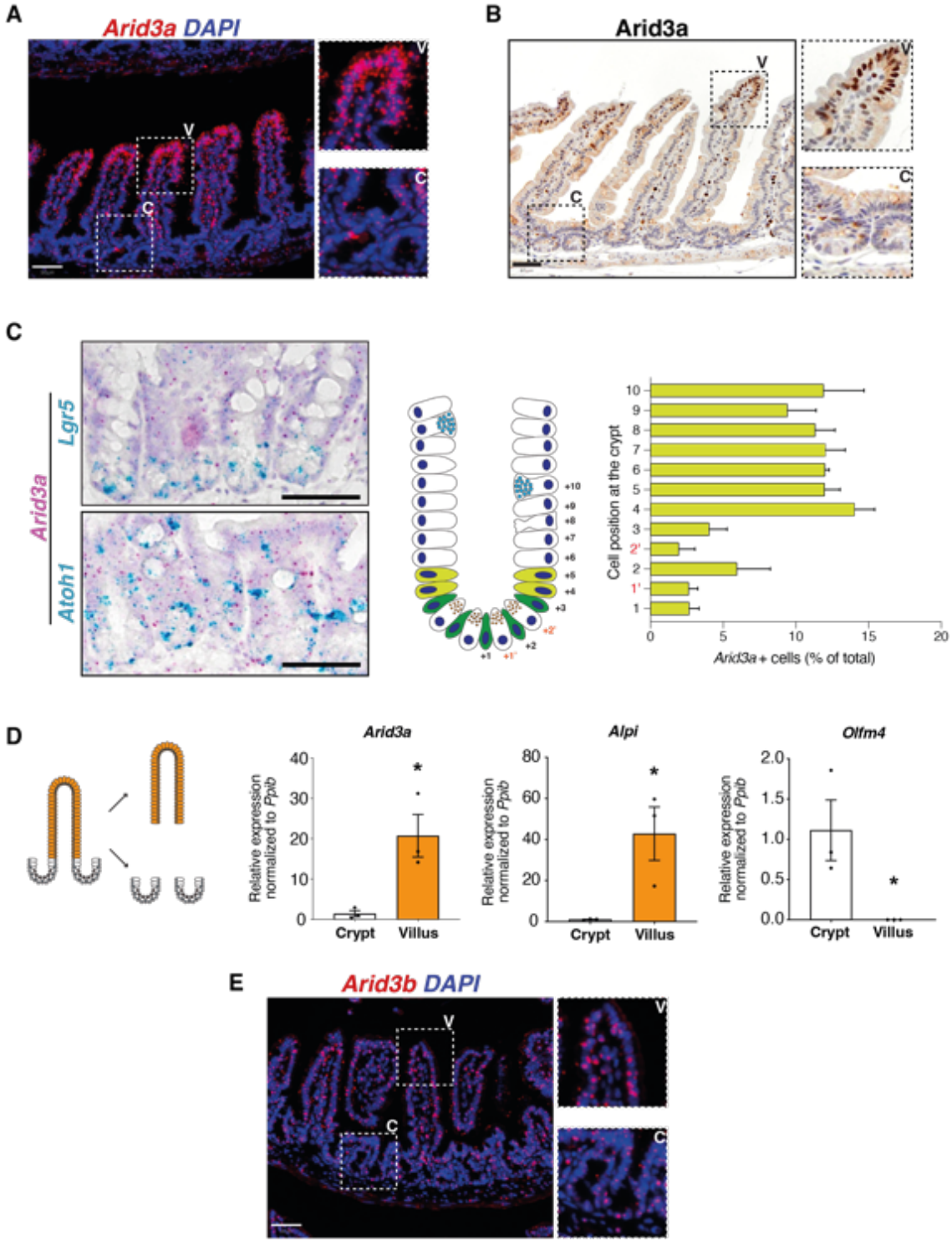

Figure 3.5 | Arid3a exhibits a gradient of expression throughout the crypt-villus axis.
(A) RNAscope of Arid3a at WT mouse small intestine. Staining was performed at three different animals (N=3). (B) Protein staining of Arid3a at WT mouse small intestine. Staining was performed at three different animals (N=3). (C) Dual RNAscope of Arid3a with Lgr5 or Atoh1 at WT mouse small intestine. Each staining was performed at three different animals (N=3). Quantification was performed using the Arid3a/Lgr5 co-stain. (D) qRT-PCR analysis of crypt and villus fractions. Three biologically independent animals (N=3). Data represent mean ± s.e.m. *P<0.05, **P<0.01, ***P<0.001, two-sided t-test. (E) RNAscope of Arid3b at WT mouse small intestine. Staining was performed at three different animals (N=3). Scale bars, 50μm. C: crypt, V: villus.

Enterocytes are the most prominent type of intestinal epithelial cells. High expression of Arid3a in most villus cells suggested that it is expressed at enterocytes. We further sought to test that if Arid3a is also expressed at other secretory cells in the villi. By combing RNAscope staining of *Arid3a* and immunofluorescent staining to detect the protein levels of Mucin 2 (Muc2), Chromogranin A (ChgA) and Lysozyme (Lyz), we confirmed that *Arid3a* is also expressed in goblet cells, enteroendocrine cells and Paneth cells, respectively (figure 3.6).

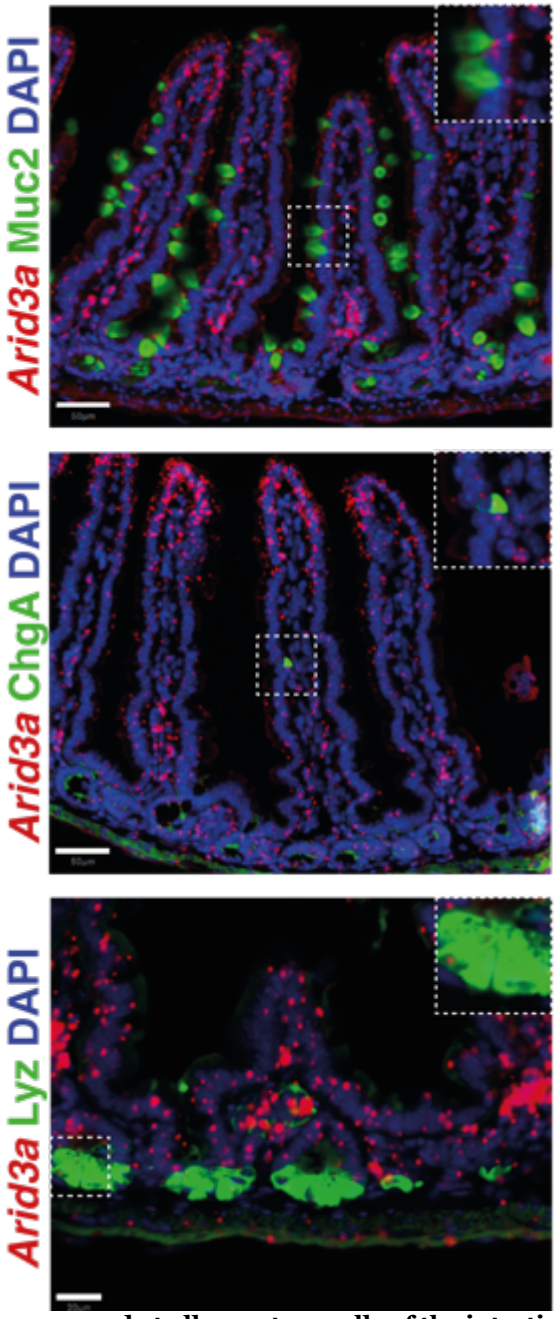

Figure 3.6 | Arid3a is expressed at all secretory cells of the intestinal epithelium.
Combined Arid3a RNAscope scope staining with immunofluorescent protein staining of Muc2, ChgA and Lyz. Each staining was performed at three different animals (N=3). Scale bar, 50µm for Arid3a/Muc2 and Arid3a/ChgA and 20µm for Arid3a/Lyz.

3.2.5 Arid3a and Arid3b are negatively regulated by Wnt

Arid3a expression was enriched at the upper crypt with minimal expression at the ISCs, in a pattern that is opposite to the Wnt gradient, implying that Wnt signalling may play a potential regulatory role in its expression. To examine this hypothesis, *ex vivo* WT mouse intestinal organoids were treated with two different Wnt inhibitors, LF3 and LGK974, for 48h. LF3 is a small molecule that robustly disturbs the β-catenin/TCF4 interaction complex, leading to inhibition of Wnt signalling (Fang et al., 2016). LGK974 is another small molecule that inhibits specifically Porcupine (Porcn), an O-acyltransferase that is required for palmitoylation and subsequent secretion of Wnt ligands (Liu et al., 2013). Successful Wnt inhibition was confirmed by downregulation of mRNA levels of known Wnt target genes, such as *Axin2* and *Cyclin D1* for LF3 inhibitor (figure 3.7A) and *Axin2* and *Sox9* for LGK974 inhibitor (figure 3.7B). In contrast, *Arid3a* expression was upregulated upon treatment with either of the two inhibitors, suggesting a suppressive role of Wnt in Arid3a expression (figure 3.7A,B). *Arid3b* expression was not changed when organoids were treated with the LF3 inhibitor but was upregulated when treated with the LGK974 inhibitor (figure 3.7A,B). Of note, the LGK974 treatment seemed to have a more drastic inhibition of Wnt signalling after 48h (figure 3.7A,B).

To validate the putative role of Wnt in *Arid3a* and *Arid3b* regulation, we further examined an independent Wnt overactivation model. To this end, isogenic Wnt-high mouse organoids carrying a truncated Apc (Apc5, generated by our lab) were used (Novellasdemunt et al., 2017). Consistent with previous observations, *Arid3a* expression was downregulated, while *Axin2* and *Cyclin D1* were significantly increased in the Wnt-high Apc5 organoids (figure 3.7C). Similarly to our LF3-treated organoid data, *Arid3b* expression was not altered in Apc5 organoids.

Wnt signalling regulates ISCs self-renewal and manipulation of Wnt in mouse organoids results in changes in cell fate, suggesting that the expression changes of *Arid3a* might be indirect due to increase or decrease of *Arid3a*+ cells. To examine if Wnt directly regulates *Arid3a* without changes of cell fate, we switched to the human colorectal cancer cell line LS174T with activated Wnt signalling driven by β-catenin mutation. LS174T cells were treated with three different doses of LF3 (10, 30 and 60μM) for 24 hours. Subsequent qRT-PCR analysis demonstrated a robust upregulated expression of both *ARID3A* and *ARID3B* in a dose-dependent manner

(figure 3.7D). Expression of Wnt target gene *AXIN2* was used to check the successful inhibition of Wnt (figure 3.7D). Western blot analysis confirmed the upregulation of ARID3A and the downregulation of Wnt target genes SOX9 and CYCLIN D1 at protein level in the same experimental set-up (figure 3.7E). Interestingly, immunofluorescence analysis of ARID3A expression of LF3-treated LS174T cells (10μM) not only confirmed upregulation of ARID3A, but also showed enriched nuclear localisation of ARID3A upon Wnt inhibition (figure 3.7F). Although the underlying mechanism still needs to be uncovered, we speculate that this could be a result of increased ARID3B binding to ARID3A, therefore retaining it at the nucleus and preventing cytoplasmic translocation.

In summary, our data indicates a suppressive role of Wnt signalling on Arid3a expression *in vitro* and *ex vivo* using a human cell line and mouse intestinal organoids, respectively. However, Wnt-mediated inhibition of Arid3b was not consistent. While some of the experimental models showed a strong suppression, others did not. This could be caused by other unknown regulators of Arid3b that have also been altered by manipulation of Wnt pathway.

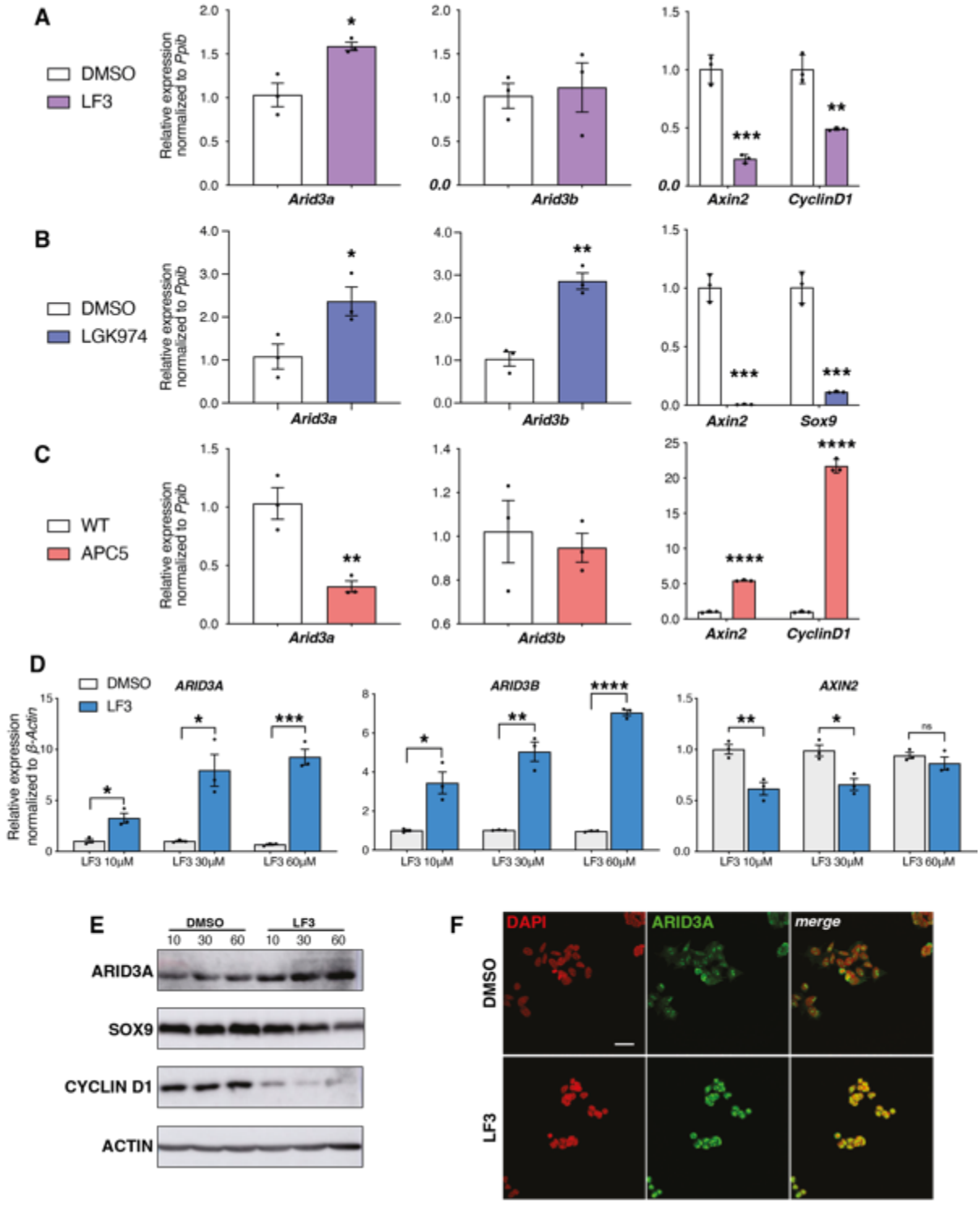

Figure 3.7 | Arid3a and Arid3b are downstream of Wnt signalling.
(A) qRT-PCR analysis of WT organoids treated with LF3 inhibitor for 48h. Organoids were established from three biologically independent animals per group (N=3). (B) qRT-PCR analysis of WT organoids treated with LGK974 inhibitor for 48h. Organoids were established from three biologically independent animals per group (N=3). (C) qRT-PCR analysis of WT versus APC5 mutant organoids. Three independent experiments were performed (n=3). (D) (B) qRT-PCR analysis of LS174T cells treated with three different doses of LF3. Three independent experiments were performed (n=3). (E) Western blot for ARID3A and Wnt target genes SOX9 and CYCLIN D1 upon LF3 treatment of LS174T cells. Two independent experiments were performed (n=2). (F) Immunofluorescence staining for ARID3A shows nuclear localization of ARID3A upon LF3 treatment of LS174T cells, scale bar 100μm. Three independent experiments were performed (n=3). Data represent mean ± s.e.m. *P<0.05, **P<0.01, ***P<0.001, two-sided t-test

3.2.6 Notch and Bmp pathways do not alter Arid3a expression

Since Arid3a is enriched at the early progenitor cells, it might be involved in the initial fate decision taking place at these cells. Notch signalling is the master regulator of this process (Baulies et al., 2020b), although Notch-independent lineage specification has been previously reported (Gerbe et al., 2011, Gracz et al., 2018). Taking this into account, we examined if Arid3a is potentially regulated by Notch. We treated mouse organoids with the γ-secretase inhibitor DAPT (10μM) for 48h and performed qRT-PCR analysis of untreated versus treated organoids. We found that both *Arid3a* and *Arid3b* were unaffected by Notch inhibition (figure 3.8A). Successful inhibition of Notch was confirmed by downregulation of *Hes1* and subsequent de-repression of its target *Atoh1* (figure 3.8A).

Based on the expression pattern of Arid3a and its accumulation at the tip of the villus, we further speculated that its expression might be regulated by Bmp signalling. Bmp is the main driver of differentiation at the villus compartment, which directly supresses Wnt signalling and Lgr5 expression by forming an expression gradient at the villus very similar to that of Arid3a (Qi et al., 2017). To test if Arid3a is regulated by Bmp, mouse organoids were treated with recombinant Bmp4 for 4h, 12h and 24h. As expected, Bmp4 treatment at 24h resulted in upregulation of differentiation markers, predominantly the enterocyte marker *Alpi* (figure 3.8B). Increased expression of the transcriptional suppressor *Id1* and downregulation of its target gene *Lgr5* was observed as soon as 4h after the initial treatment (figure 3.8B). Interestingly, expression of *Arid3a* and *Arid3b* were not altered at 4h and 12h. After 24h of treatment, mRNA levels of both genes were moderately increased but not statistically significantly (figure 3.8B). Since we showed earlier that *Arid3a* and *Arid3b* have a high expression at differentiated villus cells and their upregulation at 24h coincided with loss of stem cells and gain of differentiation, we believe that the transcriptional change of the two Arid genes is likely an indirect effect as a consequence of the cell compositional changes of the organoids rather than a direct cause of dysregulated Bmp signalling.

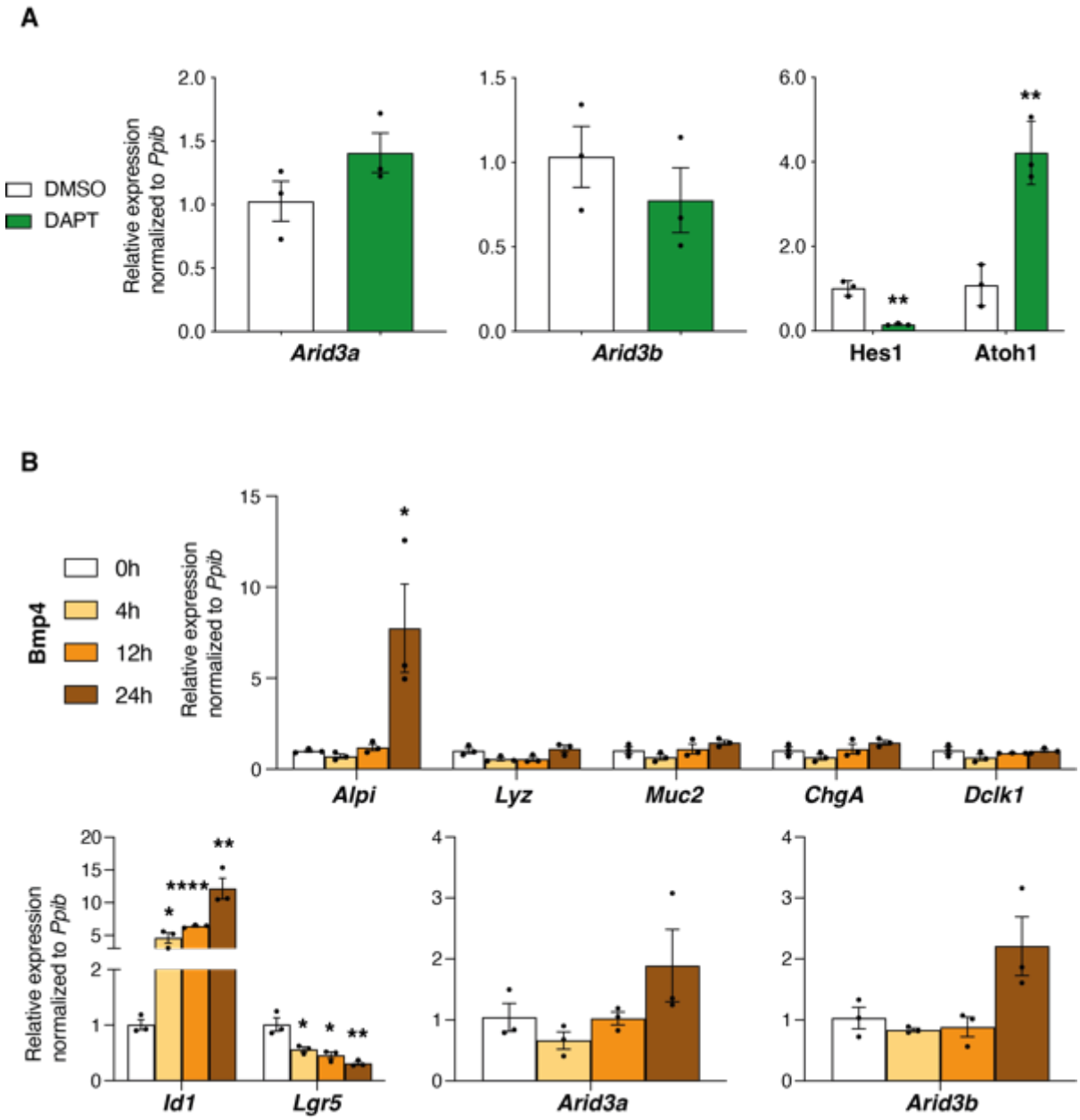

Figure 3.8 | Arid3a expression is unaffected upon modulation of Notch or Bmp pathways.
(A) qRT-PCR analysis of WT organoids treated with DAPT inhibitor for 48h. Organoids were established from three biologically independent animals per group (N=3). (B) qRT-PCT analysis of WT organoids treated with Bmp4 for 4h, 12h and 24h. Upper panel shows markers of differentiation. Lower panel shows results of control (Id1, Lgr5) and tested (Arid3a, Arid3b) genes. Organoids were established from three biologically independent animals per group (N=3). Data represent mean ± s.e.m. *P<0.05, **P<0.01, ***P<0.001, two-sided t-test.

3.2.7 Tgf-β signalling promotes expression of Arid3a at the villus

The Tgf-β family of signalling pathways plays a diverse role in development, cell proliferation, differentiation and cancer (Massague, 2012). Two different categories of secreted ligands activate the two major sub-families of the pathway in receiving cells: (1) Tgf-β ligands, including Tgf-βs, Activins and Nodal and (2) Bmp ligands. At the adult small intestine, only Tgf-β and Bmp ligands have been reported to play a role in homeostasis and disease pathogenesis. Tgf-β pathway is restricted at the villus compartment suppressing proliferation and regulating differentiation and cell death (as described on Chapter 1).

Tgf-β and Bmp pathways are both important for maintenance of intestinal homeostasis and their dysregulation has been linked to cancer and other gastrointestinal diseases (Gudino et al., 2021, Ihara et al., 2017, Tauriello et al., 2018, Zhang and Que, 2020). In particular, Bmp signalling has been reported to have a dominant role in the differentiation of epithelial cells in the gut (Qi et al., 2017). In Chapter 3.2.6, we showed that Bmp signalling does not alter expression of *Arid3a* despite sharing the exact same expression gradient peaking at the villus tip. Here, we examined if Arid3a is regulated by Tgf-β signalling. WT mouse intestinal organoids were treated with recombinant Tgf-β1 for 4h, 12h and 24h followed by qRT-PCR analysis. Interestingly, *Arid3a* expression was upregulated at all treatment timepoints, similar to the expression of Tgf-β target genes *Smad7* and *Id1* (figure 3.8A). Expression of *Arid3b* was only activated at 24h and was unchanged at earlier timepoints (figure 3.8A). Tgf-β signalling is very potent where treatment of organoid cultures with recombinant Tgf-β1 resulted in a 3-6-fold upregulation of differentiated markers of all lineages at 24h (figure 3.8B). It is interestingly to note that Tgf-β activates differentiation of all cell lineages whereas Bmp treatment induces only enterocyte differentiation at the specific timepoint. This discrepancy suggests an underappreciated role of Tgf-β in epithelial cell differentiation along with Bmp. Overall, these results led us to conclude that *Arid3a* is directly modulated by Tgf-β, while the delayed induction of *Arid3b* expression could be a consequence of increased differentiation.

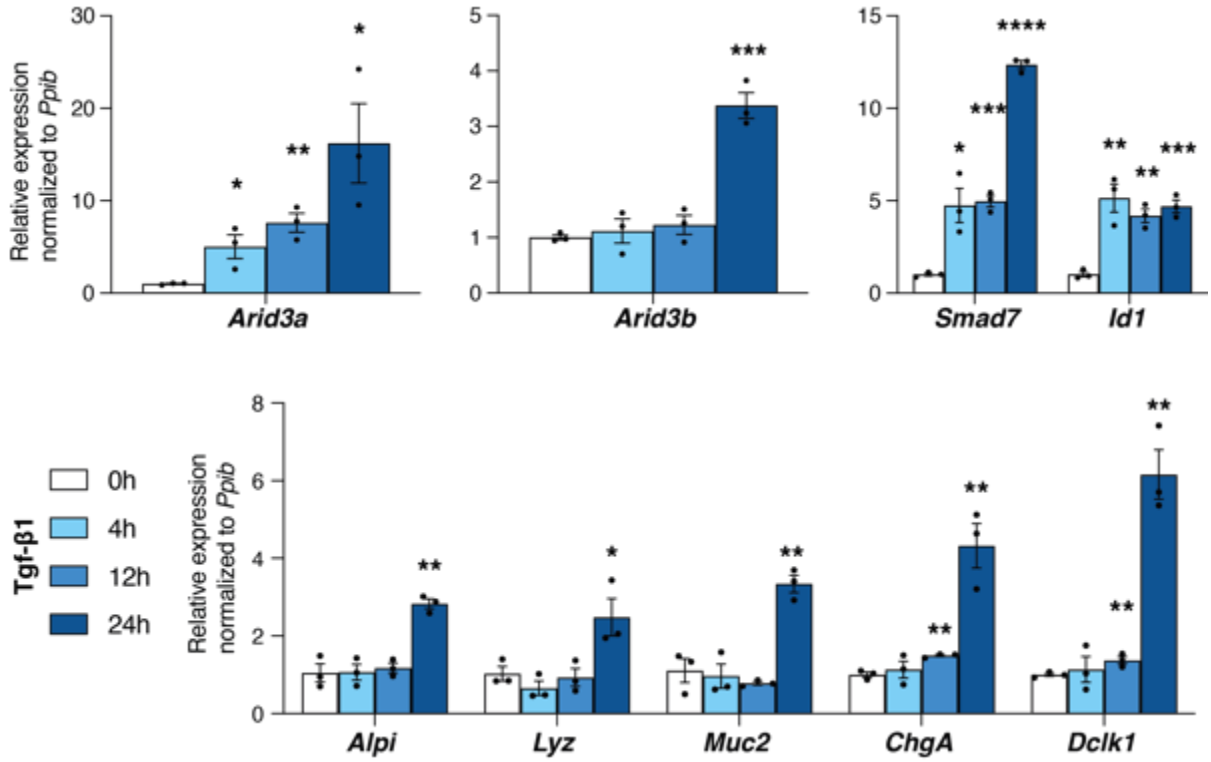

Figure 3.9 | Arid3a expression is modulated by Tgf-β signalling.
qRT-PCT analysis of WT organoids treated with Bmp4 for 4h, 12h and 24h. Upper panel shows results of tested (Arid3a, Arid3b) and control (Id1, Lgr5) genes. Lower panel shows markers of differentiation. Organoids were established from three biologically independent animals per group (N=3). Data represent mean ± s.e.m. *P<0.05, **P<0.01, ***P<0.001, two-sided t-test.

3.3 Summary and short discussion

Proliferation and differentiation of the small intestinal epithelium is tightly regulated by a very complex network of signalling pathways. Lgr5-positive ISCs reside at the bottom of the crypts and rapidly divide to fuel the needs of the epithelium to quickly replenish the upper differentiated cells responsible for food digestion and nutrient absorption. Lineage decision takes place at immediate progenitors that are positioned directly above the stem cell compartment. We hypothesise that genes enriched at the progenitor population might play a role in driving stem cell-progenitor cell transition and the subsequent differentiation. Here we compared global gene expression of ISCs and progenitor cells and we uncovered 2546 differentially expressed genes between the two populations. By focusing on transcriptional regulation, we shortlisted 3 candidate genes as putative regulators of ISC homeostasis: the transcriptional co-repressors Mtg8 and Mtg16 and the transcription factor Arid3a.

The role of Mtg8 and Mtg16 in intestinal epithelial cells has been explored before. Earlier studies showed that Mtg8 is indispensable for complete development of healthy gut (Calabi et al., 2001), but, due to embryonic lethality of Mtg8 null mice its role in adult homeostasis is unknown. On the other hand, Mtg16 has been previously reported to supress proliferation of ISCs (Poindexter et al., 2015). Using RNA-seq and immunohistochemistry, we confirmed that Mtg8 and Mtg16 supress ISC proliferation and promote niche exit, but they also promote differentiation of absorptive cells. Our full study of Mtg revealed that their very specific expression at the +4/+5 progenitor cells is absolutely essential for the initial fate decision. Mtg16 co-occupies binding sites of the transcriptional master regulator of secretory cell differentiation Atoh1 and alters chromatin accessibility (Baulies et al., 2020a), an event that has been directly linked with changes in stemness and differentiation status (Verzi and Shivdasani, 2020).

In this PhD thesis, the main objective is to understand the role of Arid3a in intestinal homeostasis and regeneration. Arid3a is a transcription factor that has been extensively studied in the haematopoietic system where it is highly expressed in in differentiated cells to promote differentiation of different lineages (Ratliff et al., 2014). Expression of Arid3a at the early progenitor cells in the intestine, along with previous studies showing its function in regulating differentiation in other contexts, prompt us to hypothesize that Arid3a might regulate proliferation and differentiation in the gut.

Arid3a share high homology with Arid3b and previous reports have shown that the two proteins work together to promote proliferation and cancer transformation (Liao et al., 2016). More specifically, this happens through formation of Arid3a/Arid3b dimer complexes that recruit Kdm4c to drive expression of stemness genes. Therefore, we decided to study both Arid3a and Arid3b and to further explore any functional redundancy of the two transcription factors. For example, loss of only one of the two genes could result in formation of homodimers of the other transcription factor and it could result in functional compensation. Our initial experiments focused on the localisation and upstream regulation of the two genes under normal physiological conditions. We revealed that both genes are expressed throughout the crypt-villus axis and expressed at all differentiated cells. In particular, *Arid3b* showed a uniform pattern of expression, whereas *Arid3a* showed a remarkable gradient of expression with highest expression at the villus tip (figure 3.10). This expression pattern is similar to that of the haematopoietic system, where their expression is higher in mature cells compared to early progenitors and function as main drivers of differentiation (Ratliff et al., 2016, Ratliff et al., 2014). Similarly, the expression of Atoh1, the main regulator of fate decision towards the secretory lineage, is not restricted only at progenitor cells, but also present in differentiated goblet and Paneth cells (Lo et al., 2017). We propose that Arid3a and Arid3b may be expressed at the early progenitor cells to drive differentiation in the intestinal epithelia.

To study the role of Arid3a and Arid3b in the intestine, we first investigated the upstream transcriptional regulation of *Arid3a* and *Arid3b*. We uncovered an inhibitory role of Wnt signalling on their expression, which could explain the lower expression at the crypt bottom. Surprisingly, Notch and Bmp pathways that drive fate decision at the progenitor cells and terminal differentiation at the villus, respectively, do not affect *Arid3a* and *Arid3b* expression. On the other hand, we found that Tgf-β signalling promotes expression of *Arid3a* (figure 3.10). This is consistent with the signalling gradient of Tgf-β that is higher at the villus compartment where *Arid3a* accumulates. It has been previously reported that Arid3a regulates Tgf-β-mediated apoptosis and cell cycle arrest in the blood, and Arid3a shares many overlapping binding sites with Tgf-β effector molecules Smad2/3 (Alejo-Valle et al., 2022). It will be interesting to further investigate if Arid3a and Tgf-β form a forward feedback loop regulating differentiation or cell death at the villus compartment of the small intestine.

After defining the localisation of the two genes at the epithelial cells, we then studied that functional role of Arid3a and Arid3b in the gut by characterising intestinal-specific loss of the two genes.

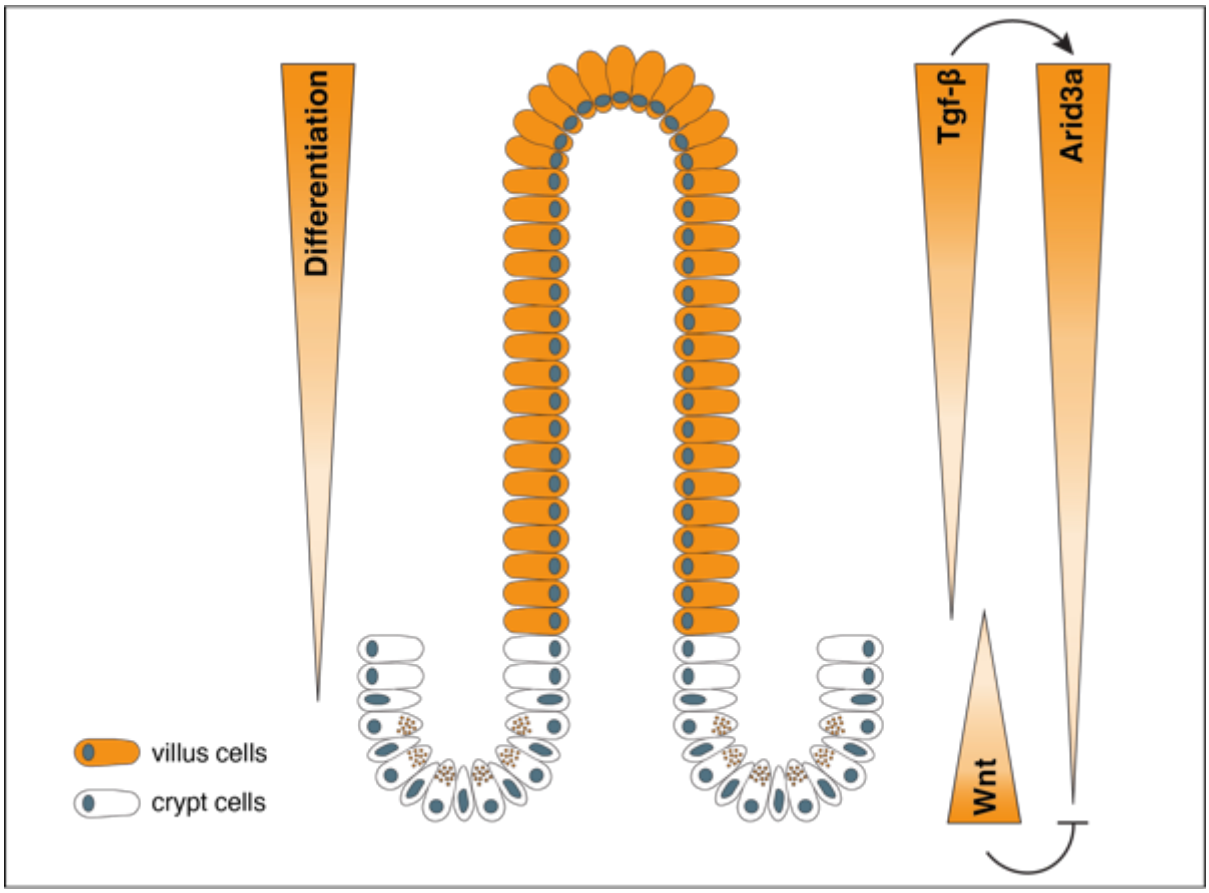

Figure 3.10 | Schematic representation of Arid3a localisation and its regulation from Wnt and Tgf-βsignalling pathways.

Chapter 4: Arid3a regulates the proliferation state of TA cells and the transdifferentiation process

4.1 Introduction

In order to fully understand the role of *Arid3a/b* in intestinal epithelial cells, we utilised *in vivo* conditional knockout mouse models for both genes. Previous studies showed that both *Arid3a* and *Arid3b* null mice exhibit embryonic lethality. In the case of Arid3a, >99% of homozygous knockout animals die at mid-gestation between E11.5 and E13.5 due to defects in haematopoiesis that are associated with highly impaired differentiation of embryonic haematopoietic stem cells (HSCs). The extremely small number of survivors are always significantly smaller in size (Webb et al., 2011). On the other side, *Arid3b* null mice die at even earlier stages of embryonic development between E7.5 and E9.5 (Webb et al., 2011). This premature death has been linked with defects in haematopoiesis, neural tissue, limb and cranial development (Casanova et al., 2011, Kurkewich et al., 2016, Takebe et al., 2006, Webb et al., 2011), signifying an important role of *Arid3b* in early embryogenesis.

To study the functional role of Arid3a and Arid3b in adult intestine, we sought to generate inducible conditional and intestinal epithelium-specific knockout animals for both genes individually as well as double knockouts. We kindly received the animals from our collaborators carrying a homozygous floxed allele for either *Arid3a* (*Arid3a*$^{fl/fl}$; Stephen Malin, Karolinska Institute) or *Arid3b* (*Arid3b*$^{fl/fl}$; Karen Cowden Dahl, University of Notre Dame). The two floxed strains were backcrossed with the *VillinCre-ERT2*$^{+/-}$ mouse line, where tamoxifen treatment induces the expression of Cre recombinase that is controlled under the promoter of the intestinal epithelial-specific marker *Villin* (*Vil1*) (el Marjou et al., 2004). This allows excision of the genomic region that is flanked by *LoxP* sites and facilitates conditional knockout only in *Villin*-expressing cells. These animal crossings resulted in the generation of three mouse lines that were used for the purpose of this study: *VillinCre-ERT2*$^{+/-}$; ***Arid3a***$^{fl/fl}$, *VillinCre-ERT2*$^{+/-}$; ***Arid3b***$^{fl/fl}$ and *VillinCre-ERT2*$^{+/-}$; ***Arid3a***$^{fl/fl}$; ***Arid3b***$^{fl/fl}$. For the rest of this thesis, the three lines are abbreviated as: Arid3a conditional knockout (Arid3a cKO), Arid3b conditional knockout (Arid3b cKO) and

double knockout (DKO), respectively. *VillinCre-ERT2*$^{+/-}$ animals are used as controls and they are abbreviated as wild-type (WT). All four lines were maintained as separate breedings. We also decided to not introduce a sex bias to our study, and we included both male and female animals for downstream analysis. All animals used were at the age of 8-12 weeks at the time of tamoxifen administration.

The bulk of our analysis of all conditional knockout animals was performed at 1 month after deletion of Arid3a and Arid3b (sections 4.2.1 – 4.2.9), but we also examined the effects of long-term deletion at 3-, 6-, 12- and 18-months post-tamoxifen administration (sections 4.2.10 – 4.2.11).

4.2 Results

4.2.1 Loss of Arid3a results in mild villus atrophy

To delete *Arid3a* and/or *Arid3b*, animals were injected with tamoxifen for 3 consecutive days and animals were culled at day 30. Both the small and large intestine were harvested for downstream histologic analysis. Of note, the pattern of Arid3a expression is conserved among the different regions of the bowel, with highest expression being observed at the villus tip (small intestine) or crypt tip (large intestine). However, the most proximal part of the small intestine was used for intestinal crypt isolation to extract RNA for downstream transcriptomics analysis and to establish intestinal organoids for functional studies (figure 4.1).

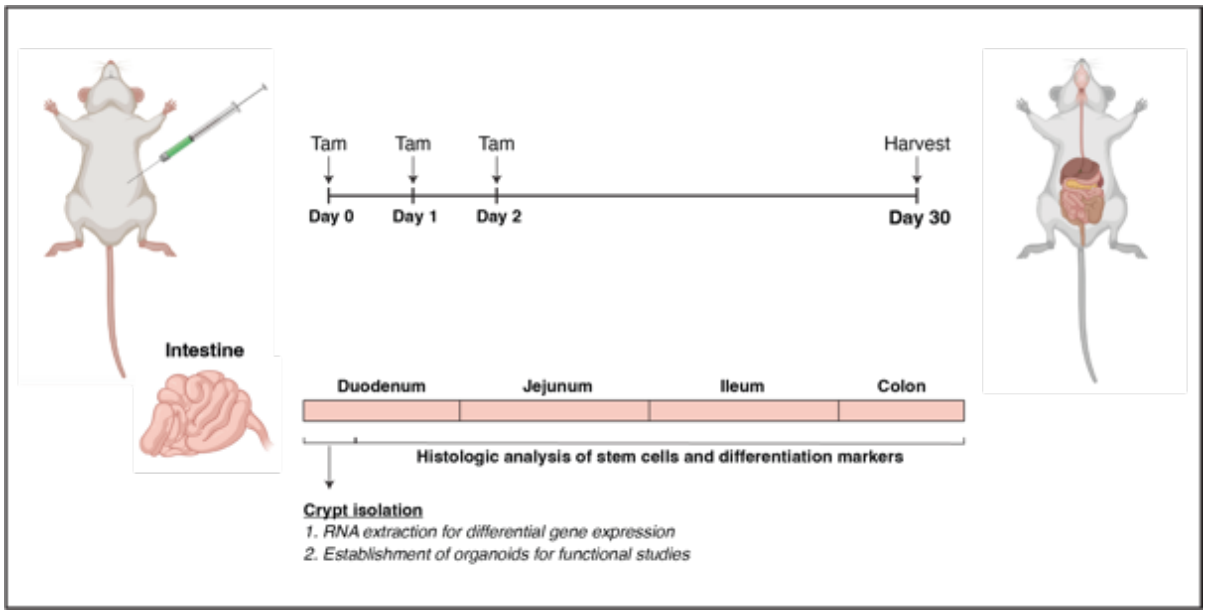

Figure 4.1 | Schematic representation of the experimental approach

Initially, we focused on characterisation of the Arid3a cKO animals. Immunohistochemistry confirmed complete abolishment of Arid3a expression at the epithelial cells, while the expression remained unchanged at stromal cells (figure 4.2A). Haematoxylin and Eosin (H&E) staining was used to assess histological differences and tissues were assessed by expert pathologists. The assessment included a semi-quantitative approach where tissue damage was scored from 0 to 5, with 0 signifying no lesion and 5 being the highest damage score. As expected, all WT animals showed no signs of tissue damage. On the other hand, Arid3a cKO animals showed a minimal to mild villus atrophy which refers to slightly reduced numbers of villi and villi lengths (figure 4.2B). No signs of mucosal inflammation or epithelial cell injury was observed at either of the two groups. We further assessed weight gain of the animals 30 days after the first tamoxifen injection. Arid3a cKO animals gained significantly less weight (mean 2.31g) compared to WT animals (mean 3.39g), and they were also found to have shorter small intestine (mean 35.35cm) than WT (mean 37.60cm) (figure 4.2C). Next, we performed a global unbiased RNA-seq analysis to characterise the transcriptomic changes caused by *Arid3a* deletion. In brief, 5 WT and 5 Arid3a cKO animals were used. Hierarchical clustering analysis showed that experimental animals with the same genotypes clustered nicely together with similar expression profile (figure 4.2D,E). Gene expression analysis revealed a total of 4387 genes differentially expressed between the two groups (FDR cut-off <0.05) (figure 4.2F). 2413 genes were upregulated at the cKO animals, while 1974 were downregulated.

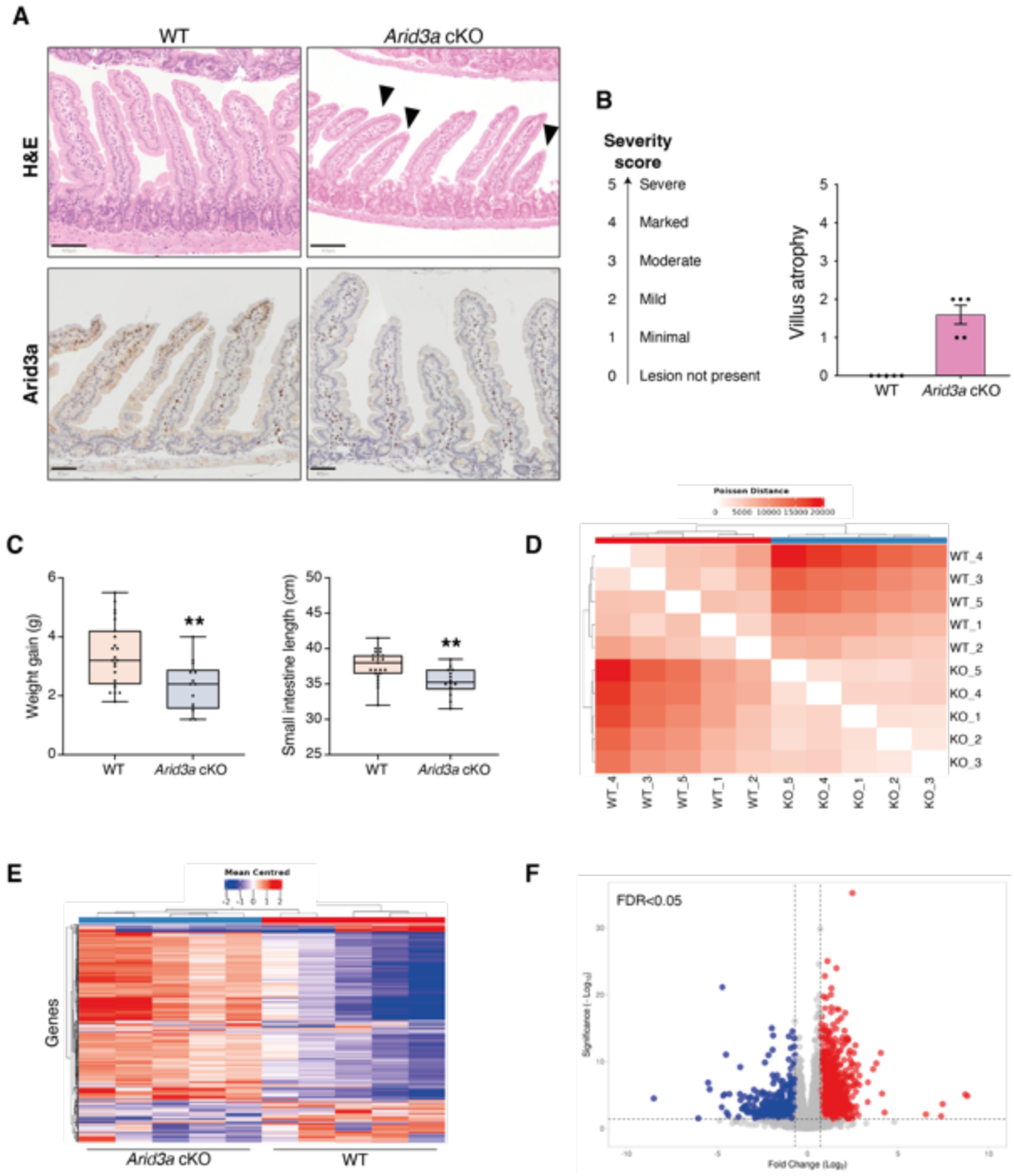

Figure 4.2 | Phenotypic analysis of Arid3a KO mice.
(A) H&E staining and Arid3a immunostaining of WT and Arid3a cKO mice. Representative images of N=23 WT animals and N=14 cKO animals for H&E and N=3 of each group for Arid3a staining. Scale bar, 100µm for H&E and 50µm for Arid3a. Arrowheads show shorter villi in Arid3a cKO animals. (B) Results of the pathologist's report of WT and Arid3a cKO small intestinal tissue. N=5 animals per experimental group. (C) Differences in weight gain (g) and small intestinal length (cm) at 1 month after tamoxifen administration. N=23 WT animals and N=14 cKO animals. Box plot shows all datapoints from min to max. *P<0.05, **P<0.01, ***P<0.001, two-sided t-test. (D) Pair-wise similarity of RNA-seq samples transcriptome-wide. This analysis compares the similarities between the two experimental groups looking at the overall gene expression per group and not only the differentially expressed genes. (E) Heatmap of blinded transcriptome-wide gene expression. The colours in the heatmap are a gene's expression in a sample, relative to its average expression. (F) Volcano plot showing differentially expressed genes (blue: downregulated in KO; red: upregulated in KO). FDR <0.05, $\log_2$(fold change)>1.5.

4.2.2 Arid3a-deficient mice exhibit reduced proliferation of the transit-amplifying cells at the upper crypt

Since expression of Arid3a is inhibited by Wnt signalling at the crypt base, we asked if loss of Arid3a can affect the proliferation status of crypt cells. Animals were injected with a short pulse of 5-ehtynyl-2'deoxyuridine (EdU) in order to assess numbers of mitotically active cells by directly measuring *de novo* DNA synthesis or S-phase synthesis of the cell cycle. Tissues were analysed at 2h after EdU injection (figure 4.3A). Arid3a cKO animals showed a reduction in total numbers of proliferative cells per crypt compared to WT animals (WT mean=9.73 cells; KO mean=7.2 cells) (figure 4.3B). The number of EdU-positive cells was further assessed by quantifying positive cells based on their positions. Interestingly, number of Edu-positive cells was mostly unaffected at positions 1-3 where Lgr5-expressing ISCs reside. Instead, reduction of EdU-positive cells was observed at positions 9-15, suggesting that Arid3a depletion inhibits proliferation at TA cells whilst ISCs at the crypt base are mostly unaffected (figure 4.3C).

Next, we analysed the transcriptional changes of proliferation markers in our RNA-seq dataset. In accordance with our EdU analysis, we observed a mild to moderate decrease of various cell cycle and cell proliferation markers in the Arid3a-depeted intestinal crypts (figure 4.3D). RNAscope analysis showed no differences in the expression of the ISC-specific marker *Olfm4* between WT and Arid3a cKO tissues, indicating that the number of stem cells are not affected upon Arid3a deletion (figure 4.3E). Gene set enrichment analysis (GSEA) analysis of our RNA-seq data revealed a significant transcriptional downregulation of gene signatures enriched in Wnt signalling (Sansom et al., 2007) and differentiating stem cells and TA cells (Busslinger et al., 2021) at Arid3a cKO crypts (figure 4.3F). Differentiating stem cells and TA cells are two slightly different populations previously identified in human duodenum (Busslinger et al., 2021). Although a big proportion of their signature is overlapping, differentiating stem cells express higher levels of stem cell markers, while TA cells have higher expression of differentiation markers. Metacore analysis further revealed that some of the most significantly affected Gene Ontology (GO) biological processes and molecular pathways included regulation of cell population proliferation (figure 4.4A) and initiation of mitosis during cell cycle (figure 4.3B). Together, the data

indicate that loss of Arid3a inhibits cell proliferation and Wnt signalling at the TA cells of the intestinal crypts.

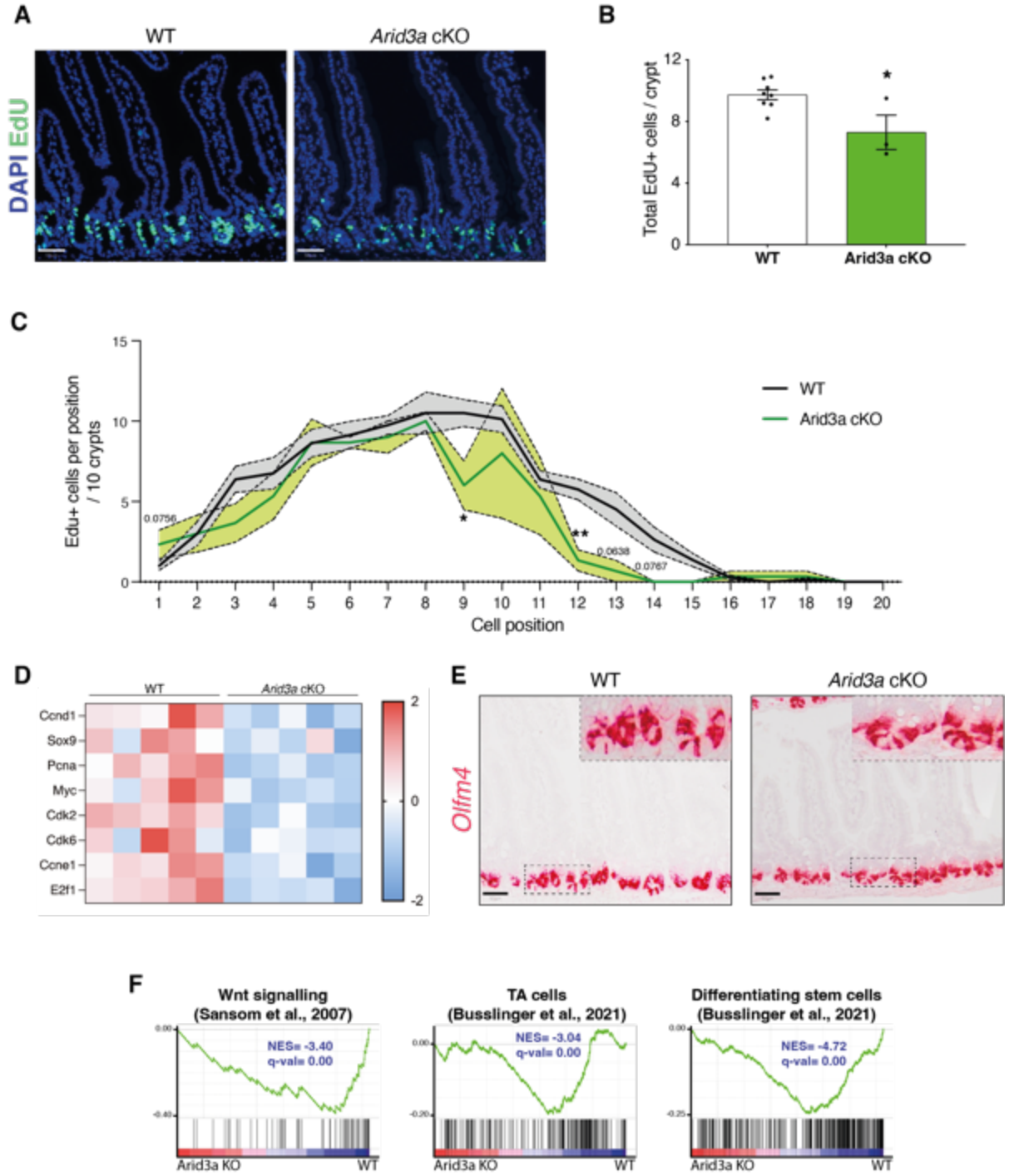

Figure 4.3 | Arid3a-deficient mice exhibit reduced proliferation at the upper crypt.
(A) EdU staining of WT and Arid3a cKO animals. Representative picture of N=8 WT and N=3 KO animals. Scale bar, 50µm. (B) Quantification of EdU-positive cells. Data represent mean ± s.e.m. *P<0.05, **P<0.01, ***P<0.001, two-sided t-test. (C) Quantification of EdU-positive cells based on their crypt position (per 10 crypts). Data represent mean ± s.e.m. (light colour area) *P<0.05, **P<0.01, ***P<0.001, multiple two-sided t-tests. (D) Heatmap of RNA-seq data of representative Wnt and stem cell markers. Z-scores are shown. (E) RNAscope staining of Olfm4 in WT and Arid3a cKO mice. Representative picture of N=3 per group. Scale bar, 50µm. (F) GSEA of previously published Wnt signalling, TA cells and differentiating stem cells gene lists.

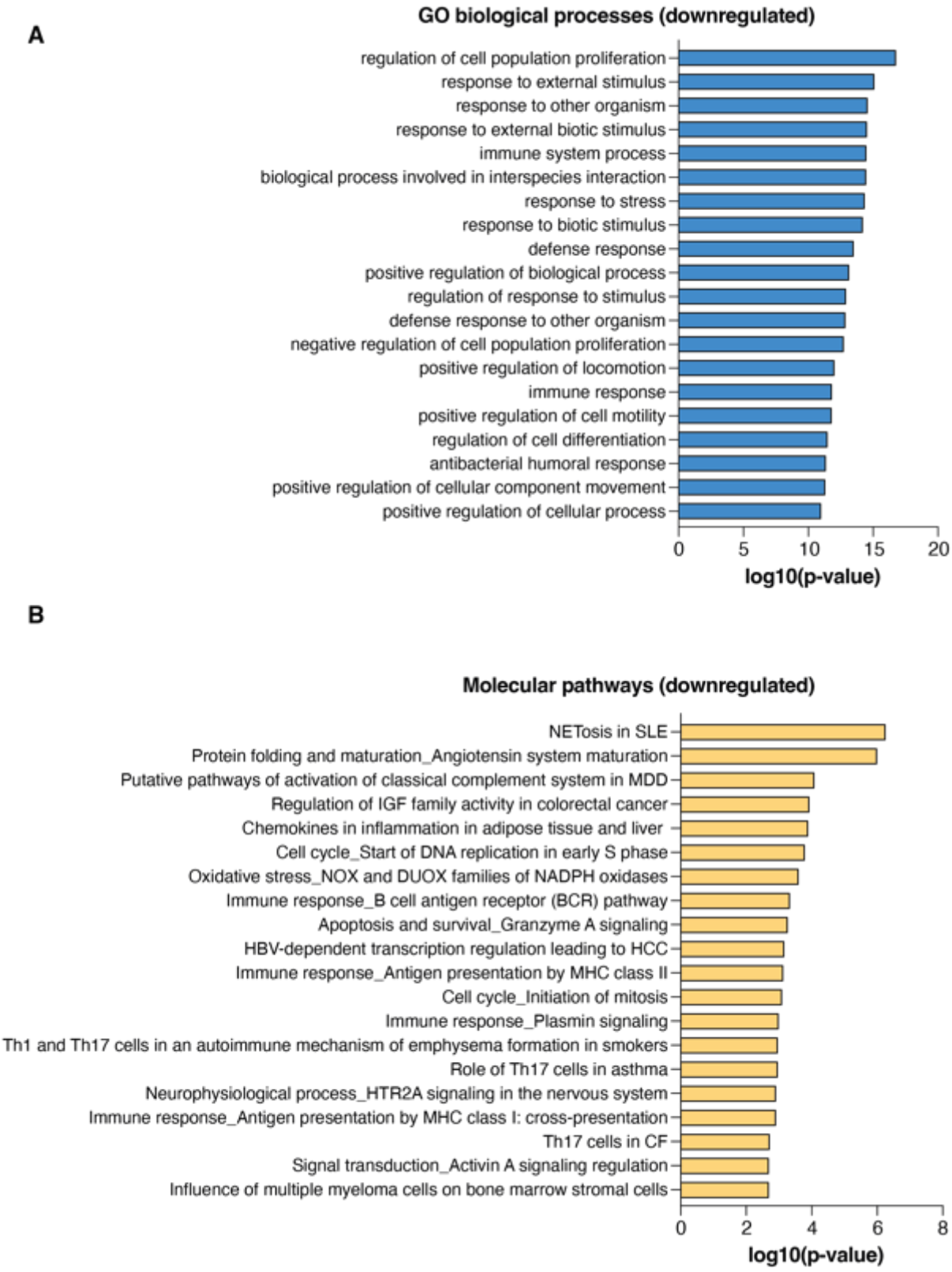

Figure 4.4 | Metacore analysis of downregulated genes in Arid3a cKO mice.
(A) Downregulated GO biological processes. (B) Downregulated molecular pathways. FDR<0.05 and fold change> 1.5 cut-offs were applied.

To validate the *in vivo* data, we utilised *ex vivo* organoid cultures to perform two different functional validation assays. Firstly, we performed an organoid formation assay. Upon crypt isolation, 200 crypts per animal were seeded in BME and organoids were counted at day 5 after isolation (figure 4.5A). A significant decrease in organoid formation capacity was observed in Arid3a cKO derived crypts (WT mean=64.1 organoids, KO mean=48.4 organoids) (figure 4.5B). Subsequently, we challenged the organoids by depleting one of the essential growth factors and Wnt agonist Rspondin (Rspo). Murine organoid cultures rely on supplementation of exogenous growth factors Rspo, Egf and Noggin to survive. Under normal condition, organoids were cultured in medium contains 5% Rspo conditioned media (CM). Organoids derived from WT and KO animals were assessed based on their phenotype and quantified: organoids with >3 buds were considered healthy, organoids with 1-3 buds were considered unhealthy and organoids that failed to bud or form cysts were considered collapsed. WT and KO organoids did not exhibit any major morphological differences in the presence of 5% Rspo CM (figure 4.5C). However, when organoids were challenged with a lower concentration of Rspo (1%), a higher percentage of collapsed and a lower percentage of healthy organoids were observed (figure 4.5D). The increased dependence on exogenous Rspo in the cKO organoids suggests a reduction of endogenous Wnt signalling in the Arid3a-depleted crypt cells, which is consistent with the GSEA data observed in figure S3F.

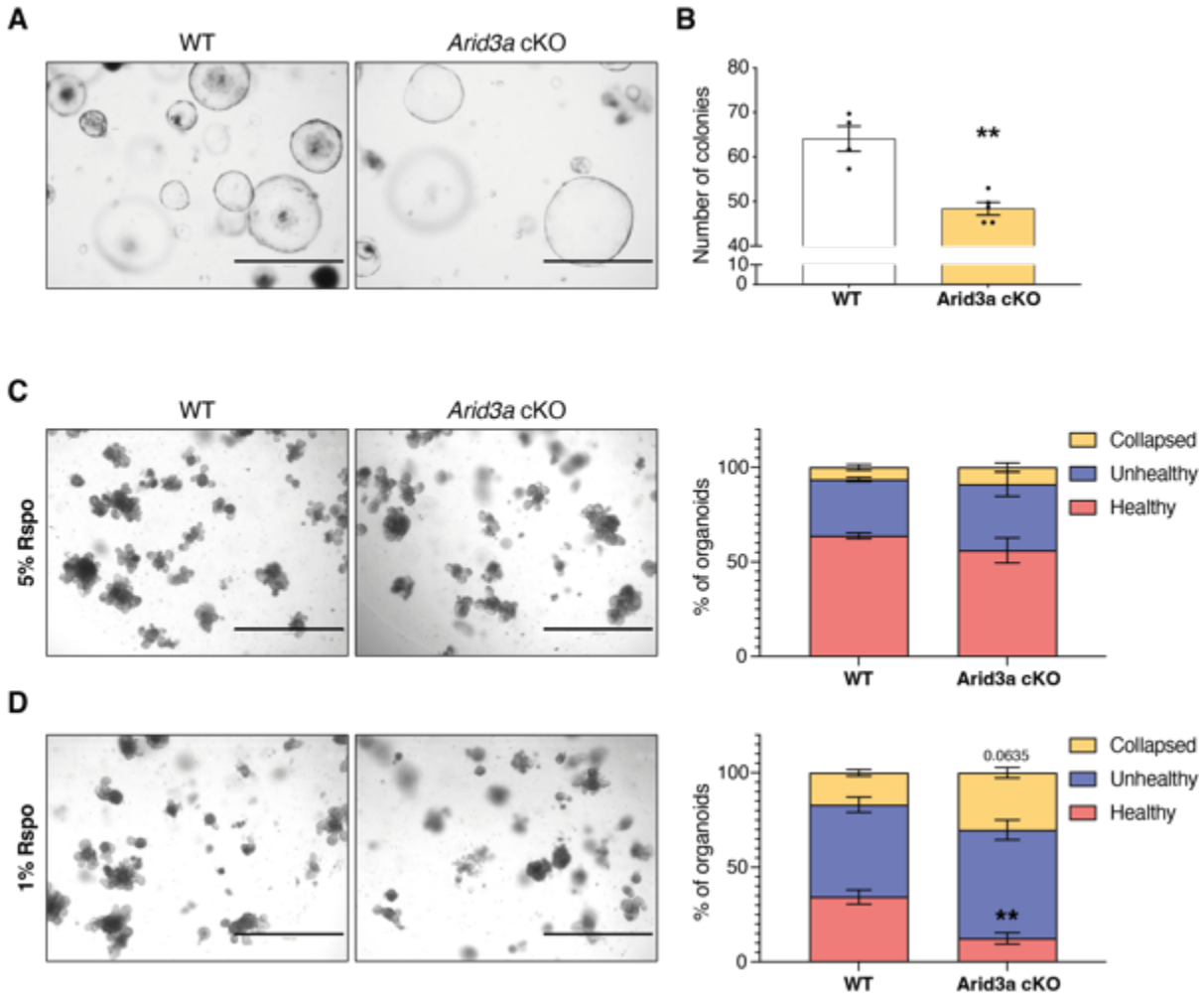

Figure 4.5 | Arid3a cKO organoids have a lower organoid formation capacity.
(A) Images of WT and Arid3a cKO organoid formation assay. Representative picture of N=4 WT and N=5 animals. Scale bar, 1000µm. (B) Quantification of organoid formation assay from (A). Data represent mean ± s.e.m. *P<0.05, **P<0.01, ***P<0.001, two-sided t-test. (C) Representative images and quantification of WT and Arid3a cKO organoids cultured in 5% Rspo CM. (D) Representative images and quantification of WT and Arid3a cKO organoids cultured in 1% Rspo CM. Scale bar, 1000µm. For both (C) and (D), N=8 WT and N=4 Arid3a cKO organoid lines were used. Stacked data represent mean ± s.e.m. *P<0.05, **P<0.01 , ***P<0.001, 2-way ANOVA

4.2.3 Loss of Arid3a alters differentiation of the small intestinal epithelium

To further study the role of Arid3a in intestinal homeostasis, we characterised if functional differentiation is affected in the cKO intestine. We first looked into differentiation of Paneth cells, the only specialised epithelial cells that live for a longer period of time (~14 days). Instead of migrating towards the villus, Paneth cells move to the crypt base upon maturation and function as stem cell niche by secreting essential growth ligands such as Wnt, Notch and Egf (Sato et al., 2011b). Our RNA-seq data revealed a downregulation of the traditional Paneth cell marker *Lyz1*, as well as of the newly discovered marker *Mptx2* (Haber et al., 2017) in Arid3a cKO intestine (figure 4.6A). Paneth cells also act as a defence mechanism to exogenous stimuli and secrete a large number of anti-microbial peptides called cryptidins or α-defensins (Vandenbroucke et al., 2014) and our RNA-seq data showed a significant decrease in majority of these peptides in KO animals (figure 4.6A). Of note, the Metacore analysis of downregulated genes presented in section 4.2.2 showed that most of the significantly downregulated biological processes in the KO animals are related to their defence response to other organisms, which could be caused by reduced Paneth cell differentiation (figure 4.4A). Immunostaining of Lyz using WT and KO tissues further confirmed the reduction of Paneth cells numbers (WT mean=14.53 cells/5 crypts, KO mean=11.82 cells/5 crypts) (figure 4.6B).

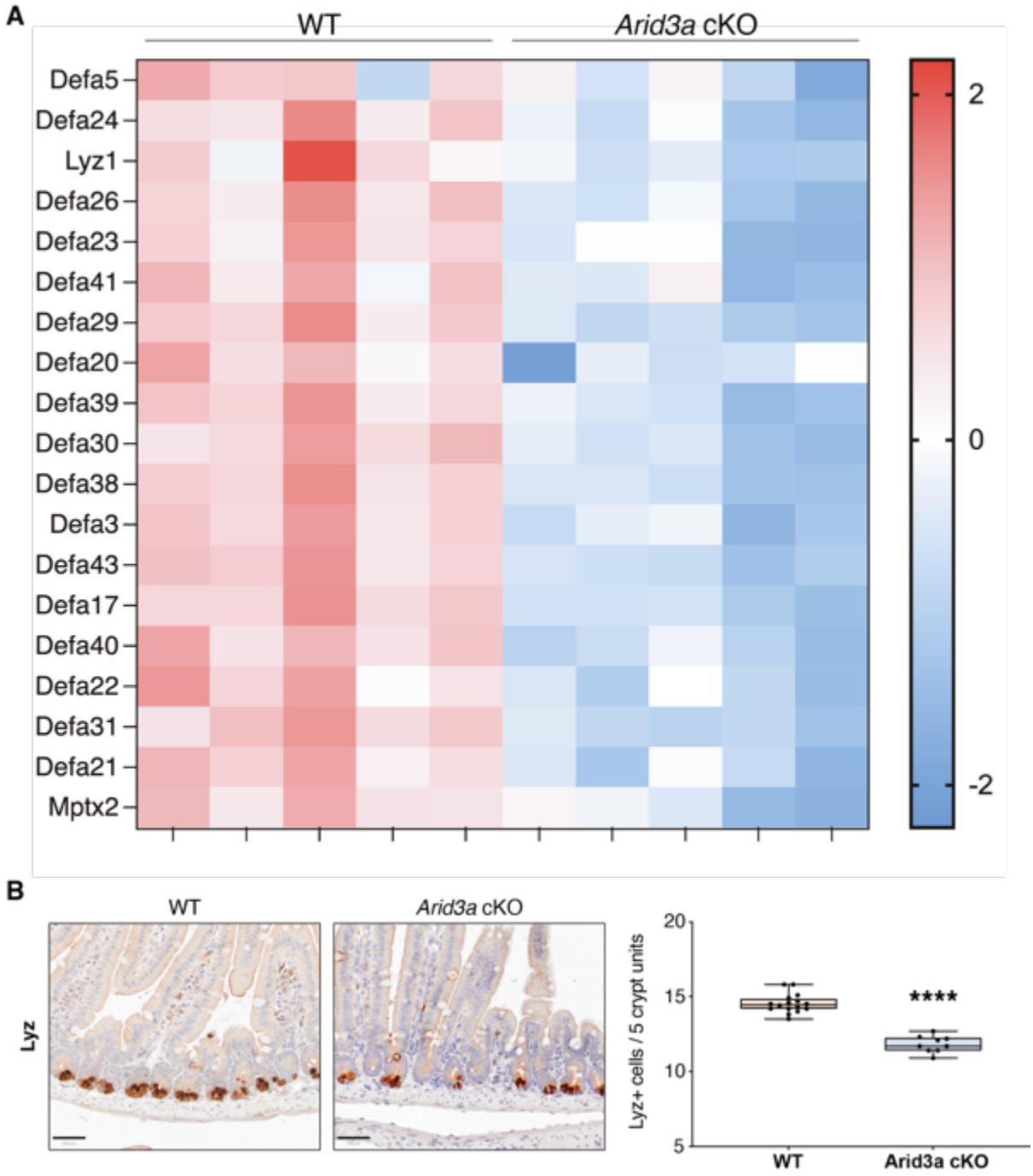

Figure 4.6 | Arid3a cKO results in reduced numbers of Paneth cells.
(A) Heatmap of RNA-seq data of representative Paneth cells markers. Z-scores are shown. (B) Lyz staining of WT and Arid3a cKO animals. Scale bar, 50 µm. Representative images and quantification of N=16 WT and N=9 KO animals. Box plot shows all datapoints from min to max. *P<0.05, **P<0.01, ***P<0.001, two-sided t-test

Next, we investigated whether loss of Arid3a affects other differentiated cells in the villus. Apart from Paneth cells, goblet and enteroendocrine cells are the two most abundant secretory cell types in the intestinal epithelium throughout the villus. To test if differentiation of the two cell types is affected, intestinal tissues derived from WT and KO mice were stained with AB-PAS and against ChgA to mark goblet and enteroendocrine cells, respectively. Quantification of the staining showed minimal reduction of both cell populations (figure 4.7A,B). In accordance with the staining results, GSEA of the RNA-seq data confirmed an overall small downregulation of secretion-related markers at the KO animals (figure 4.7C). The complex dynamics of secretory lineage differentiation will further be analysed and discussed in section 4.2.5.

Subsequently, we looked at differences in expression of absorptive genes. Differential gene expression analysis revealed a strong upregulation of various enterocyte markers, such as Alpi, Apoa4, Apoc2 and Fabp1 (figure 4.8A). The upregulation of enterocyte signature was confirmed by increased protein levels of different enterocyte markers (Alpi, Fabp1, Apoa4) in Arid3a cKO intestine (figure 4.8B). Furthermore, disaccharidase functional assay was performed to assess the enterocyte function by challenging the Arid3a cKO and WT organoids with sucrose for 1h. Disaccharidase enzymes in enterocytes function to breakdown sucrose into glucose and fructose. After incubation, supernatants were collected and glucose levels were assessed. In accordance with our *in vivo* data, supernatants from Arid3a cKO organoids contained significantly higher levels of glucose than those from WT organoids (figure 4.8C). Interestingly, Metacore analysis of all significantly upregulated genes of the RNA-seq dataset (FDR<0.05, Fold change>1.5) showed that most of the top upregulated GO biological processes and molecular pathways were related to an increase of several different metabolic processes (figure 4.9A,B), which are facilitated by absorptive enterocytes. The results confirm that loss of Arid3a increases numbers and/or functional differentiation of enterocytes in the intestine, which subsequently increases the metabolic potential of the animals.

In summary, we have demonstrated so far that loss of Arid3a affects the differentiation of intestinal epithelial cells. On one side, differentiation of absorptive enterocytes is remarkably upregulation in the KO intestine; on the other side, Paneth cells (mostly), goblet and enteroendocrine cells (to a lesser degree) are reduced.

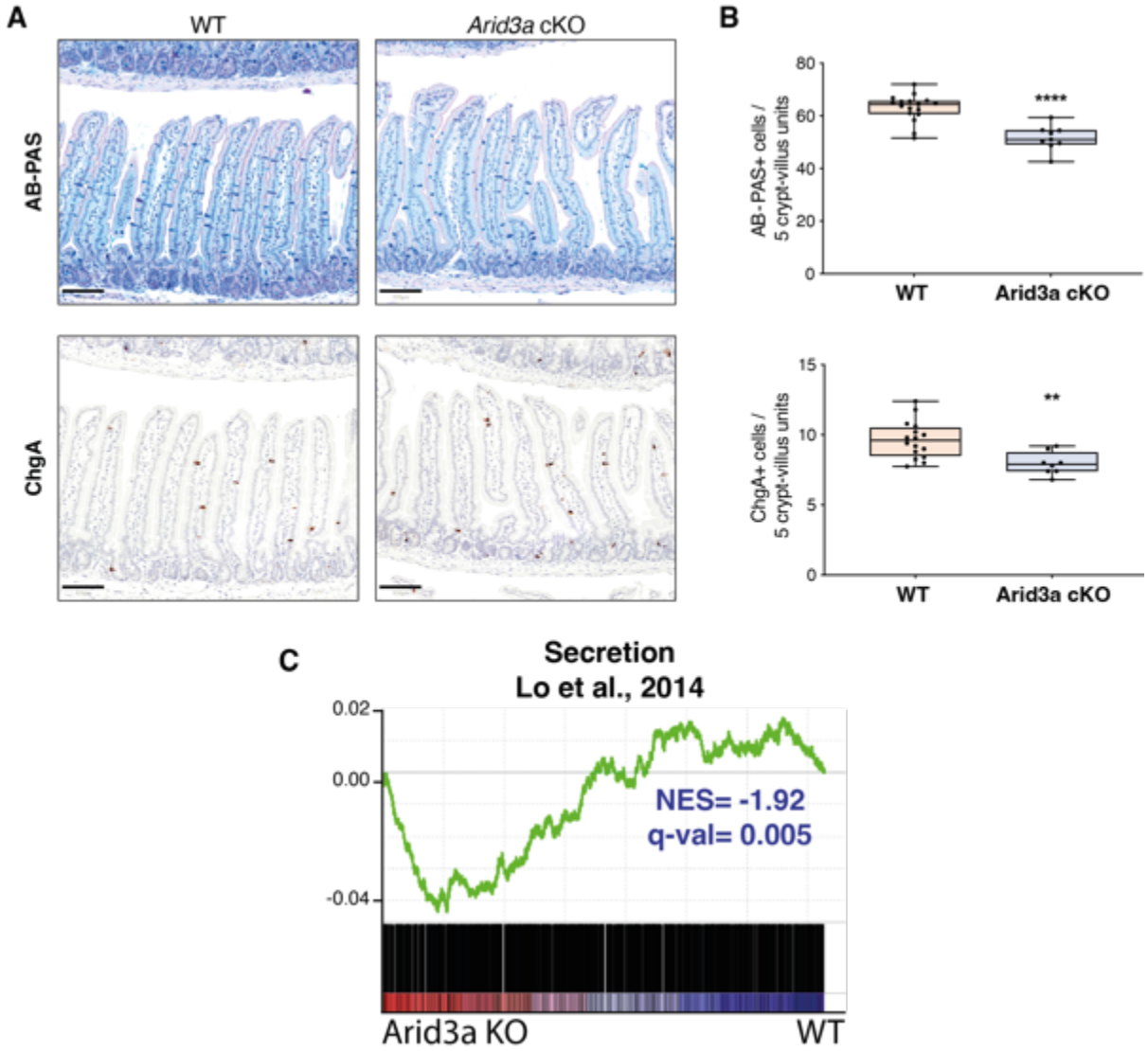

Figure 4.7 | Tissue analysis and GSEA reveal subtle differences in secretory lineages of Arid3a cKO animals.
(A) AB-PAS and ChgA staining of WT and Arid3a cKO animals. Scale bar, 100 µm. Representative images of N=17 WT and N=9 KO animals for AB-PAS and N=16 WT and N=8 KO animals for ChgA. (B) Quantification of AB-PAS and ChgA stainings. Box plot shows all datapoints from min to max. *P<0.05, **P<0.01 , ***P<0.001, two-sided t-test. (C) GSEA of previously published secretion-related genes.

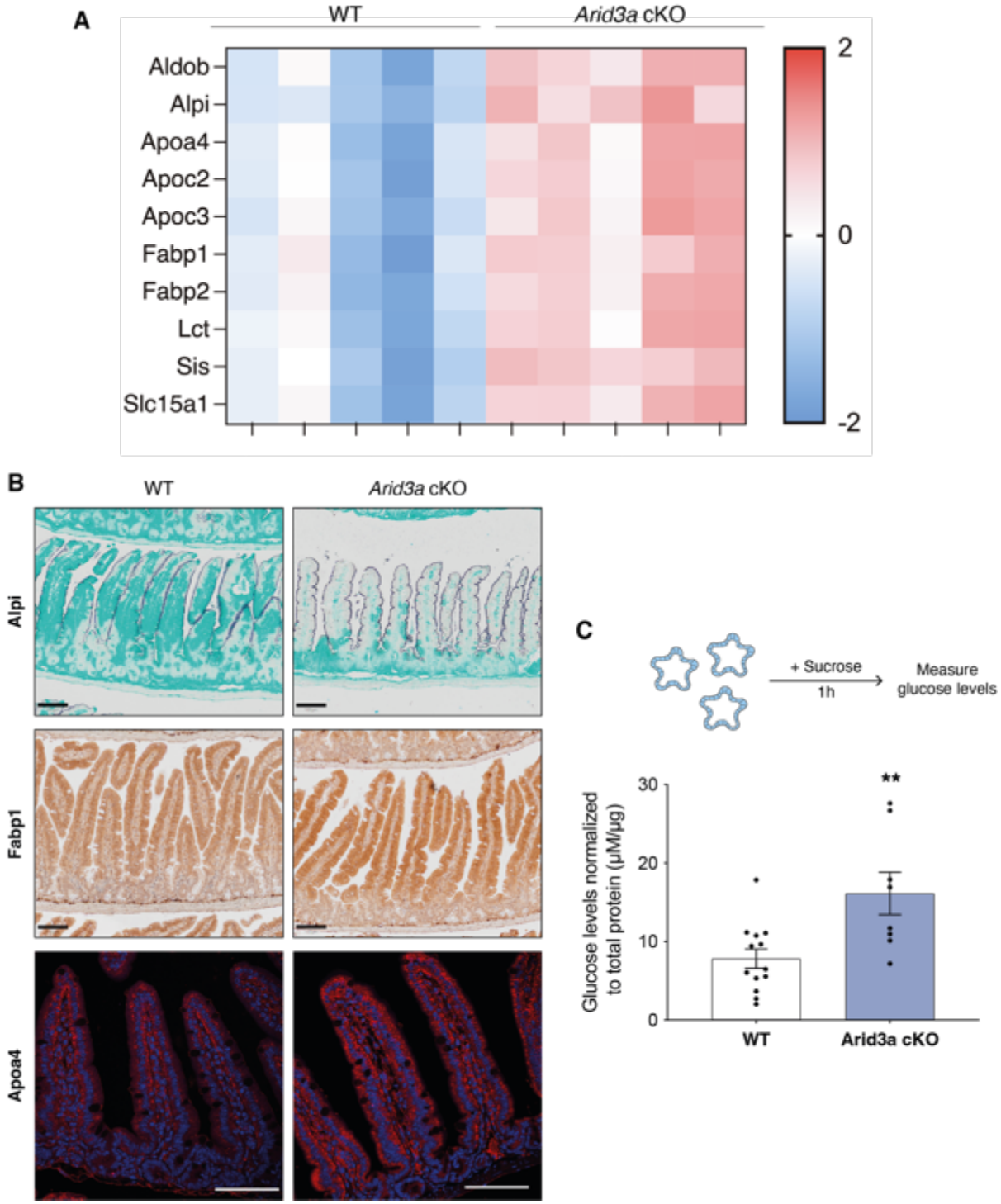

Figure 4.8 | Enterocyte signature is upregulated upon loss of Arid3a.
(A) Heatmap of RNA-seq data of representative enterocytes markers. Z-scores are shown. (B) Immunostainings against three different enterocyte markers: Alpi, Fabp1 and Apoa4. Representative images from N=5 per group. Scale bar, 100µm. (C) WT and Arid3a cKO organoids were treated with sucrose for 1h. Graph shows absorbance levels of glucose normalised to total protein. Data represent mean ± s.e.m. *P<0.05, **P<0.01 , ***P<0.001, two-sided t-test.

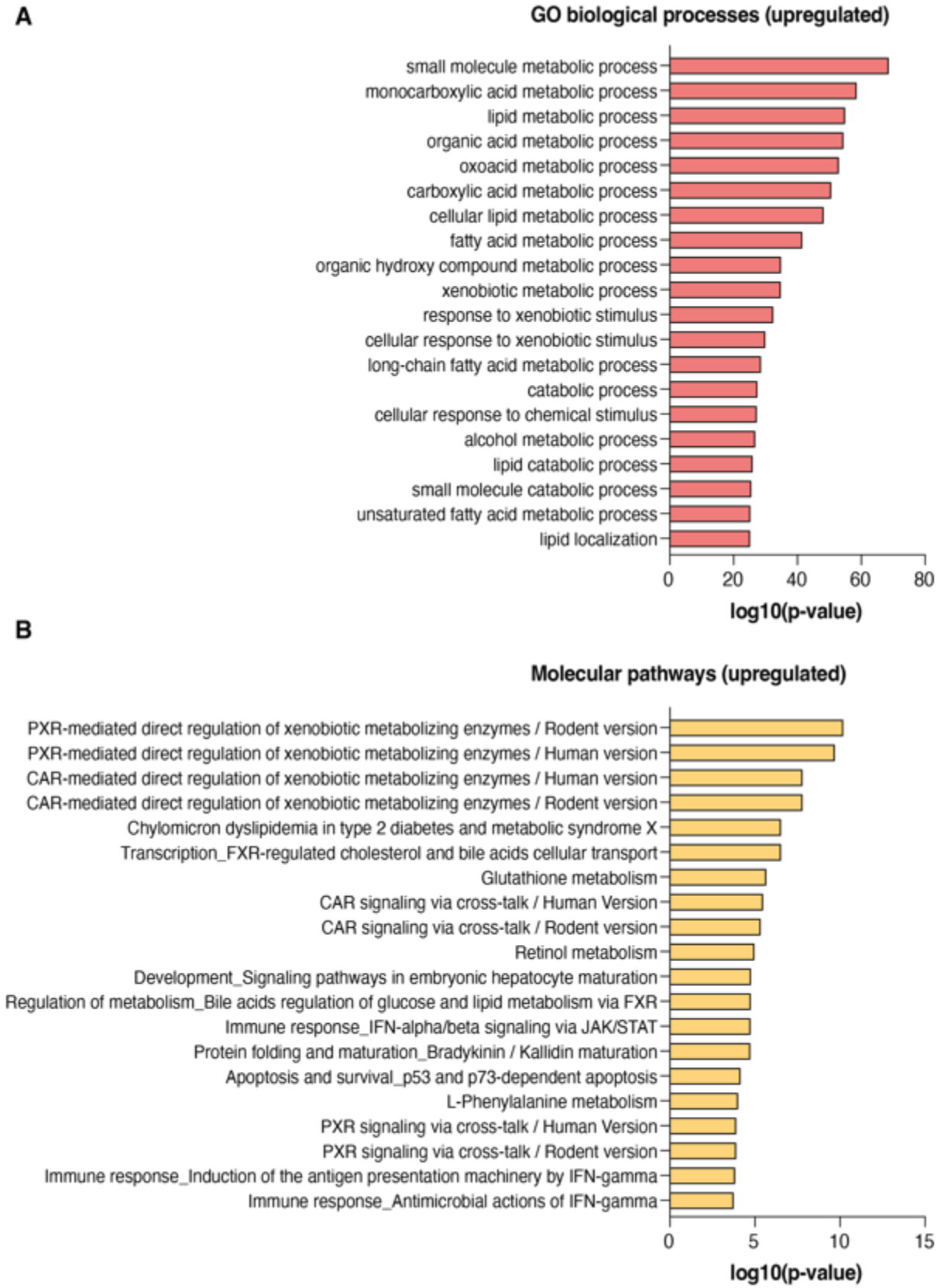

Figure 4.9 | Metacore analysis of upregulated genes in Arid3a cKO mice.
(A) Upregulated GO biological processes. (B) Upregulated molecular pathways. FDR<0.05 and fold change> 1.5 cut-offs were applied.

4.2.4 Arid3a controls the transdifferentiation of enterocytes

The conventional differentiation programme of the small intestinal epithelium follows a simple hierarchy where ISCs residing at the bottom of the crypt give rise to progenitor cells at positions +4/+5. Lineage decision takes place at these progenitors, where cells will adopt either absorptive or secretory fate and will subsequently migrate towards the villus. However, a recent study from the Itzkovitz lab revealed that cells do not acquire their terminal identity at the progenitor cells. Rather, the epithelial cells transdifferentiate as they move upwards to facilitate diverse functions (Moor et al., 2018). They showed that enterocytes exhibit a broad zonation of gene expression from the crypt to the villus bottom, which can be grouped into five clusters (figure 4.10A) based on their functionality (Moor et al., 2018). Of note, the term "enterocyte transdifferentiation" refers to the continuous changes in gene expression of enterocytes as they move upwards the crypt/villus axis, that result in facilitation of different biological processes from the same cells.

In section 4.2.3, we showed that enterocyte signature is increased upon Arid3a deletion. To further investigate if Arid3a is involved in the transdifferentiation process, alterations in the expression of the gene signature of the five clusters between WT and Arid3a cKO intestine were examined. Interestingly, differential gene expression analysis showed that cluster 1 is strongly enriched at WT animals, while expression of clusters 2-5 is upregulated in Arid3a cKO animals (figure 4.10B). Consistently, GSEA further confirmed this result (figure 4.10C). Cluster 1 contains genes that are mainly enriched at the early crypt enterocytes. GO term analysis has associated these genes with increased translation and transcription, while genes in clusters 2-5 are associated with mitochondrial activity (cluster 2), acute phase response (cluster 2), absorption, nutrient transport, brush border function and cell adhesion (clusters 3-5) (Moor et al., 2018). Decreased gene expression of crypt enterocytes (cluster 1) in Arid3a cKO intestine can be caused by the reduced proliferation in the upper crypt as shown earlier in figure 4.3, while increased absorption capacity (cluster 2-5) can be explained by the increased enterocyte signature and function in the Arid3a cKO animals (figure 4.7). Of note, our RNA-seq analysis showed that various mid-villus and villus-tip transporters that are zonated at clusters 2-5 are upregulated upon loss of Arid3a to facilitate absorption of different nutrients (figure 4.10D). Collectively, our data suggest that Arid3a regulates

enterocyte differentiation in the intestine, possibly by regulating the proliferation-to-differentiation rate of TA cells.

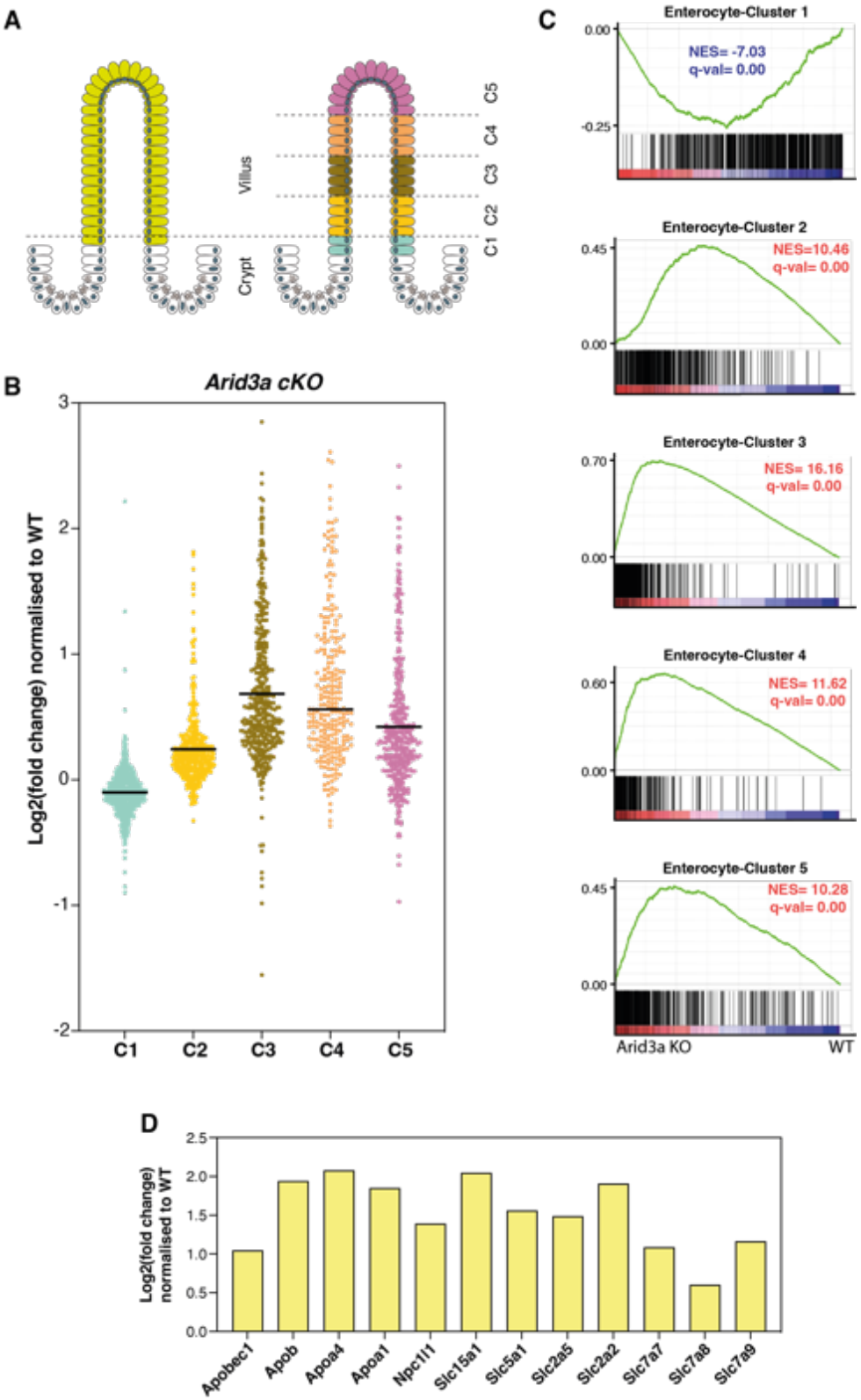

Figure 4.10 | Arid3a controls the transdifferentiation of villus enterocytes.
(A) Schematic representation of traditional and updated model of enterocyte differentiation. (B) RNA-seq expression data of all signature genes of the five enterocyte clusters. Data represents log2(fold change) of expression in Arid3a cKO animals against WT animals. (C) GSEA of the five enterocyte clusters (Moor et al., 2018). (D) RNA-seq expression data different transporters enriched across clusters 2-5. Data represents log2(fold change) of expression in Arid3a cKO animals against WT animals.

4.2.5 Loss of Arid3a increases the signature of goblet and tuft cells at the villus-tip

Several recent studies have focused on understanding the differentiation dynamics of secretory cells (Beumer et al., 2018, Gehart et al., 2019, Manco et al., 2021). Goblet cells and tuft cells show a spatial expression programme across the crypt-villus axis similar to the one of enterocytes, while enteroendocrine cells show a more complex spatio-temporal migration pattern (Manco et al., 2021).

Since GSEA of secretion-related genes on our RNA-seq dataset showed a mixed enrichment of genes towards WT or Arid3a cKO animals (figure 4.7C), we hypothesized that Arid3a may regulate the spatial expression programs of secretory cells. To test the hypothesis, the spatial gene expression programme of goblet, tuft and enteroendocrine cells was examined in the KO animals. Similar to enterocytes, we noted enrichment of the villus-tip gene expression programme in all three secretory lineages upon Arid3a deletion (figure 4.11A,B,C). Goblet and tuft cells further showed an enrichment of mid-villus genes and a reduction in expression of crypt genes (figure 4.11A,B). On the other hand, enteroendocrine genes at the crypt and mid-villus showed a more heterogeneous expression at WT or KO animals, which may be due to their complex spatio-temporal migration pattern (figure 4.11C).

A recent study on scRNA-seq of the intestinal epithelium has uncovered two distinct population of Tuft cells – Tuft1 and Tuft2 cells (Haber et al., 2017). Tuft1 cells express neuronal-like genes that are mostly localised at the bottom of the villus and Tuft2 cells exhibits higher expression of immune-related programs that are enriched at the villus tip (Manco et al., 2021). Indeed, GSEA of the RNA-seq data showed that Tuft1 population seems to be largely unaffected, whereas Tuft2 cells are enriched in the Arid3a cKO intestine (figure 4.12). Together, our results show that Arid3a is important for maintenance of the spatial differentiation/zonation of both absorptive and secretory genes across the crypt-villus axis. Since loss of Arid3a inhibits TA cell proliferation and increases the gene signatures of all cell lineages at the villus-tip, we propose that Arid3a is expressed at the TA cells to balance the transition from proliferation to terminal differentiation of the intestinal epithelium.

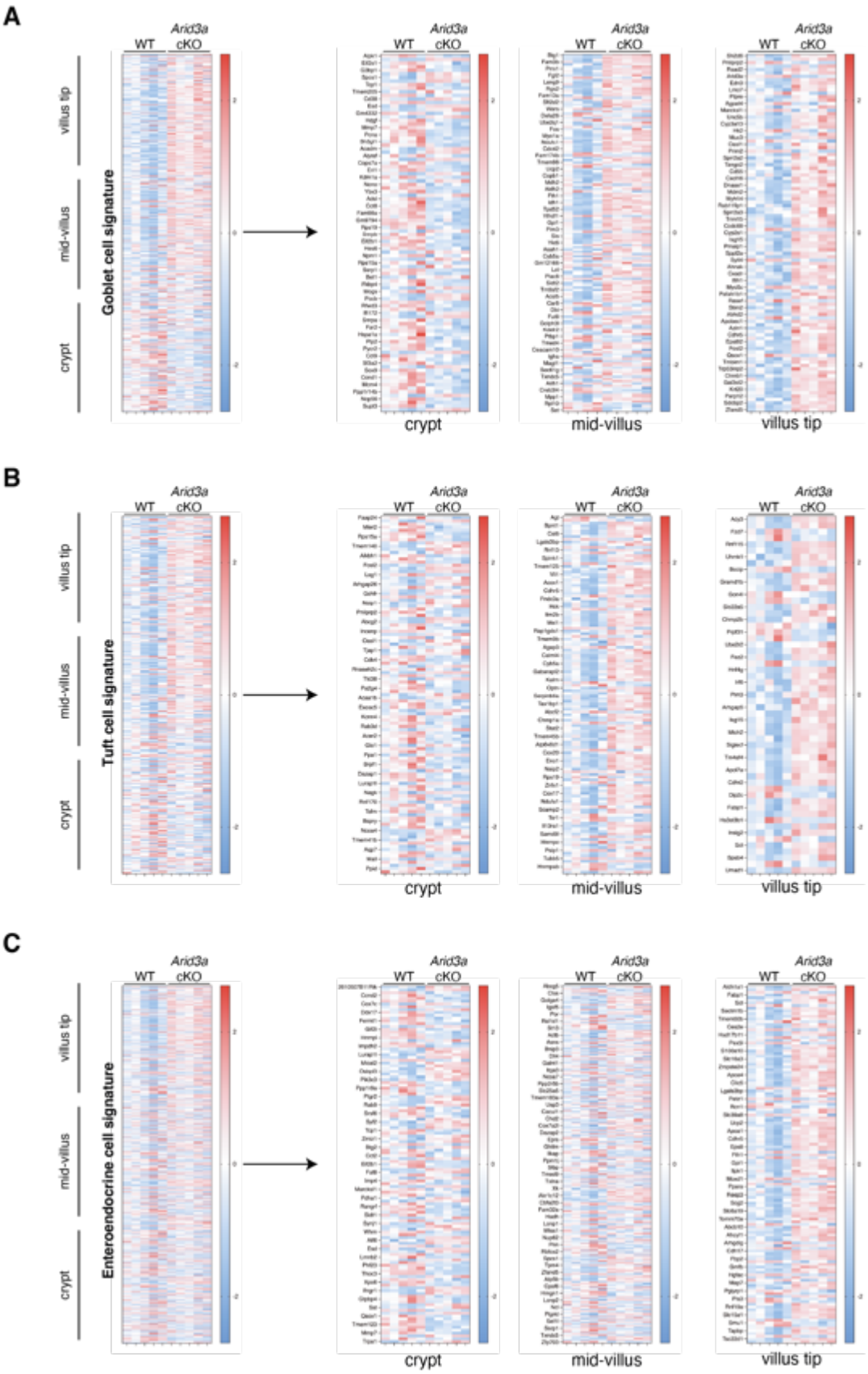

Figure 4.11 | Loss of Arid3a increases the signature of villus-tip secretory cells.
Heatmap of RNA-seq data of zonated goblet (A), tuft (B) and enteroendocrine (C) genes. Full lists of significantly differentially expressed genes are shown on the left side of each panel. Genes are shown based on their centre of mass with crypt genes at the bottom of the heatmap and villus tip genes at the top (Manco et al., 2021). Genes that are mostly enriched at the crypt, mid-villus and villus tip are shown on the right side of each panel. Z-scores are shown. FDR cut-off <0.05.

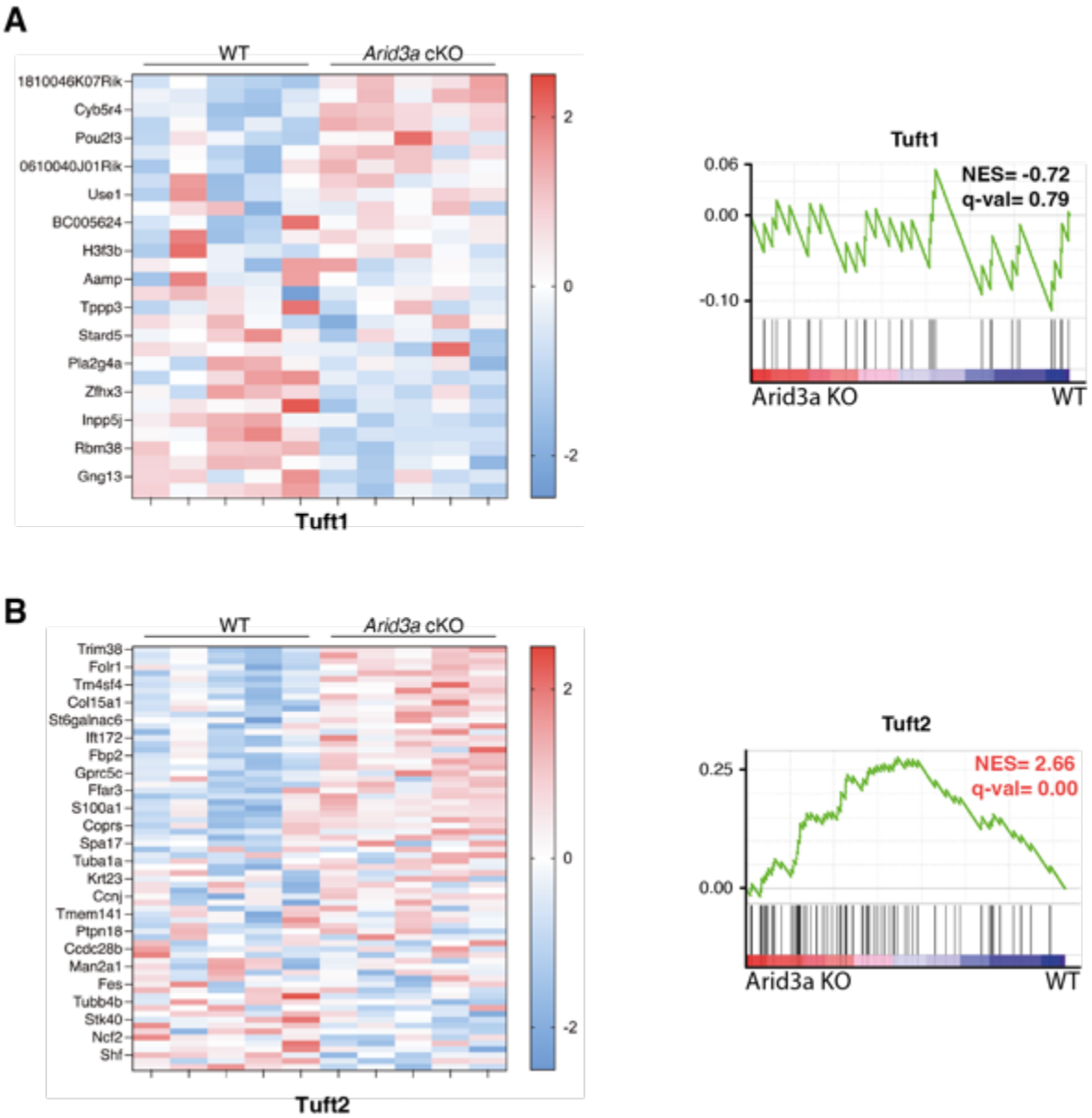

Figure 4.12 | Tuft2 cells are enriched in Arid3a cKO animals.
(A) Heatmap of all Tuft1 signature genes and subsequent GSEA of the same genes. (B) Heatmap of all Tuft2 signature genes and subsequent GSEA of the same genes. No FDR or log2(fold change) cut-offs were applied.Tuft1 and Tuft2 gene lists are from (Haber et al., 2017).

4.2.6 Expression analysis of villus samples confirms enrichment of villus-tip differentiated cells

Thus far, our RNA-seq experiment was performed using intestinal crypts isolated by either WT or KO animals. It has been previously reported that crypt fractions contain representative cells from all differentiated populations of the intestinal epithelium (Haber et al 2017). Since Arid3a expression is enriched at the villus tip and the crypt RNA-seq data showed increased differentiated gene signatures at the villus-tip, we asked whether sequencing of the villus fractions isolated from the WT and Arid3a cKO animals would confirm this result. In general, RNA quality extracted from villus samples is of lower quality. This can be attributed to the high proportions of apoptotic cells that are accumulated mainly at the villus tip, or it could be related to increased mucus content surrounding the intestinal brush border.

To characterise the gene expression changes in the villus, we isolated the villus fractions of the same animals that were previously used for crypt-based RNA-seq (figure 4.2). As expected, Bioanalyzer-based quality control (QC) of the extracted RNA showed that several samples had a lower RNA Integrity Number (RIN) and failed to pass the QC threshold. Low RIN signifies higher degradation of RNA or, less often, DNA contamination. Library preparation for of these samples always contains a DNase treatment step to purify the samples. To overcome the issues related to possible RNA degradation, total RNA libraries were prepared instead of mRNA libraries. This would include degraded RNA fragments in the libraries that could be aligned back to the reference genome upon sequencing.

Remarkably, RNA-seq analysis of the villus samples highly resembled that of the crypt samples described earlier. GSEA confirmed the enrichment of the villus-tip gene expression programme in all cell lineages (enterocyte, goblet, tuft and enteroendocrine cells) upon Arid3a deletion (figure 4.13A-D). Moreover, expression of crypt or villus bottom expression signatures of enterocytes, goblet and enteroendocrine cells (but not tuft cells) were downregulated in Arid3a cKO animals, while expression of mid-villus genes of these three cell types was largely unaffected. Only tuft mid-villus cells showed an enrichment upon Arid3a KO. Overall, RNA-seq of villus samples confirmed the upregulation of gene expression programme of villus tip differentiated cells in Arid3a cKO animals. Small discrepancies that were observed in crypt/villus bottom genes expression between crypts and villi samples are possibly due to absence or very low presence of these cells in the villus samples. Deeper sequencing

of villus samples derived from total RNA could increase the resolution of these results and confirm enrichment of mid-villus genes.

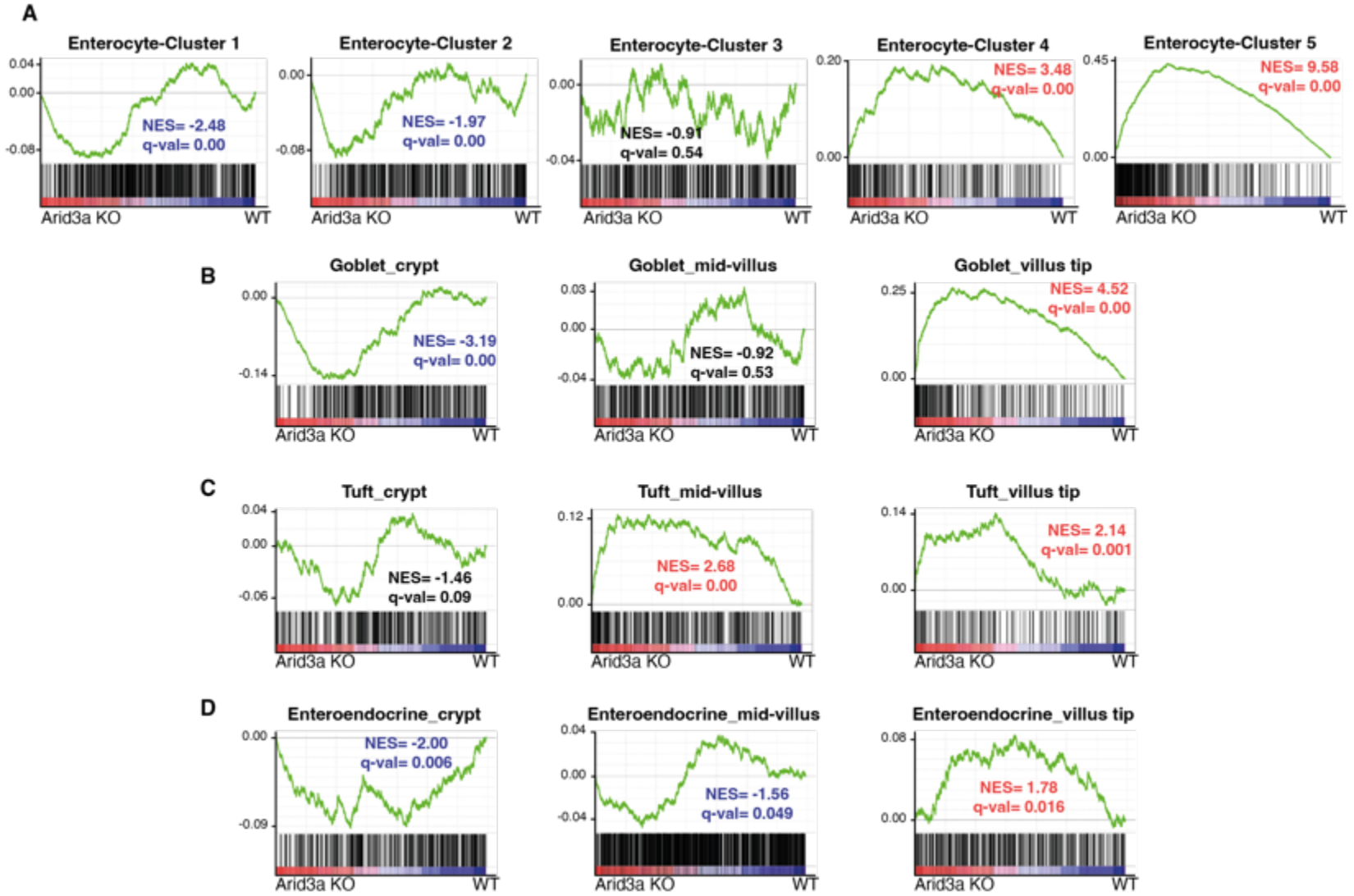

Figure 4.13 | Bulk RNA-seq of villi confirms enrichment of villus tip differentiated cells in Arid3a cKO animals.
GSEA of zonation programmes of enterocytes (A) (Moor et al., 2018), goblet (B), tuft (C) and enteroendocrine cells (D)(Manco et al., 2021)

4.2.7 ChIP-seq analysis of Arid3a targetome

To understand how Arid3a regulates the proliferation and differentiation transition at the TA cells, ChIP-seq analysis was performed to identify its transcriptional targets.

Before proceeding to ChIP-seq analysis, we first performed a multi-step validation of the antibody in order to confirm its binding specificity. We have shown earlier that the same antibody gave specific immunostaining against Arid3a in mouse FFPE tissue (figure 4.2A), as well as in Western blot analysis of protein lysates from Ls174T human colorectal cells (figure 3.7E). To further validate the antibody specificity, we overexpressed (OE) Arid3a in mouse organoids and confirm higher Arid3a protein expression (figure 4.14A). Immunostaining of ARID3A in LS174T showed high expression levels of *ARID3A* in both nuclear and cytoplasm (figure 4.14B). Immunoprecipitation (IP) of endogenous ARID3A in LS174T cells showed enrichment of ARID3A in the pull down but not in the IgG control (figure 4.14C). We further proceeded to test if the antibody can be used for ChIP-qPCR analysis using isolated WT intestinal crypts. The previously published data set of Arid3a binding sites during embryonic development (GSE56877) was used as reference where several peaks were chosen for downstream RT-qPCR upon successful ChIP. Enrichment of the selected binding sites close to the genes of potential interest (such as *Arid3b, Ascl2* and *Hes1*) was successfully confirmed (figure 4.14D), suggesting that the antibody could be used for ChIP-seq analysis.

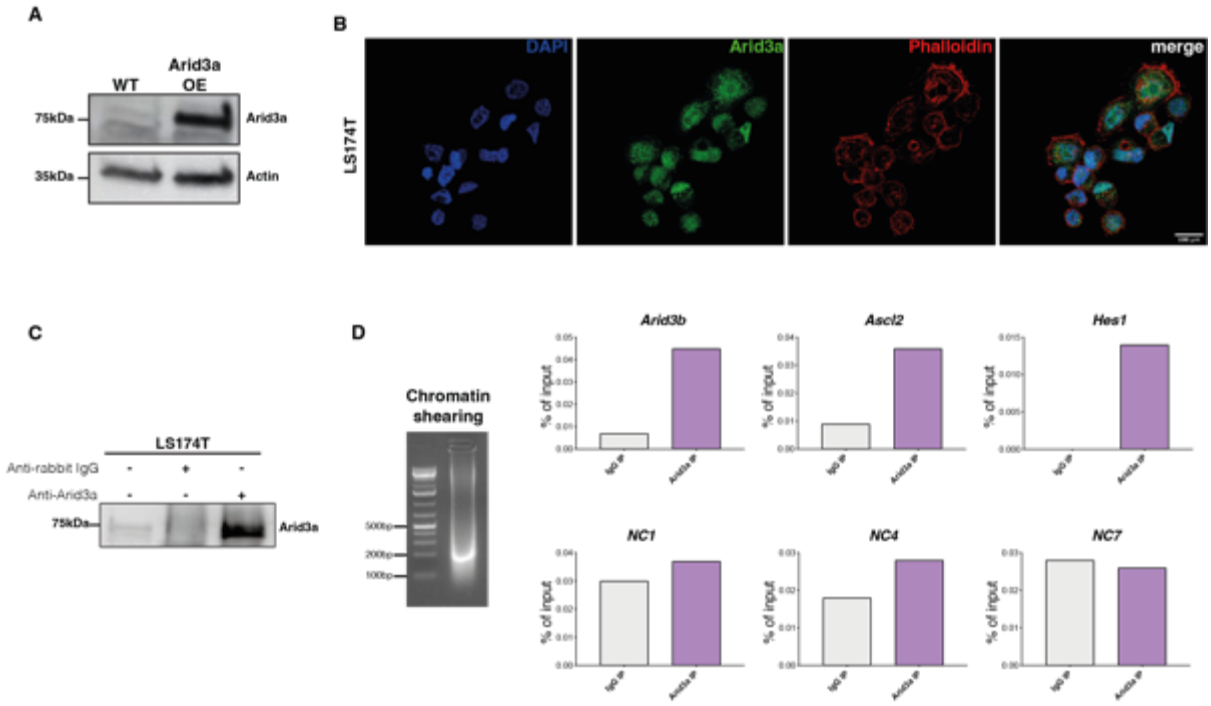

Figure 4.14 | Multi-step antibody validation for ChIP-seq.
(A) Western blot analysis of lysates from WT and Arid3a OE mouse intestinal organoids. Image from n=1 technical replicate. (B) Immunofluorescence staining of ARID3A using LS174T cells. Images from n=1 technical replicate. (C) Immunoprecipitation of ARID3A in lysates of LS174T cells. Representative image from n=2 technical replicates. (D) Optimised chromatin shearing and ChIP-qPCR analysis of Arid3a using intestinal crypts. N=1 biological replicate.

Next, we proceeded to downstream ChIP-seq analysis. Intestinal crypts from full-length intestine of both WT and Arid3a cKO animals were used. Although the purpose of the experiment was to unravel the binding sites in WT animals and to understand how binding correlates with the transcriptional changes observed in the RNA-seq of KO animals, we utilised Arid3a cKO animals as a control. From our experience crypt fractions contain ~5% of non-epithelial stromal cells. This contamination does not affect our RNA-seq results since Arid3a is conditionally deleted specifically in epithelial cells. Thus, any gene expression changes observed can be attributed to the epithelial cells. However, since Arid3a is also strongly expressed in stromal cells (figure 3.5A,B), any detected ChIP-seq binding sites in WT animals could be associated with non-epithelial cells. By analysing Arid3a cKO mice, we believed that we will be able to normalise the WT data since any peaks detected in the cKO tissues would likely be coming from stromal cells.

Several quality control (QC) steps were performed prior to analysing the sequencing data. We first created a fingerprint plot, a useful QC for visualisation of the genome-wide relative enrichment of the IP samples with respect to the input control

(figure 4.15A). The plot shows a profile of cumulative read coverage for each sample and determines how well the signal in the ChIP-seq sample can be differentiated from the background distribution of reads in the input control sample. Ideally, the input control should form a straight diagonal line and the distance of each ChIP sample line would indicate a very strong and specific enrichment. However, in this case, neither the input control formed a straight line, nor the ChIP samples were very distant from the input, although they all indeed showed binding enrichment (figure 4.15A,B). Next, the signal-to-noise ratio in our experiment was assessed using two different metrics: (1) the normalized ratio between the fragment-length cross-correlation peak and the background cross-correlation (normalized strand coefficient, NSC) and (2) the ratio between the fragment-length peak and the read-length peak (relative strand correlation, RSC). Successful ChIP-seq experiments have NSC>1.05 and RSC>0.8. Our data set failed to pass the cut-off value for NSC, but it passed the RSC threshold (figure 4.15B,C). Subsequently, peaks were called for each sample. Unfortunately, only one sample per group (WT and KO) showed a high number of peaks (>30000, typical of a transcription factor). Two WT and two KO samples only called for a few hundred peaks (figure 4.15D). Interestingly, when comparing the one WT and one KO sample with sufficient number of peaks, we saw that almost ~50% of these peaks was different between the two samples (figure 4.15D), suggesting that there could be cell-type specific (epithelial vs stromal) binding targets of Arid3a.

The low reproducibility among samples and the multiple failed QC steps indicated that no safe conclusions could be withdrawn from this experiment. Although antibody validation was successful, good chromatin immunoprecipitation requires very high antibody specificity and decent endogenous protein expression. The antibody used here is polyclonal which may partly explain the poor ChIP-seq quality. Future experiments using a specific monoclonal antibody against Arid3a would likely improve the result.

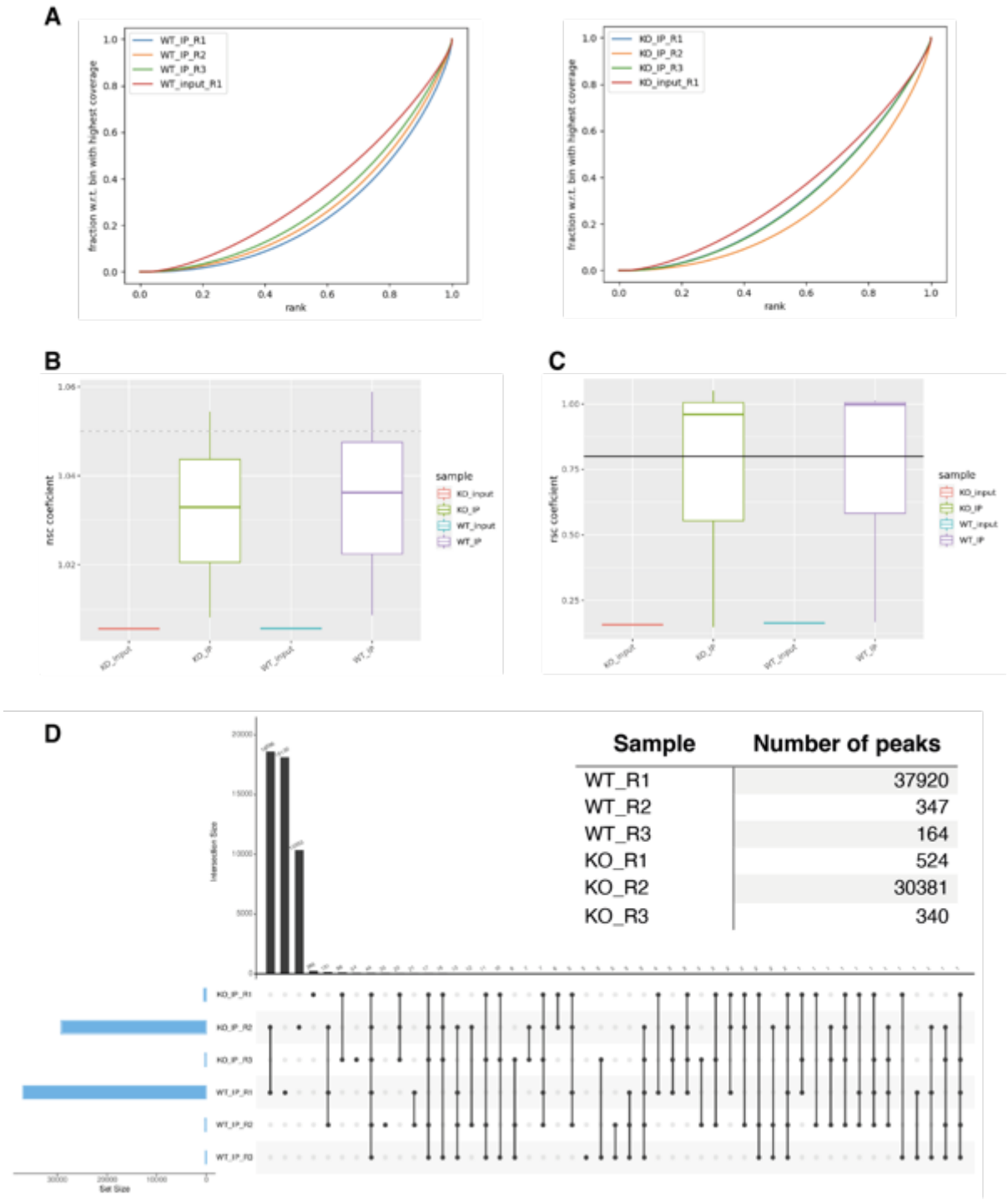

Figure 4.15 | Arid3a ChIP-seq analysis.
(A) Fingerprint plot of WT and Arid3a cKO input and IP samples. (B) Normalised strand coefficient (NSC) plot. (C) Relative strand correlation (RSC) plot. (D) Number of peaks called per IP sample and their distribution across samples.

4.2.8 Arid3a regulates TA cell transition by inhibiting Hnf-mediated epithelial differentiation

Over the past two decades, a variety of new techniques has been developed to allow the study of gene regulation on an epigenetic level. These techniques include DNase I hypersensitive sites sequencing (DNase-seq), Formaldehyde-Assisted Isolation of Regulatory Elements sequencing (FAIRE-seq) and Assay of Transposase Accessible Chromatin sequencing (ATAC-seq) (Yan et al., 2020). The latter relies on the hyperactive Tn5 transposase to cleave open chromatin and ligate sequencing adapters to cleaved regions (Buenrostro et al., 2015), which has become one of the most commonly used techniques due its high sensitivity and the low input of cell requirement.

Here we used ATAC-seq to assess the differences in chromatin accessibility between WT and Arid3a cKO intestine, which will provide mechanistic understanding of how Arid3a regulates the proliferation/differentiation balance of the intestinal epithelium. Similar to the RNA-seq experimental design, 3 WT and 3 Arid3a cKO animals were used for ATAC-seq 1 month after tamoxifen administration. Analysis of the ATAC-seq data showed that the Arid3a cKO intestine exhibits a more global open chromatin pattern when compared to WT (figure 4.16A). The result was unexpected considering that Arid3a deletion caused increased differentiation, while differentiation is often associated with less open chromatin. However, when comparing the expression of histone genes in WT and Arid3a cKO animals, we noted that loss of Arid3a led to a reduction of histone genes, which could partially explain the less packed DNA (figure 4.16B). Next, we sought to examine the chromatin status in more detail. By using the gene lists associated with villus-tip and crypt of differentiated cells, we compared the chromatin status around the transcription start sites (TSS) of these gene signatures. In accordance with increased gene expression at the villus tip, chromatin was found more open around the TSS of these genes (figure 4.16C). However, similar pattern of more open chromatin was also observed around the TSS of crypt-associated genes (figure 4.16C), making it more difficult to understand how Arid3a modulates chromatin status to control the proliferation-to-differentiation transition. To gain more insight into the mechanism of Arid3a function, we used a recently published methodology (Transcription factor Occupancy prediction By Investigation of ATAC-seq Signal – TOBIAS) for footprinting analysis of

ATAC-seq (Bentsen et al., 2020). TOBIAS enables genome-wide analysis of transcription factor dynamics and calculates enriched motif binding using publicly available binding motifs of hundreds of transcription factors. Interestingly, TOBIAS analysis of our ATAC-seq data showed that there was an enrichment of transcription factor binding sites in genomic regions that are rich in A+T in the Arid3a cKO animals (figure 4.16D). These transcription factors include members of the Arid family (Arid3b and Arid5a) as well as members of the Hnf family (Hnf1 and Hnf4) (figure 4.16D). Interestingly, Hnf proteins have been previously associated with terminal maturation of enterocytes (Babeu et al., 2009, Chen et al., 2019, D'Angelo et al., 2010). Hnf proteins are expressed across the crypt/villus axis, although their expression is stronger in the villus. It is conceivable that enrichment of Hnf activity in the Arid3a cKO intestine results in increased gene expression of terminally differentiated villus cells. Of note, our RNA-seq data confirmed transcriptional upregulation of Hnf4γ in Arid3a-deficient intestine. The results suggest that Arid3a may function to regulate the TA cell transition by inhibiting Hnf-mediated epithelial differentiation.

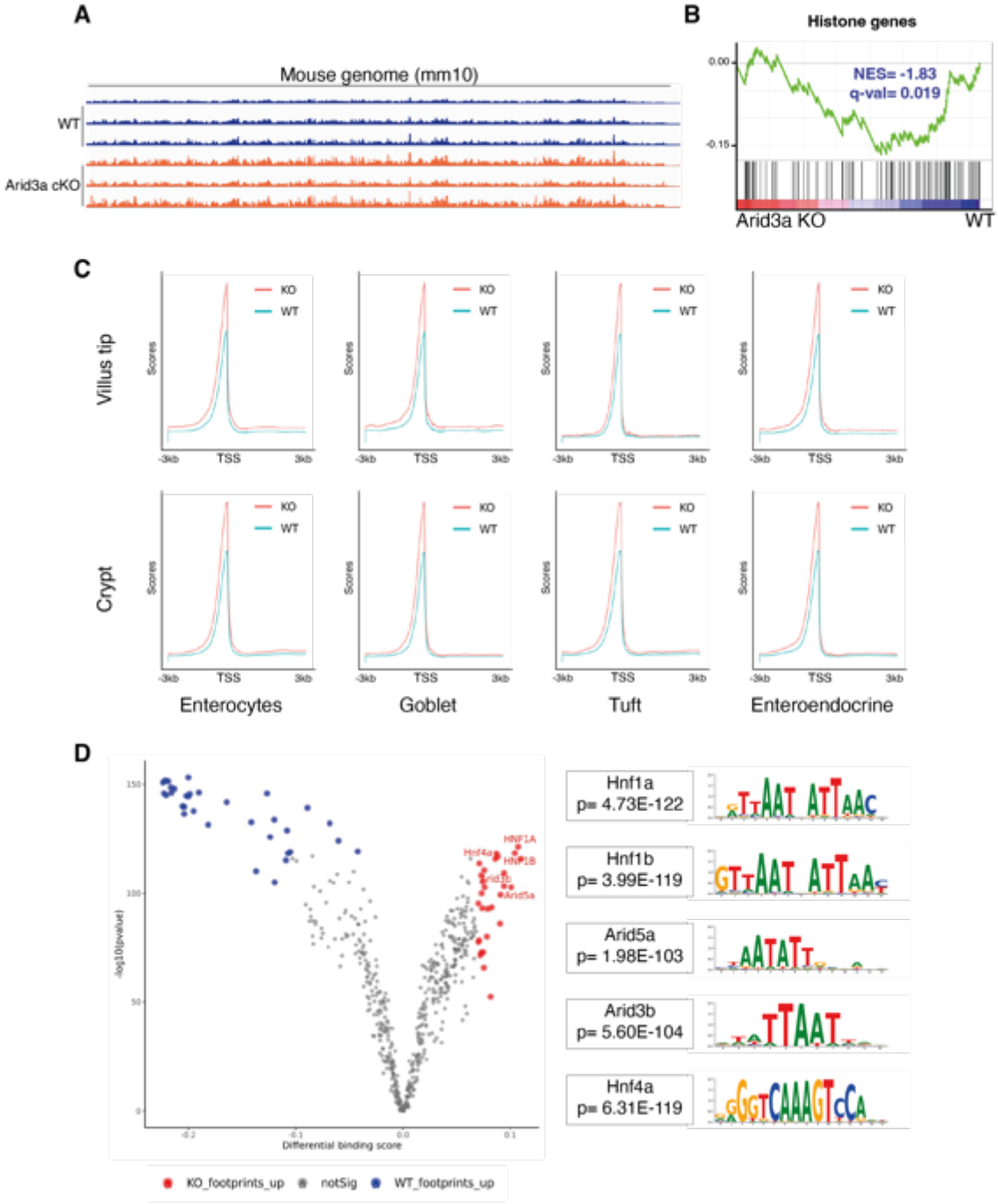

Figure 4.16 | Deletion of Arid3a allows Hnf- family of transcription factors to bind to A+T rich regions.
(A) Genome-wide comparison of open ATAC-seq chromatin peaks between WT and Arid3a cKO animals (tracks extracted from IGV). (B) GSEA of histone genes based on RNA-seq analysis of WT versus Arid3a cKO animals (1 month after tamoxifen administration). (C) PlotProfile visualisation to compare the enrichment of WT and Arid3a cKO animals at transcription start sites (TSS) of crypt and villus tip -associated genes. (D) Analysis of the ATAC-seq using the TOBIAS package (see methods). Volcano plot shows the differential binding activity against the -log10(p-value) of all investigated transcription factor motifs. Each dot represents one motif; blue dots represent motif enrichment in WT; red dots represent motif enrichment in Arid3a cKO. Representative examples of transcription factors enriched in Arid3a cKO animals is shown of the right.

4.2.9 Loss of Arid3b does not affect proliferation and differentiation

As discussed in Chapter 3, Arid3a interplays with its nuclear paralogue Arid3b in a variety of biological processes. Since Arid3b is expressed throughout the crypt-villus axis, we hypothesized that it might be functionally redundant to Arid3a in the TA cells to regulate the proliferation/differentiation transition. To characterise the potential functional overlap, we also generated and analysed the Arid3b cKO and DKO animals (section 4.1, figure 4.1). Analysis of H&E-stained tissues revealed that both Arid3b and DKO animals did not exhibit any major morphological differences (figure 4.17A). However, pathological review of these tissues (review criteria from figure 4.2B) unveiled that these mouse lines also exhibited a minimal villus atrophy, which was less notable compared to the one observed in Arid3a cKO animals (figure 4.17B). To our surprise, DKO did not contribute to cumulative phenotype. In contrast to the Arid3a cKO animals, there was no significant difference in the weight these animals (figure 4.17C). Arid3b cKO showed a variable but significant increase in small intestinal length (figure 4.17C). To further characterise the phenotypes of Arid3b cKO and DKO, intestinal crypts from both lines were collected for RNA-seq analysis in parallel with WT and Arid3a cKO samples. Principal component analysis (PCA) revealed a very interesting result. Arid3a cKO animals were the only group to differentiate and clustered separately, while WT, Arid3b cKO and DKO showed no clustering (figure 4.17D). This was confirmed by the differential gene expression analysis. While Arid3a cKO animals had a large number of upregulated or downregulated genes compared to WT (3211 genes, FDR cut-off <0.05), Arid3b cKO showed very limited differences (54 genes) and DKO had an intermediate phenotype (1339 genes) (figure 4.17E).

To validate the RNA-seq results, we performed immunostaining of differentiation (expression of enterocyte marker Apoa4, figure 4.17F) and proliferation (number of EdU-positive cells per crypt, figure 4.17G) markers on Arid3b cKO and DKO intestine. No differences were observed in any of the two KO lines, although DKO animals showed a reduced but not statistically significant reduction of EdU-positive cells (figure 4.17G). The lack of phenotypes of the Arid3b cKO animals indicates that Arid3a and Arid3b may function differently at the intestinal epithelial cells. The intermediate phenotype of DKO animals further suggests that there might be opposing functions of the two paralogues. It would be interesting to further explore the distinct role of Arid3b in intestinal homeostasis.

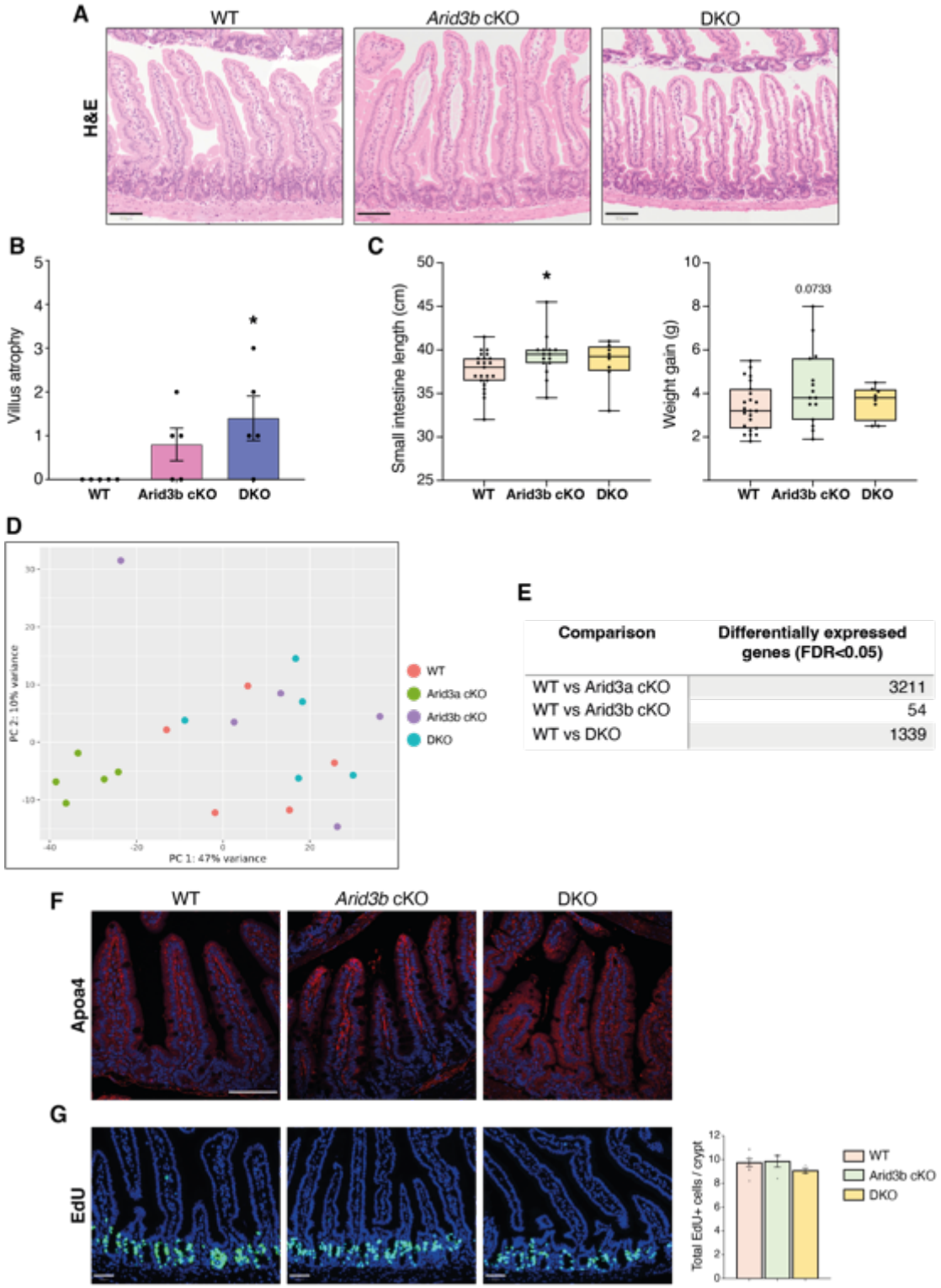

Figure 4.17 | Loss of Arid3b does not affect proliferation and differentiation at 1 month after tamoxifen administration.
(A) H&E staining of WT, Arid3b cKO and DKO mice. Representative images of N=23 WT animals, N=15 Arid3b cKO animals and N=8 DKO animals. Scale bar, 100μm for H&E. (B) Results of the pathologist's report of WT, Arid3ab cKO and DKO small intestinal tissue. N=5 animals per experimental group. (C) Differences in small intestinal length(cm) and weight gain (g) at 1 month after tamoxifen administration. N=23 WT animals, N=15 Arid3b cKO animals and N=8 DKO animals. Box plots show all datapoints from min to max. *P<0.05, **P<0.01 , ***P<0.001, two-sided t-test. (D) PCA plot of all RNA-seq samples. (E) Table showing the number of differentially expressed genes based on RNA-seq analysis. FDR <0.05 (F) Immunostaining of WT, Arid3b and DKO animals against enterocyte marker Apoa4. Representative images from N=5 per group. Scale bar, 100μm. (G)EdU staining of WT, Arid3b cKO and DKO animals. Representative images of N=8 WT animals, N=4 Arid3b cKO animals and N=3 DKO animals. Data represent mean ± s.e.m. *P<0.05, **P<0.01 , ***P<0.001, two-sided t-test. Scale bar, 100μm.

4.2.10 Long-term phenotypic analysis of the conditional knockout animals

Analysis of WT and KO animals in sections 4.2.1 – 4.2.9 was performed at 1 month after tamoxifen administration. At this timepoint, Arid3a was uncovered as a major modulator of intestinal homeostasis by regulating proliferation and differentiation, while the role of Arid3b was found to be dispensable. We sought to further explore the effects of KO of the two genes at later timepoints, more specifically at 3, 6, 12 and 18 months after tamoxifen administration. We focussed on understanding how long-term health of the animals is affected by deletion of Arid3a, including imbalanced differentiation dynamics of the intestinal epithelium and alterations in digestion, absorption and response to external stimulus. Since 1 month deletion of Arid3b did not show any noticeable impairment, we explored whether long-term deletion of Arid3b would exhibit any delayed phenotype in the intestine in both single and double KO animals. For these later timepoints, we also assessed whether the upper gastrointestinal tract (stomach), spleen and liver were affected as a consequence of altered intestinal homeostasis (figure 4.18).

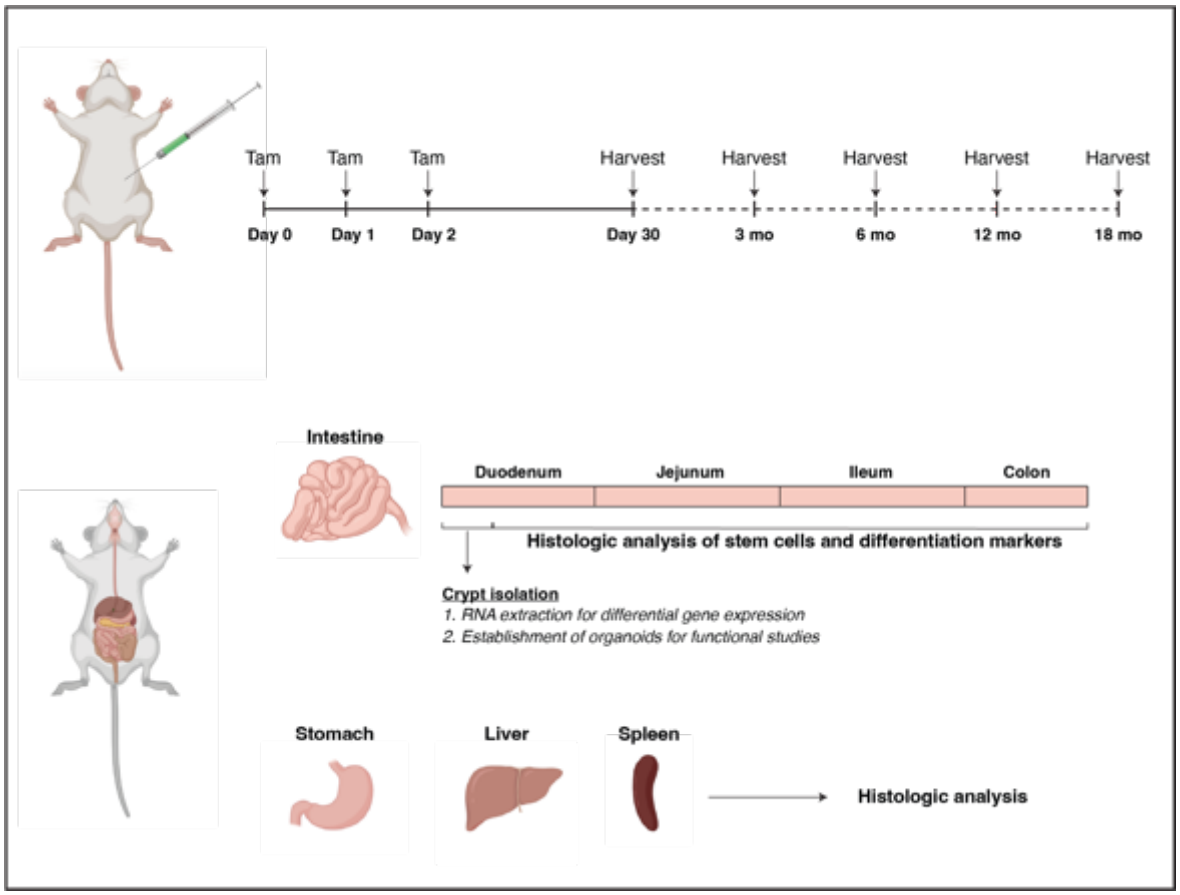

Figure 4.18 | Schematic representation of the experimental approach at later timepoints.

To validate our findings on the role of Arid3a in regulating intestinal proliferation and differentiation, RNA-seq of WT and Arid3a cKO animals was performed on intestinal crypts isolated 3 months after tamoxifen administration. Samples from this RNA-seq run were pooled together with samples from the 1-month RNA-seq analysis for the same genotypes. PCA showed distinct clustering of WT and Arid3a cKO intestine independent of timepoint (figure 4.19A). However, samples from the two experimental time points (1 month vs 3 months) appeared to cluster separately (figure 4.19A). This could be attributed to either batch effect from different RNA-seq runs or to the age differences between animals. To characterise the gene expression changes upon Arid3a loss, WT and KO samples of both timepoints were pooled together for analysis. Differential gene expression analysis showed a total of 1792 genes significantly changed upon Arid3a deletion in both timepoints (FDR <0.05, figure 4.19B). GSEA was performed on the combined data set and confirmed a downregulation of Wnt signalling and TA cell signature (figure 4.19C). We further confirmed that gene expression of early enterocyte and secretory cells at the crypt was downregulated, while the expression signature of the mid-villus and villus tip of both cell types was highly upregulated in the Arid3a cKO intestine in both timepoints (figure 4.19D, 4.20A-C). The results demonstrate that loss of Arid3a perturbs the TA cell transition by pushing the proliferating progenitor cells to terminal differentiation, and such effect persists even 3 months after tamoxifen induction.

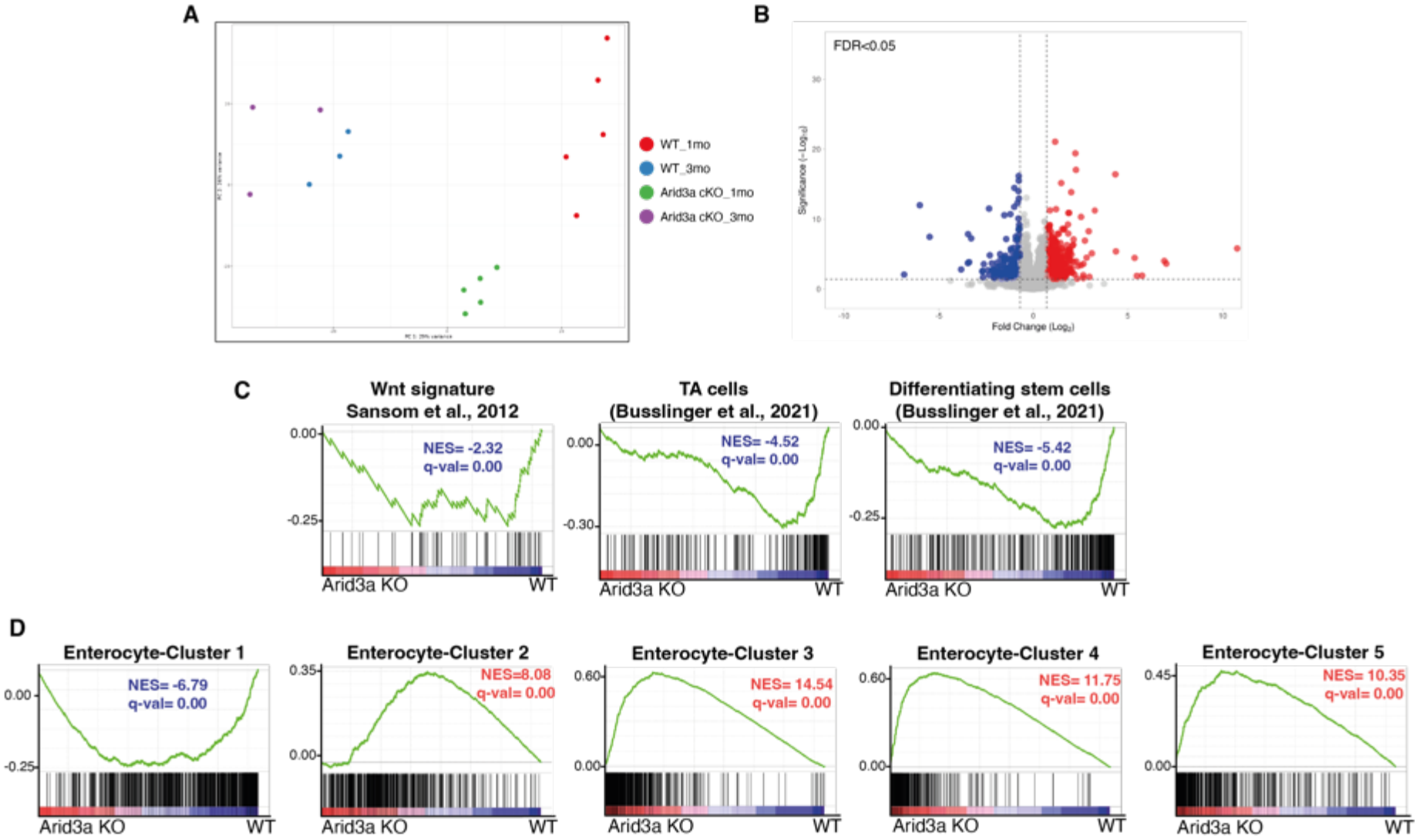

Figure 4.19 | Loss of Arid3a leads to increased transcriptional signature of upper villus enterocytes independently of timepoint.
(A) PCA of WT and Arid3a cKO animals from 1mo and 3mo timepoints. (B) Volcano plot showing differentially expressed genes in WT versus KO comparison independently of timepoint (blue: downregulated in KO; red: upregulated in KO). FDR <0.05, $\log_2$(fold change)>1.5. (C) GSEA of Wnt signalling, TA cells and differentiating stem cells signatures. (D) GSEA of the five enterocyte clusters (Moor et al., 2018).

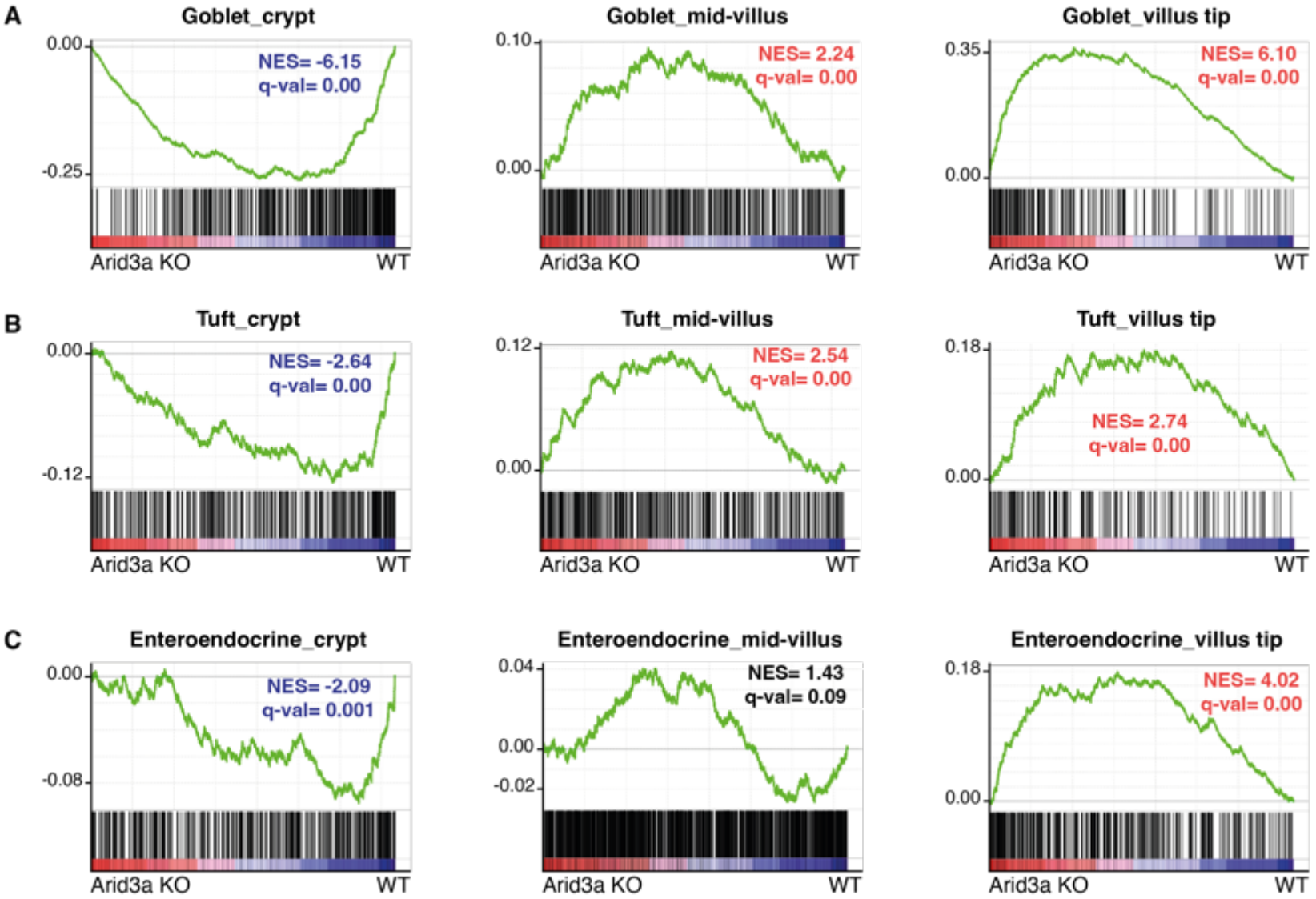

Figure 4.20 | Loss of Arid3a leads to increased transcriptional signature of upper villus secretory cells independently of timepoint.
GSEA of zonation programmes of goblet (A), tuft (B) and enteroendocrine cells (C) (Manco et al., 2021).

Despite the TA transition perturbation, the Arid3a KO animals survived over the course of 18 months after tamoxifen administration and did not present major health issues. Similarly, no phenotype was observed in the Arid3b and DKO animals. H&E staining of small intestinal sections at later timepoints showed no significant difference in their tissue architecture (figure 4.21). Pathological analysis of tissues at 12 months showed that KO animals showed no signs of inflammation, epithelial injury or villus atrophy. Moreover, assessment of stomach H&E sections at the same timepoint also showed no differences between WT and KO animals (data not shown).

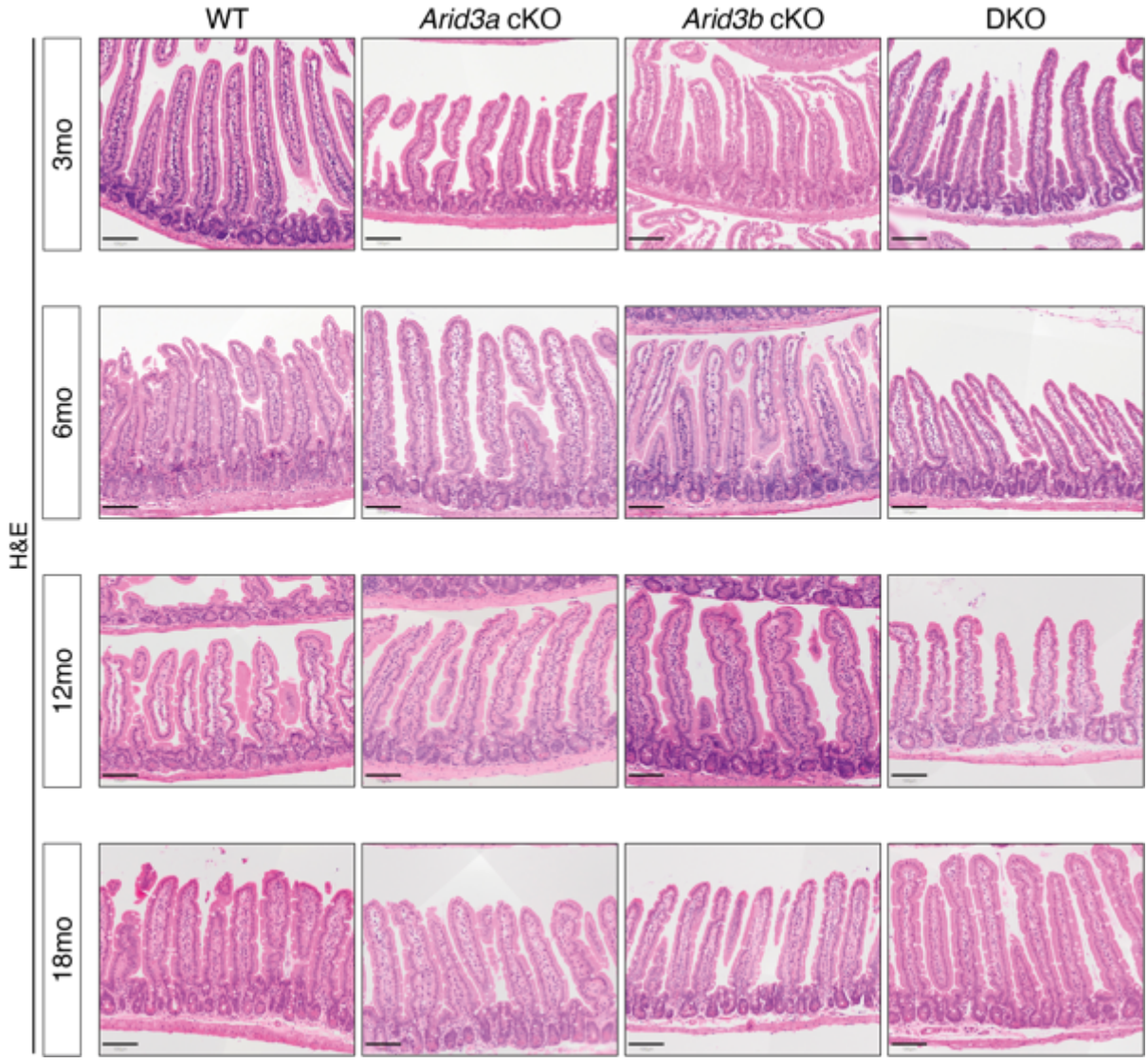

Figure 4.21 | Phenotypic analysis of small intestine after long-term deletion of Arid3a and/or Arid3b.
H&E staining of WT, Arid3a cKO, Arid3b cKO and DKO animals at 3-, 6-, 12- and 18-months post-tamoxifen administration. Representative images of minimum N=5 animals for each genotype at all timepoints. Scale bar, 100μm.

The weight gain and small intestinal length were also measured at various timepoints to assess how Arid3a and Arid3b affect the long-term homeostasis of the animals. Our data showed that all KO animals gain slightly more weight than the WT after 6 months, although the increase was not statistically significant in most cases (figure 4.22). Moreover, and in accordance with the 1-month data, Arid3a cKO showed a reduction in small intestinal length compared to WT (figure 4.22). Interestingly, the shortening was increasingly obvious and at later timepoints, suggesting an important role of epithelial Arid3a in maintenance of the small intestinal length. On the other side, Arid3b cKO animals and DKO animals exhibited longer small intestines than WT animals (figure 4.22). Together with the RNA-seq data, the results suggest a unique and possibly redundant role of Arid3b in the intestine. The exact role of Arid3b poses an interesting biological situation whereas single Arid3b KO does not produce any major differences in gene expression, but in absence of Arid3a, loss of Arid3b causes a milder phenotype than the single Arid3a KO. This will be further discussed at the end of this chapter.

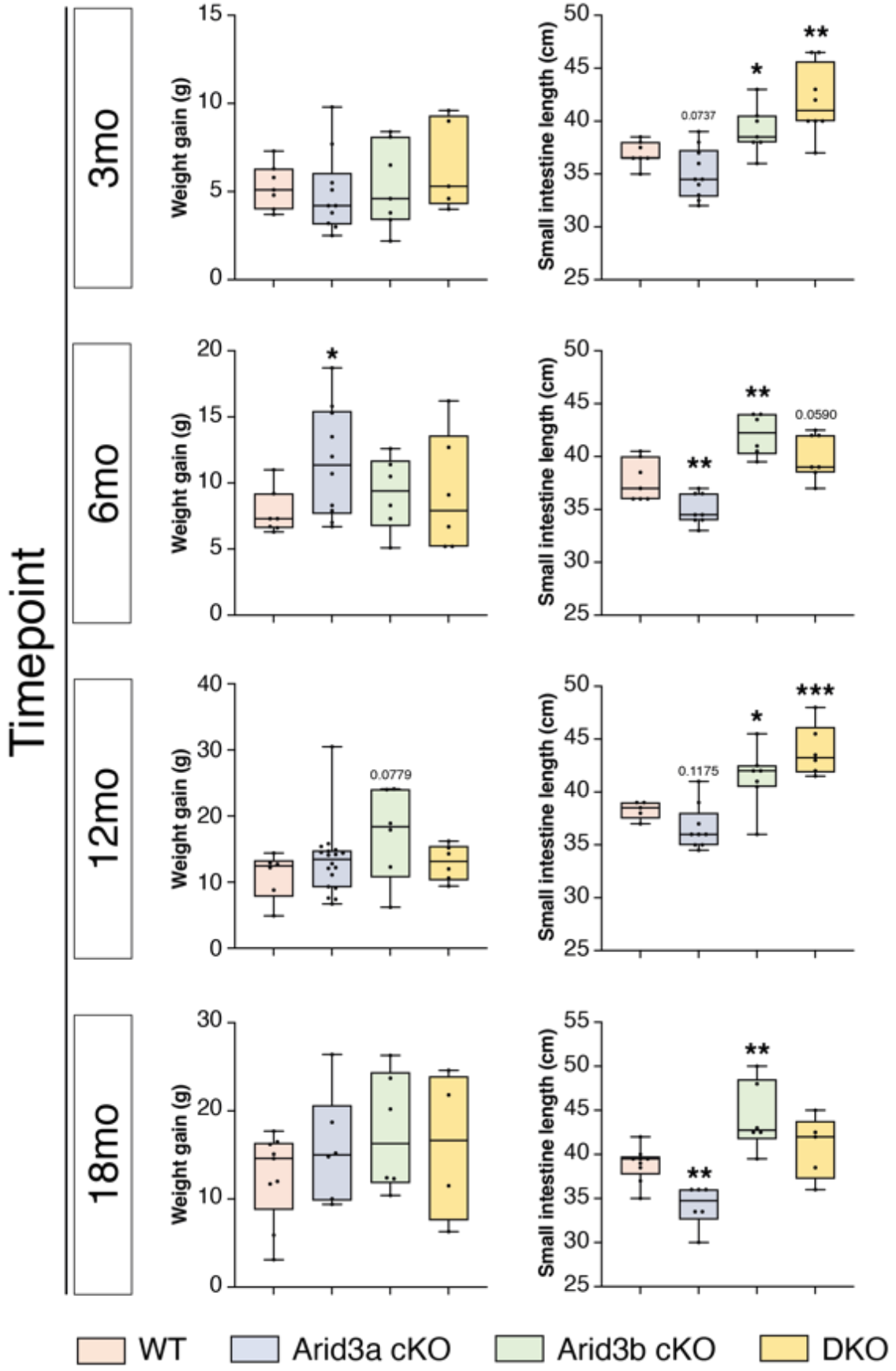

Figure 4.22 | Weight loss and small intestinal length after long-term deletion of Arid3a and/or Arid3b.
Box plots show all datapoints from min to max. *P<0.05, **P<0.01 , ***P<0.001, two-sided t-test. Minimum N=5 animals for each genotype at all timepoints.

Lastly, immunofluorescence staining against the late enterocyte marker Apoa4 was used to assess upper villus differentiation at later timepoints. Interestingly, we noted that not only Arid3a cKO but also Arid3b cKO and DKO intestine showed an increased expression of Apoa4 at all timepoints (figure 4.25). This indicated a delayed effect of Arid3b in enterocyte differentiation. Whether this is dependent or independent to Arid3a is yet to be examined. Since Apoa4 is involved in lipid absorption (Wang et al., 2015), we asked whether the fat percentage of the KO animals is increased. To address this question, the mesenteric and abdominal fat of WT and KO animals was assessed at 12- and 18-month timepoints. Interestingly, Arid3a cKO exhibited 26.6% increase (WT mean= 9.12% ; Arid3a cKO mean=11.55%; p-value=0.17) in total fat and 37.8% increase (WT mean= 6.24% ; Arid3a cKO mean=8.60%; p-value = 0.12) in abdominal fat at 18 months (figure 4.26B). On the other hand, Arid3b cKO and DKO animals showed no differences at either timepoints (figure 4.26A,B).

In summary, we conclude that the effects of Arid3a deletion on intestinal epithelium proliferation and differentiation persist in the long-term, which affect intestinal length and body fat but without impairing their survival. Arid3b seems to affect differentiation at later timepoints, but its overall effect is much milder compared to Arid3a. Collectively, our analysis from 1 to 18 months KO animals suggests that Arid3a and Arid3b may have distinct function in intestinal epithelial homeostasis. This will be further discussed at the end of this chapter and in Chapter 6.

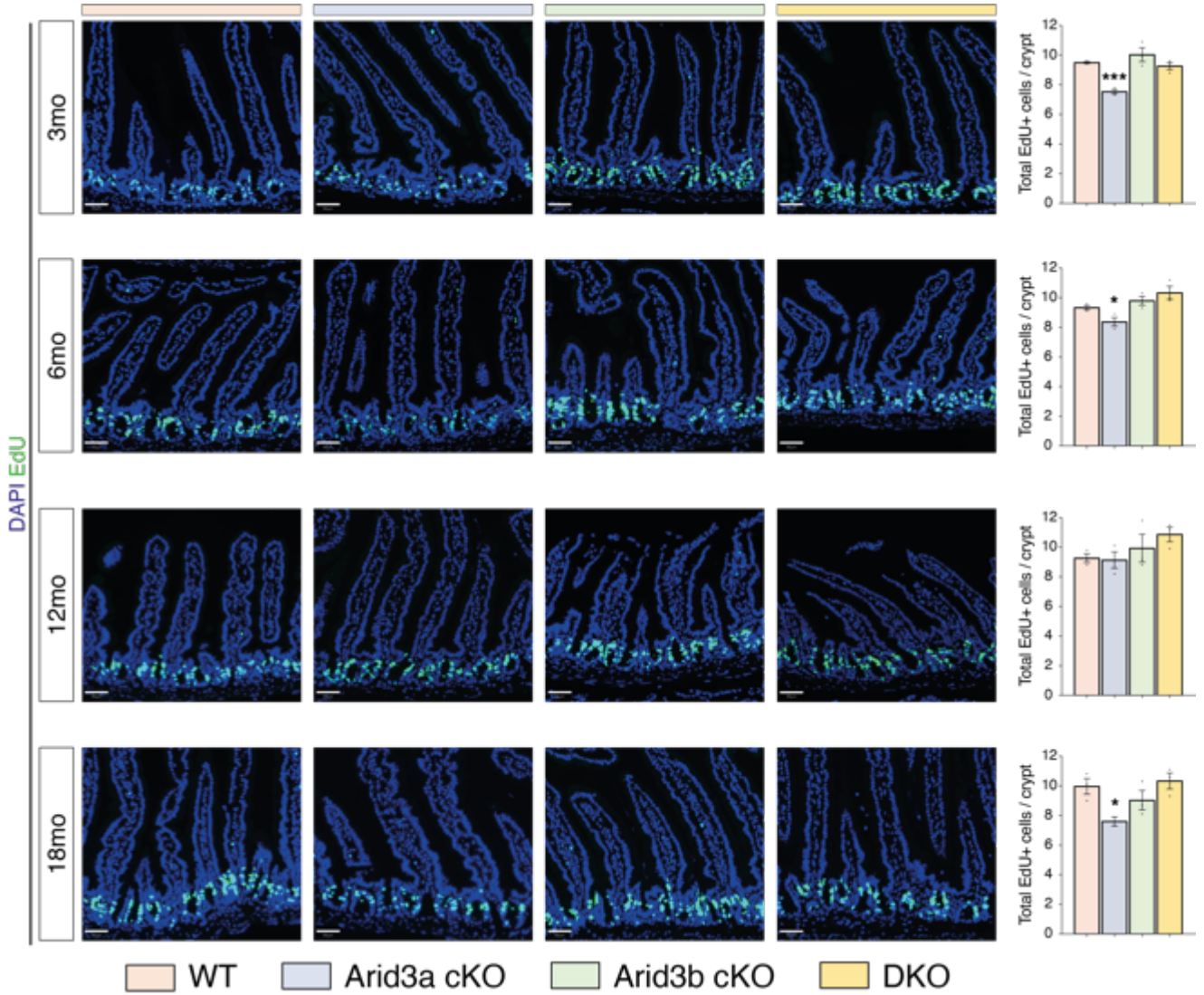

Figure 4.23 | Loss of Arid3a results in a sustained loss of EdU-positive cells.
EdU staining at 3-, 6-, 12- and 18-months post-tamoxifen administration and quantification of positive cells at each timepoint. Representative images of N=3 animals for each genotype at all timepoints. Scale bar, 50μm. Data represent mean ± s.e.m. *P<0.05, **P<0.01 , ***P<0.001, two-sided t-test.

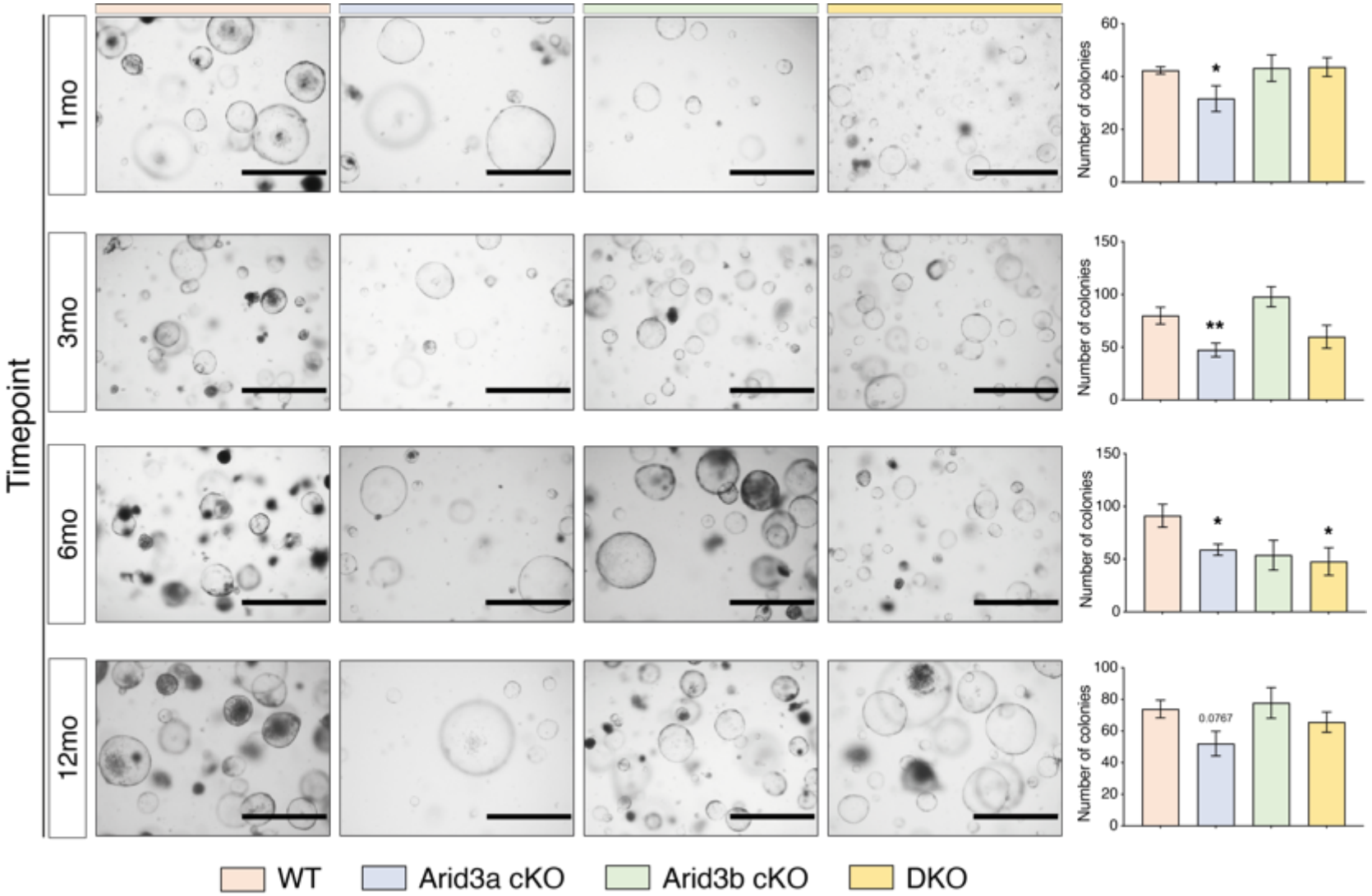

Figure 4.24 | Arid3a cKO organoids show a reduced capacity to form organoids over time.
Organoid formation assay was performed at 1- ,3- , 6- and 12-months post-tamoxifen administration. Representative images of minimum N=5 animals for each genotype at all timepoints. Scale bar, 1000μm. Data represent mean ± s.e.m. *P<0.05, **P<0.01 , ***P<0.001, two-sided t-test.

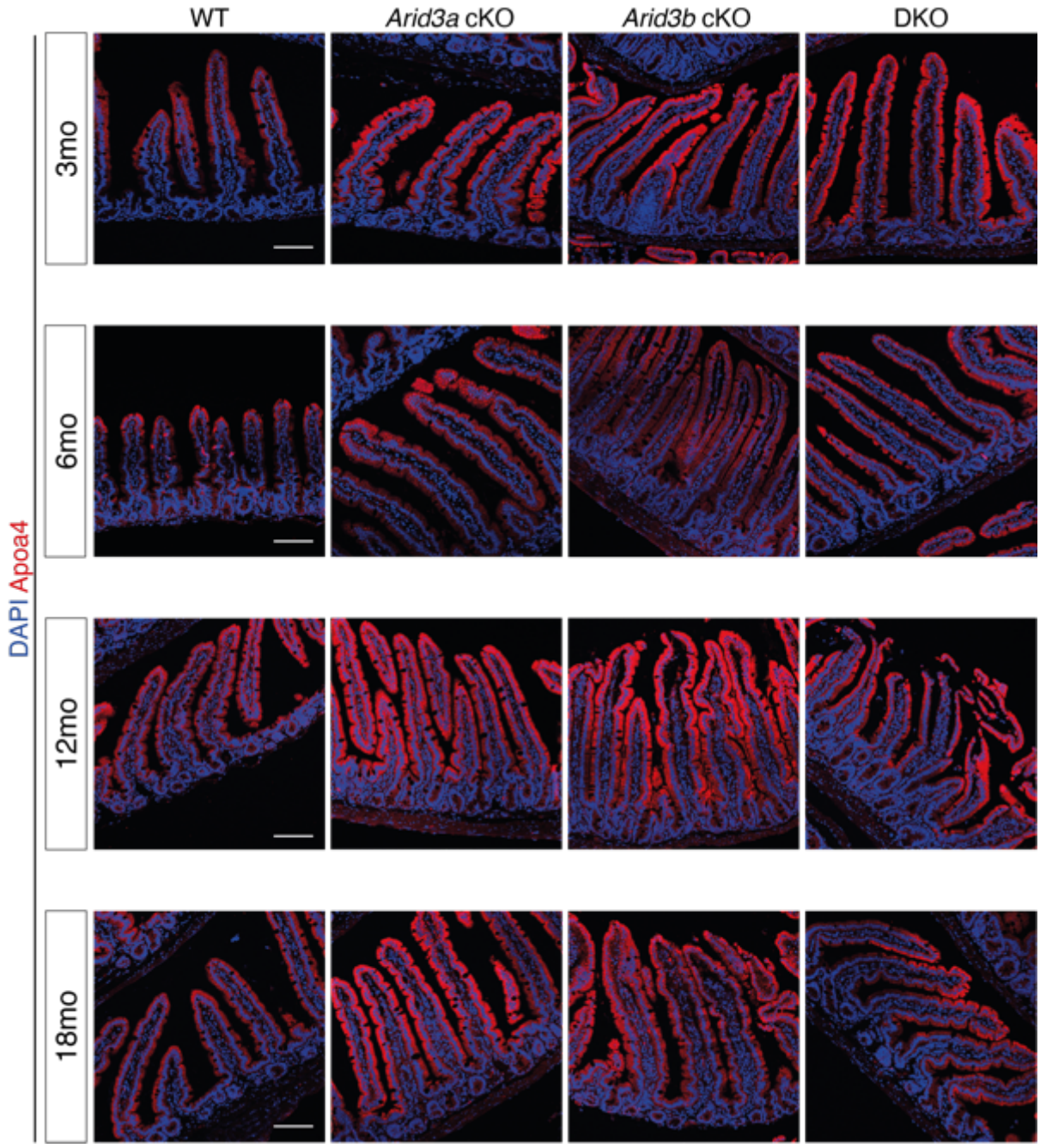

Figure 4.25 | Enterocytes are upregulated upon long-term deletion of both Arid3a and Arid3b. Apoa4 immunofluorescence staining at 3- ,6- ,12- and 18- months post-tamoxifen administration. Representative images of N=3 animals for each genotype at all timepoints. Scale bar, 100μm.

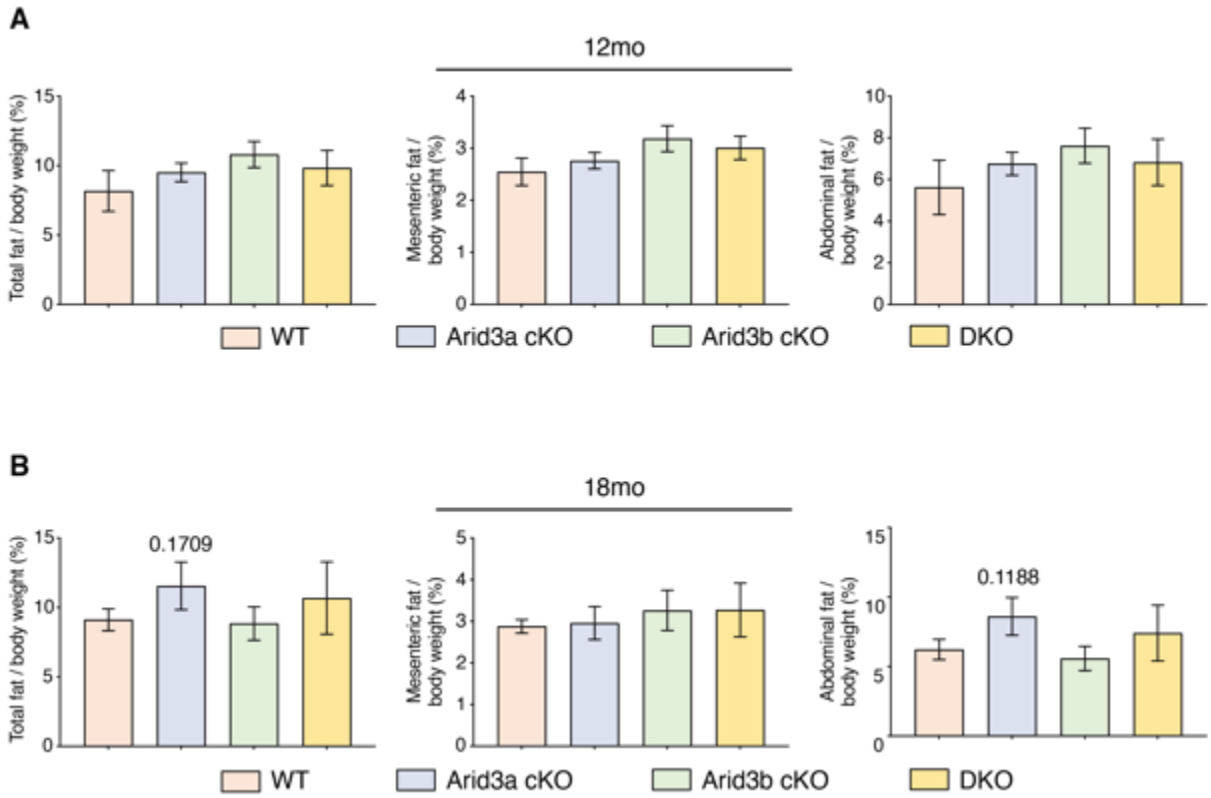

Figure 4.26 | Loss of Arid3a increases abdominal fat percentage.
Mesenteric and abdominal fat were measured at 12- and 18-months post-tamoxifen administration and their sum was used to calculate total fat. Minimum N=5 animals for each genotype at both timepoints. Data represent mean ± s.e.m. *P<0.05, **P<0.01 , ***P<0.001, two-sided t-test.

4.2.11 Effects of long-term intestinal-specific deletion of Arid3a/b on other organs

To gain a better understanding on how intestinal deletion affects the overall animal health, we examined any potential changes in organ size and histology of spleen and liver 3-18 months after tamoxifen administration.

Apart from food digestion and absorption, small intestinal epithelial cells exhibit immunomodulatory programmes in response to external stimulus or inflammation caused by dysregulated barrier function. The spleen plays a central role in the immune system and serves as a source of antibody-producing lymphocytes in response to inflammation. This response can be accompanied by an increase in spleen size. Histologic analysis of spleen sections revealed no structural differences in the KO animals (figure 4.27), and the size of spleen was also unaffected (figure 4.29). Moreover, pathological review assessing white pulp hyperplasia and red pulp hemosiderosis found no significant differences between WT and KO animals at 12 months after tamoxifen administration (figure 4.30A). The results are consistent with our earlier findings that the KO animals do not exhibit disrupted barrier function and, under normal homeostatic conditions, have no signs of inflammation.

On the other side, the liver plays a central role in metabolism. Our RNA-seq data revealed that Arid3a cKO animals showed a dramatic increase in metabolic processes, especially lipid metabolism. Increased intestinal lipid absorption can cause an accumulation of lipids in the liver. Hence, we examined any potential phenotypic changes in livers of the KO animals. Macroscopically, livers isolated from WT and KO animals did not show any significant differences regarding to their weight (figure 4.29). However, H&E staining of liver sections revealed morphological differences. All KO animals showed signs of cellular swelling and, in some cases, microvesicular fatty changes (figure 4.28). Moreover, pathologic review and quantification of tissue damage confirmed that Arid3a cKO liver exhibited an increase in hydropic changes and cellular swelling (p-value=0.085), while no differences were observed with regards to extramedullary haematopoiesis, degeneration and necrosis (figure 4.30B). Arid3b cKO and DKO also showed mild, but not significant, increase in liver hydropic degeneration (figure 4.30B).

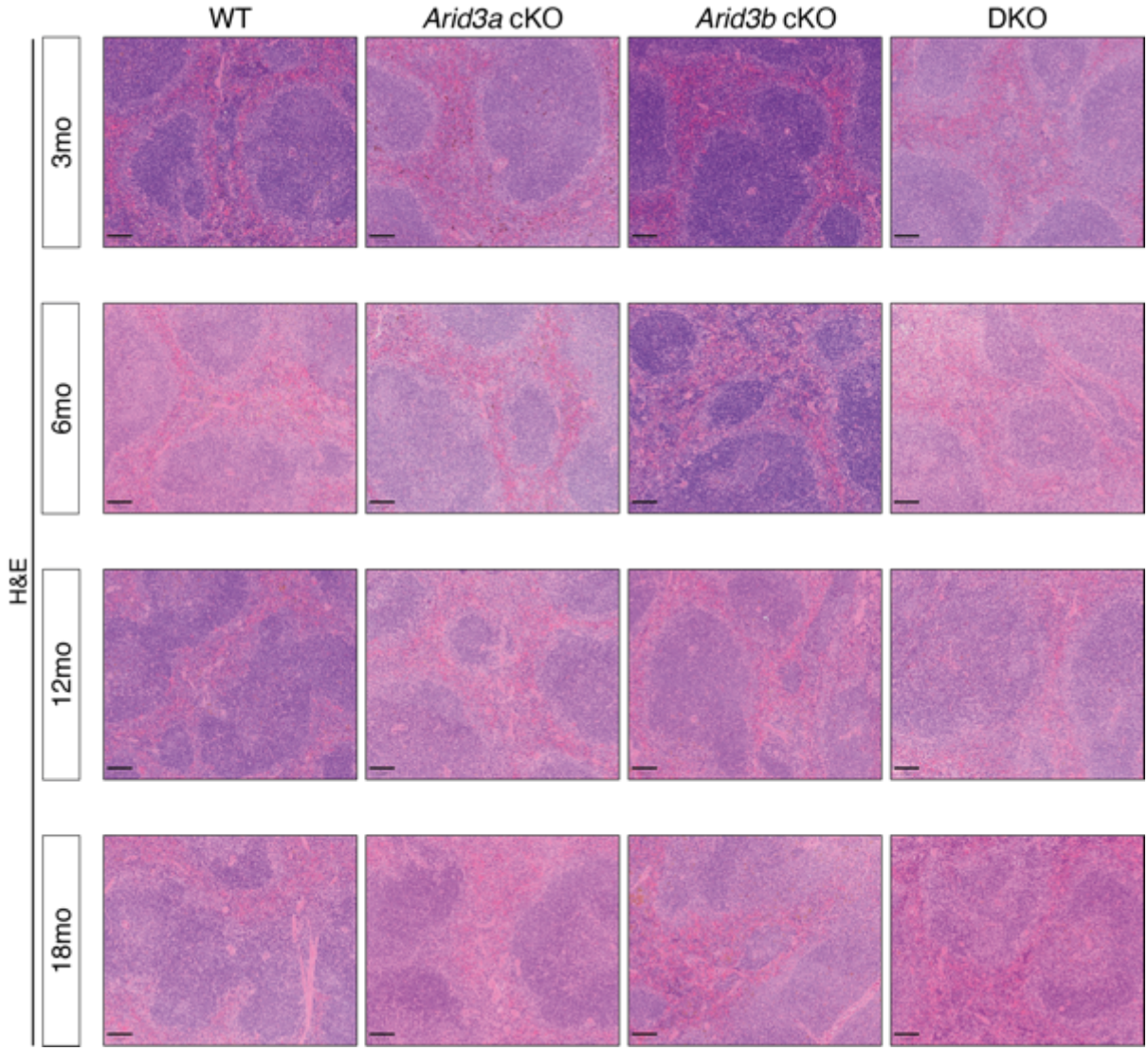

Figure 4.27 | Phenotypic analysis of spleen after long-term deletion of Arid3a and/or Arid3b.
H&E staining of WT, Arid3a cKO, Arid3b cKO and DKO animals at 3-, 6-, 12- and 18-months post-tamoxifen administration. Representative images of minimum N=5 animals for each genotype at all timepoints. Scale bar, 100μm.

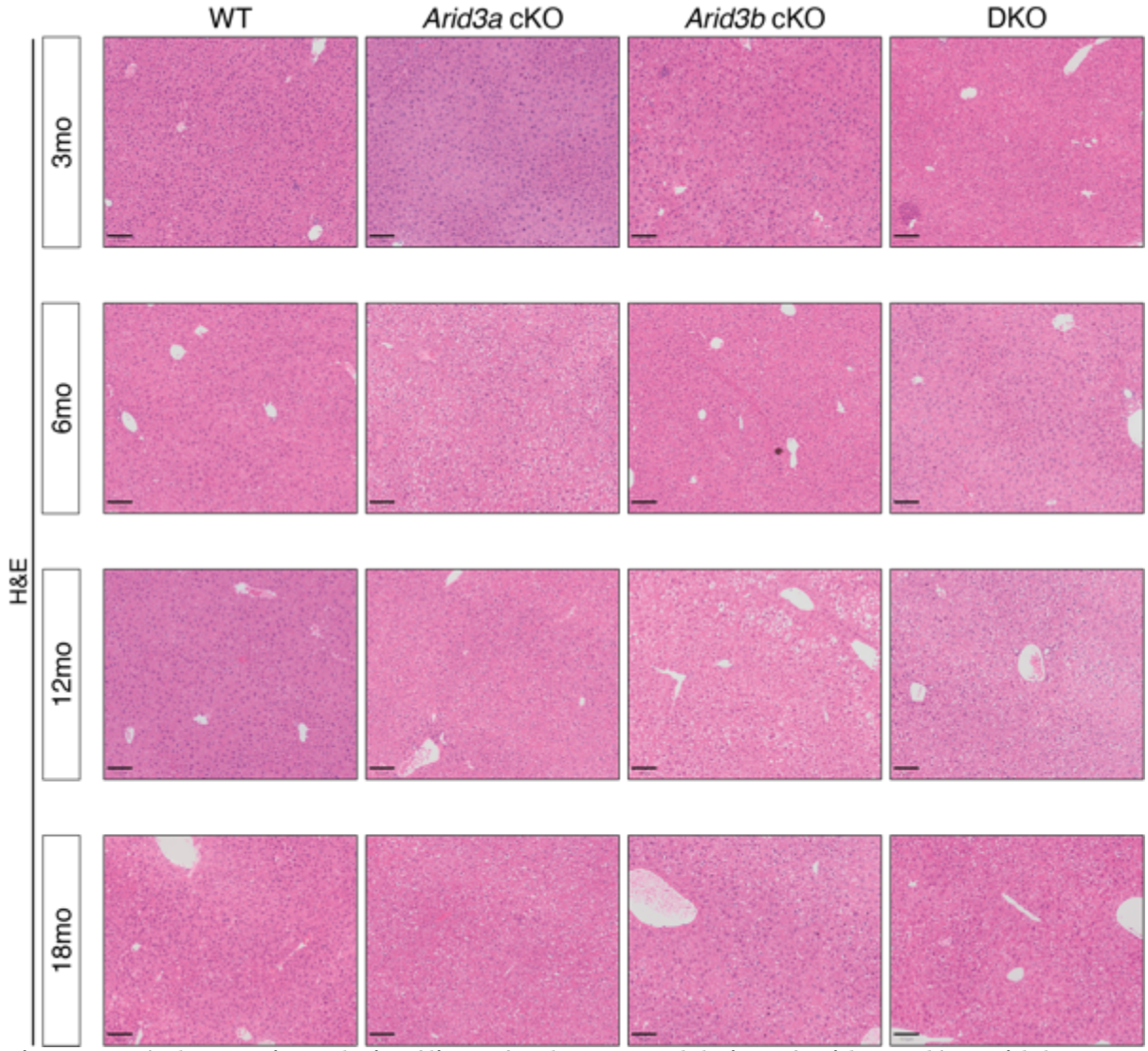

Figure 4.28 | Phenotypic analysis of liver after long-term deletion of Arid3a and/or Arid3b.
H&E staining of WT, Arid3a cKO, Arid3b cKO and DKO animals at 3-, 6-, 12- and 18-months post-tamoxifen administration. Representative images of minimum N=5 animals for each genotype at all timepoints. Scale bar, 100μm.

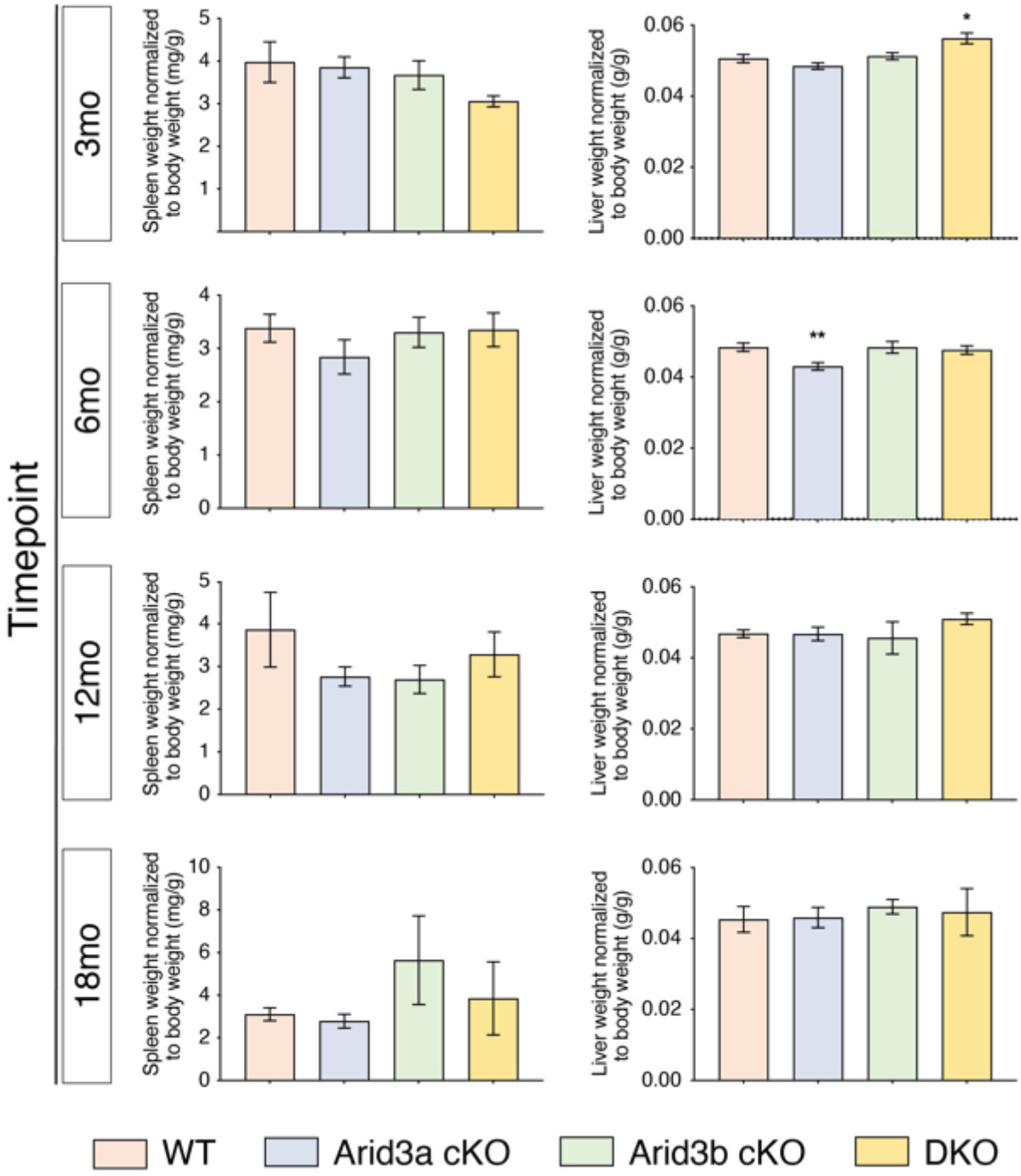

Figure 4.29 | No differences are observed in spleen and liver weight upon deletion of Arid3a and Arid3b.
Spleen and liver weight were normalised to the total body weight. Minimum N=5 animals for each genotype at each timepoint. Data represent mean ± s.e.m. *P<0.05, **P<0.01 , ***P<0.001, two-sided t-test.

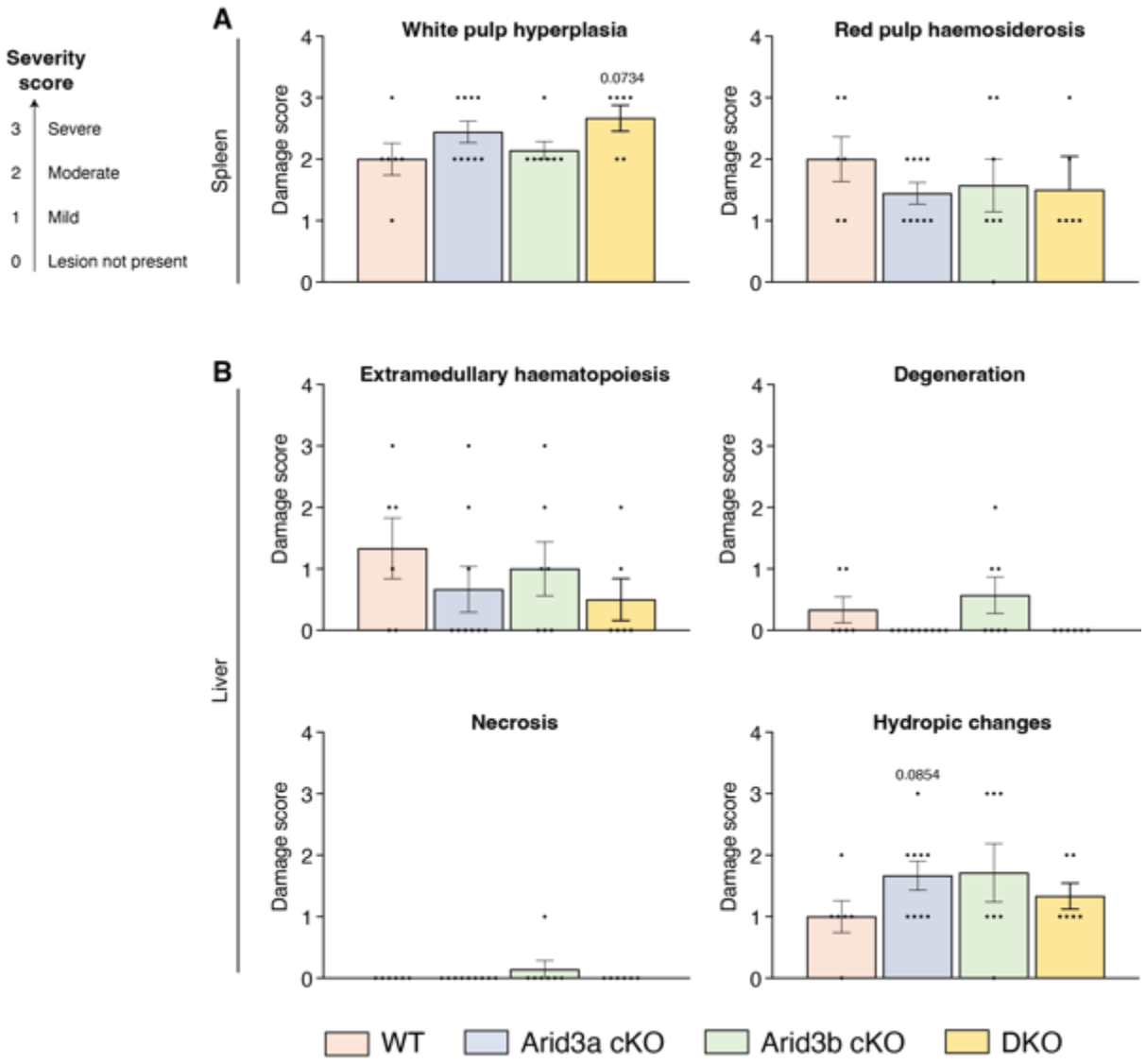

Figure 4.30 | Arid3a cKO animals show increased liver hydropic changes at 12 months after tamoxifen administration.
Spleen and liver H&E tissue sections were reviewed by pathologists and a semi-quantitative scoring system was used for their assessment. (A) Spleen sections were assessed for white pulp hyperplasia and red pulp hemosiderosis. (B) Liver sections were assessed for extramedullary haematopoiesis, degeneration, necrosis and hydropic changes. Minimum N=5 animals for each genotype. Data represent mean ± s.e.m. *P<0.05, **P<0.01 , ***P<0.001, two-sided t-test.

4.3 Summary and short discussion

The continuous self-renewal of the intestinal epithelium relies heavily on the ISCs at the crypt bottom which divide, differentiate and move to the villus to facilitate various functions of the intestine. Upon stem cell niche exit, lineage decision is taking place at the early progenitor cells at positions +4/+5 of the crypt and cells will commit to either absorptive or secretory lineages.

Our initial screening of transcription factors enriched at the +4/5 progenitors in Chapter 3 identified Arid3a as a putative regulator of epithelial differentiation. Expression analysis showed that Arid3a is not only localised at +4/5 early progenitors, but also throughout the differentiated cells at the villus with strong enrichment at the villus tip. The results suggest that Arid3a may have a broader functional role than decision making only at the +4/5 cells. Deletion of Arid3a in the intestinal epithelium resulted in reduced proliferation in TA cells whilst ISC numbers were unaffected, indicating that Arid3a functions to maintain the proliferation state in TA cells. Interestingly, transcriptomic analysis of the Arid3a cKO intestine revealed that Arid3a is not a conventional regulator of the absorptive vs secretory lineages at the early progenitor cells. Rather, it regulates the zonation programme of the entire intestinal epithelium. Expression analysis of the Arid3a cKO intestine showed a reduction of upper crypt committed cell signatures and a strong enrichment of mid-villus to villus-tip gene signatures (figure 4.31), suggesting that TA cells enter their differentiated status earlier. Indeed, ATAC-seq analysis revealed that this is likely due to the increased occupancy of A+T rich regions (previously occupied by Arid3a) by Hnf-family transcription factors which drive differentiation. Importantly, loss of Arid3a perturbs zonation of all intestinal cell lineages, highlighting its unique role in regulating intestinal epithelial cell differentiation. Of note, these perturbation phenotypes persist after long-term deletion, pointing to a central role of Arid3a in regulating the transitional programme of the TA cells.

Upregulation of the gene signatures of the mid-villus and villus tip cells in the Arid3a cKO animals would likely increase absorption and metabolic capabilities by increasing the carbohydrate, peptide and fat absorption machineries (Moor et al., 2018). Indeed, these animals seem to gain slightly more weight in the long-term with a mild increase in body fat percentage. There also seem to have more fat accumulation in the Arid3a cKO liver, although not in significant amounts. The fact that a strong upregulation of enterocyte-driven absorption is not translated into an equally strong

increase in weight and fat percentage can be explained by the loss of proliferation and early enterocytes at the crypt and a slightly shorter intestine. It would be interesting to further examine the effects of high-fat diet or calorie restriction upon Arid3a deletion to test if these animals will have higher or lower tolerance when given an altered diet. Villus-tip enterocytes and goblet cells have been previously reported to exhibit immunomodulatory programmes (Manco et al., 2021, Moor et al., 2018). Indeed, Metacore analysis of our RNA-seq data (figure 4.8) showed an increase in immune response pathways. It would also be of great importance to further investigate how these changes affect animal response to inflammation.

Since Arid3a has a nuclear paralogue Arid3b that is also expressed throughout the intestinal epithelium, we tested if there is functional redundancy by analysing the Arid3b cKO and DKO animals. We found that loss of Arid3b caused minimal transcriptional changes in the small intestine at 1 month after deletion, whereas deletion of both genes showed an intermediate phenotype compared to single knockouts. This result is rather intriguing and suggests that Arid3b is not only dispensable for the homeostatic function of the gut but may also have a distinct and opposing role that ameliorates the effects of Arid3a depletion. Since the two proteins are well-established chromatin modulators, it is possible that upon Arid3a loss, Arid3b occupies the binding sites of Ari3da (as shown by our ATAC-seq data) without the ability to recruit the histone modifiers. However, when both genes are deleted, other transcription factors may bind to the unoccupied chromatin and partially compensate for the loss of Arid3a. More detailed analysis on the Arid3b cKO and DKO intestine will be needed to further characterise the overlapping and distinct function of the two genes.

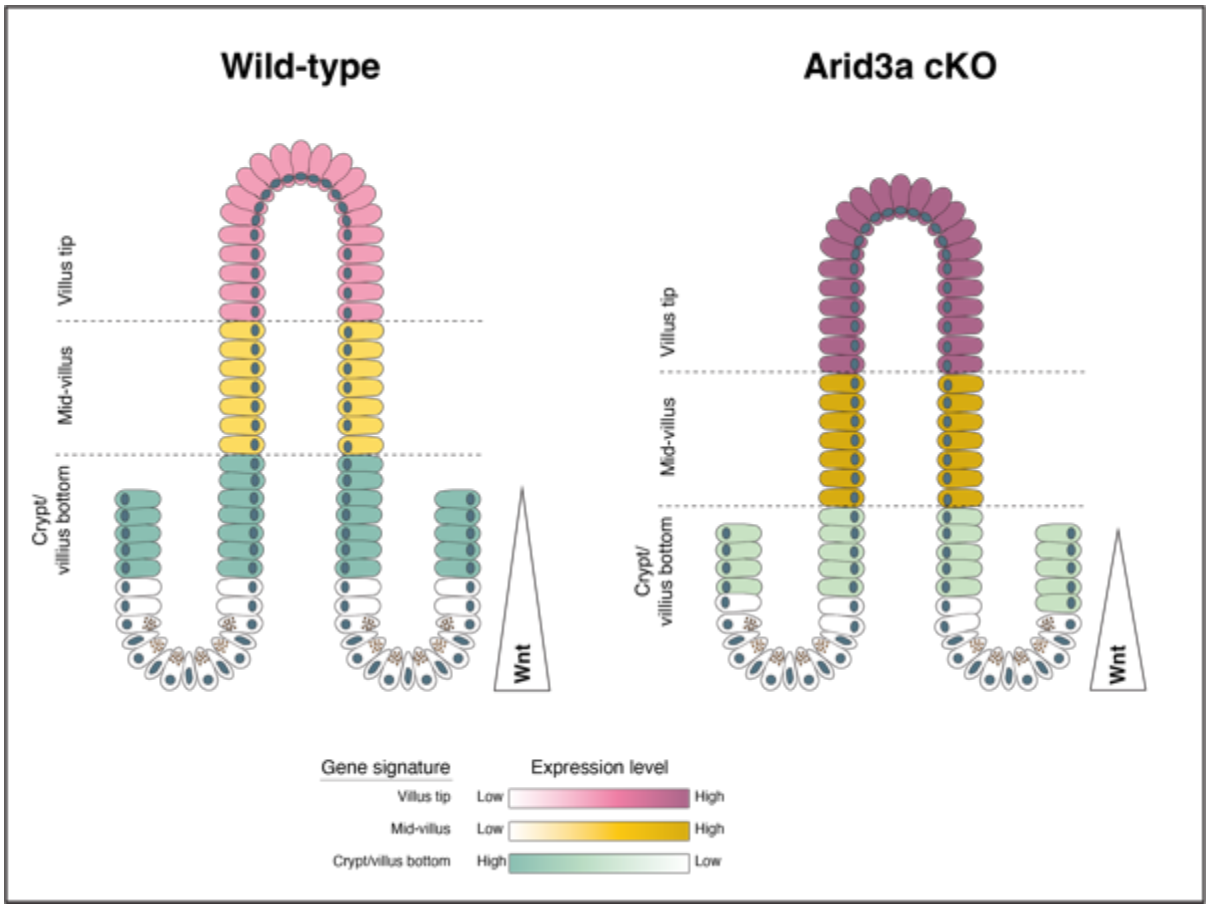

Figure 4.31 | Schematic summary of transcriptional changes of the small intestinal epithelium caused by deletion of Arid3a.
Gene expression of markers associated with TA cells/ early differentiated cells in WT animals are downregulated in Arid3a cKO epithelium, accompanied with a reduction of Wnt and proliferation markers. Conversely, mid-villus and villus-tip genes are upregulated upon loss of Arid3a.

Chapter 5: Arid3a is essential for irradiation-induced regeneration

5.1 Introduction

Apart from its self-renewal capabilities under homeostasis, the intestinal epithelium also possesses a remarkable injury-induced cellular plasticity that drives tissue regeneration (Meyer et al., 2022). Different cell types at around +4/5 cell positions, including reserve stem cells, absorptive and secretory progenitor cells as well as terminally differentiated cells, are capable of dedifferentiating after damage and re-populating the ISC niche at the bottom of the crypt upon injury (extensively discussed in Chapter 1). Such cellular plasticity of intestinal epithelial cells has been reported since early developmental stages. A recent study has shown that both Lgr5-positive and Lgr5-negative cells during development actively contribute to the adult ISC pool, signifying that stemness is acquired rather than hardwired (Guiu et al., 2019).

Irradiation-induced injury serves as a great model to study intestinal regeneration. Upon administration of a sub-lethal dose of full-body irradiation, the intestinal epithelium undergoes big morphological changes to respond to injury which can largely be divided into three phases: (1) apoptotic phase (days 1-2 post-irradiation), (2) hyperproliferation/regenerating phase (days 3-4 post-irradiation) and (3) normalisation phase (day 5 post-irradiation onwards) (Kim et al., 2017). During the first phase, irradiation induces extensive depletion of proliferating Lgr5-positive ISCs that are the workhorses of epithelial homeostasis. This leads to a dramatic increase of apoptotic crypts that are significantly smaller in size. In response to the loss of ISCs, progenitors or early differentiated cells are able to dedifferentiate and replenish the ISC pool. This leads to the hyperproliferation/regenerating phase where crypts are characterised by an increased length and all crypt cells are actively proliferating. At around day 5 after irradiation, ISCs and tissue morphology are restored back to homeostasis (Kim et al., 2017). The whole process from damage to regeneration is usually less than 7 days, which provides a unique model to study plasticity and regeneration.

In Chapter 4, we extensively described the role of Arid3a in intestinal tissue homeostasis. Since deletion of Arid3a inhibits proliferation of the TA cells where progenitors reside, we asked whether this would affect the regenerative capacity of the intestine upon irradiation. The regenerative role of Arid3b was also examined. Specifically, WT and KO mice were injected with tamoxifen and were given a single 12Gy irradiation dose at day 5 after administration of the first tamoxifen dose. To fully capture the differences in the regeneration dynamics between WT and KO conditions, animals were sacrificed on days 1, 2, 3, 4 and 5 post-irradiation (figure 5.1).

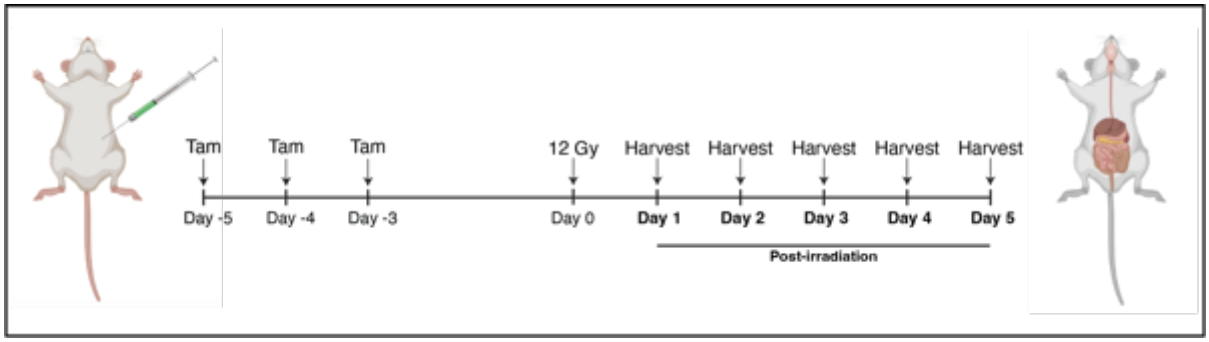

Figure 5.1 | Schematic representation of irradiation-induced injury experimental set-up.

5.2 Results

5.2.1 Arid3a is essential for intestinal regeneration upon irradiation

We have shown earlier that Arid3a is localised throughout the crypt-villus axis where the expression at the crypt is relatively low and enriched at the upper crypt (figure 3.5). We first asked if Arid3a expression is changed upon injury and during regeneration. To test that, we irradiated WT mice and collected the irradiated intestinal tissues at days 1, 2, 3 and 4 post-irradiation as well as non-irradiated controls. Immunohistochemistry analysis of the non-irradiated control confirmed the relatively low expression of Arid3a at the upper crypt (figure 5.2). On day 1 post-irradiation, crypt collapse was accompanied with a reduction of Arid3a. On day 2, as crypt began to transition from apoptotic to proliferative phase, Arid3a expression started restoring. Interestingly, on day 3, crypt elongation coincided with an increase in number of Arid3a+ cells at the crypt. Arid3a-positive cells were mainly localised at the upper crypt with a few occasionally at the crypt bottom. Approaching the

normalisation phase on day 4, numbers of Ari3a-positive cells started to fall back to normal (figure 5.2A).

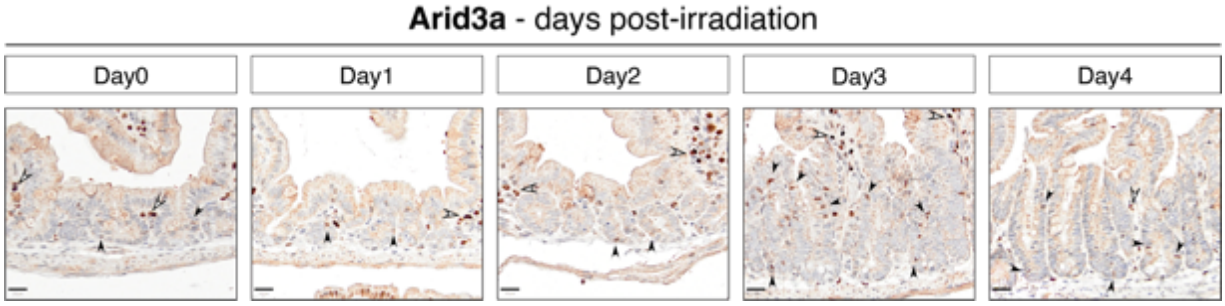

Figure 5.2 | Arid3a is upregulated upon irradiation to facilitate regeneration.
Arid3a immunostaining of WT mice during the first 4 days after administration of 12Gy irradiation. Representative images of N=5 WT animals per timepoint. Scale bar, 20μm. Black arrowheads indicate epithelial expression of Arid3a; white arrowheads indicate stromal expression of Arid3a.

Next, we investigated whether deletion of Arid3a perturbs the regenerative response. Both WT and Arid3a cKO animals were irradiated and tissues were collected for analysis histologic analysis (figure 5.1). H&E staining revealed that loss of Arid3a led to extensive damage of the intestinal tissues in the apoptotic phase with a slower recovery (figure 5.3). More specifically, on days 1 and 2, Arid3a cKO intestine showed more degenerated crypts and the overall tissue integrity was more compromised compared to WT. During the regenerative phase on day 3, the number of regenerating crypts was much lower in the Arid3a-depleted intestine with majority of them failed to elongate until day 4. Finally, WT crypts reached the normalisation phase on day 5, whereas Arid3a cKO crypts were still in the elongated regenerating phase (figure 5.3). Expert pathological analysis was performed on these tissues to assess the damage of the lamina propria, mucosa and gut-associated lymphoid tissue, and confirmed a more extensive tissue damage of KO animals from day 2 to day 4 when compared to WT (figure 5.3B,C).

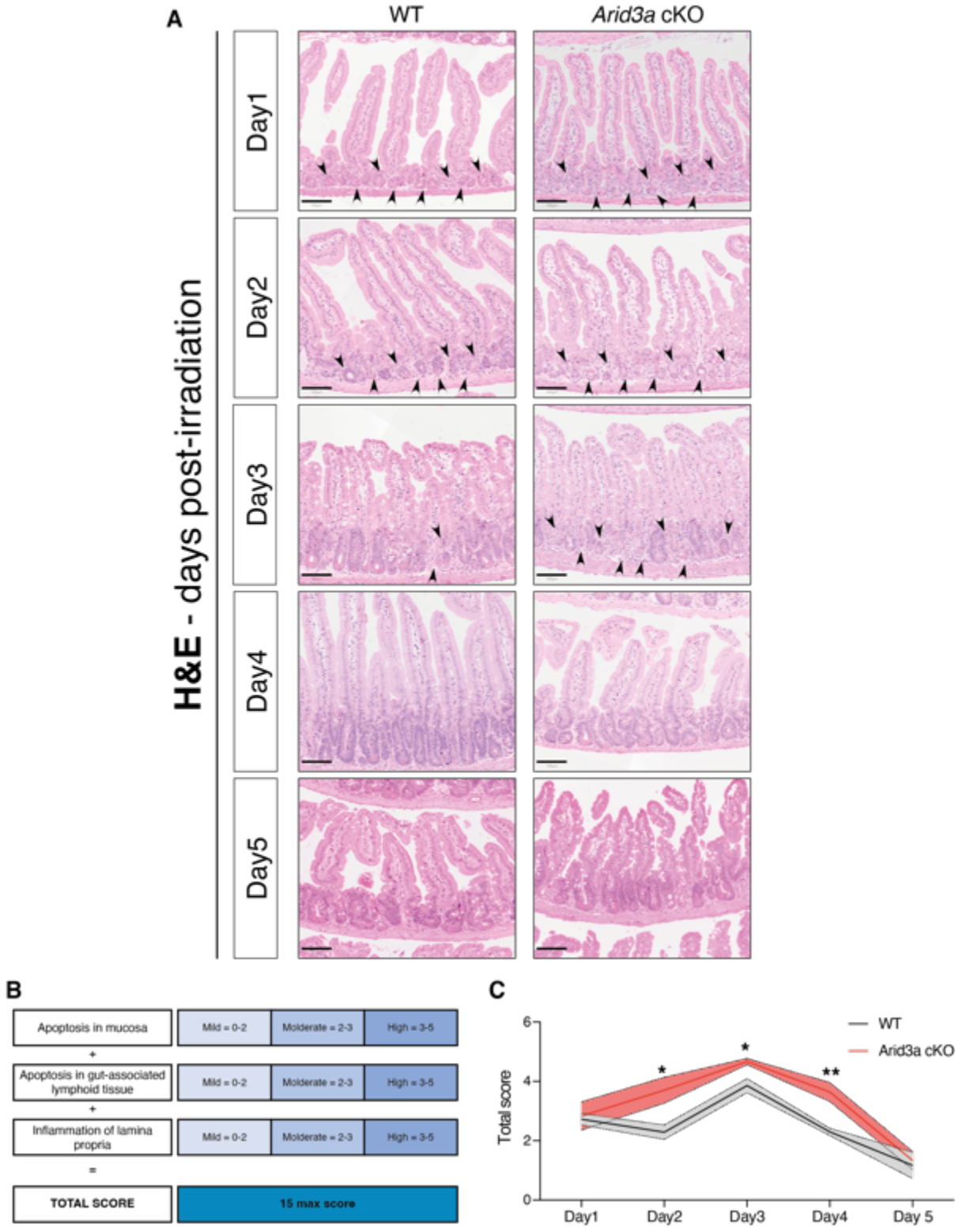

Figure 5.3 | H&E staining of WT and Arid3a cKO animals over the time-course of response to irradiation.
(A) Representative images of at least N=4 animals for each genotype per timepoint. Scale bar, 100µm. Black arrowheads indicate degenerated crypts. (B) Description of the scoring system used to assess damage of the small intestine at days. (C) Quantification of tissue damage. Data represent mean ± s.e.m. *P<0.05, **P<0.01 , ***P<0.001, two-sided t-test.

To assess the apoptosis of the epithelial cells, cleaved caspase-3 staining was performed which showed no difference on days 1, 2 and 3. However, on days 4 and 5, Arid3a cKO animals showed significantly higher percentage of apoptotic crypts (figure 5.4A). It is interesting to note that the number of apoptotic crypts appeared to decrease gradually over time in a wave rather than linear pattern (figure 5.4B). To validate the increased apoptotic crypts in the irradiated Arid3a-depleted intestine, mouse intestinal organoids were derived from either WT or Arid3a cKO animals. The organoids were treated with a 4Gy irradiation dose *ex vivo* and were subsequently stained for Annexin-V - a protein that selectively binds to phosphatidylserine (PS) that will only be presented to the cell surface in an event of early programmed cell death (Logue et al., 2009). Annexin-V staining of the WT and Arid3a cKO cells would be quantitated by FACS analysed at 4h and 24h after irradiation. These two timepoints resembles the *in vivo* apoptotic and proliferation-to-normalisation phase, respectively (Guillermin et al., 2021). In accordance with the *in vivo* data, loss of Arid3a resulted in significant increase of apoptotic cells at 4h, while both WT and KO organoids showed the similar recovery rate (figure 5.5A,B).

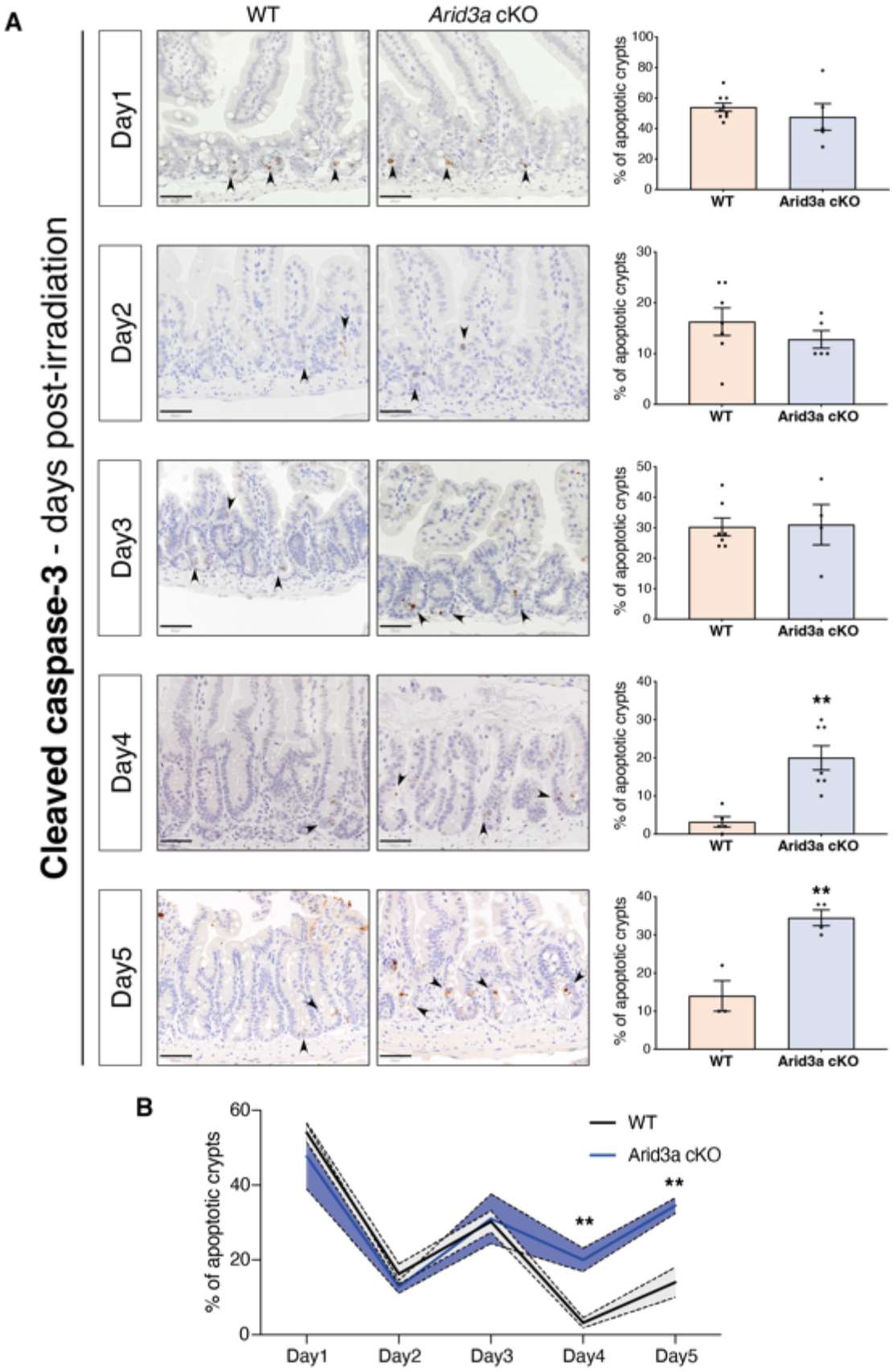

Figure 5.4 | Arid3a cKO animals exhibit higher rates of apoptotic crypts.
(A) Cleaved caspase-3 immunostaining of WT and Arid3a cKO mice. Representative images of at least N=4 animals for each genotype per timepoint. Scale bar, 50μm. Black arrowheads indicate apoptotic cells. Quantification of apoptotic crypts for each timepoint is shown on the right side. (B) Summary of quantification of apoptotic crypts in WT and Arid3a cKO animals shown in (A). Data represent mean ± s.e.m. *P<0.05, **P<0.01 , ***P<0.001, two-sided t-test.

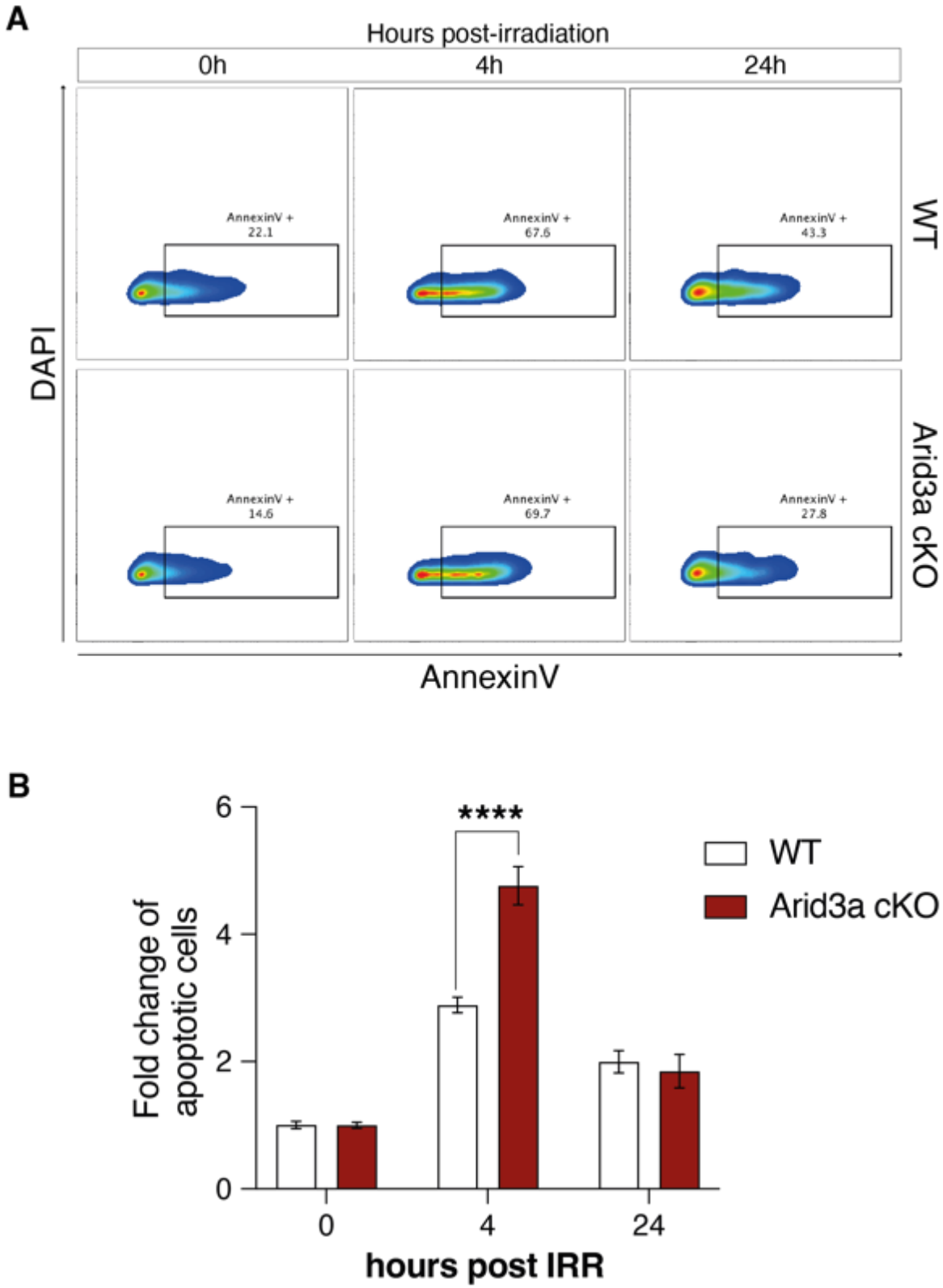

Figure 5.5 | Arid3a cKO organoids are most susceptible to irradiation-induced apoptosis.
(A) Sorting strategy for FACS analysis of apoptotic cells. Annexin-V-positive cells were selected out of the pool of live (DAPI-negative) cells. (B) Quantification of the fold change in percentage of apoptotic cells. Fold change was normalised to the non-irradiated control for each genotype. Data represent mean ± s.e.m. Adjusted p-value (q-value) was calculated with Sidak's correction for multiple testing *q<0.05, **q<0.01 , ***q<0.001, 2-way ANOVA.

We hypothesised that this extended apoptotic phase would cause a delay in entering the hyperproliferation phase at the crypts. Proliferative cells are marked by Ki67, an antigen that is expressed during cell cycle and is absent in quiescent cells. No major differences were observed between WT and KO animals on day 1, where extended cell death lead to a dramatic reduction of proliferation. On days 2 and 3, WT animals started regenerating as evident by crypt expansion and an increase in proliferation. At the same timepoints, Arid3a cKO animals showed much lower numbers of Ki67-positive cells and most of the crypts failed to expand their size. On day4, both genotypes were at the hyperproliferation phase. On day 5, WT animals had already entered their normalisation phase, while the majority of Arid3a cKO crypts were still in the hyperproliferation phase (figure 5.6A) To confirm the reduced proliferative capacity of crypts at early timepoints, we isolated crypts from WT and Arid3a cKO intestine collected on days 1 and 3 post irradiation and performed organoid formation assay by seeding equal numbers of crypts (200 crypts). No difference was observed on day 1 apoptotic phase where organoid formation efficiency was less than 10%. However, on day 3, WT crypts had restored their capacity to form organoids while Arid3a depleted crypts maintained the same low colony formation efficiency (p-value=0.099) (figure 5.6B).

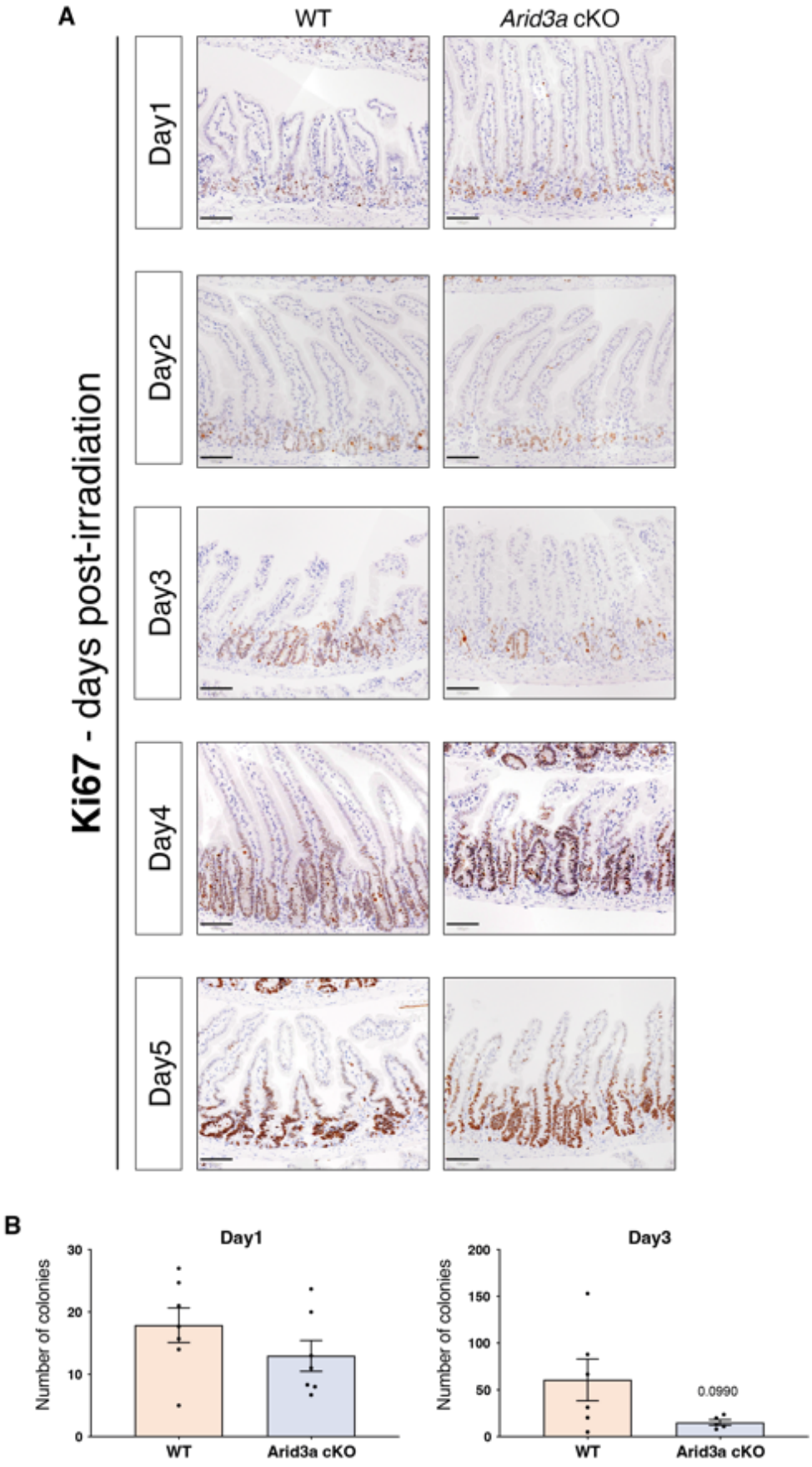

Figure 5.6 | Loss of Arid3a results in delayed crypt hyperproliferation.
(A) Ki67 immunostaining of WT and Arid3a cKO mice. Representative images of at least N=4 animals for each genotype per timepoint. Scale bar, 100µm. (B) Organoid formation assay was performed at days 1 and 3 post irradiation. Data represent mean ± s.e.m. *P<0.05, **P<0.01 , ***P<0.001, two-sided t-test.

Lastly, we asked whether the delayed response in irradiation-induced injury of Arid3a cKO animals can have an impact on the longer-term health of the animals. To address this question, the same protocol of tamoxifen administration and irradiation five days later was followed. Animals' health and their weight from the day of the first tamoxifen injection was closely monitored. Both WT and KO animals showed similar pattern of weight loss until day 5 post-irradiation. Upon tamoxifen administration (day -5), there was an initial drop in animal weight, but by the day of irradiation (day 0) animals had recovered. After irradiation, extensive tissue damage was translated to a sudden weight loss until day 4. From day 5, WT animals started recovering, and they had reached their baseline weight by day 6. In contrast, Arid3a cKO animals were not able to recover their weight and the weight loss continued until reaching the humane time point by day 10 (>20% of their original body weight) where the animals needed to be culled (figure 5.7A). It is interesting to note that, by day 12, all WT and Arid3a cKO animals had to be culled due to either weight loss or other health-related protocol restrictions. However, Arid3a cKO died earlier than the WT animals, indicating that intestinal epithelial loss of Arid3a increased the susceptibility to injury (figure 5.7B).

Since all animals died 12 days after irradiation regardless of their genotypes and weight loss, we ask if this was caused by irreversible intestinal injury or failure of other organ(s). Interestingly, histological analysis of the intestinal tissues at day 12 post irradiation did not show any apparent morphological differences between WT and KO animals based on H&E staining. Moreover, Ki67 staining showed that both genotypes maintained a normal proliferative status. However, cleaved caspase-3 based assessment of apoptosis showed extensive cell death in the Arid3a cKO intestine when compared to WT. Apoptotic cells were mostly detected in the villus tip of the WT intestine, whereas caspase-3-positive cells were located throughout the crypt-villus axis as well as in the stroma (figure 5.8). Whether the increase in apoptosis of the intestinal cells is a direct consequence of Arid3a cKO needs to be further investigated (see discussion).

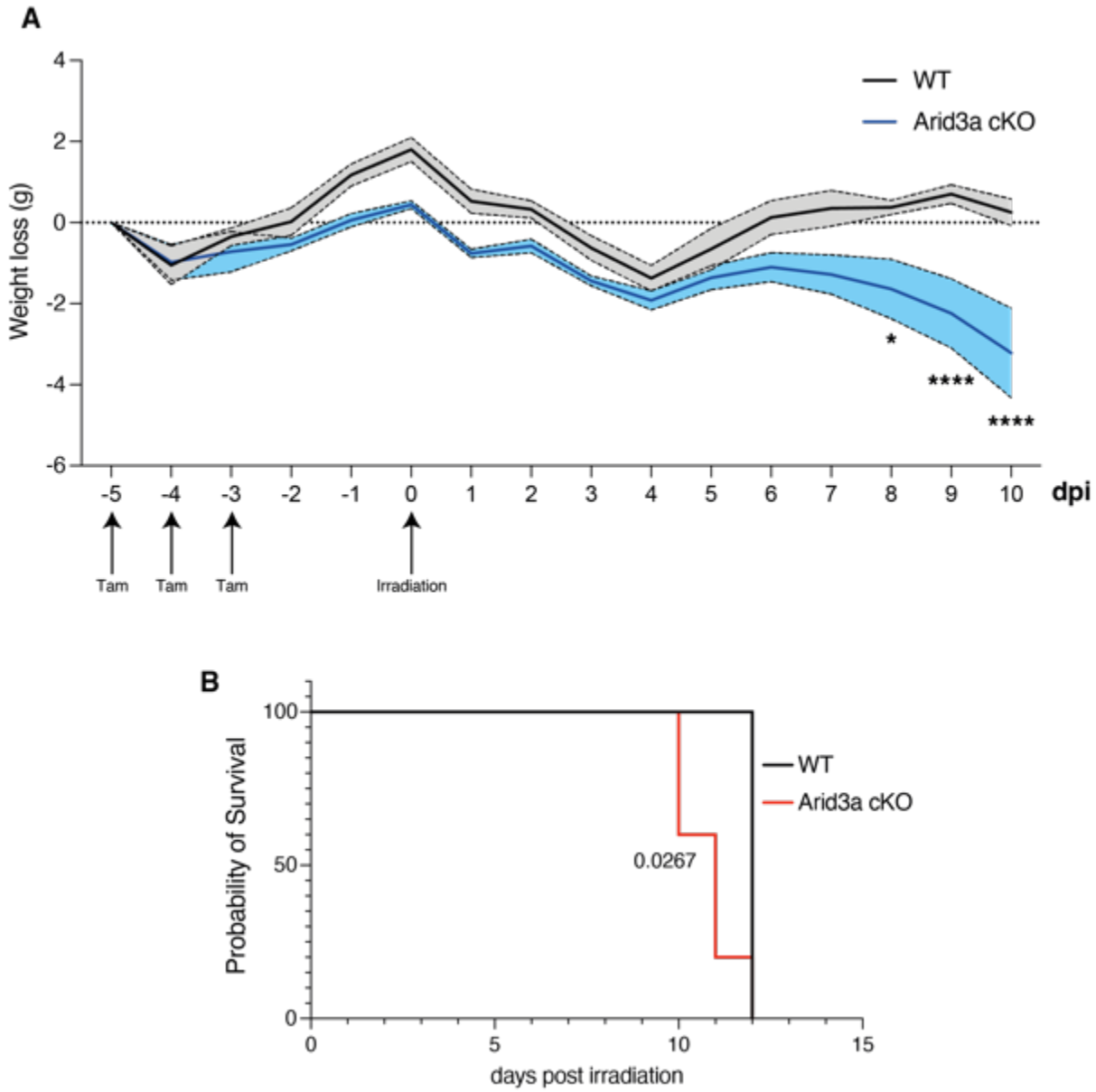

Figure 5.7 | Arid3a cKO animals have an impaired response to irradiation.
(A) Changes in animals' weight from Day -5 (first tamoxifen injection) through Day 10 post-irradiation. Data represent mean ± s.e.m. *P<0.05, **P<0.01 , ***P<0.001, two-sided t-test. (B) Kaplan-Meir survival curve of WT and Arid3a cKO animals after irradiation. *P<0.05, **P<0.01, log-rank (Mantel-Cox) test.

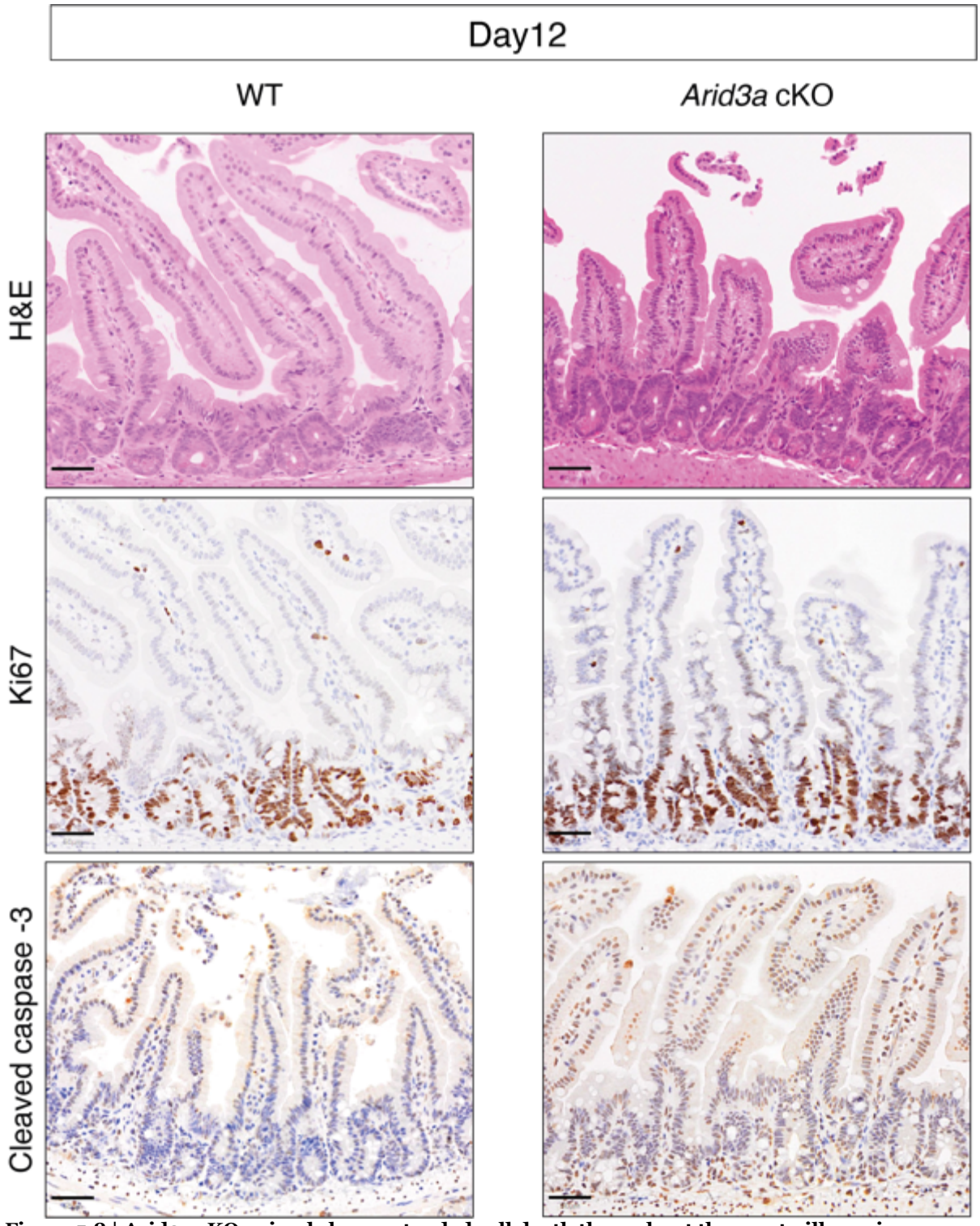

Figure 5.8 | Arid3a cKO animals have extended cell death throughout the crypt-villus axis.
H&E staining and Ki67 and Cleaved caspase-3 immunostainings of WT and Arid3a cKO animals at day 12 post-irradiation. Representative images of N=2 WT and N=3 Arid3a cKO animals. Scale bar, 50µm.

5.2.2 Loss of Arid3b leads to delayed response to irradiation

Under normal homeostatic condition, Arid3b is dispensable for the function of the small intestine. Intestinal-specific deletion of Arid3b did not affect proliferation but altered differentiation at later timepoints (Chapter 4, figure 4.17, figure 4.25). On the other hand, previous studies have shown that Arid3b regulates proliferation at non-homeostatic conditions of other tissues (Dausinas et al., 2020, Liao et al., 2016). To investigate whether deletion of Arid3b affects the regeneration process, WT and Arid3b cKO animals were given a single 12Gy irradiation dose as shown in figure 5.1 and tissues were collected at days 1, 2, 3 and 4 post-irradiation.

H&E staining of the irradiated tissues showed different dynamics in the regeneration process of WT and KO animals. Deletion of Arid3b led to more extensive tissue damage during the apoptotic phase (days 1 and 2) (figure 5.9A) and showed higher levels of degeneration throughout the crypt-villus axis which was confirmed by the same semi-quantitative approach as described earlier (figure 5.9B and Figure 5.7A). Of note, on days 3 and 4, no morphological differences were observed, implying that Arid3b is dispensable for irradiation-induced regeneration in the gut (figure 5.9A,B).

To gain a better insight on the increased damage of Arid3b-deficient intestine after irradiation, apoptosis and proliferation were evaluated using cleaved caspase-3 and Ki67 immunostainings, respectively, at all timepoints. A moderate increase in apoptotic crypts was observed on the Arid3b cKO intestine on day 4 (figure 5.10), whilst proliferation was largely unaffected (figure 5.11). The results support the notion that Arid3b is dispensable during the intestinal regeneration process.

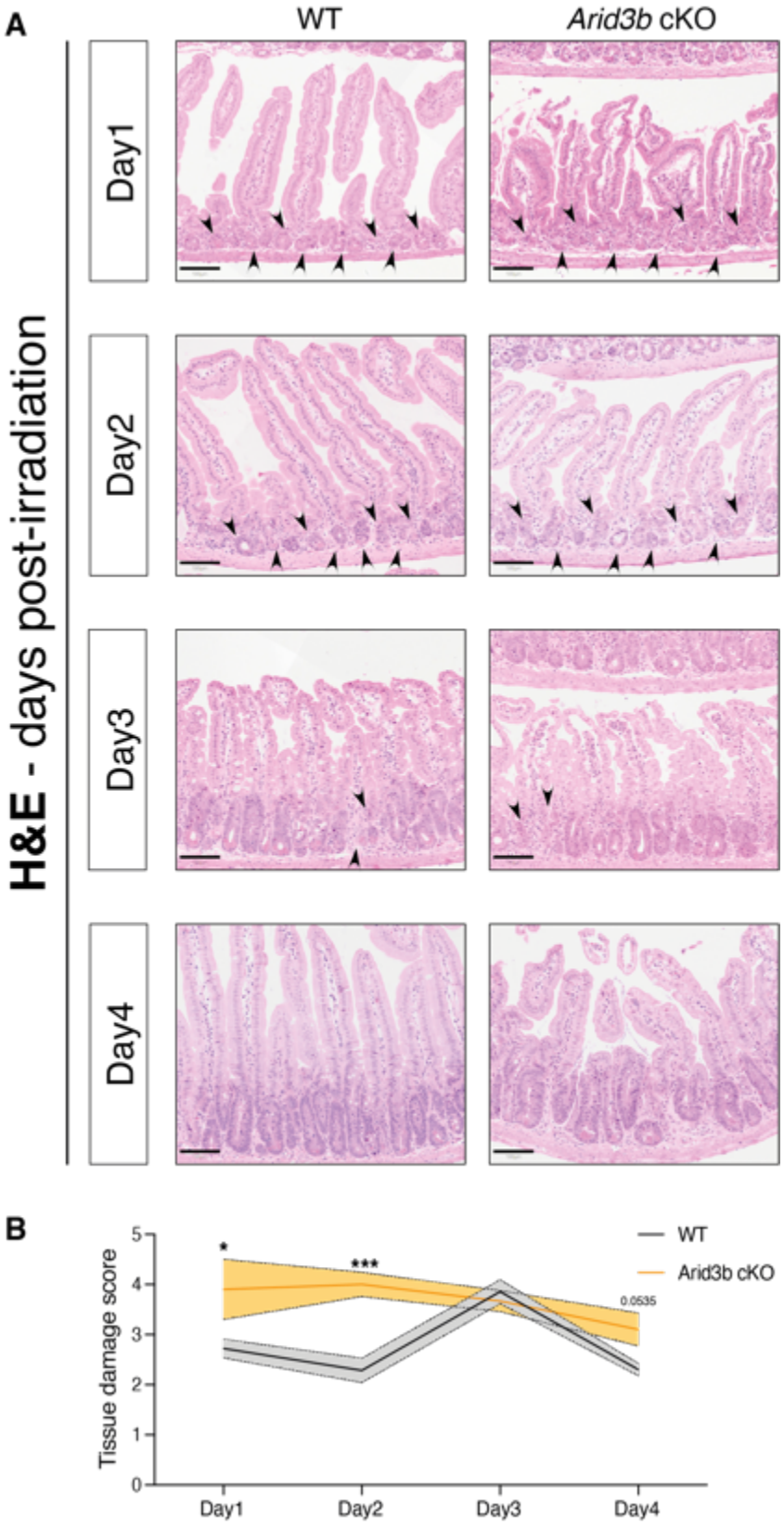

Figure 5.9 | H&E staining of WT and Arid3b cKO animals over the timecourse of response to irradiation.
(A) Representative images of at least N=4 animals for each genotype per timepoint. Scale bar, 100μm. Black arrowheads indicate degenerated crypts. (B) Quantification of tissue damage based on model from figure 5.7A. Data represent mean ± s.e.m. *P<0.05, **P<0.01 , ***P<0.001, two-sided t-test.

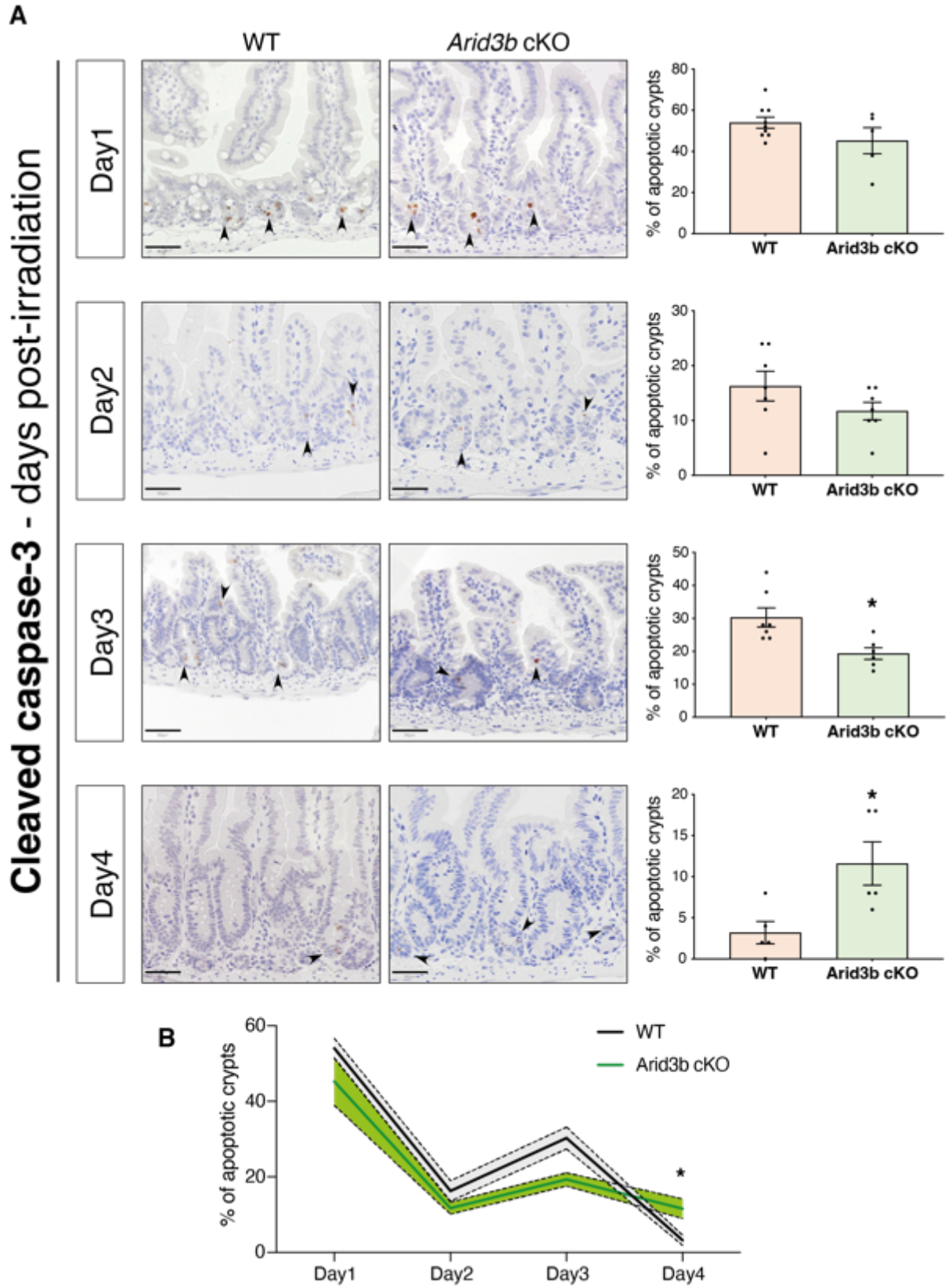

Figure 5.10 | Arid3b cKO animals show a mild increase in apoptosis at later timepoints of the regeneration process.
(A) Cleaved caspase-3 immunostaining of WT and Arid3b cKO mice. Representative images of at least N=5 animals for each genotype per timepoint. Scale bar, 50µm. Black arrowheads indicate apoptotic cells. Quantification of apoptotic crypts for each timepoint is shown on the right side. (B) Summary of quantification of apoptotic crypts in WT and Arid3b cKO animals shown in (A). Data represent mean ± s.e.m. *P<0.05, **P<0.01 , ***P<0.001, two-sided t-test.

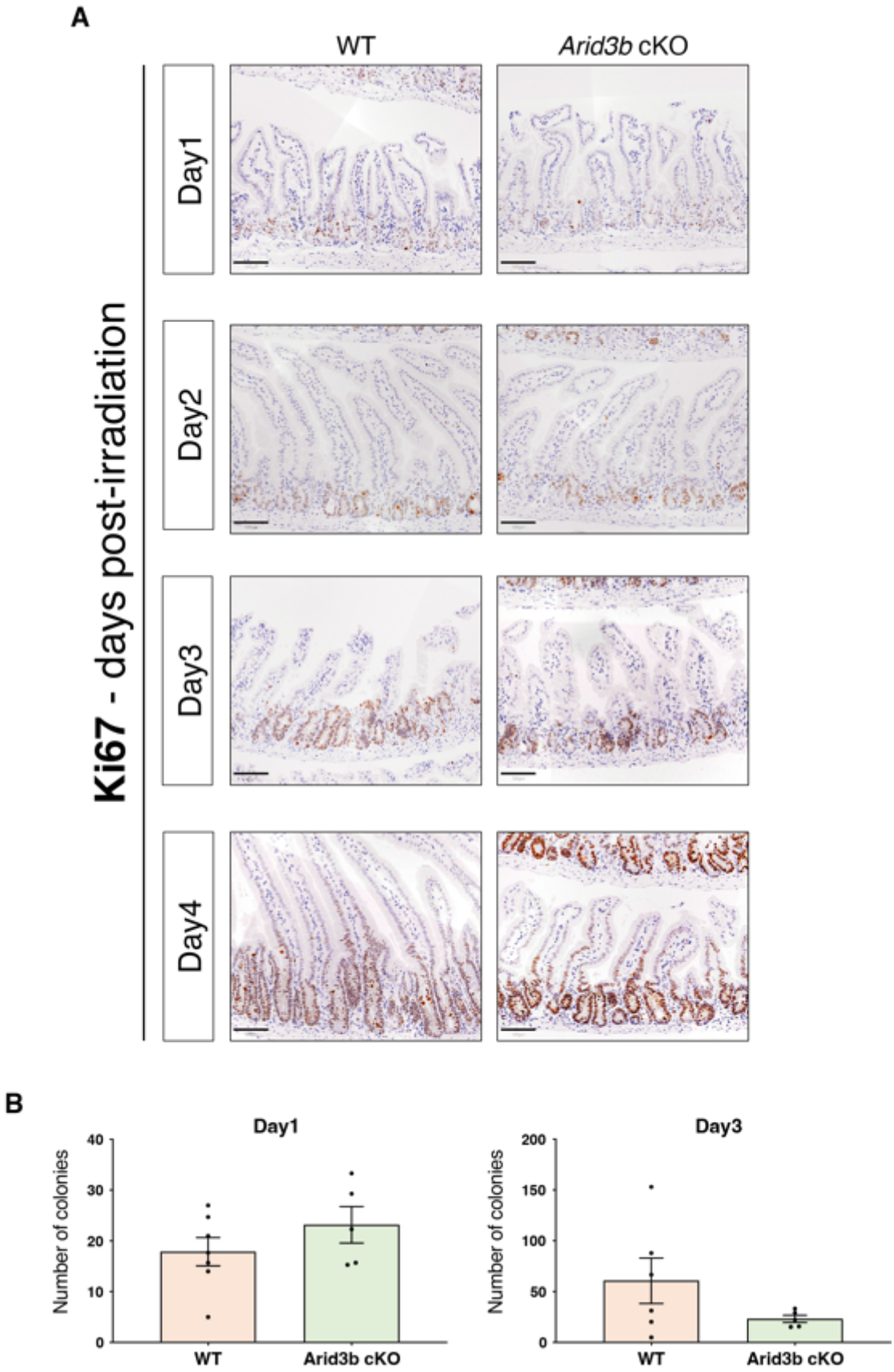

Figure 5.11 | Arid3b cKO animals do not show differences in proliferation.
(A) Ki67 immunostaining of WT and Arid3b cKO mice. Representative images of at least N=5 animals for each genotype per timepoint. Scale bar, 100μm. (B) Organoid formation assay was performed at days 1 and 3 post irradiation. Data represent mean ± s.e.m. *P<0.05, **P<0.01 , ***P<0.001, two-sided t-test.

5.2.3 Arid3a and Arid3b are not targeted by Yap

Yap signalling has long been implicated in the regenerative response upon injury. Yap is a transcriptional activator, and its nuclear localisation drives proliferation. During homeostasis, Yap is only localised at the nucleus of ISCs. Upon injury, increased Yap transcription and nuclear localisation drive intestinal regeneration (Gregorieff et al., 2015). We therefore asked whether the impaired intestinal regeneration upon Arid3a and Arid3b loss is Yap-dependent.

Since Arid3a expression was upregulated upon irradiation (figure 5.2), we first tested whether Arid3a and Arid3b are potential Yap targets. Lats1/2 kinases are key components of the Hippo pathway that phosphorylate Yap leading to its retention in the cytoplasm (Carter et al., 2021). We have previously shown that conditionally deletion of Lats1 and Lats2 in the intestine (VillinCreERT2;Lats1$^{fl/fl}$;Lats2$^{fl/fl}$ – Lats1/2 DKO) induces nuclear translocating of Yap protein which is accompanied by massive hyperproliferation (Guillermin et al., 2021). qRT-PCR analysis of Lats1/2 DKO intestine showed activation of Yap signalling as revealed by transcriptional upregulation of its downstream effectors *Ctgf* and *Cyr61,* 3 days after deletion (figure 5.12A). Interestingly at the same timepoint, *Arid3a* and *Arid3b* expression is unaffected, indicating that they are not transcriptional targets of Yap (figure 5.12A). Next, we examined if Yap signalling is affected in the Arid3a and Arid3b cKO intestine upon injury. Expression analysis of WT intestine showed that the *Ctgf* was upregulated 2 days after irradiation and its expression rapidly went back down to baseline by day 3 and 4 (figure 5.12B). Interestingly, the upregulation of *Ctgf* expression at day 2 post irradiation was significantly higher in both KO as compared to the WT intestine (figure 5.12B). We further examined the expression of another regenerative marker *Clu,* which marks a very rare reserve stem cell population that drives intestinal regeneration (Ayyaz et al., 2019). Similarly, *Clu* expression was moderately upregulated, but not significant, in the Arid3a-depleted intestine on days 2 and 3 post irradiation (figure 5.12B). Given that there are more extensive tissue damage and reduced regeneration in the irradiated Arid3a cKO animals as described earlier, we speculate that the stronger upregulation of *Ctgf* and *Clu* upon injury is an intrinsic response to the increased damage in the KO intestine. Future work is needed to further characterise the functional role of Arid3a/b in intestinal regeneration.

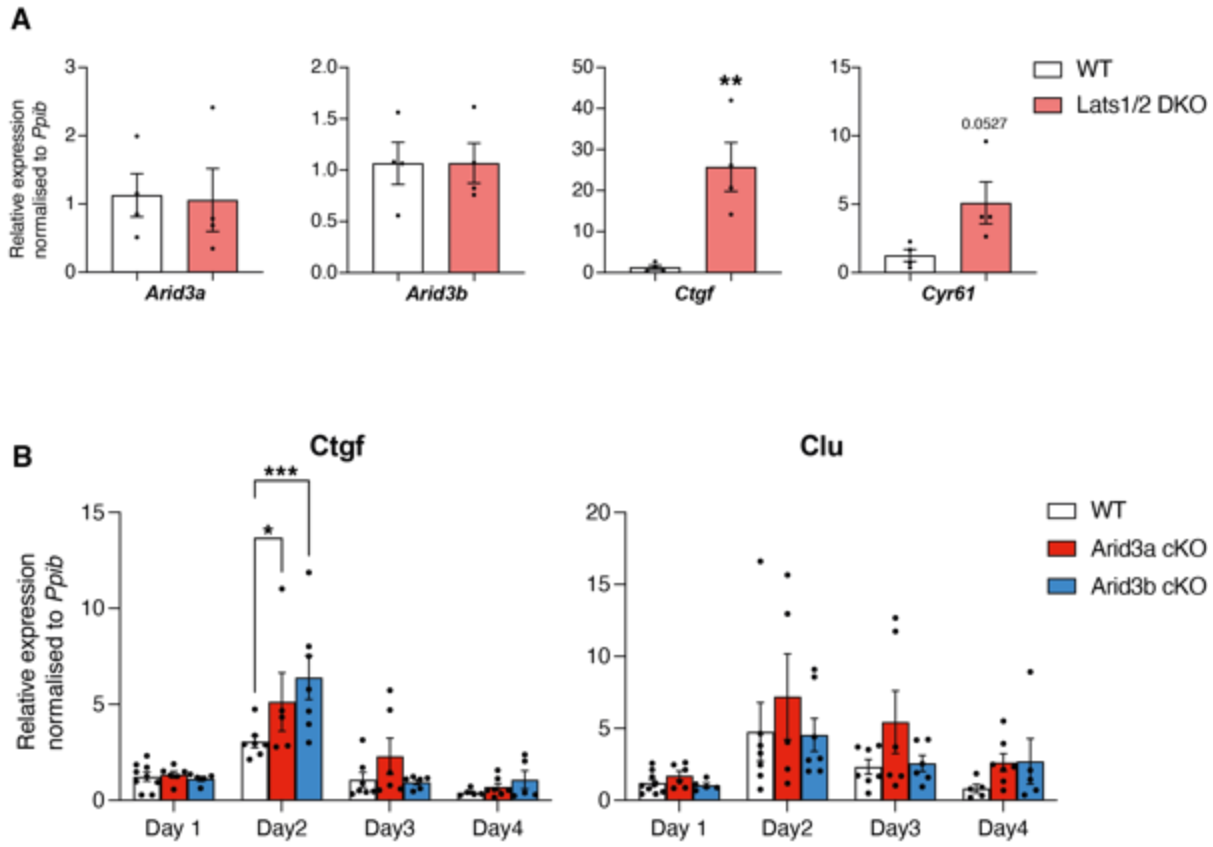

Figure 5.12 | Arid3a and Arid3b are not targeted by Yap.
(A) qRT-PCR analysis of WT and Lats1/2 DKO animals at Day 3 after tamoxifen administration. N=3 WT animals and N=4 Lats1/2 DKO animals. (B) qRT-PCR analysis of WT, Arid3a cKO and Arid3b cKO animals at Days 1,2,3 and 4 post-irradiation. For each graph data is normalised to the expression of each gene at WT animals at Day 1. At least N=5 animals per genotype per timepoint. Data represent mean ± s.e.m. *P<0.05, **P<0.01 , ***P<0.001, two-sided t-test.

5.3 Summary and short discussion

The small intestinal epithelium is continuously exposed to numerous pathogens and other environmental cues that can cause injury. Irradiation-induced injury serves a great model to study the cellular plasticity of the intestinal epithelium. Here, we report that Arid3a plays an essential role in the regeneration process. Upon injury, Arid3a is upregulated at the crypt at days 3 and 4 post-irradiation which is accompanied by hyperproliferation. Future lineage tracing experiments will be crucial to test whether Arid3a drives the dedifferentiation process of early committed cells which can re-populate the bottom of the crypt. Expression analysis showed that Arid3a is not acting downstream of Yap, one of the master regulators of epithelial response to injury. It would be interesting to further investigate what drives the Arid3a expression upon injury.

Interestingly, loss of Arid3a leads to a delayed regeneration response and reduced survival of the animals compared to WT. More specifically, Arid3a deficient mice exhibited higher degrees of tissue damage, an extended apoptotic phase and subsequently a delayed hyperproliferation phase. Although the epithelium of the KO animals seemed to be morphologically recovered at later time point, albeit slower than the WT, there was a significant increase in apoptotic cell numbers in the Arid3a KO intestine. The KO animals failed to re-gain weight, signifying an impaired function of the intestine. Of note, both WT and Arid3a cKO mice died by day 12 after irradiation. However, Arid3a cKO died sooner with much more extensive cell death throughout the intestine. We believe that the animals may die of other causes such as irradiation-mediated damage of the bone marrow and/or liver. Collectively, the results suggest that Arid3a may have a dual role in the regeneration process: on one hand, it drives hyperproliferation of early committed cells to re-acquire stemness and, on the other hand, it provides epithelial cells with radiosensitivity by protecting against programmed cell death. Future experiments will be needed to study the survival and functional role of Arid3a in regeneration using less aggressive injury models, such as lower irradiation dose or other chemical-induced damage.

In contrast to Arid3a, the role of Arid3b is dispensable during regeneration. Although Arid3b cKO animals showed an initial increase in tissue damage caused by irradiation, most animals recovered and reached the normalisation phase.

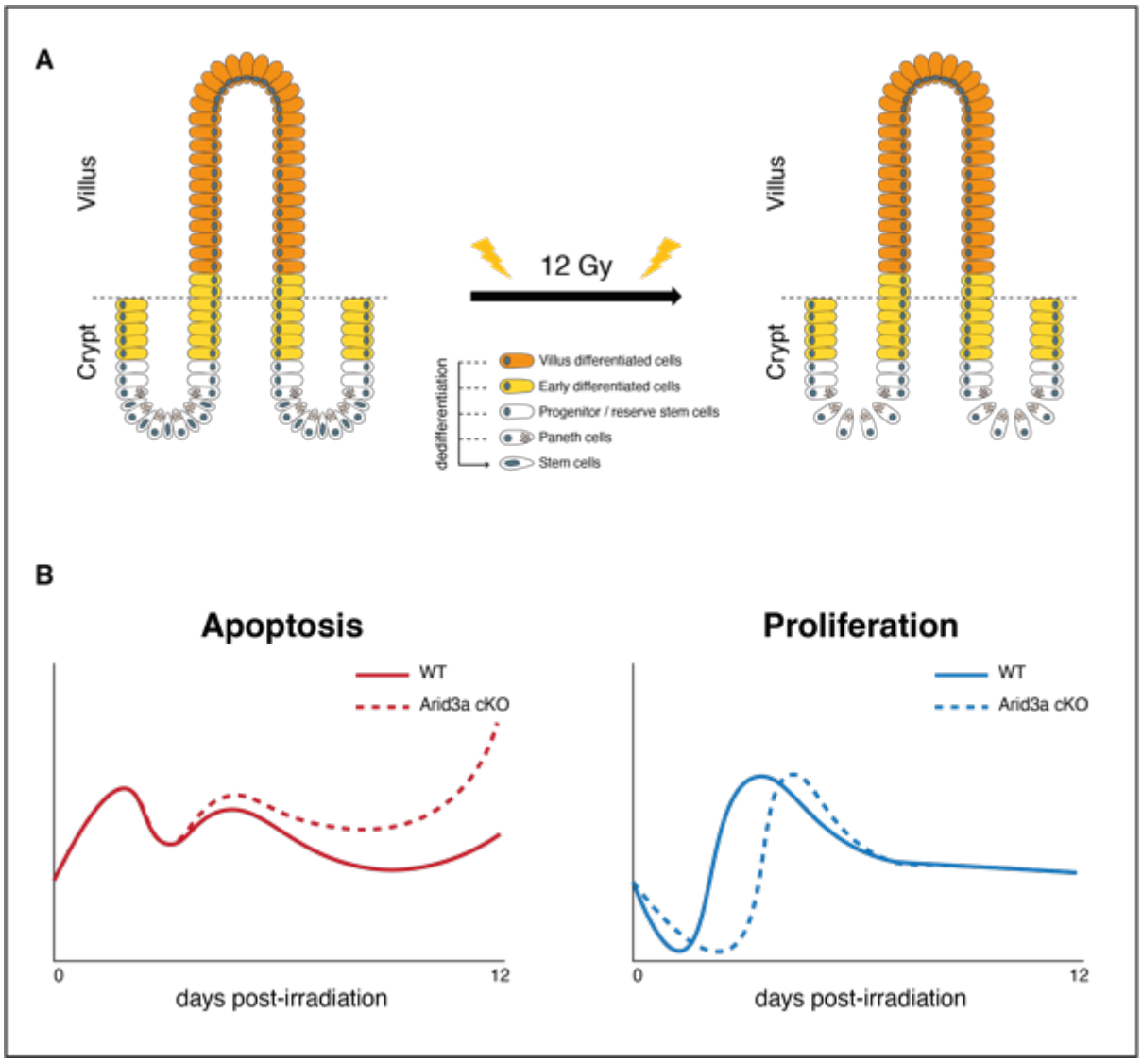

Figure 5.13 | Schematic representation of altered dynamics of irradiation-induced regeneration upon deletion of Arid3a.
(A) Irradiation-induced damage of the small intestinal epithelium causes depletion of Lgr5-positive stem cells at the bottom of the crypt. Early or terminally differentiated cells have the ability to obtain stemness and re-populate the stem cell pool at the crypt bottom. (B) Loss of Arid3a alters the dynamics of the regeneration process. Arid3a cKO animals show higher apoptosis and a delayed hyperproliferation compared to WT.

Chapter 6:Discussion and future perspectives

The intestinal epithelium is a highly organised structure that facilitates the major functions of our intestines such as food digestion and absorption as well as protection against pathogenic organisms. Extensive studies over the past decades have shed light into the mechanisms of ISC homeostasis and have greatly improved our understanding of disease pathogenesis in the gut. Actively cycling ISCs, marked by the expression of Lgr5, reside at the bottom of the crypt to fuel the remarkably high turnover of the intestinal epithelium. ISCs divide and generate daughter cells that will stochastically either self-renew to generate another ISC or exit the stem cell niche and enter the TA zone for subsequent differentiation towards the absorptive or secretory lineages. Lineage decision is taking place at the +4/+5 positions where early progenitor cells reside.

In Chapter 1, we discussed that Wnt and Notch signalling play a central role in ISC regulation during homeostasis by forming gradients of expression along the crypt. The functional roles of both pathways have been extensively studied in homeostasis and cancer. While both pathways are essential for maintaining the proliferation status of stem cells at the crypt bottom, Notch is central in the binary fate decision process at the early progenitors. Although the mechanisms of ISC self-renewal are very well characterised, the molecular controls of niche exit, stem cell-to-daughter cell transition and plasticity at the early progenitor cells remain largely unclear. Thus, the aim of this PhD was to identify new modulators of early fate decision at the +4/+5 cells of the intestinal crypts. We hypothesised the existence of a specific gene regulatory network at these cells and aimed to identify their role in stem cell maintenance and differentiation. In Chapter 3, we screened for transcription factors that are enriched in +4/+5 early progenitors by comparing the transcriptomic data of Lgr5-sorted cells. This may help elucidate the transcriptional network underlying loss of stemness and subsequent differentiation upon ISC niche exit. We identified 3 transcription factors - Mtg8, Mtg16 and Arid3a- as putative new modulators of ISC homeostasis. Indeed, the two transcription co-repressor homologues Mtg8 and Mtg16 were confirmed to play a key role in exit of stemness and the binary lineage decision at +4/+5 cells. Deletion of Mtg8/16 leads to loss of enterocytes and increased crypt proliferation. Both genes are repressed by Notch signalling acting downstream of Atoh1 to drive differentiation towards the enterocyte lineage by antagonising Atoh1 transcription. This is a

collaborative work with another colleague in the lab and the complete story has been published (Baulies et al., 2020a). The role of Mtg8 and Mtg16 in ISC maintenance will not be further discussed in this chapter.

During my PhD, I focused on characterising the role of Arid3a as a novel candidate for the regulation of proliferation and differentiation of ISCs. To our knowledge, this is the first ever report of the role of Arid3a in adult intestinal epithelium. Previously, Arid3a has been extensively studied in the blood for its role in driving transcription of IgH and in regulating differentiation of B cells and megakaryocytes (Webb et al., 2011, Alejo-Valle et al., 2022, Herrscher et al., 1995). Moreover, Arid3a has been implicated in regulation of cell cycle progression, chromatin remodelling and embryonic development (Lin et al., 2007, Peeper et al., 2002, Popowski et al., 2014, Rhee et al., 2014). Expression analysis showed that Arid3a is expressed not only at the +4/+5 cells but also in other differentiated cells, forming an expression gradient at the crypt opposite to that of Wnt and Notch signalling. In accordance with this result, we showed that Wnt pathway inhibits expression of Arid3a at the crypt bottom, while Notch has no effect on its expression. The results suggest that Arid3a may be a potential regulator of Notch-independent lineage decision. In fact, several studies in the past have uncovered genes with a central role in the differentiation process that act independently of Notch and Atoh1. For example, Sox4 is expressed at the intestinal crypts to promote differentiation of enteroendocrine and tuft cells independently of Notch (Gracz et al., 2018). Similarly, Pou2f3 has also been shown as the master regulator of Tuft cells differentiation (Gerbe et al., 2016, Long et al., 2021), although a contradictory study revealed an Atoh1-dependent tuft cell specification (Gerbe et al., 2011).

Analysis of Arid3a cKO mice showed that Arid3a regulates both proliferation and differentiation processes. Loss of Arid3a results in loss of proliferative TA cells at the upper crypt, while the number of Lgr5-positive ISCs remains unchanged. TA cells is a very unique population in the intestinal crypts, which comprises of partially committed early progenitors of various cell lineages that continue to undergo rapid cell divisions before terminal differentiation. A proper balance between the proliferation-to-differentiation ratio of these cells is essential for the maintenance of intestinal epithelial homeostasis. Indeed, a recent study has shown that TA cell proliferation rate is key in coordinating the balance of secretory and absorptive cell types (Sanman et al., 2021). The loss of TA cell proliferative capacity mediated by

Arid3a suggests that the differentiation dynamic of the epithelial cells may also be affected. In addition, RNA-seq data further showed that loss of proliferation markers was accompanied by a reduction in Wnt signature in the Arid3a-deficient crypts, which can explain the reduced numbers of Paneth cells at the crypt since Paneth cell differentiation is Wnt-dependent (Farin et al., 2012, van Es et al., 2005). It is interesting to note that Paneth cells secrete Wnt ligands to maintain the signalling gradient in the ISC niche. Expression of Arid3a in the TA cells may be important to support the Wnt gradient indirectly by maintaining Paneth cell numbers. Notably, increased Arid3a expression has been associated with colorectal cancer development (Tang et al., 2021). Tight regulation of Arid3a expression at the upper crypt is therefore important for tissue homeostasis,

Upon niche exit, ISCs are committed to differentiation, a process driven by several key developmental pathways including Bmp, Tgfβ and Notch. Bmp pathway has been proposed as the main pathway driving differentiation of intestinal epithelial cells by directly suppressing stemness genes via recruitment of Hdac1 (Qi et al., 2017). On the other hand, Notch plays a key role in fate decision at the early progenitor cells. However, it is now believed that lineage decision and specification is not a simple ON/OFF switch of Notch signalling. Recent advances in genomics and spatial transcriptomics revealed that differentiation is a continuous process along the crypt-villus axis where committed progenitor cells carry on to transdifferentiate/mature and exhibit zonated gene expression programme to facilitate different functional requirements along the axis, such as absorption of different nutrients or defence against microbes (Gehart et al., 2019, Haber et al., 2017, Manco et al., 2021, Moor et al., 2018). Recent studies have shown that zonation of enterocyte and goblet cell states as well as switch of hormone expression of enteroendocrine cells along the crypt-villus axis are driven by Bmp signalling (Beumer et al., 2018, Beumer et al., 2022). How Bmp induces zonation patterning of various cell types along the crypt-villus axis remains unknown. The findings in our current study indicate that Arid3a is key to the zonation patterning of multiple cell lineages, including enterocytes, goblet, enteroendocrine and tuft cells. RNA-seq analysis of Arid3a cKO intestine showed a reduction of gene expression of all differentiated markers that are enriched at the upper crypt/villus bottom, while expression of the mid-villus and villus tip genes was upregulated. It is important to note that bulk RNA-seq data does not provide sufficient spatial resolution to determine whether upregulation of the mid-villus and villus tip genes

occurs at cells residing at their corresponding locations or at the TA zone. Since Arid3a is expressed throughout the crypt-villus axis, it will be important to further investigate if Arid3a regulates the zonation programme at the villus directly or at TA zone by modulating the proliferation-differentiation transition. The latter would support a recently proposed working model where TA cells have a central role in fine-tuning the composition of differentiated cell types (Sanman et al., 2021). It is conceivable that Arid3a is expressed at the TA cells to ensure that they maintain their proliferative capacity and undergo enough cycles of cell division before migration to the villus and terminal maturation. Single-cell transcriptomics will help to further address this question by providing spatial clues.

Interestingly, our data demonstrate that Arid3a is regulated by Tgf-β but not Bmp signalling. This is different from other recent studies showing Bmp as the driver of the zonation programmes (Beumer et al., 2018, Beumer et al., 2022). Our results come in accordance with previous findings showing that Tgf-β promotes expression of Arid3a and vice versa (Alejo-Valle et al., 2022, Callery et al., 2005, Lin et al., 2008). As alluded to in Chapter 1, Bmp signalling has been widely associated with differentiation of intestinal epithelial cells, while only a few studies have demonstrated the contribution of Tgf-β in this process despite being in the same family. Our results possibly reveal a previously underappreciated role of Tgf-β in intestinal homeostasis and suggests that both branches of the same superfamily of pathways might contribute to the epithelial spatial differentiation programmes. Both Tgf-β and Bmp pathways recruit the same core Smad4 to activate their transcriptional targets, yet it has been shown that the level of contribution of Smad4 on each of the pathways is different in early embryogenesis (Guglielmi et al., 2021). It would be interesting to examine whether differential Smad4-dependent or Smad4-independent activity of the two pathways contributes to the differentiation programme of the intestinal epithelium.

Previous studies have showed that Tgf-β modulates expression of Arid3a in other systems (Lin et al., 2008). A very recent work from Alejo-Valle et al showed that Arid3a interacts with Smad2/3 to promote Tgf-β-driven differentiation towards megakaryocytic lineage in the haematopoietic system (Alejo-Valle et al., 2022). Interestingly, our results indicate a different regulatory process in the intestine: Tgf-β promotes expression of Arid3a, which in turn supresses the transdifferentiation of early progenitor cells. This could indicate a very interesting mechanism where Bmp and Tgf-β coordinate the differentiation process in the intestinal epithelium: Bmp

drives the transdifferentiation upon niche exit, while Tgf-β utilises Arid3a to fine-tune this process at the TA cells. Future experiments should aim to further characterise the specific role of Tgf-β in proliferation and differentiation of intestinal epithelial cells and determine its mechanism of action. It will also be of interest to further assess the role of Arid3a in pathogenesis of diseases driven by dysregulation of Tgf-β such as inflammatory bowel disease, fibrosis and colorectal cancer.

The mechanism underlying Arid3a-mediated transdifferentiation of different cell lineages remains unclear. Unfortunately, we were not able to directly demonstrate the transcriptional targets of Arid3a due to the lack of reliable antibodies for ChIP-seq experiment. However, ATAC-seq analysis of Arid3a-deficient intestinal crypts has provided some valuable insights into the mechanism of action. The results showed that members of the Hnf family of transcription factors have increased occupancy of A+T rich genomic regions upon loss of Arid3a, which are normally bound by Arid3a under homeostasis. Hnf transcription factors have been previously associated with terminal differentiation of enterocytes (Babeu et al., 2009, Chen et al., 2019, D'Angelo et al., 2010). This suggests that Arid3a may regulate the transdifferentiation of enterocytes by competing with Hnf transcription. To further explore this mechanism of proliferation/differentiation balance, a series of experiments should be conducted. Firstly, a list of Hnf protein in the intestine should be identified and the expression of these genes in the Arid3a cKO animals should be examined. Secondly, the list of genomic loci with enriched binding of Hnf proteins in Arid3a cKO animals (based on the TOBIAS analysis) should be extracted and an over-representation analysis should be performed in order to validate whether this increased Hnf binding is related with biological functions related to Hnf proteins. Lastly, the binding of Hnf proteins could be compared in WT and KO conditions with ChIP-seq analysis. To this end, mouse organoids homozygous for an Arid3a floxed allele could be used and treated with hydro-tamoxifen). It would be interesting to examine the binding of Hnf proteins in the presence of Arid3a (WT), partial loss of Arid3a (a few hours after hydro-tamoxifen treatment) and complete loss of Arid3a (KO – 3 days after hydro-tamoxifen administration).

Interestingly, the ATAC-seq analysis also revealed global increase in chromatin accessibility upon loss of Arid3a, suggesting that Arid3a might be acting as a suppressor. Indeed, several reports have suggested that Arid3a can act either as an activator or as a repressor (Lin et al., 2007, Popowski et al., 2014, Webb et al., 1999).

However, these genome-wide alterations in chromatin accessibility can only partially explain the changes revealed by RNA-seq of Arid3a KO animals. Increased open chromatin around the TSS of mid/top villus genes can cause their increased expression but does not explain the reduced expression of proliferation and early differentiation gene at the crypt. One possible explanation is that ATAC-seq was performed in bulk including both crypts and villi, making it hard to distinguish the effects of Arid3a loss on chromatin accessibility of different cell types. Future single cell ATAC-seq analysis and comparison of WT and Arid3a cKO would greatly help understand the contribution of Arid3a in chromatin accessibility of different cell populations. Moreover, optimisation of ChIP-seq experiment will reveal the Arid3a targetome and help understand the direct transcriptional changes caused by Arid3a deletion. It is interesting to note that previous studies have reported a striking level of similarity in open chromatin regions of intestinal epithelial cells, especially between ISCs and enterocytes (Jadhav et al., 2017, Kim et al., 2014). The findings support a model where chromatin and cis-element status is largely established in Lgr5-positive cells and differentiation is driven by activation of these existing sites. This implies that deletion of a single transcription factor (such as Arid3a) may perturb differentiation without the need to alter chromatin remodelling during differentiation. Indeed, the vast majority of the aforementioned chromatin regions identified were present in both WT and Arid3a cKO intestines. Many of these regions showed a moderate increase in their accessibility without statistical significance. On the other hand, RNA-seq analysis revealed significant downregulation of histone genes upon deletion of Arid3a. Whether reduced expression of histone genes is the reason for more opened chromatin in KO tissues is yet to be determined.

Arid3a is not only expressed at the differentiated cells but also showed a strong enrichment at villus tip (figure 3.5). Such unique pattern of expression at the epithelium suggests that Arid3a may play an additional role at the villus tip. Intestinal epithelium renews continuously as the cells migrate towards the villus tip and undergo apoptosis before shedding into the lumen. Despite the rapid turnover of epithelial cells and the continuous cell shedding at the villus tip, the underlying molecular mechanism regulating this process is largely unknown. Since Arid3a is highly enriched at the villus tip, we speculate that Arid3a might play a role in this machinery. Moreover, Arid3a might also be involved in hypoxia. Previous studies have shown reduced oxygen availability towards the lumen (physiologic hypoxia) (Zheng et al.,

2015), which is evident by the strong expression of Hypoxia-inducible factor 1 (Hif-1) at the villus-tip similar to that or Arid3a (Rohwer et al., 2019). It will be worth further investigating if Arid3a potentially regulates response to oxygen concentration.

Arid3b is another transcription factor of the Arid3 sub-family and shows significant levels of expression at intestinal epithelial cells. Previous studies have linked the function of Arid3a and Arid3b in promoting proliferation and cancer transformation (Dausinas et al., 2020, Liao et al., 2016). Of interest, loss of Arid3b did not reveal any major phenotypic change with regards to proliferation and differentiation and does not have an additive effect in DKO animals.

Since loss of Arid3a perturbs the balance of proliferation and differentiation of the TA cells, we asked if Arid3a is also involved in tissue regeneration upon irradiation. Interestingly, we found that Arid3a cKO mice showed an impaired response to irradiation and died faster compared to WT animals, indicating that Arid3a is indispensable for the intestinal regenerative machinery. The prolonged period of initial damage and delayed hyperproliferation phase in the Arid3a cKO animals can be attributed to the reduced number of proliferative TA cells and Paneth cells, thus reduced plasticity. In addition, Arid3a cKO intestine showed increased apoptosis at the intestinal crypts. Quantitation of apoptotic crypts revealed interesting regeneration dynamics where apoptosis recovery is in waves rather than in a linear pattern (figure 5.4). Conceivably, intestinal crypts that fail to regenerate at the first proliferative phase (day 3) become apoptotic again (day 4-5) and undergo another round of regeneration until the crypt is fully recovered. Loss of Arid3a seems to impair this recovery process, leading to massive apoptosis throughout the crypt-villus axis and significant weight loss by day 12 post-irradiation. Indeed, RNA-seq data showed that loss of Arid3a increases apoptotic gene expression, suggesting that the accumulation of Arid3a expression at the villus tip may indeed be protect epithelial cells against injury-induced apoptosis. Tgf has traditionally linked with cell cycle arrest and apoptosis. It will be interesting to test if the protective role of Arid3a against apoptosis is Tgf-β-dependent. Detailed single cell RNA-seq analysis of the regenerating epithelium of Arid3a cKO mice as well as lineage tracing experiments will help understand how Arid3a regulates regeneration. It will also be importance to validate these results using different injury models such as genetic ablation of Lgr5-positive ISCs or chemotherapy-induced regeneration.

In summary, we uncovered Arid3a as a novel modulator of intestinal epithelial homeostasis, regulating the proliferation state of TA cells and the transdifferentiation process of different committed cell types. Loss of Arid3a impairs irradiation-induced intestinal regeneration due to reduced number of proliferating TA cells and increased apoptosis. Our findings provide new mechanistic insights into the regulation of TA cell transition as well as villus differentiation via Tgf-β-mediated zonation patterning.

Reference list

ABERLE, H., BAUER, A., STAPPERT, J., KISPERT, A. & KEMLER, R. 1997. beta-catenin is a target for the ubiquitin-proteasome pathway. *EMBO J,* 16**,** 3797-804.

ALEJO-VALLE, O., WEIGERT, K., BHAYADIA, R., NG, M., ISSA, H., BEYER, C., EMMRICH, S., SCHUSCHEL, K., IHLING, C., SINZ, A., ZIMMERMANN, M., WICKENHAUSER, C., FLASINSKI, M., REGENYI, E., LABUHN, M., REINHARDT, D., YASPO, M. L., HECKL, D. & KLUSMANN, J. H. 2022. The megakaryocytic transcription factor ARID3A suppresses leukemia pathogenesis. *Blood,* 139**,** 651-665.

AMANN, J. M., CHYLA, B. J., ELLIS, T. C., MARTINEZ, A., MOORE, A. C., FRANKLIN, J. L., MCGHEE, L., MEYERS, S., OHM, J. E., LUCE, K. S., OUELETTE, A. J., WASHINGTON, M. K., THOMPSON, M. A., KING, D., GAUTAM, S., COFFEY, R. J., WHITEHEAD, R. H. & HIEBERT, S. W. 2005. Mtgr1 is a transcriptional corepressor that is required for maintenance of the secretory cell lineage in the small intestine. *Mol Cell Biol,* 25**,** 9576-85.

AN, G., MINER, C. A., NIXON, J. C., KINCADE, P. W., BRYANT, J., TUCKER, P. W. & WEBB, C. F. 2010. Loss of Bright/ARID3a function promotes developmental plasticity. *Stem Cells,* 28**,** 1560-7.

AOKI, R., SHOSHKES-CARMEL, M., GAO, N., SHIN, S., MAY, C. L., GOLSON, M. L., ZAHM, A. M., RAY, M., WISER, C. L., WRIGHT, C. V. & KAESTNER, K. H. 2016. Foxl1-expressing mesenchymal cells constitute the intestinal stem cell niche. *Cell Mol Gastroenterol Hepatol,* 2**,** 175-188.

ARTAVANIS-TSAKONAS, S., RAND, M. D. & LAKE, R. J. 1999. Notch signaling: cell fate control and signal integration in development. *Science,* 284**,** 770-6.

ASFAHA, S., HAYAKAWA, Y., MULEY, A., STOKES, S., GRAHAM, T. A., ERICKSEN, R. E., WESTPHALEN, C. B., VON BURSTIN, J., MASTRACCI, T. L., WORTHLEY, D. L., GUHA, C., QUANTE, M., RUSTGI, A. K. & WANG, T. C. 2015. Krt19(+)/Lgr5(-) Cells Are Radioresistant Cancer-Initiating Stem Cells in the Colon and Intestine. *Cell Stem Cell,* 16**,** 627-38.

AYYAZ, A., KUMAR, S., SANGIORGI, B., GHOSHAL, B., GOSIO, J., OULADAN, S., FINK, M., BARUTCU, S., TRCKA, D., SHEN, J., CHAN, K., WRANA, J. L. & GREGORIEFF, A. 2019. Single-cell transcriptomes of the regenerating intestine reveal a revival stem cell. *Nature,* 569**,** 121-125.

BABEU, J. P., DARSIGNY, M., LUSSIER, C. R. & BOUDREAU, F. 2009. Hepatocyte nuclear factor 4alpha contributes to an intestinal epithelial phenotype in vitro and plays a partial role in mouse intestinal epithelium differentiation. *Am J Physiol Gastrointest Liver Physiol,* 297**,** G124-34.

BAHAR HALPERN, K., MASSALHA, H., ZWICK, R. K., MOOR, A. E., CASTILLO-AZOFEIFA, D., ROZENBERG, M., FARACK, L., EGOZI, A., MILLER, D. R., AVERBUKH, I., HARNIK, Y., WEINBERG-COREM, N., DE SAUVAGE, F. J., AMIT, I., KLEIN, O. D., SHOSHKES-CARMEL, M. & ITZKOVITZ, S. 2020. Lgr5+ telocytes are a signaling source at the intestinal villus tip. *Nat Commun,* 11**,** 1936.

BANKHEAD, P., LOUGHREY, M. B., FERNANDEZ, J. A., DOMBROWSKI, Y., MCART, D. G., DUNNE, P. D., MCQUAID, S., GRAY, R. T., MURRAY, L. J., COLEMAN, H. G., JAMES, J. A., SALTO-TELLEZ, M. & HAMILTON, P. W. 2017. QuPath: Open source software for digital pathology image analysis. *Sci Rep,* 7**,** 16878.

BARKER, N. 2014. Adult intestinal stem cells: critical drivers of epithelial homeostasis and regeneration. *Nat Rev Mol Cell Biol,* 15**,** 19-33.

BARKER, N., VAN ES, J. H., KUIPERS, J., KUJALA, P., VAN DEN BORN, M., COZIJNSEN, M., HAEGEBARTH, A., KORVING, J., BEGTHEL, H., PETERS, P. J. & CLEVERS, H. 2007. Identification of stem cells in small intestine and colon by marker gene Lgr5. *Nature,* 449**,** 1003-7.

BARNETT, D. W., GARRISON, E. K., QUINLAN, A. R., STROMBERG, M. P. & MARTH, G. T. 2011. BamTools: a C++ API and toolkit for analyzing and managing BAM files. *Bioinformatics,* 27**,** 1691-2.

BARRIGA, F. M., MONTAGNI, E., MANA, M., MENDEZ-LAGO, M., HERNANDO-MOMBLONA, X., SEVILLANO, M., GUILLAUMET-ADKINS, A., RODRIGUEZ-ESTEBAN, G., BUCZACKI, S. J. A., GUT, M., HEYN, H., WINTON, D. J., YILMAZ, O. H., ATTOLINI, C. S., GUT, I. & BATLLE, E. 2017. Mex3a Marks a Slowly Dividing Subpopulation of Lgr5+ Intestinal Stem Cells. *Cell Stem Cell,* 20**,** 801-816 e7.

BARRY, E. R., MORIKAWA, T., BUTLER, B. L., SHRESTHA, K., DE LA ROSA, R., YAN, K. S., FUCHS, C. S., MAGNESS, S. T., SMITS, R., OGINO, S., KUO, C. J. & CAMARGO, F. D. 2013. Restriction of intestinal stem cell expansion and the regenerative response by YAP. *Nature,* 493**,** 106-10.

BASAK, O., BEUMER, J., WIEBRANDS, K., SENO, H., VAN OUDENAARDEN, A. & CLEVERS, H. 2017. Induced Quiescence of Lgr5+ Stem Cells in Intestinal Organoids Enables Differentiation of Hormone-Producing Enteroendocrine Cells. *Cell Stem Cell,* 20**,** 177-190.e4.

BASAK, O., VAN DE BORN, M., KORVING, J., BEUMER, J., VAN DER ELST, S., VAN ES, J. H. & CLEVERS, H. 2014. Mapping early fate determination in Lgr5+ crypt stem cells using a novel Ki67-RFP allele. *Embo j,* 33**,** 2057-68.

BATLLE, E., BACANI, J., BEGTHEL, H., JONKHEER, S., GREGORIEFF, A., VAN DE BORN, M., MALATS, N., SANCHO, E., BOON, E., PAWSON, T., GALLINGER, S., PALS, S. & CLEVERS, H. 2005. EphB receptor activity suppresses colorectal cancer progression. *Nature,* 435**,** 1126-30.

BATLLE, E., HENDERSON, J. T., BEGHTEL, H., VAN DEN BORN, M. M., SANCHO, E., HULS, G., MEELDIJK, J., ROBERTSON, J., VAN DE WETERING, M., PAWSON, T. & CLEVERS, H. 2002. Beta-catenin and TCF mediate cell positioning in the intestinal epithelium by controlling the expression of EphB/ephrinB. *Cell,* 111**,** 251-63.

BAULIES, A., ANGELIS, N., FOGLIZZO, V., DANIELSEN, E. T., PATEL, H., NOVELLASDEMUNT, L., KUCHARSKA, A., CARVALHO, J., NYE, E., DE COPPI, P. & LI, V. S. W. 2020a. The Transcription Co-Repressors MTG8 and MTG16 Regulate Exit of Intestinal Stem Cells From Their Niche and Differentiation Into Enterocyte vs Secretory Lineages. *Gastroenterology,* 159**,** 1328-1341 e3.

BAULIES, A., ANGELIS, N. & LI, V. S. W. 2020b. Hallmarks of intestinal stem cells. *Development,* 147.

BENTSEN, M., GOYMANN, P., SCHULTHEIS, H., KLEE, K., PETROVA, A., WIEGANDT, R., FUST, A., PREUSSNER, J., KUENNE, C., BRAUN, T., KIM, J. & LOOSO, M. 2020. ATAC-seq footprinting unravels kinetics of transcription factor binding during zygotic genome activation. *Nat Commun,* 11**,** 4267.

BEUMER, J., ARTEGIANI, B., POST, Y., REIMANN, F., GRIBBLE, F., NGUYEN, T. N., ZENG, H., VAN DEN BORN, M., VAN ES, J. H. & CLEVERS, H. 2018. Enteroendocrine cells switch hormone expression along the crypt-to-villus BMP signalling gradient. *Nat Cell Biol,* 20**,** 909-916.

BEUMER, J. & CLEVERS, H. 2016. Regulation and plasticity of intestinal stem cells during homeostasis and regeneration. *Development,* 143**,** 3639-3649.

BEUMER, J. & CLEVERS, H. 2021. Cell fate specification and differentiation in the adult mammalian intestine. *Nat Rev Mol Cell Biol,* 22**,** 39-53.

BEUMER, J., PUSCHHOF, J., YENGEJ, F. Y., ZHAO, L., MARTINEZ-SILGADO, A., BLOTENBURG, M., BEGTHEL, H., BOOT, C., VAN OUDENAARDEN, A., CHEN, Y. G. & CLEVERS, H. 2022. BMP gradient along the intestinal villus axis controls zonated enterocyte and goblet cell states. *Cell Rep,* 38**,** 110438.

BHANOT, P., BRINK, M., SAMOS, C. H., HSIEH, J. C., WANG, Y., MACKE, J. P., ANDREW, D., NATHANS, J. & NUSSE, R. 1996. A new member of the frizzled family from Drosophila functions as a Wingless receptor. *Nature,* 382**,** 225-30.

BIRCHENOUGH, G. M., JOHANSSON, M. E., GUSTAFSSON, J. K., BERGSTROM, J. H. & HANSSON, G. C. 2015. New developments in goblet cell mucus secretion and function. *Mucosal Immunol,* 8**,** 712-9.

BJERKNES, M. & CHENG, H. 1999. Clonal analysis of mouse intestinal epithelial progenitors. *Gastroenterology,* 116**,** 7-14.

BJERKNES, M. & CHENG, H. 2005. Gastrointestinal stem cells. II. Intestinal stem cells. *Am J Physiol Gastrointest Liver Physiol,* 289**,** G381-7.

BJERKNES, M. & CHENG, H. 2010. Cell Lineage metastability in Gfi1-deficient mouse intestinal epithelium. *Dev Biol,* 345**,** 49-63.

BREAULT, D. T., MIN, I. M., CARLONE, D. L., FARILLA, L. G., AMBRUZS, D. M., HENDERSON, D. E., ALGRA, S., MONTGOMERY, R. K., WAGERS, A. J. & HOLE, N. 2008. Generation of mTert-GFP mice as a model to identify and study tissue progenitor cells. *Proc Natl Acad Sci U S A,* 105**,** 10420-5.

BUCZACKI, S. J., ZECCHINI, H. I., NICHOLSON, A. M., RUSSELL, R., VERMEULEN, L., KEMP, R. & WINTON, D. J. 2013. Intestinal label-retaining cells are secretory precursors expressing Lgr5. *Nature,* 495**,** 65-9.

BUENROSTRO, J. D., WU, B., CHANG, H. Y. & GREENLEAF, W. J. 2015. ATAC-seq: A Method for Assaying Chromatin Accessibility Genome-Wide. *Curr Protoc Mol Biol,* 109**,** 21.29.1-9.

BUSSLINGER, G. A., WEUSTEN, B. L. A., BOGTE, A., BEGTHEL, H., BROSENS, L. A. A. & CLEVERS, H. 2021. Human gastrointestinal epithelia of the esophagus, stomach, and duodenum resolved at single-cell resolution. *Cell Rep,* 34**,** 108819.

CAI, J., ZHANG, N., ZHENG, Y., DE WILDE, R. F., MAITRA, A. & PAN, D. 2010. The Hippo signaling pathway restricts the oncogenic potential of an intestinal regeneration program. *Genes Dev,* 24**,** 2383-8.

CALABI, F., PANNELL, R. & PAVLOSKA, G. 2001. Gene targeting reveals a crucial role for MTG8 in the gut. *Mol Cell Biol,* 21**,** 5658-66.

CALLERY, E. M., SMITH, J. C. & THOMSEN, G. H. 2005. The ARID domain protein dril1 is necessary for TGF(beta) signaling in Xenopus embryos. *Dev Biol,* 278**,** 542-59.

CARTER, P., SCHNELL, U., CHANEY, C., TONG, B., PAN, X., YE, J., MERNAUGH, G., COTTON, J. L., MARGULIS, V., MAO, J., ZENT, R., EVERS, B. M., KAPUR, P. & CARROLL, T. J. 2021. Deletion of Lats1/2 in adult kidney epithelia leads to renal cell carcinoma. *J Clin Invest,* 131.

CARULLI, A. J., KEELEY, T. M., DEMITRACK, E. S., CHUNG, J., MAILLARD, I. & SAMUELSON, L. C. 2015. Notch receptor regulation of intestinal stem cell homeostasis and crypt regeneration. *Dev Biol,* 402**,** 98-108.

CASANOVA, J. C., URIBE, V., BADIA-CAREAGA, C., GIOVINAZZO, G., TORRES, M. & SANZ-EZQUERRO, J. J. 2011. Apical ectodermal ridge morphogenesis in limb development is

controlled by Arid3b-mediated regulation of cell movements. *Development,* 138**,** 1195-205.

CASTILLO-AZOFEIFA, D., FAZIO, E. N., NATTIV, R., GOOD, H. J., WALD, T., PEST, M. A., DE SAUVAGE, F. J., KLEIN, O. D. & ASFAHA, S. 2019. Atoh1(+) secretory progenitors possess renewal capacity independent of Lgr5(+) cells during colonic regeneration. *EMBO J,* 38.

CAVALLO, R. A., COX, R. T., MOLINE, M. M., ROOSE, J., POLEVOY, G. A., CLEVERS, H., PEIFER, M. & BEJSOVEC, A. 1998. Drosophila Tcf and Groucho interact to repress Wingless signalling activity. *Nature,* 395**,** 604-8.

CHEN, L., TOKE, N. H., LUO, S., VASOYA, R. P., FULLEM, R. L., PARTHASARATHY, A., PEREKATT, A. O. & VERZI, M. P. 2019. A reinforcing HNF4-SMAD4 feed-forward module stabilizes enterocyte identity. *Nat Genet,* 51**,** 777-785.

CHENG, H. & LEBLOND, C. P. 1974. Origin, differentiation and renewal of the four main epithelial cell types in the mouse small intestine. V. Unitarian Theory of the origin of the four epithelial cell types. *Am J Anat,* 141**,** 537-61.

CHENG, H., MERZEL, J. & LEBLOND, C. P. 1969. Renewal of Paneth cells in the small intestine of the mouse. *Am J Anat,* 126**,** 507-25.

CHIN, A. M., TSAI, Y. H., FINKBEINER, S. R., NAGY, M. S., WALKER, E. M., ETHEN, N. J., WILLIAMS, B. O., BATTLE, M. A. & SPENCE, J. R. 2016. A Dynamic WNT/beta-CATENIN Signaling Environment Leads to WNT-Independent and WNT-Dependent Proliferation of Embryonic Intestinal Progenitor Cells. *Stem Cell Reports,* 7**,** 826-839.

CHYLA, B. J., MORENO-MIRALLES, I., STEAPLETON, M. A., THOMPSON, M. A., BHASKARA, S., ENGEL, M. & HIEBERT, S. W. 2008. Deletion of Mtg16, a target of t(16;21), alters hematopoietic progenitor cell proliferation and lineage allocation. *Mol Cell Biol,* 28**,** 6234-47.

CLEVERS, H. 2013. The Intestinal Crypt, A Prototype Stem Cell Compartment. *Cell,* 154**,** 274-284.

CLEVERS, H. & NUSSE, R. 2012. Wnt/beta-catenin signaling and disease. *Cell,* 149**,** 1192-205.

CLEVERS, H. C. & BEVINS, C. L. 2013. Paneth cells: maestros of the small intestinal crypts. *Annu Rev Physiol,* 75**,** 289-311.

COHEN, S., CARPENTER, G. & KING, L., JR. 1980. Epidermal growth factor-receptor-protein kinase interactions. Co-purification of receptor and epidermal growth factor-enhanced phosphorylation activity. *J Biol Chem,* 255**,** 4834-42.

COLLIER, C. A., MENDIONDO, C. & RAGHAVAN, S. 2022. Tissue engineering of the gastrointestinal tract: the historic path to translation. *J Biol Eng,* 16**,** 9.

CORCES, M. R., TREVINO, A. E., HAMILTON, E. G., GREENSIDE, P. G., SINNOTT-ARMSTRONG, N. A., VESUNA, S., SATPATHY, A. T., RUBIN, A. J., MONTINE, K. S., WU, B., KATHIRIA, A., CHO, S. W., MUMBACH, M. R., CARTER, A. C., KASOWSKI, M., ORLOFF, L. A., RISCA, V. I., KUNDAJE, A., KHAVARI, P. A., MONTINE, T. J., GREENLEAF, W. J. & CHANG, H. Y. 2017. An improved ATAC-seq protocol reduces background and enables interrogation of frozen tissues. *Nat Methods,* 14**,** 959-962.

D'ANGELO, A., BLUTEAU, O., GARCIA-GONZALEZ, M. A., GRESH, L., DOYEN, A., GARBAY, S., ROBINE, S. & PONTOGLIO, M. 2010. Hepatocyte nuclear factor 1alpha and beta control terminal differentiation and cell fate commitment in the gut epithelium. *Development,* 137**,** 1573-82.

DALEY, T. & SMITH, A. D. 2013. Predicting the molecular complexity of sequencing libraries. *Nat Methods,* 10**,** 325-7.

DAUSINAS, P., PULAKANTI, K., RAO, S., COLE, J. M., DAHL, R. & COWDEN DAHL, K. D. 2020. ARID3A and ARID3B induce stem promoting pathways in ovarian cancer cells. *Gene,* 738**,** 144458.

DAVIS, H., IRSHAD, S., BANSAL, M., RAFFERTY, H., BOITSOVA, T., BARDELLA, C., JAEGER, E., LEWIS, A., FREEMAN-MILLS, L., GINER, F. C., RODENAS-CUADRADO, P., MALLAPPA, S., CLARK, S., THOMAS, H., JEFFERY, R., POULSOM, R., RODRIGUEZ-JUSTO, M., NOVELLI, M., CHETTY, R., SILVER, A., SANSOM, O. J., GRETEN, F. R., WANG, L. M., EAST, J. E., TOMLINSON, I. & LEEDHAM, S. J. 2015. Aberrant epithelial GREM1 expression initiates colonic tumorigenesis from cells outside the stem cell niche. *Nat Med,* 21**,** 62-70.

DE LAU, W., BARKER, N., LOW, T. Y., KOO, B. K., LI, V. S., TEUNISSEN, H., KUJALA, P., HAEGEBARTH, A., PETERS, P. J., VAN DE WETERING, M., STANGE, D. E., VAN ES, J. E., GUARDAVACCARO, D., SCHASFOORT, R. B., MOHRI, Y., NISHIMORI, K., MOHAMMED, S., HECK, A. J. & CLEVERS, H. 2011. Lgr5 homologues associate with Wnt receptors and mediate R-spondin signalling. *Nature,* 476**,** 293-7.

DE LAU, W., PENG, W. C., GROS, P. & CLEVERS, H. 2014. The R-spondin/Lgr5/Rnf43 module: regulator of Wnt signal strength. *Genes Dev,* 28**,** 305-16.

DEGIRMENCI, B., VALENTA, T., DIMITRIEVA, S., HAUSMANN, G. & BASLER, K. 2018. GLI1-expressing mesenchymal cells form the essential Wnt-secreting niche for colon stem cells. *Nature,* 558**,** 449-453.

DEMITRACK, E. S. & SAMUELSON, L. C. 2016. Notch regulation of gastrointestinal stem cells. *J Physiol,* 594**,** 4791-803.

DI TOMMASO, P., CHATZOU, M., FLODEN, E. W., BARJA, P. P., PALUMBO, E. & NOTREDAME, C. 2017. Nextflow enables reproducible computational workflows. *Nat Biotechnol,* 35**,** 316-319.

DURAND, A., DONAHUE, B., PEIGNON, G., LETOURNEUR, F., CAGNARD, N., SLOMIANNY, C., PERRET, C., SHROYER, N. F. & ROMAGNOLO, B. 2012. Functional intestinal stem cells after Paneth cell ablation induced by the loss of transcription factor Math1 (Atoh1). *Proc Natl Acad Sci U S A,* 109**,** 8965-70.

EL MARJOU, F., JANSSEN, K. P., CHANG, B. H., LI, M., HINDIE, V., CHAN, L., LOUVARD, D., CHAMBON, P., METZGER, D. & ROBINE, S. 2004. Tissue-specific and inducible Cre-mediated recombination in the gut epithelium. *Genesis,* 39**,** 186-93.

ELPHICK, D. A. & MAHIDA, Y. R. 2005. Paneth cells: their role in innate immunity and inflammatory disease. *Gut,* 54**,** 1802-9.

ENGEL, M. E., NGUYEN, H. N., MARIOTTI, J., HUNT, A. & HIEBERT, S. W. 2010. Myeloid translocation gene 16 (MTG16) interacts with Notch transcription complex components to integrate Notch signaling in hematopoietic cell fate specification. *Mol Cell Biol,* 30**,** 1852-63.

EWELS, P. A., PELTZER, A., FILLINGER, S., PATEL, H., ALNEBERG, J., WILM, A., GARCIA, M. U., DI TOMMASO, P. & NAHNSEN, S. 2020. The nf-core framework for community-curated bioinformatics pipelines. *Nat Biotechnol,* 38**,** 276-278.

FANG, L., ZHU, Q., NEUENSCHWANDER, M., SPECKER, E., WULF-GOLDENBERG, A., WEIS, W. I., VON KRIES, J. P. & BIRCHMEIER, W. 2016. A Small-Molecule Antagonist of the beta-Catenin/TCF4 Interaction Blocks the Self-Renewal of Cancer Stem Cells and Suppresses Tumorigenesis. *Cancer Res,* 76**,** 891-901.

FARIN, H. F., JORDENS, I., MOSA, M. H., BASAK, O., KORVING, J., TAURIELLO, D. V., DE PUNDER, K., ANGERS, S., PETERS, P. J., MAURICE, M. M. & CLEVERS, H. 2016. Visualization of a short-range Wnt gradient in the intestinal stem-cell niche. *Nature,* 530**,** 340-3.

FARIN, H. F., VAN ES, J. H. & CLEVERS, H. 2012. Redundant sources of Wnt regulate intestinal stem cells and promote formation of Paneth cells. *Gastroenterology,* 143**,** 1518-1529.e7.

FAWKNER-CORBETT, D., ANTANAVICIUTE, A., PARIKH, K., JAGIELOWICZ, M., GEROS, A. S., GUPTA, T., ASHLEY, N., KHAMIS, D., FOWLER, D., MORRISSEY, E., CUNNINGHAM, C., JOHNSON, P. R. V., KOOHY, H. & SIMMONS, A. 2021. Spatiotemporal analysis of human intestinal development at single-cell resolution. *Cell,* 184**,** 810-826 e23.

FRE, S., HANNEZO, E., SALE, S., HUYGHE, M., LAFKAS, D., KISSEL, H., LOUVI, A., GREVE, J., LOUVARD, D. & ARTAVANIS-TSAKONAS, S. 2011. Notch lineages and activity in intestinal stem cells determined by a new set of knock-in mice. *PLoS One,* 6**,** e25785.

FUJII, M., MATANO, M., NANKI, K. & SATO, T. 2015. Efficient genetic engineering of human intestinal organoids using electroporation. *Nat Protoc,* 10**,** 1474-85.

FUJII, M., MATANO, M., TOSHIMITSU, K., TAKANO, A., MIKAMI, Y., NISHIKORI, S., SUGIMOTO, S. & SATO, T. 2018. Human Intestinal Organoids Maintain Self-Renewal Capacity and Cellular Diversity in Niche-Inspired Culture Condition. *Cell Stem Cell,* 23**,** 787-793.e6.

GARABEDIAN, E. M., ROBERTS, L. J., MCNEVIN, M. S. & GORDON, J. I. 1997. Examining the role of Paneth cells in the small intestine by lineage ablation in transgenic mice. *J Biol Chem,* 272**,** 23729-40.

GEHART, H. & CLEVERS, H. 2019. Tales from the crypt: new insights into intestinal stem cells. *Nat Rev Gastroenterol Hepatol,* 16**,** 19-34.

GEHART, H., VAN ES, J. H., HAMER, K., BEUMER, J., KRETZSCHMAR, K., DEKKERS, J. F., RIOS, A. & CLEVERS, H. 2019. Identification of Enteroendocrine Regulators by Real-Time Single-Cell Differentiation Mapping. *Cell*.

GENANDER, M. & FRISEN, J. 2010. Ephrins and Eph receptors in stem cells and cancer. *Curr Opin Cell Biol,* 22**,** 611-6.

GERBE, F., LEGRAVEREND, C. & JAY, P. 2012. The intestinal epithelium tuft cells: specification and function. *Cell Mol Life Sci,* 69**,** 2907-17.

GERBE, F., SIDOT, E., SMYTH, D. J., OHMOTO, M., MATSUMOTO, I., DARDALHON, V., CESSES, P., GARNIER, L., POUZOLLES, M., BRULIN, B., BRUSCHI, M., HARCUS, Y., ZIMMERMANN, V. S., TAYLOR, N., MAIZELS, R. M. & JAY, P. 2016. Intestinal epithelial tuft cells initiate type 2 mucosal immunity to helminth parasites. *Nature,* 529**,** 226-30.

GERBE, F., VAN ES, J. H., MAKRINI, L., BRULIN, B., MELLITZER, G., ROBINE, S., ROMAGNOLO, B., SHROYER, N. F., BOURGAUX, J. F., PIGNODEL, C., CLEVERS, H. & JAY, P. 2011. Distinct ATOH1 and Neurog3 requirements define tuft cells as a new secretory cell type in the intestinal epithelium. *J Cell Biol,* 192**,** 767-80.

GRACZ, A. D., PUTHOFF, B. J. & MAGNESS, S. T. 2012. Identification, isolation, and culture of intestinal epithelial stem cells from murine intestine. *Methods Mol Biol,* 879**,** 89-107.

GRACZ, A. D., SAMSA, L. A., FORDHAM, M. J., TROTIER, D. C., ZWARYCZ, B., LO, Y. H., BAO, K., STARMER, J., RAAB, J. R., SHROYER, N. F., REINHARDT, R. L. & MAGNESS, S. T. 2018. Sox4 Promotes Atoh1-Independent Intestinal Secretory Differentiation Toward Tuft and Enteroendocrine Fates. *Gastroenterology,* 155**,** 1508-1523.e10.

GREGORIEFF, A., LIU, Y., INANLOU, M. R., KHOMCHUK, Y. & WRANA, J. L. 2015. Yap-dependent reprogramming of Lgr5(+) stem cells drives intestinal regeneration and cancer. *Nature,* 526**,** 715-8.

GREGORIEFF, A., PINTO, D., BEGTHEL, H., DESTREE, O., KIELMAN, M. & CLEVERS, H. 2005. Expression pattern of Wnt signaling components in the adult intestine. *Gastroenterology,* 129**,** 626-38.

GREICIUS, G., KABIRI, Z., SIGMUNDSSON, K., LIANG, C., BUNTE, R., SINGH, M. K. & VIRSHUP, D. M. 2018. PDGFRalpha(+) pericryptal stromal cells are the critical source of Wnts and RSPO3 for murine intestinal stem cells in vivo. *Proc Natl Acad Sci U S A,* 115**,** E3173-e3181.

GUDINO, V., CAMMARERI, P., BILLARD, C. V. & MYANT, K. B. 2021. Negative regulation of TGFbeta-induced apoptosis by RAC1B enhances intestinal tumourigenesis. *Cell Death Dis,* 12**,** 873.

GUGLIELMI, L., HELIOT, C., KUMAR, S., ALEXANDROV, Y., GORI, I., PAPALEONIDOPOULOU, F., BARRINGTON, C., EAST, P., ECONOMOU, A. D., FRENCH, P. M. W., MCGINTY, J. & HILL, C. S. 2021. Smad4 controls signaling robustness and morphogenesis by differentially contributing to the Nodal and BMP pathways. *Nat Commun,* 12**,** 6374.

GUILLERMIN, O., ANGELIS, N., SIDOR, C. M., RIDGWAY, R., BAULIES, A., KUCHARSKA, A., ANTAS, P., ROSE, M. R., CORDERO, J., SANSOM, O., LI, V. S. W. & THOMPSON, B. J. 2021. Wnt and Src signals converge on YAP-TEAD to drive intestinal regeneration. *EMBO J,* 40**,** e105770.

GUIU, J., HANNEZO, E., YUI, S., DEMHARTER, S., ULYANCHENKO, S., MAIMETS, M., JORGENSEN, A., PERLMAN, S., LUNDVALL, L., MAMSEN, L. S., LARSEN, A., OLESEN, R. H., ANDERSEN, C. Y., THUESEN, L. L., HARE, K. J., PERS, T. H., KHODOSEVICH, K., SIMONS, B. D. & JENSEN, K. B. 2019. Tracing the origin of adult intestinal stem cells. *Nature,* 570**,** 107-111.

HABER, A. L., BITON, M., ROGEL, N., HERBST, R. H., SHEKHAR, K., SMILLIE, C., BURGIN, G., DELOREY, T. M., HOWITT, M. R., KATZ, Y., TIROSH, I., BEYAZ, S., DIONNE, D., ZHANG, M., RAYCHOWDHURY, R., GARRETT, W. S., ROZENBLATT-ROSEN, O., SHI, H. N., YILMAZ, O., XAVIER, R. J. & REGEV, A. 2017. A single-cell survey of the small intestinal epithelium. *Nature,* 551**,** 333-339.

HABIR, K., AEINEHBAND, S., WERMELING, F. & MALIN, S. 2017. A Role for the Transcription Factor Arid3a in Mouse B2 Lymphocyte Expansion and Peritoneal B1a Generation. *Front Immunol,* 8**,** 1387.

HAO, H. X., XIE, Y., ZHANG, Y., CHARLAT, O., OSTER, E., AVELLO, M., LEI, H., MICKANIN, C., LIU, D., RUFFNER, H., MAO, X., MA, Q., ZAMPONI, R., BOUWMEESTER, T., FINAN, P. M., KIRSCHNER, M. W., PORTER, J. A., SERLUCA, F. C. & CONG, F. 2012. ZNRF3 promotes Wnt receptor turnover in an R-spondin-sensitive manner. *Nature,* 485**,** 195-200.

HARAMIS, A. P., BEGTHEL, H., VAN DEN BORN, M., VAN ES, J., JONKHEER, S., OFFERHAUS, G. J. & CLEVERS, H. 2004. De novo crypt formation and juvenile polyposis on BMP inhibition in mouse intestine. *Science,* 303**,** 1684-6.

HE, X. C., ZHANG, J., TONG, W. G., TAWFIK, O., ROSS, J., SCOVILLE, D. H., TIAN, Q., ZENG, X., HE, X., WIEDEMANN, L. M., MISHINA, Y. & LI, L. 2004. BMP signaling inhibits intestinal stem cell self-renewal through suppression of Wnt-beta-catenin signaling. *Nat Genet,* 36**,** 1117-21.

HEINZ, S., BENNER, C., SPANN, N., BERTOLINO, E., LIN, Y. C., LASLO, P., CHENG, J. X., MURRE, C., SINGH, H. & GLASS, C. K. 2010. Simple combinations of lineage-determining transcription factors prime cis-regulatory elements required for macrophage and B cell identities. *Mol Cell,* 38**,** 576-89.

HERRING, C. A., BANERJEE, A., MCKINLEY, E. T., SIMMONS, A. J., PING, J., ROLAND, J. T., FRANKLIN, J. L., LIU, Q., GERDES, M. J., COFFEY, R. J. & LAU, K. S. 2018. Unsupervised Trajectory Analysis of Single-Cell RNA-Seq and Imaging Data Reveals Alternative Tuft Cell Origins in the Gut. *Cell Syst,* 6**,** 37-51 e9.

HERRSCHER, R. F., KAPLAN, M. H., LELSZ, D. L., DAS, C., SCHEUERMANN, R. & TUCKER, P. W. 1995. The immunoglobulin heavy-chain matrix-associating regions are bound by Bright: a B cell-specific trans-activator that describes a new DNA-binding protein family. *Genes Dev,* 9**,** 3067-82.

HEUBERGER, J., KOSEL, F., QI, J., GROSSMANN, K. S., RAJEWSKY, K. & BIRCHMEIER, W. 2014. Shp2/MAPK signaling controls goblet/paneth cell fate decisions in the intestine. *Proc Natl Acad Sci U S A,* 111**,** 3472-7.

HOWE, K. L., REARDON, C., WANG, A., NAZLI, A. & MCKAY, D. M. 2005. Transforming growth factor-beta regulation of epithelial tight junction proteins enhances barrier function and blocks enterohemorrhagic Escherichia coli O157:H7-induced increased permeability. *Am J Pathol,* 167**,** 1587-97.

HUBER, W., CAREY, V. J., GENTLEMAN, R., ANDERS, S., CARLSON, M., CARVALHO, B. S., BRAVO, H. C., DAVIS, S., GATTO, L., GIRKE, T., GOTTARDO, R., HAHNE, F., HANSEN, K. D., IRIZARRY, R. A., LAWRENCE, M., LOVE, M. I., MACDONALD, J., OBENCHAIN, V., OLES, A. K., PAGES, H., REYES, A., SHANNON, P., SMYTH, G. K., TENENBAUM, D., WALDRON, L. & MORGAN, M. 2015. Orchestrating high-throughput genomic analysis with Bioconductor. *Nat Methods,* 12**,** 115-21.

IHARA, S., HIRATA, Y. & KOIKE, K. 2017. TGF-beta in inflammatory bowel disease: a key regulator of immune cells, epithelium, and the intestinal microbiota. *J Gastroenterol,* 52**,** 777-787.

IMAJO, M., EBISUYA, M. & NISHIDA, E. 2015. Dual role of YAP and TAZ in renewal of the intestinal epithelium. *Nat Cell Biol,* 17**,** 7-19.

IRELAND, H., HOUGHTON, C., HOWARD, L. & WINTON, D. J. 2005. Cellular inheritance of a Cre-activated reporter gene to determine Paneth cell longevity in the murine small intestine. *Dev Dyn,* 233**,** 1332-6.

ITZKOVITZ, S., LYUBIMOVA, A., BLAT, I. C., MAYNARD, M., VAN ES, J., LEES, J., JACKS, T., CLEVERS, H. & VAN OUDENAARDEN, A. 2011. Single-molecule transcript counting of stem-cell markers in the mouse intestine. *Nat Cell Biol,* 14**,** 106-14.

JADHAV, U., SAXENA, M., O'NEILL, N. K., SAADATPOUR, A., YUAN, G. C., HERBERT, Z., MURATA, K. & SHIVDASANI, R. A. 2017. Dynamic Reorganization of Chromatin Accessibility Signatures during Dedifferentiation of Secretory Precursors into Lgr5+ Intestinal Stem Cells. *Cell Stem Cell,* 21**,** 65-77.e5.

JENNY, M., UHL, C., ROCHE, C., DULUC, I., GUILLERMIN, V., GUILLEMOT, F., JENSEN, J., KEDINGER, M. & GRADWOHL, G. 2002. Neurogenin3 is differentially required for endocrine cell fate specification in the intestinal and gastric epithelium. *EMBO J,* 21**,** 6338-47.

JONES, J. C., BRINDLEY, C. D., ELDER, N. H., MYERS, M. G., JR., RAJALA, M. W., DEKANEY, C. M., MCNAMEE, E. N., FREY, M. R., SHROYER, N. F. & DEMPSEY, P. J. 2019. Cellular Plasticity of Defa4(Cre)-Expressing Paneth Cells in Response to Notch Activation and Intestinal Injury. *Cell Mol Gastroenterol Hepatol,* 7**,** 533-554.

JOOSTEN, S. P. J., ZEILSTRA, J., VAN ANDEL, H., MIJNALS, R. C., ZAUNBRECHER, J., DUIVENVOORDEN, A. A. M., VAN DE WETERING, M., CLEVERS, H., SPAARGAREN, M. & PALS, S. T. 2017. MET Signaling Mediates Intestinal Crypt-Villus Development, Regeneration, and Adenoma Formation and Is Promoted by Stem Cell CD44 Isoforms. *Gastroenterology,* 153**,** 1040-1053 e4.

KABIRI, Z., GREICIUS, G., MADAN, B., BIECHELE, S., ZHONG, Z., ZARIBAFZADEH, H., EDISON, ALIYEV, J., WU, Y., BUNTE, R., WILLIAMS, B. O., ROSSANT, J. & VIRSHUP, D. M. 2014.

Stroma provides an intestinal stem cell niche in the absence of epithelial Wnts. *Development,* 141**,** 2206-15.

KALO, M. S. & PASQUALE, E. B. 1999. Multiple in vivo tyrosine phosphorylation sites in EphB receptors. *Biochemistry,* 38**,** 14396-408.

KANIA, A. & KLEIN, R. 2016. Mechanisms of ephrin-Eph signalling in development, physiology and disease. *Nat Rev Mol Cell Biol,* 17**,** 240-56.

KARASOV, W. H. 2017. Integrative physiology of transcellular and paracellular intestinal absorption. *J Exp Biol,* 220**,** 2495-2501.

KATZ, J. P., PERREAULT, N., GOLDSTEIN, B. G., LEE, C. S., LABOSKY, P. A., YANG, V. W. & KAESTNER, K. H. 2002. The zinc-finger transcription factor Klf4 is required for terminal differentiation of goblet cells in the colon. *Development,* 129**,** 2619-28.

KAY, S. K., HARRINGTON, H. A., SHEPHERD, S., BRENNAN, K., DALE, T., OSBORNE, J. M., GAVAGHAN, D. J. & BYRNE, H. M. 2017. The role of the Hes1 crosstalk hub in Notch-Wnt interactions of the intestinal crypt. *PLoS Comput Biol,* 13**,** e1005400.

KAZAKEVYCH, J., SAYOLS, S., MESSNER, B., KRIENKE, C. & SOSHNIKOVA, N. 2017. Dynamic changes in chromatin states during specification and differentiation of adult intestinal stem cells. *Nucleic Acids Res,* 45**,** 5770-5784.

KENT, W. J., ZWEIG, A. S., BARBER, G., HINRICHS, A. S. & KAROLCHIK, D. 2010. BigWig and BigBed: enabling browsing of large distributed datasets. *Bioinformatics,* 26**,** 2204-7.

KIM, C. K., YANG, V. W. & BIALKOWSKA, A. B. 2017. The Role of Intestinal Stem Cells in Epithelial Regeneration Following Radiation-Induced Gut Injury. *Curr Stem Cell Rep,* 3**,** 320-332.

KIM, D., PROBST, L., DAS, C. & TUCKER, P. W. 2007. REKLES is an ARID3-restricted multifunctional domain. *J Biol Chem,* 282**,** 15768-77.

KIM, D. & TUCKER, P. W. 2006. A regulated nucleocytoplasmic shuttle contributes to Bright's function as a transcriptional activator of immunoglobulin genes. *Mol Cell Biol,* 26**,** 2187-201.

KIM, T. H., ESCUDERO, S. & SHIVDASANI, R. A. 2012. Intact function of Lgr5 receptor-expressing intestinal stem cells in the absence of Paneth cells. *Proc Natl Acad Sci U S A,* 109**,** 3932-7.

KIM, T. H., LI, F., FERREIRO-NEIRA, I., HO, L. L., LUYTEN, A., NALAPAREDDY, K., LONG, H., VERZI, M. & SHIVDASANI, R. A. 2014. Broadly permissive intestinal chromatin underlies lateral inhibition and cell plasticity. *Nature,* 506**,** 511-5.

KIM, T. H. & SHIVDASANI, R. A. 2011. Genetic evidence that intestinal Notch functions vary regionally and operate through a common mechanism of Math1 repression. *J Biol Chem,* 286**,** 11427-33.

KOCH, S. 2017. Extrinsic control of Wnt signaling in the intestine. *Differentiation,* 97**,** 1-8.

KOO, B. K., LIM, H. S., CHANG, H. J., YOON, M. J., CHOI, Y., KONG, M. P., KIM, C. H., KIM, J. M., PARK, J. G. & KONG, Y. Y. 2009. Notch signaling promotes the generation of EphrinB1-positive intestinal epithelial cells. *Gastroenterology,* 137**,** 145-55, 155 e1-3.

KORN, S. M. & SCHLUNDT, A. 2022. Structures and nucleic acid-binding preferences of the eukaryotic ARID domain. *Biol Chem*.

KORTSCHAK, R. D., TUCKER, P. W. & SAINT, R. 2000. ARID proteins come in from the desert. *Trends Biochem Sci,* 25**,** 294-9.

KOSINSKI, C., LI, V. S., CHAN, A. S., ZHANG, J., HO, C., TSUI, W. Y., CHAN, T. L., MIFFLIN, R. C., POWELL, D. W., YUEN, S. T., LEUNG, S. Y. & CHEN, X. 2007. Gene expression patterns of human colon tops and basal crypts and BMP antagonists as intestinal stem cell niche factors. *Proc Natl Acad Sci U S A,* 104**,** 15418-23.

KOSINSKI, C., STANGE, D. E., XU, C., CHAN, A. S., HO, C., YUEN, S. T., MIFFLIN, R. C., POWELL, D. W., CLEVERS, H., LEUNG, S. Y. & CHEN, X. 2010. Indian hedgehog regulates intestinal stem cell fate through epithelial-mesenchymal interactions during development. *Gastroenterology,* 139**,** 893-903.

KURKEWICH, J. L., KLOPFENSTEIN, N., HALLAS, W. M., WOOD, C., SATTLER, R. A., DAS, C., TUCKER, H., DAHL, R. & COWDEN DAHL, K. D. 2016. Arid3b Is Critical for B Lymphocyte Development. *PLoS One,* 11**,** e0161468.

KURTZER, G. M., SOCHAT, V. & BAUER, M. W. 2017. Singularity: Scientific containers for mobility of compute. *PLoS One,* 12**,** e0177459.

LEBLOND, C. P. & WALKER, B. E. 1956. Renewal of cell populations. *Physiol Rev,* 36**,** 255-76.

LESTARI, W., ICHWAN, S. J., OTSU, M., YAMADA, S., ISEKI, S., SHIMIZU, S. & IKEDA, M. A. 2012. Cooperation between ARID3A and p53 in the transcriptional activation of p21WAF1 in response to DNA damage. *Biochem Biophys Res Commun,* 417**,** 710-6.

LI, H., HANDSAKER, B., WYSOKER, A., FENNELL, T., RUAN, J., HOMER, N., MARTH, G., ABECASIS, G., DURBIN, R. & GENOME PROJECT DATA PROCESSING, S. 2009. The Sequence Alignment/Map format and SAMtools. *Bioinformatics,* 25**,** 2078-9.

LI, H. J., KAPOOR, A., GIEL-MOLONEY, M., RINDI, G. & LEITER, A. B. 2012a. Notch signaling differentially regulates the cell fate of early endocrine precursor cells and their maturing descendants in the mouse pancreas and intestine. *Dev Biol,* 371**,** 156-69.

LI, V. S. & CLEVERS, H. 2013. Intestinal regeneration: YAP-tumor suppressor and oncoprotein? *Curr Biol,* 23**,** R110-2.

LI, V. S., NG, S. S., BOERSEMA, P. J., LOW, T. Y., KARTHAUS, W. R., GERLACH, J. P., MOHAMMED, S., HECK, A. J., MAURICE, M. M., MAHMOUDI, T. & CLEVERS, H. 2012b. Wnt signaling through inhibition of beta-catenin degradation in an intact Axin1 complex. *Cell,* 149**,** 1245-56.

LI, Y., TANG, J., LI, J., DU, Y., BAI, F., YANG, L., LI, X., JIN, X. & WANG, T. 2022. ARID3A promotes the chemosensitivity of colon cancer by inhibiting AKR1C3. *Cell Biol Int*.

LIAO, T.-T., HSU, W.-H., HO, C.-H., HWANG, W.-L., LAN, H.-Y., LO, T., CHANG, C.-C., TAI, S.-K. & YANG, M.-H. 2016. let-7 Modulates Chromatin Configuration and Target Gene Repression through Regulation of the ARID3B Complex. *Cell Reports,* 14**,** 520-533.

LIAO, Y., SMYTH, G. K. & SHI, W. 2014. featureCounts: an efficient general purpose program for assigning sequence reads to genomic features. *Bioinformatics,* 30**,** 923-30.

LIAO, Y., ZHANG, M. & LONNERDAL, B. 2013. Growth factor TGF-beta induces intestinal epithelial cell (IEC-6) differentiation: miR-146b as a regulatory component in the negative feedback loop. *Genes Nutr,* 8**,** 69-78.

LIN, D., IPPOLITO, G. C., ZONG, R. T., BRYANT, J., KOSLOVSKY, J. & TUCKER, P. 2007. Bright/ARID3A contributes to chromatin accessibility of the immunoglobulin heavy chain enhancer. *Mol Cancer,* 6**,** 23.

LIN, L., ZHOU, Z., ZHENG, L., ALBER, S., WATKINS, S., RAY, P., KAMINSKI, N., ZHANG, Y. & MORSE, D. 2008. Cross talk between Id1 and its interactive protein Dril1 mediate fibroblast responses to transforming growth factor-beta in pulmonary fibrosis. *Am J Pathol,* 173**,** 337-46.

LINDEBOOM, R. G., VAN VOORTHUIJSEN, L., OOST, K. C., RODRIGUEZ-COLMAN, M. J., LUNA-VELEZ, M. V., FURLAN, C., BARAILLE, F., JANSEN, P. W., RIBEIRO, A., BURGERING, B. M., SNIPPERT, H. J. & VERMEULEN, M. 2018. Integrative multi-omics analysis of intestinal organoid differentiation. *Mol Syst Biol,* 14**,** e8227.

LIU, C., LI, Y., SEMENOV, M., HAN, C., BAEG, G. H., TAN, Y., ZHANG, Z., LIN, X. & HE, X. 2002. Control of beta-catenin phosphorylation/degradation by a dual-kinase mechanism. *Cell,* 108**,** 837-47.

LIU, J., PAN, S., HSIEH, M. H., NG, N., SUN, F., WANG, T., KASIBHATLA, S., SCHULLER, A. G., LI, A. G., CHENG, D., LI, J., TOMPKINS, C., PFERDEKAMPER, A., STEFFY, A., CHENG, J., KOWAL, C., PHUNG, V., GUO, G., WANG, Y., GRAHAM, M. P., FLYNN, S., BRENNER, J. C., LI, C., VILLARROEL, M. C., SCHULTZ, P. G., WU, X., MCNAMARA, P., SELLERS, W. R., PETRUZZELLI, L., BORAL, A. L., SEIDEL, H. M., MCLAUGHLIN, M. E., CHE, J., CAREY, T. E., VANASSE, G. & HARRIS, J. L. 2013. Targeting Wnt-driven cancer through the inhibition of Porcupine by LGK974. *Proc Natl Acad Sci U S A,* 110**,** 20224-9.

LO, Y. H., CHUNG, E., LI, Z., WAN, Y. W., MAHE, M. M., CHEN, M. S., NOAH, T. K., BELL, K. N., YALAMANCHILI, H. K., KLISCH, T. J., LIU, Z., PARK, J. S. & SHROYER, N. F. 2017. Transcriptional Regulation by ATOH1 and its Target SPDEF in the Intestine. *Cell Mol Gastroenterol Hepatol,* 3**,** 51-71.

LOGUE, S. E., ELGENDY, M. & MARTIN, S. J. 2009. Expression, purification and use of recombinant annexin V for the detection of apoptotic cells. *Nat Protoc,* 4**,** 1383-95.

LONG, T., ABBASI, N., HERNANDEZ, J. E., LI, Y., SAYED, I. M., MA, S., IEMOLO, A., YEE, B. A., YEO, G. W., TELESE, F., GHOSH, P., DAS, S. & HUANG, W. J. M. 2021. RNA binding protein DDX5 directs tuft cell specification and function to regulate microbial repertoire and disease susceptibility in the intestine. *Gut*.

LOPEZ-DIAZ, L., JAIN, R. N., KEELEY, T. M., VANDUSSEN, K. L., BRUNKAN, C. S., GUMUCIO, D. L. & SAMUELSON, L. C. 2007. Intestinal Neurogenin 3 directs differentiation of a bipotential secretory progenitor to endocrine cell rather than goblet cell fate. *Dev Biol,* 309**,** 298-305.

LOVE, M. I., HUBER, W. & ANDERS, S. 2014. Moderated estimation of fold change and dispersion for RNA-seq data with DESeq2. *Genome Biol,* 15**,** 550.

MA, K., ARAKI, K., ICHWAN, S. J., SUGANUMA, T., TAMAMORI-ADACHI, M. & IKEDA, M. A. 2003. E2FBP1/DRIL1, an AT-rich interaction domain-family transcription factor, is regulated by p53. *Mol Cancer Res,* 1**,** 438-44.

MADISON, B. B., BRAUNSTEIN, K., KUIZON, E., PORTMAN, K., QIAO, X. T. & GUMUCIO, D. L. 2005. Epithelial hedgehog signals pattern the intestinal crypt-villus axis. *Development,* 132**,** 279-89.

MANCO, R., AVERBUKH, I., PORAT, Z., BAHAR HALPERN, K., AMIT, I. & ITZKOVITZ, S. 2021. Clump sequencing exposes the spatial expression programs of intestinal secretory cells. *Nat Commun,* 12**,** 3074.

MASSAGUE, J. 2012. TGFbeta signalling in context. *Nat Rev Mol Cell Biol,* 13**,** 616-30.

MATSU-URA, T., DOVZHENOK, A., AIHARA, E., ROOD, J., LE, H., REN, Y., ROSSELOT, A. E., ZHANG, T., LEE, C., OBRIETAN, K., MONTROSE, M. H., LIM, S., MOORE, S. R. & HONG, C. I. 2016. Intercellular Coupling of the Cell Cycle and Circadian Clock in Adult Stem Cell Culture. *Mol Cell,* 64**,** 900-912.

MAURY, J., NICOLETTI, C., GUZZO-CHAMBRAUD, L. & MAROUX, S. 1995. The filamentous brush border glycocalyx, a mucin-like marker of enterocyte hyper-polarization. *Eur J Biochem,* 228**,** 323-31.

MCCONNELL, R. E., HIGGINBOTHAM, J. N., SHIFRIN, D. A., JR., TABB, D. L., COFFEY, R. J. & TYSKA, M. J. 2009. The enterocyte microvillus is a vesicle-generating organelle. *J Cell Biol,* 185**,** 1285-98.

MCDOLE, J. R., WHEELER, L. W., MCDONALD, K. G., WANG, B., KONJUFCA, V., KNOOP, K. A., NEWBERRY, R. D. & MILLER, M. J. 2012. Goblet cells deliver luminal antigen to CD103+ dendritic cells in the small intestine. *Nature,* 483**,** 345-9.

MENG, Z., MOROISHI, T. & GUAN, K. L. 2016. Mechanisms of Hippo pathway regulation. *Genes Dev,* 30**,** 1-17.

MERAN, L., BAULIES, A. & LI, V. S. W. 2017. Intestinal Stem Cell Niche: The Extracellular Matrix and Cellular Components. *Stem Cells Int,* 2017**,** 7970385.

MEYER, A. R., BROWN, M. E., MCGRATH, P. S. & DEMPSEY, P. J. 2022. Injury-Induced Cellular Plasticity Drives Intestinal Regeneration. *Cell Mol Gastroenterol Hepatol,* 13**,** 843-856.

MOLENAAR, M., VAN DE WETERING, M., OOSTERWEGEL, M., PETERSON-MADURO, J., GODSAVE, S., KORINEK, V., ROOSE, J., DESTREE, O. & CLEVERS, H. 1996. XTcf-3 transcription factor mediates beta-catenin-induced axis formation in Xenopus embryos. *Cell,* 86**,** 391-9.

MONTGOMERY, R. K., CARLONE, D. L., RICHMOND, C. A., FARILLA, L., KRANENDONK, M. E., HENDERSON, D. E., BAFFOUR-AWUAH, N. Y., AMBRUZS, D. M., FOGLI, L. K., ALGRA, S. & BREAULT, D. T. 2011. Mouse telomerase reverse transcriptase (mTert) expression marks slowly cycling intestinal stem cells. *Proc Natl Acad Sci U S A,* 108**,** 179-84.

MOOR, A. E., HARNIK, Y., BEN-MOSHE, S., MASSASA, E. E., ROZENBERG, M., EILAM, R., BAHAR HALPERN, K. & ITZKOVITZ, S. 2018. Spatial Reconstruction of Single Enterocytes Uncovers Broad Zonation along the Intestinal Villus Axis. *Cell,* 175**,** 1156-1167.e15.

MOOSEKER, M. S. 1985. Organization, chemistry, and assembly of the cytoskeletal apparatus of the intestinal brush border. *Annu Rev Cell Biol,* 1**,** 209-41.

MOWAT, A. M. & AGACE, W. W. 2014. Regional specialization within the intestinal immune system. *Nat Rev Immunol,* 14**,** 667-85.

MUNOZ, J., STANGE, D. E., SCHEPERS, A. G., VAN DE WETERING, M., KOO, B. K., ITZKOVITZ, S., VOLCKMANN, R., KUNG, K. S., KOSTER, J., RADULESCU, S., MYANT, K., VERSTEEG, R., SANSOM, O. J., VAN ES, J. H., BARKER, N., VAN OUDENAARDEN, A., MOHAMMED, S., HECK, A. J. & CLEVERS, H. 2012. The Lgr5 intestinal stem cell signature: robust expression of proposed quiescent '+4' cell markers. *Embo j,* 31**,** 3079-91.

MURATA, K., JADHAV, U., MADHA, S., VAN ES, J., DEAN, J., CAVAZZA, A., WUCHERPFENNIG, K., MICHOR, F., CLEVERS, H. & SHIVDASANI, R. A. 2020. Ascl2-Dependent Cell Dedifferentiation Drives Regeneration of Ablated Intestinal Stem Cells. *Cell Stem Cell,* 26**,** 377-390 e6.

NADJSOMBATI, M. S., MCGINTY, J. W., LYONS-COHEN, M. R., JAFFE, J. B., DIPESO, L., SCHNEIDER, C., MILLER, C. N., POLLACK, J. L., NAGANA GOWDA, G. A., FONTANA, M. F., ERLE, D. J., ANDERSON, M. S., LOCKSLEY, R. M., RAFTERY, D. & VON MOLTKE, J. 2018. Detection of Succinate by Intestinal Tuft Cells Triggers a Type 2 Innate Immune Circuit. *Immunity,* 49**,** 33-41 e7.

NASH, K. L. & LEVER, A. M. 2004. Green fluorescent protein: green cells do not always indicate gene expression. *Gene Ther,* 11**,** 882-3.

NIGMATULLINA, L., NORKIN, M., DZAMA, M. M., MESSNER, B., SAYOLS, S. & SOSHNIKOVA, N. 2017. Id2 controls specification of Lgr5(+) intestinal stem cell progenitors during gut development. *Embo j,* 36**,** 869-885.

NOAH, T. K., DONAHUE, B. & SHROYER, N. F. 2011. Intestinal development and differentiation. *Exp Cell Res,* 317**,** 2702-10.

NOAH, T. K. & SHROYER, N. F. 2013. Notch in the Intestine: Regulation of Homeostasis and Pathogenesis. *Annual Review of Physiology,* 75**,** 263-288.

NOVELLASDEMUNT, L., FOGLIZZO, V., CUADRADO, L., ANTAS, P., KUCHARSKA, A., ENCHEVA, V., SNIJDERS, A. P. & LI, V. S. W. 2017. USP7 Is a Tumor-Specific WNT Activator for APC-Mutated Colorectal Cancer by Mediating beta-Catenin Deubiquitination. *Cell Rep,* 21**,** 612-627.

NOWARSKI, R., JACKSON, R., GAGLIANI, N., DE ZOETE, M. R., PALM, N. W., BAILIS, W., LOW, J. S., HARMAN, C. C., GRAHAM, M., ELINAV, E. & FLAVELL, R. A. 2015. Epithelial IL-18 Equilibrium Controls Barrier Function in Colitis. *Cell,* 163**,** 1444-56.

NUSSE, R. & CLEVERS, H. 2017. Wnt/beta-Catenin Signaling, Disease, and Emerging Therapeutic Modalities. *Cell,* 169**,** 985-999.

NUSSE, Y. M., SAVAGE, A. K., MARANGONI, P., ROSENDAHL-HUBER, A. K. M., LANDMAN, T. A., DE SAUVAGE, F. J., LOCKSLEY, R. M. & KLEIN, O. D. 2018. Parasitic helminths induce fetal-like reversion in the intestinal stem cell niche. *Nature,* 559**,** 109-113.

ORCHARD, P., KYONO, Y., HENSLEY, J., KITZMAN, J. O. & PARKER, S. C. J. 2020. Quantification, Dynamic Visualization, and Validation of Bias in ATAC-Seq Data with ataqv. *Cell Syst,* 10**,** 298-306 e4.

PARANG, B., ROSENBLATT, D., WILLIAMS, A. D., WASHINGTON, M. K., REVETTA, F., SHORT, S. P., REDDY, V. K., HUNT, A., SHROYER, N. F., ENGEL, M. E., HIEBERT, S. W. & WILLIAMS, C. S. 2015. The transcriptional corepressor MTGR1 regulates intestinal secretory lineage allocation. *Faseb j,* 29**,** 786-95.

PATSIALOU, A., WILSKER, D. & MORAN, E. 2005. DNA-binding properties of ARID family proteins. *Nucleic Acids Res,* 33**,** 66-80.

PEEPER, D. S., SHVARTS, A., BRUMMELKAMP, T., DOUMA, S., KOH, E. Y., DALEY, G. Q. & BERNARDS, R. 2002. A functional screen identifies hDRIL1 as an oncogene that rescues RAS-induced senescence. *Nat Cell Biol,* 4**,** 148-53.

PELASEYED, T., BERGSTROM, J. H., GUSTAFSSON, J. K., ERMUND, A., BIRCHENOUGH, G. M., SCHUTTE, A., VAN DER POST, S., SVENSSON, F., RODRIGUEZ-PINEIRO, A. M., NYSTROM, E. E., WISING, C., JOHANSSON, M. E. & HANSSON, G. C. 2014. The mucus and mucins of the goblet cells and enterocytes provide the first defense line of the gastrointestinal tract and interact with the immune system. *Immunol Rev,* 260**,** 8-20.

PELLEGRINET, L., RODILLA, V., LIU, Z., CHEN, S., KOCH, U., ESPINOSA, L., KAESTNER, K. H., KOPAN, R., LEWIS, J. & RADTKE, F. 2011. Dll1- and dll4-mediated notch signaling are required for homeostasis of intestinal stem cells. *Gastroenterology,* 140**,** 1230-1240.e1-7.

POINDEXTER, S. V., REDDY, V. K., MITTAL, M. K., WILLIAMS, A. M., WASHINGTON, M. K., HARRIS, E., MAH, A., HIEBERT, S. W., SINGH, K., CHATURVEDI, R., WILSON, K. T., LUND, P. K. & WILLIAMS, C. S. 2015. Transcriptional corepressor MTG16 regulates small intestinal crypt proliferation and crypt regeneration after radiation-induced injury. *Am J Physiol Gastrointest Liver Physiol,* 308**,** G562-71.

POPOWSKI, M., TEMPLETON, T. D., LEE, B.-K., RHEE, C., LI, H., MINER, C., DEKKER, JOSEPH D., ORLANSKI, S., BERGMAN, Y., IYER, VISHWANATH R., WEBB, CAROL F. & TUCKER, H. 2014. Bright/Arid3A Acts as a Barrier to Somatic Cell Reprogramming through Direct Regulation of Oct4, Sox2, and Nanog. *Stem Cell Reports,* 2**,** 26-35.

POTTEN, C. S. 1977. Extreme sensitivity of some intestinal crypt cells to X and gamma irradiation. *Nature,* 269**,** 518-21.

POTTEN, C. S., HUME, W. J., REID, P. & CAIRNS, J. 1978. The segregation of DNA in epithelial stem cells. *Cell,* 15**,** 899-906.

POTTEN, C. S., KOVACS, L. & HAMILTON, E. 1974. Continuous labelling studies on mouse skin and intestine. *Cell Tissue Kinet,* 7**,** 271-83.

POWELL, A. E., WANG, Y., LI, Y., POULIN, E. J., MEANS, A. L., WASHINGTON, M. K., HIGGINBOTHAM, J. N., JUCHHEIM, A., PRASAD, N., LEVY, S. E., GUO, Y., SHYR, Y., ARONOW, B. J., HAIGIS, K. M., FRANKLIN, J. L. & COFFEY, R. J. 2012. The pan-ErbB negative regulator Lrig1 is an intestinal stem cell marker that functions as a tumor suppressor. *Cell,* 149**,** 146-58.

QI, Z., LI, Y., ZHAO, B., XU, C., LIU, Y., LI, H., ZHANG, B., WANG, X., YANG, X., XIE, W., LI, B., HAN, J. J. & CHEN, Y. G. 2017. BMP restricts stemness of intestinal Lgr5(+) stem cells by directly suppressing their signature genes. *Nat Commun,* 8**,** 13824.

QUINLAN, A. R. & HALL, I. M. 2010. BEDTools: a flexible suite of utilities for comparing genomic features. *Bioinformatics,* 26**,** 841-2.

RAMIREZ, F., RYAN, D. P., GRUNING, B., BHARDWAJ, V., KILPERT, F., RICHTER, A. S., HEYNE, S., DUNDAR, F. & MANKE, T. 2016. deepTools2: a next generation web server for deep-sequencing data analysis. *Nucleic Acids Res,* 44**,** W160-5.

RATLIFF, M. L., MISHRA, M., FRANK, M. B., GUTHRIDGE, J. M. & WEBB, C. F. 2016. The Transcription Factor ARID3a Is Important for In Vitro Differentiation of Human Hematopoietic Progenitors. *J Immunol,* 196**,** 614-23.

RATLIFF, M. L., TEMPLETON, T. D., WARD, J. M. & WEBB, C. F. 2014. The Bright Side of Hematopoiesis: Regulatory Roles of ARID3a/Bright in Human and Mouse Hematopoiesis. *Front Immunol,* 5**,** 113.

RHEE, C., LEE, B. K., BECK, S., ANJUM, A., COOK, K. R., POPOWSKI, M., TUCKER, H. O. & KIM, J. 2014. Arid3a is essential to execution of the first cell fate decision via direct embryonic and extraembryonic transcriptional regulation. *Genes Dev,* 28**,** 2219-32.

RIOS-ESTEVES, J. & RESH, M. D. 2013. Stearoyl CoA desaturase is required to produce active, lipid-modified Wnt proteins. *Cell Rep,* 4**,** 1072-81.

ROBERTS, S. A., HENDRY, J. H. & POTTEN, C. S. 1995. Deduction of the clonogen content of intestinal crypts: a direct comparison of two-dose and multiple-dose methodologies. *Radiat Res,* 141**,** 303-8.

ROHWER, N., JUMPERTZ, S., ERDEM, M., EGNERS, A., WARZECHA, K. T., FRAGOULIS, A., KUHL, A. A., KRAMANN, R., NEUSS, S., RUDOLPH, I., ENDERMANN, T., ZASADA, C., APOSTOLOVA, I., GERLING, M., KEMPA, S., HUGHES, R., LEWIS, C. E., BRENNER, W., MALINOWSKI, M. B., STOCKMANN, M., SCHOMBURG, L., FALLER, W., SANSOM, O. J., TACKE, F., MORKEL, M. & CRAMER, T. 2019. Non-canonical HIF-1 stabilization contributes to intestinal tumorigenesis. *Oncogene,* 38**,** 5670-5685.

ROMERA-HERNANDEZ, M., APARICIO-DOMINGO, P., PAPAZIAN, N., KARRICH, J. J., CORNELISSEN, F., HOOGENBOEZEM, R. M., SAMSOM, J. N. & CUPEDO, T. 2020. Yap1-Driven Intestinal Repair Is Controlled by Group 3 Innate Lymphoid Cells. *Cell Rep,* 30**,** 37-45 e3.

ROSSETTI, S., HOOGEVEEN, A. T. & SACCHI, N. 2004. The MTG proteins: chromatin repression players with a passion for networking. *Genomics,* 84**,** 1-9.

ROTHENBERG, M. E., NUSSE, Y., KALISKY, T., LEE, J. J., DALERBA, P., SCHEEREN, F., LOBO, N., KULKARNI, S., SIM, S., QIAN, D., BEACHY, P. A., PASRICHA, P. J., QUAKE, S. R. & CLARKE, M. F. 2012. Identification of a cKit(+) colonic crypt base secretory cell that supports Lgr5(+) stem cells in mice. *Gastroenterology,* 142**,** 1195-1205 e6.

SANCHO, R., CREMONA, C. A. & BEHRENS, A. 2015. Stem cell and progenitor fate in the mammalian intestine: Notch and lateral inhibition in homeostasis and disease. *EMBO Rep,* 16**,** 571-81.

SANGIORGI, E. & CAPECCHI, M. R. 2008. Bmi1 is expressed in vivo in intestinal stem cells. *Nat Genet,* 40**,** 915-20.

SANMAN, L. E., CHEN, I. W., BIEBER, J. M., STERI, V., TRENTESAUX, C., HANN, B., KLEIN, O. D., WU, L. F. & ALTSCHULER, S. J. 2021. Transit-Amplifying Cells Coordinate Changes in Intestinal Epithelial Cell-Type Composition. *Dev Cell,* 56**,** 356-365 e9.

SANSOM, O. J., MENIEL, V. S., MUNCAN, V., PHESSE, T. J., WILKINS, J. A., REED, K. R., VASS, J. K., ATHINEOS, D., CLEVERS, H. & CLARKE, A. R. 2007. Myc deletion rescues Apc deficiency in the small intestine. *Nature,* 446**,** 676-9.

SANTOS, A. J. M., LO, Y. H., MAH, A. T. & KUO, C. J. 2018. The Intestinal Stem Cell Niche: Homeostasis and Adaptations. *Trends Cell Biol,* 28**,** 1062-1078.

SASAKI, N., SACHS, N., WIEBRANDS, K., ELLENBROEK, S. I., FUMAGALLI, A., LYUBIMOVA, A., BEGTHEL, H., VAN DEN BORN, M., VAN ES, J. H., KARTHAUS, W. R., LI, V. S., LOPEZ-IGLESIAS, C., PETERS, P. J., VAN RHEENEN, J., VAN OUDENAARDEN, A. & CLEVERS, H. 2016. Reg4+ deep crypt secretory cells function as epithelial niche for Lgr5+ stem cells in colon. *Proc Natl Acad Sci U S A,* 113**,** E5399-407.

SATO, A. 2007. Tuft cells. *Anat Sci Int,* 82**,** 187-99.

SATO, T., STANGE, D. E., FERRANTE, M., VRIES, R. G., VAN ES, J. H., VAN DEN BRINK, S., VAN HOUDT, W. J., PRONK, A., VAN GORP, J., SIERSEMA, P. D. & CLEVERS, H. 2011a. Long-term expansion of epithelial organoids from human colon, adenoma, adenocarcinoma, and Barrett's epithelium. *Gastroenterology,* 141**,** 1762-72.

SATO, T., VAN ES, J. H., SNIPPERT, H. J., STANGE, D. E., VRIES, R. G., VAN DEN BORN, M., BARKER, N., SHROYER, N. F., VAN DE WETERING, M. & CLEVERS, H. 2011b. Paneth cells constitute the niche for Lgr5 stem cells in intestinal crypts. *Nature,* 469**,** 415-8.

SATO, T., VRIES, R. G., SNIPPERT, H. J., VAN DE WETERING, M., BARKER, N., STANGE, D. E., VAN ES, J. H., ABO, A., KUJALA, P., PETERS, P. J. & CLEVERS, H. 2009. Single Lgr5 stem cells build crypt□villus structures in vitro without a mesenchymal niche. *Nature,* 459**,** 262-265.

SBARBATI, A. & OSCULATI, F. 2005. A new fate for old cells: brush cells and related elements. *J Anat,* 206**,** 349-58.

SCHEPERS, A. G., VRIES, R., VAN DEN BORN, M., VAN DE WETERING, M. & CLEVERS, H. 2011. Lgr5 intestinal stem cells have high telomerase activity and randomly segregate their chromosomes. *EMBO J,* 30**,** 1104-9.

SCHMIDT, C., KIM, D., IPPOLITO, G. C., NAQVI, H. R., PROBST, L., MATHUR, S., ROSAS-ACOSTA, G., WILSON, V. G., OLDHAM, A. L., POENIE, M., WEBB, C. F. & TUCKER, P. W. 2009. Signalling of the BCR is regulated by a lipid rafts-localised transcription factor, Bright. *Embo j,* 28**,** 711-24.

SCHMITT, M., SCHEWE, M., SACCHETTI, A., FEIJTEL, D., VAN DE GEER, W. S., TEEUWSSEN, M., SLEDDENS, H. F., JOOSTEN, R., VAN ROYEN, M. E., VAN DE WERKEN, H. J. G., VAN ES, J., CLEVERS, H. & FODDE, R. 2018. Paneth Cells Respond to Inflammation and Contribute to Tissue Regeneration by Acquiring Stem-like Features through SCF/c-Kit Signaling. *Cell Rep,* 24**,** 2312-2328.e7.

SCHUIJERS, J., JUNKER, J. P., MOKRY, M., HATZIS, P., KOO, B. K., SASSELLI, V., VAN DER FLIER, L. G., CUPPEN, E., VAN OUDENAARDEN, A. & CLEVERS, H. 2015. Ascl2 acts as an R-spondin/Wnt-responsive switch to control stemness in intestinal crypts. *Cell Stem Cell,* 16**,** 158-70.

SEI, Y., FENG, J., SAMSEL, L., WHITE, A., ZHAO, X., YUN, S., CITRIN, D., MCCOY, J. P., SUNDARESAN, S., HAYES, M. M., MERCHANT, J. L., LEITER, A. & WANK, S. A. 2018. Mature enteroendocrine cells contribute to basal and pathological stem cell dynamics in the small intestine. *Am J Physiol Gastrointest Liver Physiol,* 315**,** G495-G510.

SHANDALA, T., KORTSCHAK, R. D. & SAINT, R. 2002. The Drosophila retained/dead ringer gene and ARID gene family function during development. *Int J Dev Biol,* 46**,** 423-30.

SHROYER, N. F., HELMRATH, M. A., WANG, V. Y., ANTALFFY, B., HENNING, S. J. & ZOGHBI, H. Y. 2007. Intestine-specific ablation of mouse atonal homolog 1 (Math1) reveals a role in cellular homeostasis. *Gastroenterology,* 132**,** 2478-88.

SHROYER, N. F., WALLIS, D., VENKEN, K. J., BELLEN, H. J. & ZOGHBI, H. Y. 2005. Gfi1 functions downstream of Math1 to control intestinal secretory cell subtype allocation and differentiation. *Genes Dev,* 19**,** 2412-7.

SHROYER, N. F. & WONG, M. H. 2007. BMP signaling in the intestine: cross-talk is key. *Gastroenterology,* 133**,** 1035-8.

SHYER, A. E., HUYCKE, T. R., LEE, C., MAHADEVAN, L. & TABIN, C. J. 2015. Bending gradients: how the intestinal stem cell gets its home. *Cell,* 161**,** 569-580.

SHYER, A. E., TALLINEN, T., NERURKAR, N. L., WEI, Z., GIL, E. S., KAPLAN, D. L., TABIN, C. J. & MAHADEVAN, L. 2013. Villification: how the gut gets its villi. *Science,* 342**,** 212-8.

SNIPPERT, H. J., VAN DER FLIER, L. G., SATO, T., VAN ES, J. H., VAN DEN BORN, M., KROON-VEENBOER, C., BARKER, N., KLEIN, A. M., VAN RHEENEN, J., SIMONS, B. D. & CLEVERS, H. 2010. Intestinal crypt homeostasis results from neutral competition between symmetrically dividing Lgr5 stem cells. *Cell,* 143**,** 134-44.

SNOECK, V., GODDEERIS, B. & COX, E. 2005. The role of enterocytes in the intestinal barrier function and antigen uptake. *Microbes Infect,* 7**,** 997-1004.

SOLANAS, G., CORTINA, C., SEVILLANO, M. & BATLLE, E. 2011. Cleavage of E-cadherin by ADAM10 mediates epithelial cell sorting downstream of EphB signalling. *Nat Cell Biol,* 13**,** 1100-7.

SONG, M., KIM, H., KIM, W. K., HONG, S. P., LEE, C. & KIM, H. 2014. High expression of AT-rich interactive domain 3A (ARID3A) is associated with good prognosis in colorectal carcinoma. *Ann Surg Oncol,* 21 Suppl 4**,** S481-9.

SPIT, M., KOO, B. K. & MAURICE, M. M. 2018. Tales from the crypt: intestinal niche signals in tissue renewal, plasticity and cancer. *Open Biol,* 8.

STAMATAKI, D., HOLDER, M., HODGETTS, C., JEFFERY, R., NYE, E., SPENCER-DENE, B., WINTON, D. J. & LEWIS, J. 2011. Delta1 expression, cell cycle exit, and commitment to a specific secretory fate coincide within a few hours in the mouse intestinal stem cell system. *PLoS One,* 6**,** e24484.

STOLFI, C., TRONCONE, E., MARAFINI, I. & MONTELEONE, G. 2020. Role of TGF-Beta and Smad7 in Gut Inflammation, Fibrosis and Cancer. *Biomolecules,* 11.

STONE, D. M., HYNES, M., ARMANINI, M., SWANSON, T. A., GU, Q., JOHNSON, R. L., SCOTT, M. P., PENNICA, D., GODDARD, A., PHILLIPS, H., NOLL, M., HOOPER, J. E., DE SAUVAGE, F. & ROSENTHAL, A. 1996. The tumour-suppressor gene patched encodes a candidate receptor for Sonic hedgehog. *Nature,* 384**,** 129-34.

STORM, E. E., DURINCK, S., DE SOUSA E MELO, F., TREMAYNE, J., KLJAVIN, N., TAN, C., YE, X., CHIU, C., PHAM, T., HONGO, J. A., BAINBRIDGE, T., FIRESTEIN, R., BLACKWOOD, E., METCALFE, C., STAWISKI, E. W., YAUCH, R. L., WU, Y. & DE SAUVAGE, F. J. 2016. Targeting PTPRK-RSPO3 colon tumours promotes differentiation and loss of stem-cell function. *Nature,* 529**,** 97-100.

STZEPOURGINSKI, I., NIGRO, G., JACOB, J. M., DULAUROY, S., SANSONETTI, P. J., EBERL, G. & PEDUTO, L. 2017. CD34+ mesenchymal cells are a major component of the intestinal stem cells niche at homeostasis and after injury. *Proc Natl Acad Sci U S A,* 114**,** E506-e513.

SUZUKI, M., OKUYAMA, S., OKAMOTO, S., SHIRASUNA, K., NAKAJIMA, T., HACHIYA, T., NOJIMA, H., SEKIYA, S. & ODA, K. 1998. A novel E2F binding protein with Myc-type HLH motif stimulates E2F-dependent transcription by forming a heterodimer. *Oncogene,* 17**,** 853-65.

TAIPALE, J., COOPER, M. K., MAITI, T. & BEACHY, P. A. 2002. Patched acts catalytically to suppress the activity of Smoothened. *Nature,* 418**,** 892-7.

TAKADA, R., SATOMI, Y., KURATA, T., UENO, N., NORIOKA, S., KONDOH, H., TAKAO, T. & TAKADA, S. 2006. Monounsaturated fatty acid modification of Wnt protein: its role in Wnt secretion. *Dev Cell,* 11**,** 791-801.

TAKEBE, A., ERA, T., OKADA, M., MARTIN JAKT, L., KURODA, Y. & NISHIKAWA, S. 2006. Microarray analysis of PDGFR alpha+ populations in ES cell differentiation culture identifies genes involved in differentiation of mesoderm and mesenchyme including ARID3b that is essential for development of embryonic mesenchymal cells. *Dev Biol,* 293**,** 25-37.

TAKEDA, N., JAIN, R., LEBOEUF, M. R., WANG, Q., LU, M. M. & EPSTEIN, J. A. 2011. Interconversion between intestinal stem cell populations in distinct niches. *Science,* 334**,** 1420-4.

TAN, S. & BARKER, N. 2015. Epithelial stem cells and intestinal cancer. *Seminars in Cancer Biology,* 32**,** 40-53.

TANG, J., YANG, L., LI, Y., NING, X., CHAULAGAIN, A., WANG, T. & WANG, D. 2021. ARID3A promotes the development of colorectal cancer by upregulating AURKA. *Carcinogenesis,* 42**,** 578-586.

TANIGUCHI, K., WU, L. W., GRIVENNIKOV, S. I., DE JONG, P. R., LIAN, I., YU, F. X., WANG, K., HO, S. B., BOLAND, B. S., CHANG, J. T., SANDBORN, W. J., HARDIMAN, G., RAZ, E., MAEHARA, Y., YOSHIMURA, A., ZUCMAN-ROSSI, J., GUAN, K. L. & KARIN, M. 2015. A gp130-Src-YAP module links inflammation to epithelial regeneration. *Nature,* 519**,** 57-62.

TAURIELLO, D. V. F., PALOMO-PONCE, S., STORK, D., BERENGUER-LLERGO, A., BADIA-RAMENTOL, J., IGLESIAS, M., SEVILLANO, M., IBIZA, S., CANELLAS, A., HERNANDO-MOMBLONA, X., BYROM, D., MATARIN, J. A., CALON, A., RIVAS, E. I., NEBREDA, A. R., RIERA, A., ATTOLINI, C. S. & BATLLE, E. 2018. TGFbeta drives immune evasion in genetically reconstituted colon cancer metastasis. *Nature,* 554**,** 538-543.

TETTEH, PAUL W., BASAK, O., FARIN, HENNER F., WIEBRANDS, K., KRETZSCHMAR, K., BEGTHEL, H., VAN DEN BORN, M., KORVING, J., DE SAUVAGE, F., VAN ES, JOHAN H., VAN OUDENAARDEN, A. & CLEVERS, H. 2016. Replacement of Lost Lgr5-Positive Stem Cells through Plasticity of Their Enterocyte-Lineage Daughters. *Cell Stem Cell,* 18**,** 203-213.

TETTEH, P. W., FARIN, H. F. & CLEVERS, H. 2015. Plasticity within stem cell hierarchies in mammalian epithelia. *Trends in Cell Biology,* 25**,** 100-108.

TIAN, H., BIEHS, B., WARMING, S., LEONG, K. G., RANGELL, L., KLEIN, O. D. & DE SAUVAGE, F. J. 2011. A reserve stem cell population in small intestine renders Lgr5-positive cells dispensable. *Nature,* 478**,** 255-9.

TOMIC, G., MORRISSEY, E., KOZAR, S., BEN-MOSHE, S., HOYLE, A., AZZARELLI, R., KEMP, R., CHILAMAKURI, C. S. R., ITZKOVITZ, S., PHILPOTT, A. & WINTON, D. J. 2018. Phospho-regulation of ATOH1 Is Required for Plasticity of Secretory Progenitors and Tissue Regeneration. *Cell Stem Cell*.

UEO, T., IMAYOSHI, I., KOBAYASHI, T., OHTSUKA, T., SENO, H., NAKASE, H., CHIBA, T. & KAGEYAMA, R. 2012. The role of Hes genes in intestinal development, homeostasis and tumor formation. *Development,* 139**,** 1071-82.

VALENTA, T., DEGIRMENCI, B., MOOR, A. E., HERR, P., ZIMMERLI, D., MOOR, M. B., HAUSMANN, G., CANTU, C., AGUET, M. & BASLER, K. 2016. Wnt Ligands Secreted by Subepithelial Mesenchymal Cells Are Essential for the Survival of Intestinal Stem Cells and Gut Homeostasis. *Cell Rep,* 15**,** 911-918.

VAN DER FLIER, L. G., HAEGEBARTH, A., STANGE, D. E., VAN DE WETERING, M. & CLEVERS, H. 2009. OLFM4 is a robust marker for stem cells in human intestine and marks a subset of colorectal cancer cells. *Gastroenterology,* 137**,** 15-7.

VAN DER FLIER, L. G., SABATES-BELLVER, J., OVING, I., HAEGEBARTH, A., DE PALO, M., ANTI, M., VAN GIJN, M. E., SUIJKERBUIJK, S., VAN DE WETERING, M., MARRA, G. & CLEVERS, H. 2007. The Intestinal Wnt/TCF Signature. *Gastroenterology,* 132**,** 628-32.

VAN DOP, W. A., UHMANN, A., WIJGERDE, M., SLEDDENS-LINKELS, E., HEIJMANS, J., OFFERHAUS, G. J., VAN DEN BERGH WEERMAN, M. A., BOECKXSTAENS, G. E., HOMMES, D. W., HARDWICK, J. C., HAHN, H. & VAN DEN BRINK, G. R. 2009. Depletion of the colonic epithelial precursor cell compartment upon conditional activation of the hedgehog pathway. *Gastroenterology,* 136**,** 2195-2203 e1-7.

VAN ES, J. H., DE GEEST, N., VAN DE BORN, M., CLEVERS, H. & HASSAN, B. A. 2010. Intestinal stem cells lacking the Math1 tumour suppressor are refractory to Notch inhibitors. *Nat Commun,* 1**,** 18.

VAN ES, J. H., JAY, P., GREGORIEFF, A., VAN GIJN, M. E., JONKHEER, S., HATZIS, P., THIELE, A., VAN DEN BORN, M., BEGTHEL, H., BRABLETZ, T., TAKETO, M. M. & CLEVERS, H. 2005. Wnt signalling induces maturation of Paneth cells in intestinal crypts. *Nat Cell Biol,* 7**,** 381-6.

VAN ES, J. H., SATO, T., VAN DE WETERING, M., LYUBIMOVA, A., YEE NEE, A. N., GREGORIEFF, A., SASAKI, N., ZEINSTRA, L., VAN DEN BORN, M., KORVING, J., MARTENS, A. C. M., BARKER, N., VAN OUDENAARDEN, A. & CLEVERS, H. 2012. Dll1+ secretory progenitor cells revert to stem cells upon crypt damage. *Nat Cell Biol,* 14**,** 1099-1104.

VANDENBROUCKE, R. E., VANLAERE, I., VAN HAUWERMEIREN, F., VAN WONTERGHEM, E., WILSON, C. & LIBERT, C. 2014. Pro-inflammatory effects of matrix metalloproteinase 7 in acute inflammation. *Mucosal Immunol,* 7**,** 579-88.

VERZI, M. P. & SHIVDASANI, R. A. 2020. Epigenetic regulation of intestinal stem cell differentiation. *Am J Physiol Gastrointest Liver Physiol,* 319**,** G189-G196.

VON MOLTKE, J., JI, M., LIANG, H. E. & LOCKSLEY, R. M. 2016. Tuft-cell-derived IL-25 regulates an intestinal ILC2-epithelial response circuit. *Nature,* 529**,** 221-5.

WANG, F., KOHAN, A. B., LO, C. M., LIU, M., HOWLES, P. & TSO, P. 2015. Apolipoprotein A-IV: a protein intimately involved in metabolism. *J Lipid Res,* 56**,** 1403-18.

WANG, Y., GIEL-MOLONEY, M., RINDI, G. & LEITER, A. B. 2007. Enteroendocrine precursors differentiate independently of Wnt and form serotonin expressing adenomas in response to active beta-catenin. *Proc Natl Acad Sci U S A,* 104**,** 11328-33.

WEBB, C., ZONG, R. T., LIN, D., WANG, Z., KAPLAN, M., PAULIN, Y., SMITH, E., PROBST, L., BRYANT, J., GOLDSTEIN, A., SCHEUERMANN, R. & TUCKER, P. 1999. Differential regulation of immunoglobulin gene transcription via nuclear matrix-associated regions. *Cold Spring Harb Symp Quant Biol,* 64**,** 109-18.

WEBB, C. F., BRYANT, J., POPOWSKI, M., ALLRED, L., KIM, D., HARRISS, J., SCHMIDT, C., MINER, C. A., ROSE, K., CHENG, H. L., GRIFFIN, C. & TUCKER, P. W. 2011. The ARID family

transcription factor bright is required for both hematopoietic stem cell and B lineage development. *Mol Cell Biol,* 31**,** 1041-53.

WEHKAMP, J. & STANGE, E. F. 2020. An Update Review on the Paneth Cell as Key to Ileal Crohn's Disease. *Front Immunol,* 11**,** 646.

WILEN, C. B., LEE, S., HSIEH, L. L., ORCHARD, R. C., DESAI, C., HYKES, B. L., JR., MCALLASTER, M. R., BALCE, D. R., FEEHLEY, T., BRESTOFF, J. R., HICKEY, C. A., YOKOYAMA, C. C., WANG, Y. T., MACDUFF, D. A., KREAMALMAYER, D., HOWITT, M. R., NEIL, J. A., CADWELL, K., ALLEN, P. M., HANDLEY, S. A., VAN LOOKEREN CAMPAGNE, M., BALDRIDGE, M. T. & VIRGIN, H. W. 2018. Tropism for tuft cells determines immune promotion of norovirus pathogenesis. *Science,* 360**,** 204-208.

WILLERT, K., BROWN, J. D., DANENBERG, E., DUNCAN, A. W., WEISSMAN, I. L., REYA, T., YATES, J. R., 3RD & NUSSE, R. 2003. Wnt proteins are lipid-modified and can act as stem cell growth factors. *Nature,* 423**,** 448-52.

WILSKER, D., PROBST, L., WAIN, H. M., MALTAIS, L., TUCKER, P. W. & MORAN, E. 2005. Nomenclature of the ARID family of DNA-binding proteins. *Genomics,* 86**,** 242-51.

WONG, V. W., STANGE, D. E., PAGE, M. E., BUCZACKI, S., WABIK, A., ITAMI, S., VAN DE WETERING, M., POULSOM, R., WRIGHT, N. A., TROTTER, M. W., WATT, F. M., WINTON, D. J., CLEVERS, H. & JENSEN, K. B. 2012. Lrig1 controls intestinal stem-cell homeostasis by negative regulation of ErbB signalling. *Nat Cell Biol,* 14**,** 401-8.

YAN, F., POWELL, D. R., CURTIS, D. J. & WONG, N. C. 2020. From reads to insight: a hitchhiker's guide to ATAC-seq data analysis. *Genome Biol,* 21**,** 22.

YAN, K. S., GEVAERT, O., ZHENG, G. X. Y., ANCHANG, B., PROBERT, C. S., LARKIN, K. A., DAVIES, P. S., CHENG, Z. F., KADDIS, J. S., HAN, A., ROELF, K., CALDERON, R. I., CYNN, E., HU, X., MANDLEYWALA, K., WILHELMY, J., GRIMES, S. M., CORNEY, D. C., BOUTET, S. C., TERRY, J. M., BELGRADER, P., ZIRALDO, S. B., MIKKELSEN, T. S., WANG, F., VON FURSTENBERG, R. J., SMITH, N. R., CHANDRAKESAN, P., MAY, R., CHRISSY, M. A. S., JAIN, R., CARTWRIGHT, C. A., NILAND, J. C., HONG, Y. K., CARRINGTON, J., BREAULT, D. T., EPSTEIN, J., HOUCHEN, C. W., LYNCH, J. P., MARTIN, M. G., PLEVRITIS, S. K., CURTIS, C., JI, H. P., LI, L., HENNING, S. J., WONG, M. H. & KUO, C. J. 2017a. Intestinal Enteroendocrine Lineage Cells Possess Homeostatic and Injury-Inducible Stem Cell Activity. *Cell Stem Cell,* 21**,** 78-90.e6.

YAN, K. S., JANDA, C. Y., CHANG, J., ZHENG, G. X. Y., LARKIN, K. A., LUCA, V. C., CHIA, L. A., MAH, A. T., HAN, A., TERRY, J. M., OOTANI, A., ROELF, K., LEE, M., YUAN, J., LI, X., BOLEN, C. R., WILHELMY, J., DAVIES, P. S., UENO, H., VON FURSTENBERG, R. J., BELGRADER, P., ZIRALDO, S. B., ORDONEZ, H., HENNING, S. J., WONG, M. H., SNYDER, M. P., WEISSMAN, I. L., HSUEH, A. J., MIKKELSEN, T. S., GARCIA, K. C. & KUO, C. J. 2017b. Non-equivalence of Wnt and R-spondin ligands during Lgr5(+) intestinal stem-cell self-renewal. *Nature,* 545**,** 238-242.

YANG, E. & SHEN, J. 2021. The roles and functions of Paneth cells in Crohn's disease: A critical review. *Cell Prolif,* 54**,** e12958.

YANG, S. & YU, M. 2021. Role of Goblet Cells in Intestinal Barrier and Mucosal Immunity. *J Inflamm Res,* 14**,** 3171-3183.

YANG, Y. P., MA, H., STARCHENKO, A., HUH, W. J., LI, W., HICKMAN, F. E., ZHANG, Q., FRANKLIN, J. L., MORTLOCK, D. P., FUHRMANN, S., CARTER, B. D., IHRIE, R. A. & COFFEY, R. J. 2017. A Chimeric Egfr Protein Reporter Mouse Reveals Egfr Localization and Trafficking In Vivo. *Cell Rep,* 19**,** 1257-1267.

YIN, X., FARIN, H. F., VAN ES, J. H., CLEVERS, H., LANGER, R. & KARP, J. M. 2014. Niche-independent high-purity cultures of Lgr5+ intestinal stem cells and their progeny. *Nat Methods,* 11**,** 106-12.

YU, S., TONG, K., ZHAO, Y., BALASUBRAMANIAN, I., YAP, G. S., FERRARIS, R. P., BONDER, E. M., VERZI, M. P. & GAO, N. 2018. Paneth Cell Multipotency Induced by Notch Activation following Injury. *Cell Stem Cell,* 23**,** 46-59.e5.

YUI, S., AZZOLIN, L., MAIMETS, M., PEDERSEN, M. T., FORDHAM, R. P., HANSEN, S. L., LARSEN, H. L., GUIU, J., ALVES, M. R. P., RUNDSTEN, C. F., JOHANSEN, J. V., LI, Y., MADSEN, C. D., NAKAMURA, T., WATANABE, M., NIELSEN, O. H., SCHWEIGER, P. J., PICCOLO, S. & JENSEN, K. B. 2018. YAP/TAZ-Dependent Reprogramming of Colonic Epithelium Links ECM Remodeling to Tissue Regeneration. *Cell Stem Cell,* 22**,** 35-49 e7.

ZACHARIAS, W. J., MADISON, B. B., KRETOVICH, K. E., WALTON, K. D., RICHARDS, N., UDAGER, A. M., LI, X. & GUMUCIO, D. L. 2011. Hedgehog signaling controls homeostasis of adult intestinal smooth muscle. *Dev Biol,* 355**,** 152-62.

ZHANG, Y., LIU, T., MEYER, C. A., EECKHOUTE, J., JOHNSON, D. S., BERNSTEIN, B. E., NUSBAUM, C., MYERS, R. M., BROWN, M., LI, W. & LIU, X. S. 2008. Model-based analysis of ChIP-Seq (MACS). *Genome Biol,* 9**,** R137.

ZHANG, Y. & QUE, J. 2020. BMP Signaling in Development, Stem Cells, and Diseases of the Gastrointestinal Tract. *Annu Rev Physiol,* 82**,** 251-273.

ZHENG, L., KELLY, C. J. & COLGAN, S. P. 2015. Physiologic hypoxia and oxygen homeostasis in the healthy intestine. A Review in the Theme: Cellular Responses to Hypoxia. *Am J Physiol Cell Physiol,* 309**,** C350-60.